UNIVERSITÀ DEGLI STUDI DI PADOVA

Sede Amministrativa: Università degli Studi di Padova

Dipartimento di Scienze Chimiche

SCUOLA DI DOTTORATO DI RICERCA IN : SCIENZE MOLECOLARI
INDIRIZZO: SCIENZE CHIMICHE
CICLO XXII

Non-thermal plasma processing for the decomposition of organic pollutants

Direttore della Scuola: Ch.mo Prof. Maurizio Casarin
Supervisore: Ch.ma Prof.ssa Cristina Paradisi

Dottorando: Milko Schiorlin

INDEX

SUMMARY

Plasma chemistry is a rapidly growing field to develop and exploit the great potential of plasma to perform chemical reactions. This thesis deals with the oxidation of organic pollutants in air and water promoted by the action of air non-thermal plasma (NTP). Such plasmas, which are conveniently produced by electric non-thermalizing discharges like corona and dielectric barrier discharges in air at atmospheric pressure and ambient temperature, provide highly reactive oxidizing environments comprising electrons, excited molecules, atomic and radical species (O, OH), ions ($O_2^{+\bullet}$, $N_2^{+\bullet}$, NO^+, $O^{-\bullet}$, $O_2^{-\bullet}$, $O_3^{-\bullet}$), O_3 and NO. Despite the numerous successful applications of NTP in processes of environmental and commercial relevance, the chemistry of organic compounds within air non-thermal plasmas is still not well characterized, both as far as products and mechanisms are concerned. This thesis developed as a contribution to this field of research along three lines dealing, respectively, with plasma processing of: volatile organic compounds (VOCs) in air with plasma alone; VOCs in air with plasma plus an heterogeneous catalyst; organic pollutants in aqueous solutions above which an air plasma is generated. All three projects had a common focus in the mechanistic characterization of the oxidation processes within these very complex and highly reactive systems.

The study of VOC oxidation in air NTP was carried out with a large prototype corona reactor developed at the Department of Chemical Sciences in Padova, which can be energized with DC or pulsed high voltage of either polarity. Comparative studies were carried out to evaluate the response of selected model VOCs to different corona regimes (+DC, –DC and +pulsed). The VOCs considered include two alkanes (n-hexane and i-octane), toluene and two halogenated methanes, dibromomethane (CH_2Br_2) and dibromodifluoromethane (CF_2Br_2, halon 1202). Remarkably, all these different VOCs, including the highly inert halon, can be oxidized to CO_2 at room temperature with efficiencies which depend on VOC type (despite their high reactivity NTPs display some selectivity), on VOC concentration (the efficiency increases linearly with the reciprocal of VOC concentration) but also on the way energy is given to the plasma. Thus, for all VOCs examined the efficiency decreases in the order: +pulsed > -DC > +DC corona. This means that any given amount of energy

produces an extent of VOC conversion ($[VOC]/[VOC]_0$) which depends on the corona regime and decreases in the order +pulsed > –DC > +DC. The greater efficiency of +pulsed corona is due to the higher mean electron energy achieved, for any given input of energy, with this type of power supply with respect to DC high voltage. The mean electron energy of the plasma under the different corona regimes was experimentally determined in our reactor by emission spectroscopy measurements following a published procedure. Another important variable tested was the humidity in the air, which is known to produce the strongly oxidizing OH radicals via electron induced dissociation or via reaction with $O_2^{+\bullet}$ and $N_2^{+\bullet}$ ions. Thus, the greater efficiency in humid with respect to dry air observed for the oxidation of hydrocarbons and of CH_2Br_2 with –DC and +pulsed corona was attributed to reaction with OH radicals. Surprisingly, in experiments with + DC the same VOCs undergo less efficient oxidation in humid air than in dry air, despite the presence of OH radicals. Analysis of the plasma ionized species, performed by APCI-MS (Atmospheric Pressure Chemical Ionization – Mass Spectrometry), coupled to the determination of current/voltage characteristics of DC coronas, led to the proposal that in the case of +DC corona the oxidation of hydrocarbons and of CH_2Br_2 is initiated by reactions with ions ($O_2^{+\bullet}$, H_3O^+ and their hydrates, NO^+) both in dry as well as in humid air. In contrast, with –DC and +pulsed corona in humid air, OH radicals are involved in the initial stage of hydrocarbons and of CH_2Br_2 oxidation. Consistent with its very low reactivity with the OH radical, the oxidation of CF_2Br_2 in humid air proceeds less efficiently with both +DC and –DC corona. It was thus proposed that the oxidation of CF_2Br_2 occurs via a common mechanism under all corona regimes tested, the initial step being electron induced C-Br dissociation. The process efficiency is lower in humid air because the mean electron energy is lowered due to reaction of the electrons with water molecules. The two halomethanes also form different products: FT-IR analysis of post-discharge gas has shown that CH_2Br_2 produces both CO_2 and CO, whereas CF_2Br_2 forms CO_2 and $F_2C{=}O$. The latter product is a long-lived oxidation intermediate due to its low reactivity with atmospheric radicals. It is however very rapidly hydrolized to CO_2 and HF as shown by combined ion chromatography and FT-IR analysis of the solution and of the exhaust gas obtained after a water scrubbing step. Other non-carbon containing products of the discharge were analyzed by FT-IR analysis, including ozone, HNO_3 and

N_2O. In experiments with both halomethanes evidence was found for bromine-sustained catalytic ozone destruction cycles, responsible also for increased conversion of NOx into HNO_3.

Efficiency and, especially, product selectivity can be improved by the combined action of plasma and heterogeneous catalysts which usually result in synergic effects. The nature and origin of this synergy was the focus of the research I carried out in my second year in graduate school during a stage at the Advanced Industrial Science and Technology Institute (AIST) in Tsukuba (Japan), in the group of dr. Hyun-Ha Kim. As molecular probe to compare the effects of plasma alone and plasma plus catalyst we selected the O-scrambling reaction to form $^{16}O^{18}O$ starting from a mixture of $^{16}O_2$ and $^{18}O_2$. Four different reactors were used and various catalysts, including TiO_2, MS-13X and γAl_2O_3 also containing a few % of Ag. It was possible to conclude that, in the absence of a catalyst the O-exchange reaction occurs in the gas phase and not on the electrodes surface. It was also possible to use the results of these experiments to estimate, for any given energy input the average concentration of O atoms within the plasma. This is a most interesting outcome of these studies since the traditional method for obtaining O atom density involves sophisticated laser spectroscopy instrumentation and procedures. As for the catalyst/plasma interaction, using again a labelled molecular probe, $^{18}O_2$, it was possible to conclude that the plasma induces oxygen fission on the catalyst surface and that this oxygen is then used in the oxidation of VOCs.

The third project dealt with the plasma induced oxidation of phenol in aqueous solution. For these studies two prototype reactors were developed and tested, both characterized by application of electric discharges in the air above the solution. The first is a dielectric barrier discharge reactor which afforded the efficient removal of phenol from the aqueous solution according to an exponential decay as a function of treatment time at constant power. A qualitative analysis of the intermediate and final products of phenol oxidation was performed and the major reactive species formed upon the application of the discharge in air were identified and determined. It is concluded that the decomposition of phenol is initiated by reactions with ozone, taking place on the surface of the solution, and with hydroxyl radicals, both at the surface and within the bulk of the solution. An interesting and most convenient result is the better efficiency of phenol removal in tap water than in milliQ water. After ruling out

possible effects due to conductivity, to Fenton's reaction due to Fe_2^+ and to active chlorine, it was concluded that the efficiency increase is due to the higher pH of the solution mantained by the presence of bicarbonate salts. The second developed reactor allowed us to perform some interesting comparisons since it can be powered by different types of high voltage for the generation of plasma. The possibility to apply this technology to the treatment of waste water depends on many factors: the process efficiency, the final composition of the treated solution, the general applicability of the system to the organic pollutants. The data obtained so far are very promising due to the efficient oxidation all the way to CO_2 and to the absence of any hazardous organic byproduct after a proper treatment time.

The results of this thesis confirm that plasma processing is a promising highly efficient means for the advanced oxidation of organic pollutants both in air and in aqueous solution.

RIASSUNTO

Lo studio di processi chimici indotti da plasmi sta suscitando un notevole interesse per il grande potenziale che questi sistemi possono sviluppare. Questa tesi riguarda l'ossidazione di inquinanti organici in aria e in soluzione acquosa promossa dall'interazione con plasma non-termico (NTP). Questi plasmi, che sono convenientemente generati da scariche elettriche non termalizzanti, principalmente scariche corona e a barriera di dielettrico, in aria a temperatura e pressione ambiente, costituiscono ambienti di reazione molto reattivi e fortemente ossidanti per la presenza di elettroni, molecole eccitate, specie atomiche e radicali (O, OH), ioni ($O_2^{+\bullet}$, $N_2^{+\bullet}$, NO^+, $O^{-\bullet}$, $O_2^{-\bullet}$, $O_3^{-\bullet}$), O_3 e NO. Nonostante siano numerose le applicazioni tecnologiche di questi plasmi in processi di rilevanza ambientale e commerciale, la chimica dei composti organici in questi sistemi è tuttora non ben nota sia per quanto riguarda i prodotti che i meccanismi di reazione. Questa tesi è uno studio meccanicistico che si è sviluppato lungo tre linee di ricerca riguardanti l'ossidazione di: i) composti organici volatili (VOC) in aria con solo plasma; ii) VOC in aria con plasma e un catalizzatore eterogeno; inquinanti organici in soluzioni acquose poste a contatto con plasma non termico in aria. I tre progetti hanno un obiettivo comune che riguarda la caratterizzazione dei meccanismi di ossidazione che operano in questi sistemi di enorme complessità chimica.

Lo studio dell'ossidazione di VOC in plasmi non termici in aria è stato condotto utilizzando un reattore prototipo a scarica corona sviluppato presso il Dipartimento di Scienze Chimiche a Padova, che può essere alimentato da alta tensione DC o ad impulsi di polarità sia positiva che negativa. Sono stati svolti studi comparativi per valutare la risposta di alcuni modelli di VOC a diversi regimi di scarica corona, precisamente +DC, -DC e +pulsed. I composti studiati sono due alcani (esano ed iso-ottano), il toluene e gli alometani dibromometano (CH_2Br_2) e dibromodifluorometane (CF_2Br_2, halon 1202). E' notevole il fatto che tutti questi VOC, compreso l'halon notoriamente molto inerte, possono essere ossidati a CO_2 in questi plasmi a temperatura ambiente con un'efficienza che dipende dal tipo di VOC (nonostante la loro elevata reattività questi plasmi presentano comunque un certo grado di selettività), dalla concentrazione del VOC (l'efficienza aumenta linearmente col reciproco della concentrazione

iniziale del VOC) e dal modo in cui l'energia viene fornita al reattore. Infatti, per tutti i VOC considerati, l'efficienza del trattamento aumenta nell'ordine: +DC < -DC < +pulsed. Questo significa che il grado di conversione ($[VOC]/[VOC]_0$) prodotto da una certa quantità di energia fornita al sistema dipende dal tipo di scarica utilizzato, che a sua volta determina la composizione e natura del plasma e quindi la sua reattività. La maggiore efficienza del corona ad impulsi rispetto al corona DC è attribuibile alla maggiore energia media degli elettroni in questo regime di scarica. L'energia media degli elettroni è stata determinata sperimentalmente nel nostro reattore nelle diverse condizioni di scarica mediante esperimenti di spettroscopia di emissione utilizzando un metodo pubblicato in letteratura. Un'altra importante variabile di questi processi è il grado di umidità dell'aria, che determina la formazione di maggiori o minori concentrazioni del radicale OH. Questo radicale si forma dall'acqua attraverso reazione con elettroni ad alta energia o reazione con gli ioni $O_2^{+\bullet}$ and $N_2^{+\bullet}$. La maggior efficienza dell'ossidazione di idrocarburi e del CH_2Br_2 osservata con -DC in aria umida rispetto all'aria secca è stata quindi attribuita alla reazione con radicali OH. Sorprendentemente, con +DC l'umidità produce un effetto opposto per gli stessi VOC, nonostante la presenza in aria umida di radicali OH. L'analisi degli ioni del plasma, effettuata mediante spettrometria di massa APCI-MS (Atmospheric Pressure Chemical Ionization – Mass Spectrometry), accoppiata allo studio della caratteristica corrente/tensione del corona DC, ha portato a concludere che nel caso del corona +DC l'ossidazione degli idrocarburi e del dibromometano è iniziata da reazione con ioni ($O_2^{+\bullet}$, H_3O^+ e i loro idrati, NO^+) sia in aria secca che in aria umida. Al contrario, nel caso del corona –DC e del corona +pulsed la principale reazione di attacco a questi VOC risulta essere quella del radicale OH. Per quanto riguarda invece l'halon CF_2Br_2, sia con +DC che con –DC l'ossidazione in aria umida risulta meno efficiente che in aria secca, un risultato coerente con la nota scarsa reattività di questo VOC con il radicale OH. E' stata quindi avanzata l'ipotesi che l'ossidazione di questo halon proceda attraverso un meccanismo comune, indipendentemente dal regime di scarica applicato, che comporta la dissociazione iniziale del legame C-Br indotta da interazione con elettroni del plasma. Il processo è meno efficiente in aria umida probabilmente perché la reazione di dissociazione dell'acqua provoca una riduzione dell'energia media degli elettroni rispetto a quella in aria secca. L'ossidazione dei due alometani in aria secca dà prodotti diversi: l'analisi

FT-IR del gas in uscita dal reattore ha individuato sia CO_2 che CO fra i prodotti di CH_2Br_2 mentre nel caso di CF_2Br_2 i prodotti sono CO_2 e $F_2C=O$. Quest'ultimo è un intermedio di ossidazione con tempo di vita sufficientemente lungo da poter essere rivelato in quanto notoriamente poco reattivo nelle reazioni con radicali. E' tuttavia idrolizzato molto velocemente a CO_2 e HF come dimostrato da analisi integrate di cromatografia ionica e FT-IR della soluzione e del gas ottenuti dopo gorgogliamento del gas trattato in acqua. Altri prodotti di questi trattamenti rivelati e quantificati mediante spettroscopia FT-IR sono l'ozono, l'acido nitrico e l'ossido N_2O. Con entrambi gli alometani si è osservato l'intervento di cicli catalitici di distruzione dell'ozono in cui il bromo atomico è la specie propagatrice. Gli stessi cicli sono inoltre responsabili della conversione degli NOx in HNO_3.

L'efficienza e la selettività dei processi di ossidazione al plasma possono essere migliorati attraverso l'azione combinata del plasma e di catalizzatori eterogenei. Ne deriva un effetto sinergico, la cui origine e natura sono tuttora in fase di studio. Di questo problema mi sono occupato durante un soggiorno presso l'Advanced Industrial Science and Technology Institute (AIST) a Tsukuba (Giappone), presso il gruppo del Prof. Hyun-Ha Kim. Per confrontare gli effetti di solo plasma e plasma più catalizzatore abbiamo utilizzato come sonda molecolare la reazione di scambio di ossigeno che produce $^{16}O^{18}O$ partendo da miscele di $^{16}O_2$ e $^{18}O_2$. Sono stati utilizzati diversi reattori al plasma con diverse alimentazioni elettriche e parecchi catalizzatori fra cui TiO_2, MS-13X e γAl_2O_3 contentente varie modeste percentuali di Ag. Questi studi hanno permesso di concludere che, in assenza di catalizzatore, la reazione di scambio di ossigeno avviene in fase gas e non sulle superfici degli elettrodi. I risultati di questi esperimenti sono stati utilizzati per sviluppare un metodo basato sulla reazione di scambio isotopico al fine di determinare la concentrazione di ossigeno atomico in questi plasmi. Questo è un risultante importante che si propone come alternativa al metodo tradizionale per la determinazione della concentrazione di ossigeno atomico con strumentazioni ottiche laser e procedure piuttosto sofisticate. Per quanto riguarda l'interazione catalizzatore/plasma, è stato possibile concludere, sempre utilizzando la sonda molecolare $^{18}O_2$, marcata isotopicamente, che il plasma determina la fissazione dell'ossigeno sulla superficie del catalizzatore e che questo ossigeno è quindi trasferito al VOC nel processo di ossidazione.

Infine, il terzo progetto ha riguardato l'ossidazione del fenolo in soluzioni acquose esposte all'azione di plasma non-termico in aria. Per questi studi sono stati sviluppati due prototipi di reattore caratterizzati entrambi dall'applicazione di scariche elettriche nell'aria sovrastante la soluzione da trattare. L'ossidazione del fenolo nel primo reattore, che utilizza scariche a barriera di dielettrico, procede efficacemente fino a CO_2 seguendo un decadimento esponenziale in funzione del tempo di trattamento a potenza applicata costante. Dall'analisi dei prodotti ed intermedi di ossidazione nonché dalla determinazione delle principali specie reattive è emerso che la decomposizione del fenolo avviene per reazione con l'ozono sulla superficie della soluzione a contatto con il plasma, e con il radicale OH, sia sulla superficie che all'interno della soluzione. Un risultato molto interessante e utile in vista di applicazioni pratiche di questi processi riguarda la maggiore efficienza dell'ossidazione del fenolo in acqua di rubinetto rispetto all'acqua milliQ. Dopo aver escluso che all'origine di questo fenomeno potessero esserci effetti dovuti alla conduttività maggiore, alla presenza di ioni Fe_2^+ capaci di indurre la reazione di Fenton, e alla presenza di cloro attivo nell'acqua potabile, è stato verificato che l'effetto tampone esercitato dallo ione bicarbonato mantiene un pH elevato e consente al processo di procedere velocemente.

1. INTRODUCTION

The present condition of our environment and the worrying perspective for its future are raising increasing awareness and preoccupation at all levels of the human society. The scientific community is called upon to contribute knowledge and innovative proposals aiming at reducing and at remediating the negative impact on the environment due to human activities. Some effects are immediate, others require longer times to develop so that it is often difficult to predict the consequences in the long range. A most famous example is given by the chemically and biochemically inert chlorofluorocarbons (CFCs) which were developed and successfully used as safe substitutes for dangerous refrigerating fluids like ammonia. Unexpectedly the very same lack of reactivity which had made them so valuable in the short term turned out to be the origin of nowadays well understood environmental problems: CFCs are too stable to undergo reactions in the troposphere, live long enough to reach the stratosphere where they undergo photolysis releasing chlorine atoms which contribute greatly to the depletion of the stratospheric ozone layer, our shield against dangerous UV radiation. This problem was overcome by developing a new generation of substitutes, likewise inert and non toxic, which do not contain labile carbon halogen bonds, the hydrofluorocarbons (HFCs). Such compounds, however, are proving to be harmful for their impact as green house gases. It appears obvious from the above cited example that the term ‘pollutant’ must be used in a wide context and not be limited to toxic or dangerous compounds released into the environment.

This thesis deals with the study of innovative remediation processes based on use of non-thermal plasmas in air. Such plasmas, which are conveniently produced through the application of electric discharges in air at room temperature and atmospheric pressure, provide a highly reactive, strongly oxidizing environment capable of decomposing any organic pollutant present in the air itself or in aqueous solutions which are in contact with it. Since some of the major reactive species involved in air non-thermal plasma processes are the same which occur in nature, a brief account is given in the following paragraphs of natural remediation mechanisms of the troposphere. Such natural processes have been studied for a long time and are nowadays rather well understood and characterized. These data are thus most useful in interpreting the results of

experiments in which model organic compounds are subjected to non-thermal plasma induced oxidation.

The first part of this chapter gives a brief account on air and water pollution, on natural remediation mechanism and on current and developing remediation techniques. Next an introduction on plasma is provided leading to a more detailed description of the electric corona and dielectric barrier discharges which were used in this thesis to produce non-thermal plasma (NTP) in air at room temperature and atmospheric pressure. Finally, a brief account is given of the state-of-the art of organic pollutant NTP processing in air and in aqueous solution.

1.1. AIR POLLUTION

Environmental chemistry for the control of air pollution is a field of research that has expanded enormously in recent years and continues to grow with the increasing awareness of the effects due to release of pollutants into the atmosphere. Major research areas regard the study of the complex reactions organic pollutants undergo in the atmosphere and the treatment of harmful emissions from human activities. The atmosphere is a very complex dynamic system, so that the complete understanding of all phenomena occurring inside it is anything but simple: one must take into account both transport phenomena faced by primary pollutants and reactions which they undergo producing secondary pollutants. Moreover, these reactions can occur under homogeneous conditions, i.e. between gaseous reagents in the gas phase, or under heterogeneous conditions (gas-liquid and gas-solid systems, including aerosols).

The major components of the earth atmosphere are molecular nitrogen (about 78%), molecular oxygen (about 20.9%) and argon (about 0.9%). The remaining fraction is due to a huge range of different compounds, the most abundant of which are water (0.02% average on the global scale, but widely changing with season, latitude etc.), CO_2 (377 ppm), noble gases (Ne, He, Kr and Xe, amounting in total to about 25 ppm) and methane (1.7 ppm). Despite their low concentrations many other components are even more important players of the chemistry in the atmosphere: these components differ widely for

their chemical and physical properties and reactivity, and thus life-times and average concentrations. Most important species are the following:

- oxidizing species (O_3, H_2O_2, $^{\bullet}OH$, $^{\bullet}OOH$, $ROO^{\bullet}$, $NO_3^{\bullet}$);
- reducing species (CO, SO_2, H_2S);
- volatile organic compounds, VOCs, (hydrocarbons, halogenated hydrocarbons, organic acids, aldehydes, and many more as detailed in the next section);
- photochemically active species (NO_2, O_3, halogenated hydrocarbons, formaldehyde, …);
- inorganic compounds (HNO_3, H_2SO_4, NH_3, inorganic salts);
- particulate matter.

Primary pollutants are released in the atmosphere as a result of human activities (anthropogenic pollution) and of natural phenomena (biogenic pollution). The major biogenic sources are represented by volcano eruptions, fires, the metabolism of plants and some animals; the sources of anthropogenic pollution are related mainly to the use of fossil fuels and to industrial activities. Major primary pollutants include thus nitrogen and sulphur oxides (referred to respectively as NOx and SOx), carbon oxides (CO_2 and CO), many VOCs (Volatile Organic Compounds), and particulate matter. Secondary pollutants are formed by reactions involving primary pollutants. Examples of secondary pollutants are ground-level ozone and PAN (Peroxy Acetyl Nitrate).

Several studies have shown the correlation between the release of pollutants into the atmosphere and the appearance of major environmental problems:

- Stratospheric ozone depletion, cited above, and formation of Antarctic “ozone holes” by halogenated organic compounds, primarily CFCs, CCl_4 and Halons. Ozone depleting substances are regulated by the Montreal Protocol and subsequent amendments. [1]
- Accumulation of ozone at ground level, due to the action of volatile organic compounds. Ozone, harmful both to human health and to crops and vegetation, can be transported far from the production area also crossing national borders. The VOCs which cause this effect are subjected to the discipline of the Geneva Protocol. [2]
- ‘Photochemical smog’, typical of hot sunny days in high vehicular traffic areas, formed by the combined action of direct sunlight, VOCs and NOx.

- Global greenhouse effect, due to persistent chemical substances which absorb the IR radiation emitted by the Earth: CO_2, H_2O, many VOCs, including methane, CFCs and HFCs, dimethylsulfide.
- Accumulation and persistence: some organic compounds tend to adsorb on suspended particles and are subjected to long-range transport before being removed by precipitations. Then they can re-evaporate and repeat the cycle until they reach their final sink in the cold waters of the polar areas. Examples include the PCBs (Poly Chlorinated Byphenyls, regulated by the Stockholm Convention 2001 [3]), the PCTs (Poly Chlorinated Terphenyls, regulated by the Rotterdam Convention 1998 [4]) phthalic acids and their derivatives.
- Toxic and carcinogenic effects: the most important organic compounds that can potentially cause cancer in humans and are widely distributed in the atmosphere include benzene, polycyclic aromatic hydrocarbons (PAHs), 1,3-butadiene, formaldehyde, polinuclear aromatic hydrocarbons, polychlorodibenzo dioxins (PCDD) and polychlorodibenzo furans (PCDF).

1.1.1 Volatile Organic Compounds (VOCs)

Volatile Organic Compounds (VOCs) are organic compounds that have high enough vapor pressures under normal conditions to significantly vaporize and enter the Earth's atmosphere. Therefore hundreds of compounds fall within the VOC class, including hydrocarbons as well as many oxygen-, halogen-, nitrogen- and sulphur-containing derivatives. VOCs are an important class of air pollutants, generally present in the atmosphere both in urban or industrial sites and in rural areas or remote locations.

The input into the atmosphere of big amounts of VOCs is due both to anthropogenic and biogenic causes. Major anthropogenic sources are emissions of vehicles with combustion engine, fuel storage and distribution, emissions of chemical and petrochemical industries. Biogenic sources of VOCs are emissions of plants and animals, spontaneous forest fires and metabolic processes of anaerobic bacteria and marine organisms.

Relevant data about total emissions of VOCs in Europe community are reported in *Table 1*.

Table 1: VOCs emission in the past decades for the most relevant European countries.

Country	VOCs (kt•year^{-1})			
	1980	1990	2000	2007
France	2734	2414	1658	1199
Germany	3224	3584	1569	1278
Italy	2032	2023	1538	1194
Poland	1036	832	606	596
Romania	829	517	378	330
Spain	1392	1135	1162	921
United Kingdom	2100	2396	1348	942
Sum EU27	**17575**	**16811**	**11060**	**8612**
Belarus	549	497	340	222
Russia	3410	3659	2445	2294
Ukraine	1626	1053	641	408
Sum Non-EU	**6542**	**6263**	**4301**	**3630**
Sum Europe	**24117**	**23074**	**15361**	**12242**

Major natural mechanisms of removal of VOCs from air include physical processes of dry or humid deposition and chemical processes, all of which have in common the generation of VOC-derived organic carbon radicals. Depending on the specific VOC and environmental conditions, radicals can be formed in the troposphere via four major routes: reaction with the hydroxyl radical $^{\bullet}OH$, reaction with the nitrate radical $NO_3^{\bullet}$, photolysis and reaction with ozone O_3. The reaction with $^{\bullet}OH$ radicals, which is the most important one for the majority of VOCs, forms VOC-derived radicals via H atom abstraction or addition to multiple bonds. Once such radicals are produced they are rapidly oxidized via reaction with molecular oxygen, as shown in Scheme 1 for methane, the simplest and most abundant VOC of all.

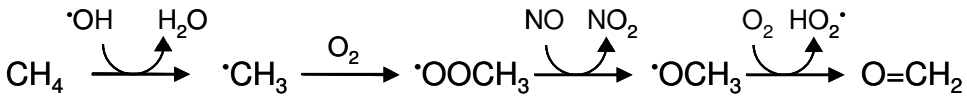

Scheme 1

Formaldehyde is an oxidation intermediate which is in turn oxidized to CO and CO_2, faster than the precursor methane, via photolysis or attack by $^{\bullet}OH$. In general, hydrocarbons and most other VOCs which contain C-H or double or

triple bonds are oxidized in the troposphere all the way to CO_2. The CFCs cited above are among the exceptions which live long-enough to reach the stratosphere where they undergo photolysis.

1.1.2 Technologies for the removal of VOCs from air

The removal of VOCs from emissions from stationary sources can be pursued with different approaches. [5] Abatement techniques can be divided into two categories: those that destroy VOCs and those that recover them.

Destructive technologies include thermal incineration, one of the oldest, which requires that the waste gas temperature is raised to 750 °C and higher; catalytic incineration systems, which use platinum group metals or transition metal oxides to lower the destruction temperature of VOCs; biodegradation which exploits the ability of certain microorganisms to metabolize the VOCs. [6,7]

Among the techniques to recover VOCs the most common one is based on adsorption on a solid substrate, usually charcoal (active carbon). Alternatives include VOC adsorption in a liquid, water or a hydrocarbon, and condensation.

Each of the conventional techniques described above has some serious drawbacks which limit the scope of their applicability. Thermal incineration requires the use of auxiliary fuel when the concentration of VOCs is not high enough to sustain combustion; catalysts are sensible to poisoning by halogenated and sulfurated compounds [8] and can be scratched and dirtied if the process gas contains also solid particles. [9] Bio-filters are useful only for VOCs that have a certain solubility in water and in some cases have poor efficiency. Adsorption based technologies suffer for problems arising by deposition of dirt or clog on filters. [5]

Thus, there is much interest in finding alternative removing technologies applicable where conventional methods are technically or economically unprofitable or unsatisfactory. Among these novel technologies being studied and developed are photo-induced decomposition [10] and abatement processes using thermal or non-thermal plasma.

1.2 WATER POLLUTION

Water is the vital element for the survival of our planet and the proper management of water resources is a major challenge in the new millennium. The steady growth of world population, together with a development model primarily focused on profit with scarce attention to the proper use and management of resources of the planet, has already led to dramatic consequences. About 1 billion people currently can not rely on a continuous supply of potable water and, with the increasing world population (the current number of 6.5 billion people is estimated to grow to 9 billion in 2050), it is expected that within 2025 this number could go up to 3.5 billion. [11-16]

In March 2007 at the European Parliament in Brussels was held the first European Water Conference and March 22 of each year the world celebrates World Water Day, proclaimed for the first time in 1993 by United Nations General Assembly. The main issue of that conference was scarcity of water in the world and the importance of cooperative approach in the management of water resources, both international and local levels. In fact, the amount of water actually used for human use is really negligible and equal to about 0.01% of total on Earth. Like other resources, distribution of water on the planet is unequal and only human activity, whether driven by principles of economic solidarity and intelligent technology can promote equitable access of populations to the resource. The growth in industry and agriculture which have taken place with economic development led to the over-exploitation of water resources. Alongside civil activities which exploiting the overall 10% of available water, agricultural and industrial use more substantial amount of the resource, 70% and 20% respectively.

In this context, the development of new technologies for water decontamination polluted by agricultural and industrial applications is a fundamental part of an integrated approach that will lead to greater availability of water for all. [11-16]

Water contamination may occur by natural or anthropogenic causes. Among the natural causes are the activity of volcanoes, fires and decomposition of biomass. Anthropogenic pollution can be from point or diffuse sources. Examples of point sources are: factories, discharge of waste water, mines and

oil wells. Among the diffuse sources we mention the deposition from acid rains, traffic and agriculture.

1.2.1 Organic pollutants of water

Organic compounds, which are among the most dangerous pollutants, derive from anthropogenic sources such as agriculture (widespread use of pesticides, herbicides and insecticides), incinerators, landfills and industry. In addition to surface water (rivers, lakes), pollution also affects groundwater. In particular, among the most common organic contaminants in water, listed below, the first three classes also exist in groundwater: [17]

- Chlorinated solvents, in particular trichloroethylene ($HClC=CCl_2$), perchloroethylene ($Cl_2C=CCl_2$), chloroform ($CHCl_3$);
- Aromatic hydrocarbons coming from petrol (BTX: benzene, toluene, xylenes) and other petroleum products;
- Methyl-terbutyl ether (MTBE) from petrol;
- Polycyclic aromatic hydrocarbons (benzo-[a]-pyrene, dibenzoanthracene, etc.) from soot, coal and from incomplete combustion of hydrocarbons;
- Fertilizers and pesticides (DDT, Chepone, Lindane, etc.);
- Compounds belonging to different chemical classes used as solvents or precursors in synthetic processes (benzene, nitrobenzene, phenol, p-dichlorobenzene, o-diaminobenzene, acrylonitrile, vinylchloride, urethane), dyes, explosives (TNT, picric acid, nitroaniline) and others.

A very dangerous characteristic for some classes of compounds widely used in the past (PCBs, PBBs, DDTs and others) is persistence due to their low reactivity.

Among the various organic pollutants of water phenol occupies a prominent place. It is a compound used in many industrial processes as an intermediate or feedstock in the production of pesticides, insecticides, wood preservatives, glues, tar, drugs, cosmetics, dyes and polymers. An example of phenol-based polymer is bakelite obtained by reaction of phenol with formaldehyde. For its antiseptic property phenol is used also as a disinfectant.

Given the great variety and use of its derivatives, phenol is not only present in industrial effluents, but also in soil and surface and ground water.

Phenol is toxic by ingestion, inhalation and skin contact, causing digestive disorders, nervous system disorders, headaches, fatigue, and rashes on the skin. Also causes burns if it comes into contact with the throat. The ingestion of 1 gram of phenol is lethal to humans. In water has a negative effect already at ppb concentrations. In concentrations between 0.01 and 0.1 ppb gives a bad smell and taste to water. It is toxic to some aquatic life in concentrations above 50 ppb. It also has a high demand for oxygen, 2.4 mg O_2/mg.

Another serious effect of phenol in water is the ability to combine with chlorine used to disinfect drinking water producing chlorophenols that are compounds even more toxic and difficult to remove.

1.2.2 Technologies for the removal of organic pollutants from water

There are numerous techniques for the removal of organic pollutants from waste water. The methods are divided into destructive (pointing to the elimination of the pollutant) or non-destructive (favour the recovery of pollutant). The destructive methods are often adopted with high concentrations of pollutants, while for low concentrations methods of recovery are usually applied. All methods require pre-treatments such as coarse/fine screening, grit removal, flocculation, sedimentation.

The most important methods for water purification are the following:

- Incineration; useful for small volumes of wastewater with high concentrations of pollutants, It requires substantial investment and energy costs. Another problem is that the combustion of organic waste may generate highly toxic compounds such as dioxins and furans. Therefore, a final combustion chamber for treatment of the exhaust gases must be present before they are released into the atmosphere.
- Air Stripping; it involves the transfer of volatile organic compounds from liquid to gas phase through injection of air. Typical methods use spray atomizers. Alternatively, wastewater is passed through porous materials upstream with respect to the air flow.
- Absorption on Activated Carbon; a separation technology in which the contaminant is absorbed from the aqueous phase on activated carbon by pumping pressurized water to be treated into the column containing the

adsorbent material. Activated charcoal is carbon treated to substantially increase the specific surface area up to 500-1500 m^2/g. The pollutants retained by the adsorbent material are then extracted or destructed by oxidation. This will regenerate the adsorbent. The efficiency of the absorption depends on concentration, polarity and molecular weight of the pollutant, and temperature.

- Chemical Oxidation; is a very effective method for removing organic pollutants, which can meet the strict legal limits on emissions. It can also be an excellent preparation for the next stage of biological oxidation. However, it is convenient only for small concentrations of pollutants and low COD (Chemical Oxygen Demand), otherwise the amount of oxidizer to be used becomes high with the consequent increase in the cost of disposal.
- Electrochemical Oxidation; it is not widely used because of the high operating costs. The conductivity of the solution to be treated has to be sufficiently high, otherwise salts must be added. The process involves three stages: electro-coagulation, electro-flotation, and electro-oxidation.
- Biological Oxidation; it usually takes place through the use of activated sludge. It is applicable only to limited ranges of pollutant concentration (for example, for phenol only up to a maximum concentration of 100 mg/L). It also requires careful adjustment of parameters such as pH, temperature, humidity. It can be implemented under aerobic or anaerobic conditions, the first being generally more effective.
- Photochemical Oxidation; it consists in irradiation of water with UV light beams. Hydroxyl radicals are thus formed by photolysis of water. UV low pressure mercury lamps were used as lamps in the past. However production of UV light is very expensive; absorption occurs only in specific wavelengths, and its reaction with other molecules present in the reaction medium generates many intermediates that slow down the process.
- Plasma treatment; one of the most promising novel AOPs (Advanced Oxidation Process) and one of the objects of this thesis. The plasma can be generated above or within the wastewater.

This thesis reports and discusses the results of studies on non-thermal plasma processes for the oxidation of organic pollutants in air and in water.

1.3 NON-THERMAL PLASMA (NTP) PROCESSES FOR AIR AND WATER PURIFICATION

1.3.1 Plasma definition, classifications and uses

Plasma is an ionized gas, and constitutes a distinct fourth state of matter. “Ionized” means that at least one electron is not bound to an atom or molecule, converting the atom or molecules into positively charged ions. As temperature increases, matter transforms in the sequence: solid, liquid, gas and finally plasma, which justifies the title “fourth state of matter”. More than 99% of matter in the entire universe is in the plasma state.

The term *plasma* was first introduced by Irving Langmuir (1928) because the multi-component, strongly interacting ionized gas reminded him of blood plasma. Langmuir wrote: “Except near the electrodes, where there are sheaths containing very few electrons, the ionized gas contains ions and electrons in about equal numbers so that the resultant space charge is very small. We shall use the name *plasma* to describe this region containing balanced charges of ions and electrons”. [18]

Plasmas occur naturally but can also be effectively produced in laboratory and in industry, and provide opportunities for numerous applications, including thermonuclear synthesis, electronics, lasers, fluorescent lamps, and many others.

Plasma comprises the majority of the universe: the solar corona, solar wind, nebula, and Earth’s ionosphere are all plasmas. The best known natural plasma phenomenon is lightning. The breakthrough experiments with this natural form of plasma were performed a long time ago by Benjamin Franklin.

At altitudes of approximately 100 km, the atmosphere no longer remains non-conducting due to ionization and formation of plasma by solar radiation. As one progresses further into near-space altitudes, the Earth’s magnetic field interacts with charged particles streaming from the sun. These particles are diverted and often become trapped by the Earth’s magnetic field. The trapped particles are most dense near the poles and account for the aurora borealis. Lightning (*Figure 1.1a*) and the aurora borealis (*Figure 1.1b*) are the most common natural plasma observed on Earth.

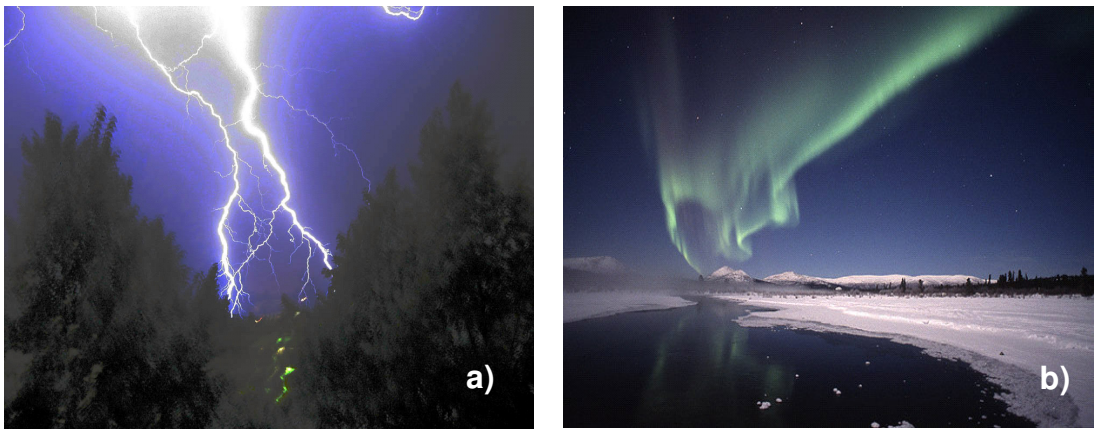

Figure 1.1: Plasma present in nature (left) lightning, (right) aurora borealis.

Man-made plasmas are widely used in practice. Plasma offers three major features that are attractive for applications in chemistry and related disciplines: (1) temperature of at least some plasma components and energy density can significantly exceed those in conventional chemical technologies, (2) plasmas are able to produce very high concentrations of energetic and chemically active species (i.e. electrons, ions, atoms and radicals, excited states, and different wavelength photons), and (3) plasma systems can essentially be far from thermodynamic equilibrium, providing extremely high concentrations of the chemically active species and keeping bulk temperature as low as room temperature. These plasma features bring about significant intensification of traditional chemical processes, essential increases of their efficiency, and often successful stimulation of chemical reactions which are hardly possible in conventional chemistry.

Plasma chemistry today is a rapidly expanding area of science and engineering, with applications which include micro-fabrication in electronics, protective coatings for aircrafts, treatment of polymer fibers and films before painting, medical cauterization and wound treatment, production of ozone, plasma TVs etc..

Natural and man-made plasmas (generated in gas discharge) occur over a wide range of pressures, electron temperatures, and electron densities (*Figure 1.2*). The temperatures of man-made plasmas range from slightly above room temperature to temperatures comparable to the interior of stars, whereas electron densities span over 15 orders of magnitude. Most plasmas of practical significance, have electron temperatures of 1–20 eV, with electron densities in

the range 10^6–10^{18} cm^{-3}. (High temperatures are conventionally expressed in electron volts; 1 eV approximately equals 11,600 K.)

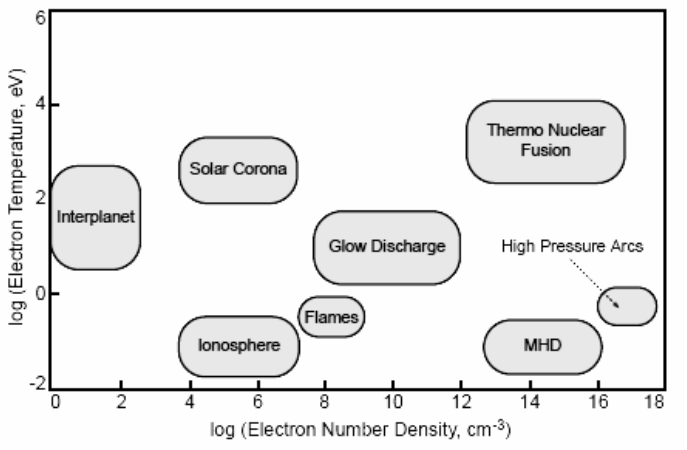

Figure 1.2: Plasma temperatures and densities.

Both natural and man-made plasmas are quasi-neutral, which means that the concentrations of positively charged particles (positive ions) and negatively charged particles (electrons and negative ions) are well balanced. A first distinction of plasmas is based on the ionization degree, i.e. the ratio of density of charged species over that of neutrals. When the ionization degree is close to unity the plasma is called **completely ionized plasma**. Completely ionized plasmas are conventional for thermonuclear plasma systems: tokomaks, stellarators, plasma pinches, focuses, and so on. Completely ionized plasma and related issues of nuclear fusion and space plasmas are the subject of several books, in particular those of Bittencourt [19] and Chen. [20] When the ionization degree is low, the plasma is called **weakly ionized plasma**, which is the main focus of plasma chemistry. The ionization degree in conventional plasma–chemical systems is in the range 10^{-7}–10^{-4}.

As in any gas, temperature in plasma is determined by the average energies of the plasma particles (neutral and charged) and their relevant degrees of freedom (translational, rotational, vibrational, and those related to electronic excitation). Thus, plasmas, as multi-component systems, are able to exhibit multiple temperatures. In electric discharges common for plasma generation in the laboratory, energy from the electric field is first accumulated by the electrons between collisions and, subsequently, is transferred from the electrons to the heavy particles. Electrons receive energy from the electric field during their mean free path and, during the following collision with a heavy particle, lose

only a small portion of that energy (because electrons are much lighter than the heavy particles). That is why the electron temperature in plasma is initially higher than that of heavy particles. Subsequently, collisions of electrons with heavy particles (Joule heating) can equilibrate their temperatures, unless time or energy are not sufficient for the equilibration (such as in coronas and pulsed discharges) or there is an intensive cooling mechanism preventing heating of the entire gas (such as in wall-cooled low-pressure discharges).

The temperature difference between electrons and heavy neutral particles due to Joule heating in the collisional weakly ionized plasma is conventionally proportional to the square of the ratio of the electric field (E) to the pressure (p). Only in the case of small values of E/p do the temperatures of electrons and heavy particles approach each other. Thus, this is a basic requirement for *Local Thermodynamic Equilibrium* (LTE) in plasma. Additionally, LTE conditions require chemical equilibrium as well as restrictions on the gradients. The LTE plasma follows the major laws of equilibrium thermodynamics and can be characterized by a single temperature at each point of space. Ionization and chemical processes in such plasmas are determined by temperature (and only indirectly by the electric fields through Joule heating). The quasi-equilibrium plasma of this kind is usually called thermal plasma. Thermal plasmas in nature can be represented by solar plasma (*Figure 1.3*).

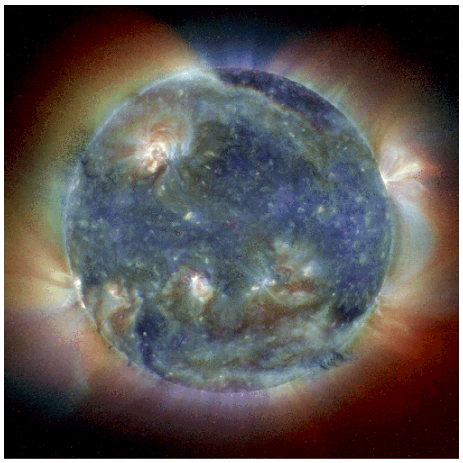

Figure 1.3: Solar plasma.

1.3.2 Non-thermal plasma (NTP)

Numerous plasmas exist very far from the thermodynamic equilibrium and are characterized by multiple different temperatures related to different

plasma particles and different degrees of freedom. It is the electron temperature that often significantly exceeds that of heavy particles ($T_e >> T_0$). Ionization and chemical processes in such non-equilibrium plasmas are directly determined by electron temperature and, therefore, are not so sensitive to thermal processes and temperature of the gas. The non-equilibrium plasma of this kind is usually called non-thermal plasma. An example of non-thermal plasmas in nature is the aurora borealis (*Figure 1.1b*).

Although the relationship between different plasma temperatures in non-thermal plasmas can be quite sophisticated, it can be conventionally presented in the collisional weakly ionized plasmas as $T_e > T_v > T_r \approx T_i \approx T_0$. Electron temperature ($T_e$) is the highest in the system, followed by the temperature of vibrational excitation of molecules (T_v). The lowest temperature is usually shared in plasma by heavy neutrals (T_0, temperature of translational degrees of freedom or simply gas temperature), ions (Ti), as well as rotational degrees of freedom of molecules (T_r). In many non-thermal plasma systems, electron temperature is about 1 eV (about 10,000 K), whereas the gas temperature is close to room temperature.

Non-thermal plasmas can be generated by interaction of a gas at room temperature and atmospheric pressure with a high energy electron beam or by the occurrence of non-thermalizing electrical discharges such as corona discharges and dielectric barrier discharges which are discussed in the following sections.

1.3.2.1 Corona discharges

A corona discharge occurs in a gas between an electrode with a small radius of curvature, called the active electrode, and a large surface external electrode, between which is applied a voltage of some kV. The electrode configurations, which are commonly used to obtain the corona effect, are the wire-to-cylinder, the point-to-plate and the wire-to-plate configurations. The terms DC, AC and Pulsed corona indicate that the discharge is driven respectively by a DC, AC and Pulsed high voltage. The active electrode generates an electric field high enough to produce free charges, while the external electrode also called passive electrode acts primarily as a collector of charges. We talk about positive

or negative corona depending on whether the active electrode is at a voltage higher or lower, respectively, than that of the earth. The electrical discharge is the passage of current through a gas due to production, multiplication and movement of free charges, ions or electrons. Under the action of a sufficiently strong electric field the free electrons in the gas may undergo a significant acceleration and cause ionization of neutral molecules of the gas and, through the production of secondary electrons, lead to electronic avalanches. The free electrons originally present in the gas are formed by cosmic radiation at a rate of about one electron per mm^3 per second. The free charges that are generated by the corona, heading towards the electrode of opposite charge, create local electric fields that modify the applied field. As a consequence of this influence the current intensity does not vary linearly with the applied voltage, but follows a pattern which is determined by the presence of space charges. The electrical discharge depends not only by the electric field applied but also by the nature of the gas used and by its pressure. The ionization of the gas is described quantitatively by the coefficient α, which indicates the number of electrons produced, both by electron ionization of neutral molecules and by electron detachment from anions, when an electron moving toward the electrode of positive potential travels a path of unit length. The energy acquired by electrons not only increases with increasing electric field E but also with their mean free path, which in turn decreases with increasing pressure p. Therefore, the production of ions via electron molecule collisions increases with the term E/p. [21] During the discharge there are also processes that lead to the reduction in the number of electrons, such as recombination and electron attachment. Electron attachment greatly reduces the mobility of charges. The process is described quantitatively by the coefficient η, which represents the average number of attachments of an electron in a path of unit length. The coefficient η depends on the nature of the gas and on the energy of the electrons. Electron attachment is very important in air discharges for the presence of oxygen, due to its high electronegativity. The corona discharge has the characteristics of a Townsend's discharge, since the applied voltage is high enough to produce impact ionization and extraction of electrons from the cathode, which trigger a process which is capable of self-sustaining. [21]

The corona reactor used in this thesis has a wire-to-cylinder configuration, for which the mean electric field is given by:

$$\mathbf{E} = \frac{\mathbf{V}}{\mathbf{R_1} \cdot \mathbf{ln}\left(\frac{\mathbf{R_2}}{\mathbf{R_1}}\right)} \quad (1)$$

where:

- V is the applied voltage between the two electrodes;
- R_1 is the radius of the active electrode;
- R_2 is the radius of the counter electrode connected to ground.

The area surrounding the active electrode is called ionization region, as the ionization process prevails over electric attachment, while the remaining space is the drift region, where electronic attachment prevail and transport of charged species occurs.

In negative DC corona, the space charge does not change appreciably the original electric field in the ionization region, where mostly radicals and positive ions are concentrated. At a distance of a few millimetres from the central wire there is the boundary between the ionization and the drift region. In the drift region electron attachment occurs, negative ions form and negatively charged species move towards the ground electrode. The discharge current is influenced by the mobility of charged species in the drift region and is lowered if a gas that favors electron attachment is used, since it reduces the number of free electrons.

In positive DC corona, the ionization region has a high density of electrons that move toward the positive electrode and dissociative attachment prevails, leading to the formation, for example, of O^- ions; the drift region is dominated by the transport of positive ions and secondary electrons will be produced as a result of extraction processes from cathode, photoemission and photo-ionization; following electron attachment negatively charged species such as O_2^- and O_3^- are produced, which together with the free electrons move towards the active electrode. [21]

The two most important forms of discharge are the so-called *glow corona* (glow discharge) and *streamer corona* (channel or filamentary discharge). The establishment of one of these two discharge regimes depends essentially on the distance between the electrodes and on the evolution in time of the applied voltage.

The streamers are filamentary discharge channels which, thanks to the electric field generated by their electric charge, extend where the value of the

geometrical electric field is lower than required for ionization. The development of streamers is different depending on whether the active electrode is positively or negatively charged.

In the case of positive polarity streamers begin to develop when the voltage is high enough for free electrons to acquire sufficient energy to ionize neutral molecules and produce an electron avalanche. Given the large difference in mobility, positive ions can be considered stationary compared to the electrons in motion. The avalanche then spreads like a cloud of electrons, rapidly increasing in number, which moves towards the anode, leaving behind a positive space charge. The geometrical electric field E_g, due to electrodes geometry and to the applied voltage, is increased by the field E_{cs}, produced by spatial charge. The ionization activity at the avalanche head is accompanied by emission of photons consequent production of photo-electrons. These photo-electrons under the action of the resulting field give rise to secondary avalanches that can neutralize, with their electrons, the positive spatial charge. Positive ions, left behind by secondary avalanches, create a spatial charge more advanced toward the cathode. For the streamer to form, it is necessary that the first avalanche reaches a critical size, due to a number of charges sufficient to create an electric field due to spatial charge which, added to the geometrical field, is capable of generating a further electron avalanche.

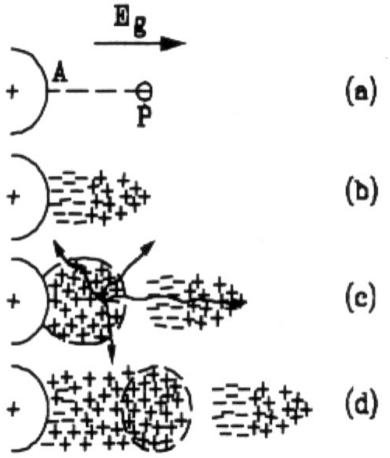

Figure 1.4: Schematic representation of positive streamer formation.

A schematic representation of the formation and propagation of a positive streamer is shown in *Figure 1.4*. The development of a positive streamer only roughly follows the lines of the applied field due to the major effect due to spatial charges present at its head. In case two secondary avalanches of

sufficient size come simultaneously from different directions at the head of the streamer, branches of the filament will occur. As the phenomenon repeats itself, the streamer developed into a highly branched structure.

In the case of negative polarity there is a discharge mechanism which is somewhat different from that for positive polarity. This mechanism is illustrated in *Figure 1.5*. When the primary avalanche, created by a free electron near the cathode, has reached the appropriate size, the electric field is greatly increased both in the vicinity of its tail and of its head. From point A in *Figure 1.5* a positive streamer is developed (reverse streamer) towards the cathode, while a photo-electron produced at a point B, under the action of the resulting field, generates a secondary avalanche. When the secondary avalanche has developed sufficiently, an opposite streamer moves from its tail to the head of the primary avalanche. The phenomenon is repeated and the negative filament moves towards the anode. The streamer propagates in areas where the applied field is reduced, leaving behind a partially ionized channel that has an excess of negative charges inside. Due to photo-ionization and bombardment by positive ions (accelerated by a strongly increasing field) there is a continuous extraction of electrons from the electrode. The neutralization of positive ions at the cathode and the extraction of new electrons determine the negative charge excess of the streamer.

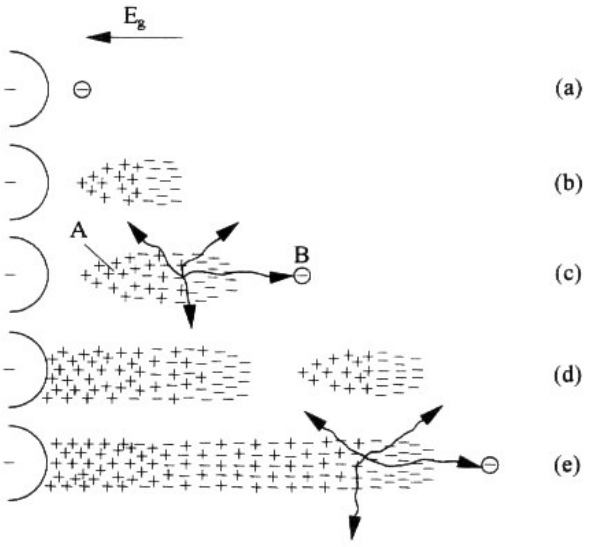

Figure 1.5: Schematic representation of negative streamer formation.

The photo-electrons that give rise to secondary avalanches are accelerated in rapidly decreasing fields due to the rapid decrease of the field component

generated by spatial charge. The applied field then, in this case, has a more pronounced influence, so the negative streamers have a development closer to the lines of the applied field and fewer branches. Moreover, they have a more limited extension than the positive streamers. It should also be noted that electron attachment reduces the mobility of negative charges where the field is lower, which corresponds to the final stages of the development of the avalanche. [22]

A *glow corona* is established when the distance between the electrodes is short enough so that the electric field is sufficiently high for the occurrence of ionization processes in a uniform manner in space and time. A stable corona discharge is obtained, consisting of a series of small electron avalanches that surround the active electrode. Visually, the glow corona appears as a faintly luminous sheath surrounding the electrode, whose intensity increases with increasing applied voltage. In the case of positive glow corona, the positive spatial charge is distributed uniformly around the positive electrode, with an effect comparable to an increase in the diameter of the electrode. The decrease of the electric field thus produced inhibits ionization avalanches induced by photo-electrons present beyond the positive space charge region. The result is a very stable discharge in which the ionization region is restricted around the active electrode. With this corona regime the discharge current remains constant in time. In contrast, for streamer corona, the discharge current is formed by a DC component with overimposed pulses.

1.3.2.2 Dielectric Barrier Discharges (DBD)

Dielectric Barrier Discharges, or simply Barrier Discharges, have been known for more than a century. The first experimental investigations were reported by Siemens in 1857 [23] and concerned the generation of ozone. This was achieved by subjecting a flow of oxygen or air to the influence of a dielectric barrier discharge (DBD) maintained in a narrow annular volume between two coaxial glass tubes by an alternating electric field of sufficient amplitude. The novel feature of this discharge apparatus was that the electrodes were positioned outside the discharge chamber and were not in contact with the plasma. A few years after Siemens' original publication, Andrews and Tait, [24] in 1860, proposed the name "silent discharge", which

still is frequently used in the English, German, and French scientific literature. Ozone and nitrogen oxide formation in DBDs became an important research issue for many decades. [25] In 1943 Manley [26] proposed a method for determining the dissipated power in DBDs by using closed voltage/charge Lissajous figures and derived an equation which became known as the power formula for Ozonizers. Occasionally, also the term corona discharge is used in connection with DBDs, although most authors prefer to use this term only for discharges between bare metal electrodes without any interposed dielectric. Both discharge types have common features: the generation of “cold” non-equilibrium plasmas at atmospheric pressure and the strong influence of the local field distortions caused by space charge accumulation.

Typical planar DBD configurations are sketched in *Figure 1.6*. As a consequence of the presence of at least one dielectric barrier these discharges require alternating voltages for their operation. The dielectric, being an insulator, cannot pass a DC current. Its dielectric constant and thickness, in combination with the time derivative of the applied voltage, dU/dt, determine the amount of displacement current that can be passed through the dielectric(s). To transport current (other than capacitive) in the discharge gap the electric field has to be high enough to cause breakdown in the gas. In most applications the dielectric limits the average current density in the gas space. Preferred materials for the dielectric barrier are glass or silica glass, in special cases also ceramic materials, and thin enamel or polymer layers.

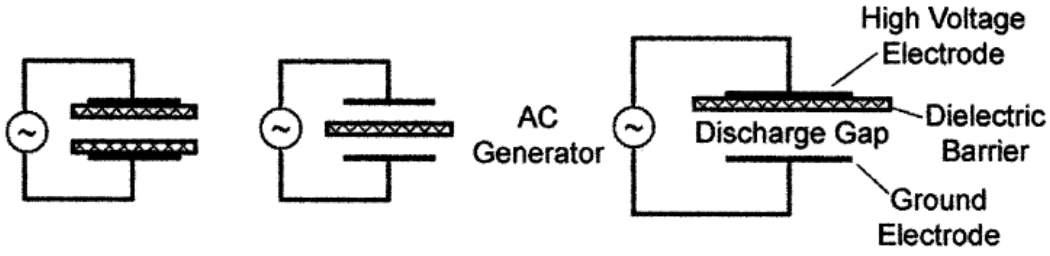

Figure 1.6: Basic dielectric barrier discharge configurations.

Besides the planar configuration showed above also annular discharge gaps between cylindrical electrodes and dielectrics are used in many technical applications. The discharge gap itself has a typical width ranging from less than 0.1 mm to several centimetres, depending on the application. To initiate a discharge in such a discharge gap filled with a gas at about atmospheric

pressure, voltages in the range of a few hundred V to several kV are required. The gas can either flow through the DBD (ozone generation, surface treatment, pollution control) or it can be re-circulated (CO_2 lasers) or fully encapsulated (excimer lamps, excimer based fluorescent lamps and light panels, plasma display panels).

At atmospheric pressure electrical breakdown in a large number of microdischarges is the normal situation for most gases in DBD configurations. Under certain circumstances also apparently homogeneous, diffuse discharges can be obtained, [27–29] or also regularly spaced glow discharge patterns. [30–33] The most common appearance of dielectric barrier discharge at elevated pressure is that shown in *Figure 1.7*. It is characterized by a large number of short-lived microdischarges. Each microdischarge has an almost cylindrical plasma channel, typically of about 100 μm of radius, and spreads into a larger surface discharge at the dielectric surface(s). *Figure 1.7* shows a schematic diagram of a single microdischarge and a simple equivalent circuit.

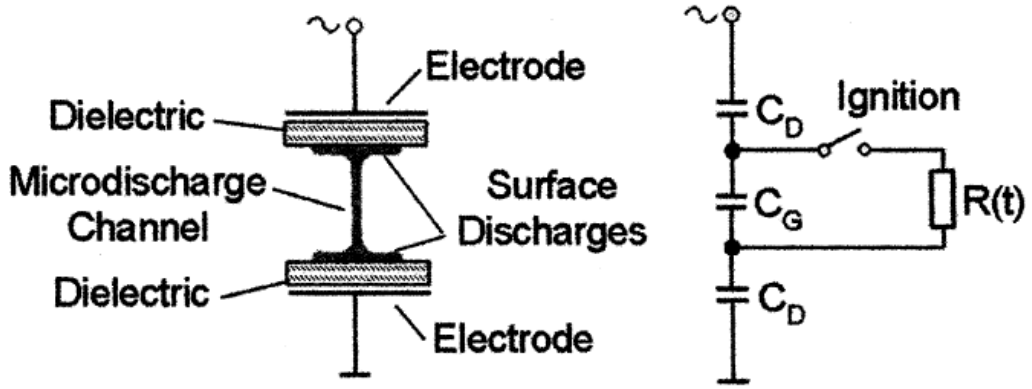

Figure 1.7: Sketch of a microdischarge and a simple equivalent circuit.

By applying an electric field larger than the breakdown field local breakdown in the gap is initiated. In the equivalent circuit this is symbolized by closing a switch and forcing some of the current through the plasma filament, whose resistance R(t) rapidly changes with time. In reality, growing electron avalanches quickly produce such a high space charge that self-propagating streamers are formed. [33-35] A space-charge induced field enhancement at the streamer head, moving much faster than the electron drift velocity, is reflected at the anode and travels back to the cathode where, within a fraction of 1 ns, an extremely thin cathode fall layer is formed. At this moment the current flow through the conductive channel bridging the electrode gap peaks.

Subsequently charge accumulation at the dielectric surface(s) reduces the local electric field to such an extent that ionization stops within a few nanoseconds and the microdischarge is choked.

Research on DBDs has focused on tailoring microdischarge characteristics by making use of special gas properties, adjusting pressure and temperature, and optimizing the electrode geometry as well as the properties of the dielectric(s).

The total charge Q transferred in a microdischarge depends on the gas properties and can be influenced by the gap spacing and by the properties of the dielectric. Q is proportional to the width of the discharge gap d, and to the quantity ε/g (ε: relative permittivity, g: thickness of dielectric). The latter relation was experimentally checked to hold up to extreme e-values of about 1000. [36,37] Contrary to what one might expect, Q does not depend on gas density. [34]

Recent advances in spectroscopic measuring techniques and in laser diagnostics provided important additional information by in situ determinations of electron, atom, free radicals and excited species concentrations in individual microdischarges. [38-40] The gas temperature inside microdischarge filaments was derived from rotational band structures [41-43] as it was done for corona discharges.

The early phases of microdischarge formation are characterized by electron multiplication, by excitation and dissociation processes initiated by energetic electrons, and by ionization processes and space charge accumulation. The ionic and excited atomic and molecular species initiate chemical reactions that finally result in the synthesis of a desired species (e.g. ozone, excimers) or the destruction of pollutants (e.g. VOCs, nerve gases, odours, NH_3, H_2S, NOx, SO_2, etc.). If the major reaction paths are dominated by charged particle reactions the term plasma chemistry adequately describes the situation. This is the case in many low-pressure discharges. In the majority of DBD applications, however, most charged particles disappear before any major changes occur. In this case it is most appropriate to speak of a free-radical chemistry primarily involving neutral species like atoms, molecular fragments and excited molecules. In any case, discharge activity and energy dissipation occur mainly within the small volume fraction occupied by microdischarges. The generated active species set the initial conditions for the ensuing chemical reactions. An adequate picture of

the physical processes during breakdown and microdischarge formation is prerequisite for a detailed understanding of DBD chemical reactor. Each individual microdischarge can be regarded as a miniature plasma chemical reactor. Scaling up or increasing the power density just means that more microdischarges are initiated per unit of time and per unit of electrode area. In principle, individual microdischarge properties are not altered during up-scaling.

1.3.4 Chemical processes in NTP plasma

The energetic electrons produced in non-thermal plasma give up their energy through inelastic collisions with the molecules in the gas, giving rise to several reactions which produce charged species, excited molecules and neutrals (atoms and radicals). The probability for any such species to form is related to the amount of energy that is released in the collision and therefore the plasma capacity to provide enough energy to induce that specific reaction to occur. The energy barriers to be overcome are: ionization energy (associated with the formation of A^+ from A neutral species), electronic excitation energy (associated with the occurrence of excited species A*), and vibrational and rotational excitation energy of molecular and atomic species that give rise to metastable states. The major reactions that may occur between the electrons of the plasma and the species present in the gaseous medium are the following: [44]

- Ionization of atomic, X, or of molecular, XY, species, with consequent formation of secondary free electrons

$$X + e^- \longrightarrow X^{+\bullet} + 2\ e^-$$

$$XY + e^- \longrightarrow XY^{+\bullet} + 2\ e^-$$

Example: $O_2 + e^- \longrightarrow O_2^{+\bullet} + 2\ e^-$ (E_a = 12.5 eV)

$N_2 + e^- \longrightarrow N_2^{+\bullet} + 2\ e^-$ (E_a = 12.5 eV)

Ionization can be associated with fragmentation resulting in the formation of free radicals:

$$XY^{+\bullet} \longrightarrow X^{\bullet} + Y^+$$

- Electron attachment:

$$X + e^- \longrightarrow X^-$$

$$XY + e^- \longrightarrow XY^-$$

Electron attachment can cause dissociation into ionic and radical fragments (dissociative electron attachment)

$$XY + e^- \longrightarrow X^\bullet + Y^-$$

Example: $O_2 + e^- \longrightarrow O^{-\bullet} + O$ (E_a = 3.5 eV)

- Excitation of atomic and molecular species:

$$X + e^- \longrightarrow X^* + e^-$$

$$XY + e^- \longrightarrow XY^* + e^-$$

Example: $O_2 + e^- \longrightarrow O_2^* + e^-$ (E_a = 1 eV)

which can be followed by dissociation into radical or atomic species

$$XY^* + e^- \longrightarrow X^\bullet + Y^\bullet + e^-$$

- Simple dissociation:

$$XY + e^- \longrightarrow X^\bullet + Y^\bullet + e^-$$

Example: $N_2 + e^- \longrightarrow 2\,N^\bullet + e^-$ (E_a = 9 eV)

- Recombination:

$$XY^{+\bullet} + e^- \longrightarrow XY$$

Corona discharges in air produce mainly the following species:

- The ions $O_2^{+\bullet}$, $N_2^{+\bullet}$, NO^+, $O^{-\bullet}$, $O_2^{-\bullet}$, $O_3^{-\bullet}$;
- The atomic species O and the $^\bullet OH$ radical;
- Excited species for atomic and molecular oxygen and nitrogen;
- The neutral species O_3 and NO.

in the presence of water molecules hydroxyl radicals also form via different possible reaction channels including an ionic path: [45, 46]

$$O_2^{+\bullet} + H_2O + N_2 \longrightarrow O_2(H_2O)^{+\bullet} + N_2$$

$$O_2(H_2O)^{+\bullet} + H_2O \longrightarrow H_3O^+ + O_2 + {}^\bullet OH$$

$$O_2(H_2O)^{+\bullet} + 2\,H_2O \longrightarrow H_3O^+ + H_2O + O_2 + {}^\bullet OH$$

and reaction of excited species of atomic oxygen and nitrogen with water: [47]

$$O(^1D) + H_2O \longrightarrow 2\ ^{\bullet}OH$$

$$N(^2D) + H_2O \longrightarrow {}^{\bullet}OH + NH$$

Considering the complexity of non-thermal plasma, due to the presence of so many different reactive species, charged and neutral which can engage into many different reactions, the characterization of the mechanisms involved in VOCs oxidation in these systems is extremely difficult. Based on the experimental results and the support by theoretical models some general mechanisms of VOCs decomposition have been proposed, which may be more or less efficient depending on the VOC type and on the adopted experimental conditions. Below are summarized some important reactions of ions and radicals produced in air discharges which can be initiation steps in VOC (here indicated as R-Y) oxidation: [44]

- Cation-induced decomposition by charge exchange:

$$X^+ + R\text{-}Y \longrightarrow R\text{-}Y^{+\bullet} + X \qquad X^{+\bullet}\ (O_2^{+\bullet},\ N_2^{+\bullet},\ \text{etc.})$$

The species $R\text{-}Y^{+\bullet}$ may dissociate through elimination of radicals:

$$R\text{-}Y^{+\bullet} \longrightarrow R^{\bullet} + Y^+$$

- Dissociative electronation, consequent to electron attachment or charge exchange with anions:

$$e^- + R\text{-}Y \longrightarrow R^{\bullet} + Y^-$$

$$X^{-\bullet} + R\text{-}Y \longrightarrow R^{\bullet} + Y^- + X \qquad X^{\bullet-}\ (O_2^{\bullet-},\ O_3^{\bullet-},\ \text{etc.})$$

- Decomposition from an electronic excited state:

$$R\text{-}Y^* \longrightarrow R^{\bullet} + Y^{\bullet}$$

For example: $Cl_2C{=}CHCl^* \longrightarrow Cl^{\bullet} + ClC^{\bullet}{=}CHCl$

- Radical induced decomposition (OH, Cl, etc…) via addition, in the case of unsaturated compounds, or H extraction:

Examples: $Cl_2C{=}CHCl + Cl^{\bullet} \longrightarrow Cl_2C^{\bullet}{-}CHCl_2$

$$CH_3CH_2CH_2CH_3 + OH \longrightarrow CH_3C^{\bullet}HCH_2CH_3 + H_2O$$

It is generally considered that the hydroxyl radicals, formed from water as described above, play a major role in the degradation of VOCs.

The reaction path for a specific VOC depends on the concentration of various radicals and ions produced in the plasma, and on the chemical characteristics of the VOC which determine the thermodynamics and the kinetics of the various possible reactions. In particular, the charge exchange reactions induced by cations are important for those VOCs which have ionization energies lower than O_2 and N_2. Charge exchange reactions involving anions are important for those compounds with high electron affinity. Since VOCs generally have lower ionization energies and larger cross sections for electron attachment than the molecules of air, the energy of the plasma is very efficiently channelled into VOC decomposition even though VOC is present in parts per million concentrations.

As mentioned earlier, the decomposition of organic compounds in non-thermal plasma can be usefully compared with the reactions which occur in the troposphere. In non-thermal plasma, however, the concentration of electrons and ions is much greater than in the troposphere and these species, therefore, play an important role in the initial attack on VOC molecules within the plasma. The four processes mentioned above as initiation stage of the decomposition of organic compounds in non-thermal plasma have in common the formation of VOC-derived organic radicals, $R^{\bullet}$; in the presence of oxygen these radicals undergo the same reactions involved in tropospheric degradations of VOCs, summarized in the following equations: [48]

$$R^{\bullet} + O_2 \longrightarrow ROO^{\bullet}$$

$$ROO^{\bullet} + NO \longrightarrow RO^{\bullet} + NO_2$$

$$2\ ROO^{\bullet} \longrightarrow 2\ RO^{\bullet} + O_2$$

$$RO^{\bullet} \longrightarrow \text{carbonylic compound} + \text{radical } (Cl^{\bullet}, R'^{\bullet}, \text{etc.})$$

The formation of alcohols occurs mainly via the following reaction: [48, 49]

$$2\ ROO^{\bullet} \longrightarrow ROH + R(\text{-}H)O + O_2$$

The final products of VOCs decomposition in non-thermal plasma are CO, CO_2, and H_2O, which are generally detected with spectroscopic methods: in the case of chlorinated compounds Cl_2 and HCl are also formed. [44] There is also evidence for the formation of aerosols in these systems. [21] It should be

emphasized that the available data on products distribution and especially on mass balance are still very deficient and incomplete.

1.3.4 Ozone generation in non-thermal plasma

Ozone production in corona discharges, in air or oxygen, can be very efficient and in fact the process has been exploited to realize Ozonizers which have various industrial applications.

The proposed mechanism for ozone formation requires the interaction between high-energy free electrons and oxygen molecules:

$$O_2 + e^- \longrightarrow 2\,O + e^-$$

The atomic oxygen thus formed is combined with molecular oxygen by the reaction:

$$O_2 + O + M \longrightarrow O_3 + M$$

where M is a mediator, such as N_2, necessary to dissipate the energy of the reaction. [50, 51]

The amount of ozone produced increases or decreases depending on the concentration of M. In particular, a concentration of nitrogen in oxygen from 0 to 7 % results in a significant increase in the production of ozone. Above 7 %, however, the ozone concentration decreases markedly due to the formation in the discharge of nitrogen oxides, which lead to the destruction of ozone: [50, 52]

$$NO + O_3 \longrightarrow NO_2 + O_2$$

$$NO_2 + O_3 \longrightarrow NO_3 + O_2$$

Moreover, the following reaction:

$$NO + O + M \longrightarrow NO_2 + M$$

is in competition with ozone formation.

Many of the findings published in the literature of the field indicate a greater production of ozone in negative polarity discharge compared to positive polarity. With wire-to-cylinder and wire-to-plate geometry concentrations of ozone produced in negative polarity were from five to nine times higher than in positive polarity. This phenomenon is explained assuming that with negative polarity a

greater number of free electrons are present and/or that electrons have higher energy than with positive polarity.

Since the production of ozone is initiated by dissociative electron impact, it is not surprising that some studies have shown that the amount of ozone produced is directly proportional to the discharge current (when all the other parameters are kept constant). [51]

1.3.5 State-of-the art of NTP processing of VOCs in air

Among the novel technologies being developed for air purification, those based on NTPs produced by electric discharges at atmospheric pressure are particularly advantageous especially for the treatment of highly diluted pollutants. [21, 53-60] NTPs provide an ideal solution for the treatment of any VOC and, particularly for specific applications such as the degradation of highly inert and persistent compounds, such as freons, and of malodorant compounds which often cause disturbance at the ppb level. Ethyl mercaptan, for example, is perceived by humans at the ppb level, and for this reason is added to methane to make gas leaks easily detectable. The literature reports a few recent works dealing with cold plasma treatment of malodorant chemicals in air at atmospheric pressure. [61-64]

As is often the case, development of technologies is more advanced than is the characterization of the chemical reactions involved in the applied process. [65-70] The desired goals of high conversion and high product selectivity (exhaustive oxidation of VOC to CO_2) are usually not easily achieved in non thermal plasma treatments. [21, 53-60] Moreover, undesired sideproducts are also formed (NOx, O_3 and aerosols). A novel approach to overcome such limits is based on the combination of plasma catalysis with heterogeneous chemical catalysis. Such hybrid processes can be performed in a two-stage reactor, with the catalyst located in a post plasma reactor (*PPC, post plasma catalysis*), or in a single-stage reactor, with the catalyst placed within the space occupied by the plasma (*IPC, in plasma catalysis*). Both configurations have been adopted with promising results and are presently investigated and developed to enhance the synergy between plasma and chemical catalysis and, in particular, to understand its origin and nature. Recent papers describe in detail the characteristic features of the two approaches and the advantages of each. [71]

Specific background and discussion relevant to the research performed during my doctoral studies is found in *Sections 4.1–4.7* of *Chapter 4* of this thesis.

1.3.6 State-of-the art of NTP processing of organic pollutants in water

Over the last decade, interest in the development of Advanced Oxidation Technologies (AOTs) for the treatment of hazardous chemical wastes has grown enormously.

High-voltage electrical discharges directly in water (electro-hydraulic discharge) or in the gas phase above the water (non-thermal plasma) have been demonstrated to produce hydrogen peroxide, [72-74] molecular oxygen and hydrogen, [75] and other radicals [74,76,77] and with the addition of air or oxygen at the high voltage electrode, ozone. [78,79] These reactive species have been shown to rapidly and efficiently degrade many organic compounds, including phenols, [80-82] polychlorinated byphenyl, [83] perchloroethylene and pentachlorophenol, [84,85] and many others. In addition the oxidation of several inorganic ions in water has been studied with the various electrical discharge processes. [86,87]

In summary, the potential advantages of electrical discharge process (e.g., electrical discharge in water, in air above water, and simultaneously in water and gas) include the following:

- Direct *in situ* production of multiple types of highly reactive chemical species, including molecule and radicals, thereby eliminating the need for externally supplied sources of hydrogen peroxide, ozone, and other highly reactive compounds;
- Enhancement and facilitation of gas phase reactions through (a) quenching of gas phase reaction products by transfer into liquid and (b) reactions of species formed in the liquid phase and subsequently transferred to the gas;
- Enhancement and facilitation of liquid-phase reactions through (a) absorption of reactive species from the gas and (b) transfer of volatile liquid-phase reaction products into the gas phase;

- Simultaneous facilitation and enhancement of gas- and liquid-phase reactions;
- Control of relative amounts of reactive species through the adjustment of applied electric fields and gas/liquid flow rates;
- Enhancement of gas/liquid mass-transfer rates through (a) electro-hydrodynamic flow at the gas/liquid interface and (b) reduction of bubble size when gas is injected through the high-voltage discharge electrode;
- Production of UV light, shock waves, and putative supercritical conditions localized in the non-homogeneous discharge channel of the discharge;
- Catalytic effects in the case of combined pulsed electrical discharge and various additive particles such as activated carbon, zeolites, photocatalysts, transition metals, and other heterogeneous catalysts, including those coated on the electrodes.

Specific background and discussion relevant to the research performed during my doctoral studies is found in *Sections 4.8–4.10* of *Chapter 4* of this thesis.

1.4 REFERENCES

[1] *The Montreal Protocol on Substances that Deplete the Ozone Layer* 1989 – website: http://ozone.unep.org/Publications/MP_Handbook/Section_1.1_The_Montreal_Protocol;

[2] *Protocol for the Prohibition of the Use in War of Asphyxiating, Poisonous or other Gases, and of Bacteriological Methods and Warfare* 1925 – website: http://www.brad.ac.uk/acad/sbtwc/keytext/genprot.htm;

[3] *Stockholm Convention on Persistent Organic Pollutants* 2001 – website: http://chm.pops.int;

[4] *Rotterdam Convention on the Prior Informed Consent Procedure for Certain Hazardous Chemicals and Pesticides in International Trade* **1988**, http://www.pic.int

[5] Barbour, A.K.; Burdett, N.A.; Cairns, J.; Derwent, R. in *Volatile Organic Compounds in the Atmosphere*, Hester, R.E.; Harrison, R.M., Eds.; Environmental Science and technology n° 4, The Royal Society of Chemistry: London, 1995;

[6] McCarty, P.L. *Science* **1997**, 276, 1521-1522;

[7] Maymò-Gatell, X; Chien, Y.; Gosset, J.M.; Zinder, S.H.; *Science* **1997**, 276 1568-1571;

[8] Nunez, C.M.; Ramsey, G.H.; Ponder, W.H.; Abbott, J.H.; Hamel, L.E.; Kariher, P.H. *J. Air Waste Manag. Assoc.* **1993**, 43, 242-249;

[9] Barresi, A.; Mazzarino, I., Ruggeri, B. *La Chimica e l'Industria*, **1989**, 71, 64-75;

[10] Bolton, J.R.; Safarzadeh-Amiri, A.; Buchley, J.A.; Notartonzo, R.; Cater, S. presented on 87th Annual Meeting and Exhibition, Air and Waste Management Association Cincinnati, OH, June 1994;
[11] IGBP, 2001 - Global Change and the Earth System: a Planet under stress - IGBP Science n.4;
[12] UNEP, 2002 - Global Environment Outlook 3 – Earth scan;
[13] Earth Policy Institute - website http://www.earth-policy.org;
[14] World Watch Institute - website http://www.worldwtach.org;
[15] World Resources Institute - website http://www.wri.org;
[16] European Pollutant Emission Register – website http://eper.eea.europa.eu/;
[17] Baird C.; Cann M. *Chimica Ambientale*, Zanichelli, 2nd Ed., 2006;
[18] Langmuir, I. *Proc. Nat. Acad. Sci. U.S.* **1928**, 14, 628;
[19] Bittencourt, J.A. *Fundamentals of Plasma Physics*, Springer, New York: Heidelberg, 2004;
[20] Chen, F.F. *Introduction to Plasma Physics and Controlled Fusion: Plasma Physics*, 2nd Edition, Plenum Press: New York, 2006;
[21] Van Veldhuizen, E.M. *Electrical Discharges for Environmental Purposes*, Nova Science Publisher, New York, 2000;
[22] Goldman, M.; Goldman, A. *Corona Discharge*, Gaseous Electronic, Academic Press Inc., 1978, vol. 1, 219-290;
[23] Siemens, W. *Poggendorff's Ann. Phys. Chem.* **1857**, 178, 66-122;
[24] Andrews, T.; Tait, P.G. *Phil. Trans. R. Soc. Lon.* **1860**, 150, 113-131;
[25] Hautefeuille, P.; Chappuis, J. *Compt. Rend. Acad. Scé.* **1881**, 92, 80 – Warburg, E.; Leithäuser, G. *Ann. Physik* **1909**, 333, 313-325;
[26] Manley, T.C. *J. Electrochem. Soc.* **1943**, 84, 83-96;
[27] Donohoe, K.G.; Wydeven, T *J. Appl. Polymer Sci.* **1979**, 23, 2591-2601;
[28] Kanazawa, S.; Kogoma, M.; Moriwaki, T; Okazaki, S. *J. Phys. D: Appl. Phys.* **1988**, 21, 838-840;
[29] Massines, F.; Rabehi, F.; Decomps, P.; Gadri, R.B.; Ségur, P.; Mayoux, C. *J. Appl. Phys.* **1998**, 83, 2950-2957;
[30] Boyers, D.G.; Tiller, W.A. *Appl. Phys. Lett.* **1982**, 41, 28-30;
[31] Ammelt, E.; Schweng, D.; Purwins, H.-G. *Phys. Lett. A* **1993**, 179, 348-354;
[32] Breazeal, W.; Flynn, K.M.; Gwinn, E.G. *Phys. Rev. E* **1995**, 52, 1503-1515;
[33] Kogelschatz, U. *IEEE Trans. Plasma Sci.* **2002**, 30, 1400-1408;
[34] Eliasson, B.; Kogelschatz, U. *IEEE Trans. Plasma Sci.* **1991**, 19, 309-323;
[35] Steinle, G.; Neundorf, D.; Hiller, W.; Pietralla, M. *J. Phys. D: Appl. Phys.* **1999,** 32, 1350-1356;
[36] Dřimal, J.; Gibalov, V.I.; Samoilovich, V.G. *Czech. J. Phys.* **1987**, B37, 1248-1255;
[37] Gibalov, V.I.; Dřimal, J.; Wronski, M.; Samoilovich, V.G. *Contrib. Plasma Phys.* **1991**, 31, 89-99;
[38] Lukas, C.; Spaan, M.; Schulz-von der Gathen, V.; Thomson, M.; Wegst, R.; Döbele, H.F.; Neiger, M. *Plasma Sources Sci. Technol.* **2001**, 10, 445-450;

[39] Kozlov, K.V.; Wagner, H.-E.; Brandenburg, R.; Michel, P. *J. Phys. D: Appl. Phys.* **2001**, 34, 3164-3176;

[40] Kunze, K.; Miclea, M.; Musa, G.; Franzke, J.; Vadla, C; Niemax, K. *Spectrochimica Acta B* **2002**, 57, 137-146;

[41] Motret, O.; Hilbert, C.; Pellerin, S.; Pouvesle, J.M. *J. Phys. D: Appl. Phys.* **2000**, 33, 1493-1498;

[42] Spaan, M.; Leistikow, J.; Schulz-von der Gathen, V.; Döbele, H.F. *Plasma Sources Sci. Technol.* **2000**, 9, 146-151;

[43] Bibinov, N.K.; Fateev, A.A.; Wiesemann, K. *Plasma Sources Sci. Technol.* **2001**, 10, 579-588;

[44] Fridman, A. *Plasma Chemistry*, Cambridge University Press, New York, 2008;

[45] Sieck, L.W.; Herron, J.T.; Green, D.S. *Plasma Chem. Plasma Process.* **2000**, 20, 235-357;

[46] Ketkar, S.N.; Dulak, J.G.; Dheandhanoo, S.; Fite, W.L. *Anal. Chim. Acta* **1991**, 245, 267-270;

[47] Herron, J.T.; Green, D.S. *Plasma Chem. Plasma Process.* **2001**, 21, 441-457;

[48] Seinfeld, J.H.; Pandis, S.N. Atmospheric Chemistry and Physics. From Air Pollution to Climate Change, John Wiley & sons, inc. 1998;

[49] Kudryashov, S.V.; Shchegoleva, G.S.; Sirotkina, E.E.; Ryabov, A.Yu. High Ene. Chem. 2000, 34, 112-115;

[50] *Ullmann's Enciclopedia of Industrial Chemistry, 5th Edition*, Elvers, B.; Hawkins, S.; Schulz, G., Wiley-VCH, **1991**, vol. A18, 349-357;

[51] Boelter, K.J.; Davidson, J.H. *Aero. Sci. Technol.* **1997**, 27, 689-708;

[52] Mason, N.J.; Skalny, J.D.; Hadj-Ziane, S. Czech. J. Phys. 2002, 52, 85-94;

[53] Harling, A. M.; Glover, D. J.; Whitehead, J. C.; Zhang, K. *Environ. Sci. Technol.* **2008**, 42, 4546-4550;

[54] Kim, H.-H. *Plasma Proces. Polym.* **2004**, 1, 91-110;

[55] Indarto, A.; Choi, J.-W.; Lee, H.; Song, H. K. *Environ. Chem. Lett.* **2008**, 6, 215-222;

[56] Mista, W.; Kacprzyk, R. *Catalysis Today* **2008**, 137, 345-349;

[57] Penetrante, B.M.; Schultheis, S.E. *Nonthermal plasma techniques for pollution control*, Springer Verlag: New York, 1993;

[58] Vercammen, K.L.L.; Berezin, A.A.; Lox, F.; Chang, J.-S. *J. Adv. Oxid. Technol.* **1997**, 2, 312-329;

[59] Pasquiers, S. *Eur. Phys. J. Appl. Phys.* **2004**, 28, 319-324;

[60] Odic, E.; Paradisi, C.; Rea, M.; Parissi, L.; Goldman, A.; Goldman, M. in *The Modern Problems of Electrostatics with Applications in Environment Protection.* NATO Science Series, 2. Environmental Security, Vol. 63, I.I. Inculet, F.T. Tanasescu, R. Cramariuc, Eds., Kluwer Academic Publishers: Dordrecht, 1999, pp. 143-160;

[61] Shi, Y.; Ruan, J.; Wang, X.; Li, W.; Tan, T. *Environ. Sci. Technol.* **2005**, 39, 6786-6791;

[62] Ruan, J.J.; Li, W.; Shi, Y.; Nie, Y.; Wang, X.; Tan, T.E. *Chemosphere* **2005**, 59, 327-333;

[63] Lock, E.H.; Saveliev, A.V.; Kennedy, L.A. *Plasma Chem. Plasma Process.* **2006**, 26, 527-542;

[64] Winands, H.G.J.J.; Yan, K.P.; Nair, S.A.; Pemen, G.A.J.M.; van Heesch, B.E.J.M. *Plasma Process. Polym.* **2005**, 2, 232-237;

[65] Van Durme, J.; Dewulf, J.; Sysmans, W.; Leys, C.; Van Langenhove, H. *Chemosphere* **2007**, 68, 1821-1829;

[66] Marotta, E.; Callea, A.; Rea, M.; Paradisi, C. *Env. Sci. Technol.* **2007**, 41, 5862-5868;

[67] Marotta, E.; Callea, A.; Ren, X.; Rea, M.; Paradisi, C. *Int. J. Plasma Env. Sci. Technol.* **2007**, 1, 39-45;

[68] Marotta, E.; Callea, A.; Ren, X.; Rea, M.; Paradisi, C. *Plasma Process. Polym.* **2008**, 5, 146-154;

[69] Jarrige, J.; Vervisch, P. *J. Appl. Phys.* **2006**, 99, 113303;

[70] Blind-Simiand, N.; Jorand, F.; Magne, L.; Pasquiers, S.; Postel, C.; Vacher, J.-R. *Plasma Chem. Plasma Process.* **2008**, 28, 429-466;

[71] (a] Van Durme, J.; Dewulf, J.; Leys, C.; Van Langenhove, H. *Appl. Cat. B: Environ.* **2008**, 78, 324-333; (b) Van Durme, J.; Dewulf, J.;. Sysmans, W; Leys, C.; Van Langenhove, H. *Appl. Catal. B: Environ.* **2007**, 74, 161-169;

[72] Sato, M.; Ohgiyama, T.; Clements, J.S. *IEEE Trans. Ind. Appl.* **1996**, 32, 106-112;

[73] Joshi, A.A.; Locke, B.R.; Arce, P.; Finney, W.C. *J. Haz. Mater.* **1995**, 41, 3-30;

[74] Sunka, P.; Babicky, V.; Clupek, M.; Lukes, P.; Simek, M.; Schmidt, J.; Cernak, M. *Plasma Sources Sci. Technol.* **1999**, 8, 258-265;

[75] Kirkpatrick, M.; Locke, B.R. *Ing. Eng. Chem. Res.* **2005**, 44, 4243-4248;

[76] Sun, B.; Sato, M.; Harano, A.; Clements, J.S. *J. Electrostat.* **1998**, 43, 115-126;

[77] Sun, B.; Sato, M.; Clements, J.S. *J. Electrostat.* **1997**, 39, 189-202;

[78] Lukes, P.; Appleton, A.; Locke, B.R. *IEEE Trans. Ind. Appl.* **2004**, 40, 60-67;

[79] Lukes, P.; Clupek, A.; Babicky, V.; Janda, V.; Sunka, P. *J. Phys. D: Appl. Phys.* **2005**, 38, 409-416;

[80] Sun, B.; Sato, M.; Clements, J.S. *Environ. Sci. Technol.* **2000**, 34, 509-513;

[81] Lukes, P.; Locke, B.R. *J. Phys. D: Appl. Phys.* **2005**, 38, 4074-4081;

[82] Lukes, P.; Clupek, M.; Sunka, P.; Peterka, F.; Sano, T.; Negishi, N.; Matsuzawa, S.; Takeuchi, K. *Res. Chem. Intermed.* **2005**, 31, 285-294;

[83] Sahni, M.; Finney, W.C.; Locke, B.R. *J. Adv. Oxid. Technol.* **2005**, 8, 105-111;

[84] Sharma, A.K.; Josephson, G.B.; Camaioni, D.M.; Goheen, S.C. *Environ. Sci. Technol.* **2000**, 34, 2267-2272;

[85] Brisset, J.L. *J. Trace Microprobe Tech.* **1998**, 16, 363-370;

[86] Benstaali, B.; Moussa, D.; Addou, A.; Brisset, J.L. *Eur. Phys. J.: Appl. Phys.* **1998**, 4, 171-179;

[87] Kutepov, A.M.; Zakharov, A.G.; Maksimov, A.I. *Theor. Found. Chem. Eng.* **2000**, 34, 70-75;

2. CONTENTS, OBJECTIVES AND ORGANIZATION OF THE THESIS

This thesis reports and discusses the results of studies on non-thermal plasma processes for the oxidation of organic pollutants in air and in water. Despite the fact that many such processes are being successfully used in applications of environmental and commercial relevance, the chemistry of organic compounds within air non-thermal plasmas is still not well characterized, both as far as products and mechanisms are concerned. In the past, major research efforts in this field, traditionally a domain of physicists and electrical/environmental engineers, focussed on improving the process energy efficiency. More recently, however, the ever stricter regulations on gaseous emissions and air quality are shifting the attention on ways to gain a better control on the emissions produced. Ideally, non-thermal plasma processing of VOCs in air should lead to their exhaustive oxidation to CO_2, a goal seldom reached. Only a partial characterization is usually available of the other VOC treatment products, which often include CO, volatile organic oxidation intermediates but also non volatile organics and aerosols. In addition, electric discharges in air produce undesired side products such as NOx and ozone. Recent developments in VOC plasma processing concern various combinations of atmospheric plasma with heterogeneous catalysts to achieve better energy efficiency but especially better product selectivity. Obviously, product control and process optimization require a good understanding of the chemical reactions involved in the VOC degradation process. This thesis developed as a contribution to this field of research along three lines of research dealing, respectively, with plasma processing of: VOCs in air with plasma alone; VOCs in air with plasma plus an heterogeneous catalyst; phenol in aqueous solutions above which an air plasma is generated. All three projects had a common focus in the mechanistic characterization of the oxidation processes within these very complex and highly reactive systems. To reach this objective I carried out experiments to determine, under various experimental conditions, the process efficiency and the reaction intermediates and stable products. Additional experiments were conducted to detect and monitor or to infer the presence of various highly reactive species produced by the discharges in air, including the

hydroxyl radical, atomic oxygen species, ozone and the ions of the plasma and to evaluate their role in the oxidation of VOCs. To interpret the results of all these experiments I made use of the extensive literature data on rate and products for the reaction of many of the reactive species of the plasma (electrons, atoms, radicals and ions) with the organic compounds I used as models in my studies. This common mechanistic approach obviously required some adaptation to fit the different conditions and experimental set-ups used in the three projects which form this thesis.

For the first project, dealing with VOC processing with plasma alone, I used the corona reactor developed at the Department of Chemical Sciences in Padova and tested in studies which preceded my doctoral work. This reactor has a wire/cylinder configuration and can be energized with DC or with pulsed voltage of either polarity. It is therefore possible to explore the reactivity of the selected model VOCs under different energization conditions but under otherwise identical experimental conditions. Previous studies dealing with saturated hydrocarbons had shown that different corona regimes (DC or pulsed, positive or negative polarity) applied within the same reactor under the same experimental conditions lead to different process efficiencies and support different mechanisms for the initial stages of VOC oxidation. It was thus proposed that, in spite of the overall rather similar general features of hydrocarbon processing with +DC, –DC and +Pulsed corona, the crucial initiation steps are different. Specifically, with +DC corona ionic reactions, which are intrinsically much faster than radical reactions, prevail in contrast with –DC and +Pulsed corona which involve initial reactions with electrons and with neutrals ($^{\bullet}OH$ and $O(^3P)$). A specific goal of my thesis was to probe the generality of these conclusions by considering additional VOCs representative of other classes of compounds, specifically aromatic and halogen containing hydrocarbons. Toluene was chosen for the first, since it is one of the environmentally most important aromatic hydrocarbons and a favorite model in testing and comparing the performance of different experimental set-ups for NTP and plasmochemical VOC processing. As for halogen-containing VOCs, two environmentally relevant compounds were chosen, CH_2Br_2 and CF_2Br_2, to test and compare the behavior of H-containing and perhalogenated hydrocarbons, respectively. A second specific goal of this part of my thesis was the set-up, performance and interpretation of in situ emission spectroscopy

measurements to detect and study excited atomic and radical species formed by corona discharges in our reactor. This project was carried out in collaboration with researchers of the Consorzio RFX, Padova.

The second topic addressed by the thesis is the synergy between non-thermal plasma and heterogeneous catalysis. This synergy is a well documented phenomenon which is being exploited to improve efficiency and selectivity of VOC advanced oxidation processes, but the origin and nature of which are still not fully understood. The occasion to take part in research on this subject was a 4 months stage at a specialized laboratory at Advanced Industrial Science Technology institute (AIST) under the supervision of Dr. H.-H. Kim. During this stage I was able to experiment with different types of NTP reactors with and without added catalysts in the active plasma region. A most interesting part of this work, propedeutic to the mechanistic studies of VOC oxidation within such hybrid systems, was the study of O-scrambling in experiments carried out with mixtures of $^{16}O_2$ and $^{18}O_2$ in various proportions. These experiments provide a novel means to determine the average concentration of atomic oxygen species within the plasma, a data which is accessible via sophisticated spectroscopy measurements (Laser Induced Fluorescence, LIF).

The third project started by testing a first prototype of plasma reactor for the treatment of polluted waters which had been developed earlier under the supervision of Prof. M. Rea of the Department of Electrical Engineering in Padova. The purpose of these tests was to verify the efficiency of this system in oxidizing phenol, used as model organic pollutant, to optimize the various electrical and experimental variables and conditions and, most importantly, to investigate on the products, oxidation intermediates and oxidizing reactive species involved in these reactions. Notably, specific chemical and spectroscopic probes were adapted and used to detect or trace the following species in the aqueous solution under treatment: ozone and the OH radical. The considerable success of this first series of experiments prompted the development of a new reactor in which, similarly to the first prototype, a plasma is produced in the air above the aqueous solution containing the organic pollutant to be oxidatively degraded. This new prototype can be powered by DC, AC and pulsed high voltage thus allowing for comparative evaluations of different plasma regimes on the efficiency and mechanisms of phenol oxidation.

As for the organization of the thesis, the following chapter (*Chapter 3*) reports details on the experimental part of the work, including the various plasma reactors and protocols used. The results and a discussion thereof are found in *Chapter 4* which is organized as a collection of scientific articles dealing each with a specific part of the research performed for the thesis. The papers presented in *Sections 4.1–4.4* have already been published, whereas those in *Sections 4.5–4.10* are to be submitted for publication in the near future. Finally, *Chapter 5* summarizes and discusses the most important conclusions which can be drawn from the thesis.

3. EXPERIENTAL METHODS AND PROCEDURES

This chapter describes the experimental set-ups, the materials and the methods used for the research activity carried out at the Department of Chemical Sciences of the University of Padova (*Sections 3.1–3.4*) and at the Advanced Industrial Science and Technology institute (AIST) in Tsukuba (Japan) (*Section 3.5*).

3.1 CHEMICALS

Pure air used in the experiments was a synthetic mixture (80% nitrogen–20% oxygen) from Air Liquide with specified impurities of H_2O (<3 ppm_v) and of C_nH_m (<0.5 ppm_v). Air mixtures of n-hexane (500 ppm_v ± 3%), toluene (500 ppm_v ± 2%), benzene (500 ppm_v ± 2%), CF_2Br_2 (500 ppm_v, ±3%), CO_2 (520 ppm_v, ±2%), CO_2 (250 ppm_v ± 1%), CO_2 (50 ppm_v ± 0.5%), CO (499 ppm_v, ±1%), CO (250 ppm_v, ±1%) and CO (50 ppm_v, ±0.5%) were purchased from Air Liquide in cylinders loaded to a pressure lower than their respective condensation limits. Liquid and solid samples of n-hexane, benzene, toluene, CH_2Br_2, acetonitrile, potassium indigo-trisulfonate, coumarin-3-carboxylic acid, 7-hydroxy-3-carboxy-coumarin, titanium oxysulfate sulfuric acid solution, phenol, 1,2-dihydroxybenzene, 1,4-dihydroxybenzene, 1,4-benzoquinone, 1,2,4-trihydroxybenzene, 1,2,3-trihydroxybenze, acetic acid, maleic acid, fumaric acid, cis-cis muconic acid, trans-trans muconic acid, formic acid, glyoxylic acid, oxalic acid, and succinic acid were the products of Sigma Aldrich, Riedel de-Haën and Fluka (purity ≥99%). Solid and liquid compounds NaH_2PO_4, Na_2HPO_4, KI, $Na_2S_2O_3$ (Normex 0.1 M) were purchased from Carlo Erba Reagenti.

3.2 INSTRUMENTATION FOR CHEMICAL ANALYSIS

Gas Chromatography

The following instrument and columns were used:

- GC/FID instrument (Varian 3600 with FID detector) equipped with a 2 m x 3 mm glass column packed with 10% SP1000 on Supelcoport 80/100 (Supelco) and an on-column injector. Nitrogen was used as carrier gas, and the injections were made manually using a gas-tight type Hamilton syringe.
- GC/FID/TCD instrument (Agilent Technologies 7890 with FID and TCD detector connected in series) equipped with a 30 m x .53 mm PlotQ column (Agilent Technologies) and a 15 m x .53 mm Molesieve column (Agilent Technologies) connected in series with a 6-way switching valve pneumatically controlled. It is possible to make analysis using only the PlotQ column or both with a time program in order to do not inject water or carbon dioxide into the Molesieve column. It has a split/split less injector, the carrier gas is helium and the injections were made manually using a gas-tight type Hamilton syringe.
- GC/MS instrument (Agilent Technologies 6850 instrument and 5973 mass detector) with electron impact source and quadrupole analyzer and equipped with a 30 m x 0.25 mm HP-5 MS column (Agilent Technologies). It has a split/splitless injector, the carrier gas is helium and the injections were made manually using a gas-tight type Hamilton syringe.

Infrared Spectroscopy

Analyses were carried out using a Fourier transform spectrometer (Nicolet 5700) equipped with a gas cell of 10 cm length. The gas cell is connected downstream to the reactor. We use two types of window cells: NaCl for experiment in dry conditions and CaF_2 for experiment in humid conditions. The acquired spectral windows vary from 4000 cm^{-1} to 650 cm^{-1} for NaCl cell, and from 4200 cm^{-1} to 1000 cm^{-1} for CaF_2 cell. The compartment where the cell houses were pre-evacuated with nitrogen in order to limit the interference on

analysis due to the presence of ambient air, particularly as regards the signal produced by CO_2.

Liquid Chromatography

Two different HPLC instrument were used:

- Shimadzu (LC-10AT pump and Shimadzu SPD-10 UV-VIS detector)
- Thermo Scientific (P2000 pump with a UV6000LP Diode array detector). Both were equipped with a Zorbax-SB Aq 4.6x150 mm (Agilent Technologies) column with particle size of 3.5 μm, and an injection loop of 20 μL. A phosphate buffer 20 mM (pH = 2) containing 1% of acetonitrile was used as eluent at a flow rate of 1.0 $mL \cdot min^{-1}$. Chromatograms were recorded at 210 and 270 nm.

Liquid Chromatography coupled with Mass Spectrometry

An HPLC instrument (Agilent Technologies 1100 Series) connected to a diode array detector and a mass spectrometer detector (MSD SL Trap) with an ElectroSpray Ionization (ESI) source (alternating positive and negative polarity) was used. The instrument is equipped with Zorbax-SB Aq 4.6x150 mm (Agilent Technologies) column with particle size of 3.5 μm, and an injection loop of 20 μL. A mixture of water/acetonitrile 9:1 containing 0.1% of formic acid was used as eluent. The operative parameters used were as follows: nebulizer 70 psi, dry gas 12 Lmin-1, dry gas temperature 350 °C, capillary voltage ±3.5 kV, capillary exit ±101.7 V, skimmer ±40 V.

Ion Chromatography

The following instruments were used:

- Ion Chromatograph instrument from Dionex (ICS-900), equipped with AG22 4x50 mm pre-column, AS22 4x250 mm column and AMMS 300 ion membrane suppressor. The used eluent was a 4.5/1.4 mM buffer solution of carbonate/bicarbonate at a flow rate of 1.2 $mL \cdot min^{-1}$, the regeneration solution for membrane suppressor was H_2SO_4 25 mM, and the injection loop was 10 μL. This instrument was used for the analysis of air processing experiments.
- Ion Chromatograph instrument from Dionex (AGP-1 pump, LCM-3 module, PED-2 detector and ACI 600 interface). This instrument was

equipped with AG4A-SC 4x50 mm pre-column, AS4A-SC 4x250 mm column and SRS ULTRA II self regenerating suppressor. The used eluent is a 1.8/1.7 mM buffer solution of carbonate/bicarbonate at a flow rate of 2.0 mL•min^{-1} and the injection loop is 10 μL. This instrument was used for the analysis of water processing experiments.

Acidity

The acidity of the water solution before, during and after the treatment is monitored using a pH meter (Metrohm 827). Before measurements, the instrument is calibrated using calibration buffer solutions (Merck).

Conductivity

Conductivity of the aqueous solution was measured with a conductometer (Metrohm 660). Before measurements, the instrument was calibrated using a calibration solution of 0.2 mM KCl (30 μS).

UV/Vis spectroscopy

UV/Vis spectra were recorded at 25 °C with a spectrophotometer (Perkin-Elmer Lamdba 16) equipped with water thermo-stated cell holders. Data were acquired with a slit of 2 nm, a spectral resolution of 0.8 nm and a sampling rate of 480 nm•min^{-1}. Quartz cells (Hellma) with an optical path-length of 1 cm were used.

Fluorescence spectroscopy

Fluorescence measurements were done with spectrofluorometer (Perkin-Elmer LS-55) equipped with a Hamamatsu R928 photomultiplier and thermo-stated cell holder. Fluorescence spectra were recorded at 25 °C by using quartz cells (Hellma) with an optical path-length of 1 cm. The excitation wavelength was 390 nm.

3.3 NTP OXIDATION OF VOCs IN AIR

3.3.1 The experimental set-up

3.3.1.1 The corona reactor

The reactor is a 38.5 mm x 600 mm (0.698 L) stainless steel cylinder set at ground potential, with a stainless steel wire (the active electrode) of 1 mm diameter fixed along its axis. The stainless steel cylinder, which has a window (1 x 10 cm) for the observation of the corona luminescence, is contained into a Pyrex glass cylinder of slightly larger diameter securely held in place by two Teflon caps connected by steel tie rods and Viton o-rings (*Figure 3.1*).

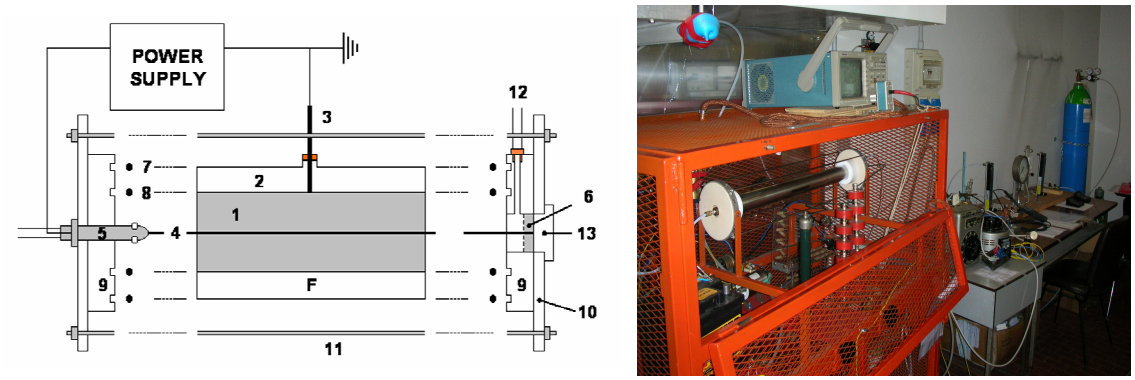

Figure 3.1: Sectional view of the gas treatment reactor (left) and photo of the experimental apparatus (right).

One of the reactor head has a hole in it (*Figure 3.1 - Detail 13*) to incorporate an optical lens at the centre of one of the end caps. Connecting an optical fiber on the lens holder is possible to measure the emission from the chemical species formed under plasma conditions.

3.3.1.2 The gas feeding line

A gas feeding line (*Figure 3.2*) was built to be used either with commercial gaseous VOC/air mixtures which are contained in gas cylinders, or to produce VOC/air mixtures of desired composition starting from liquid VOC samples. In this latter case the following procedure was used. Rotameter 2 is set to a value so as to obtain the desired total flow rate of pure air to be used in the

experiment. This flow is then split into two parts by adjusting rotameter 3, which regulates the flow of air passing through bubbler 5 which contains a sample of the liquid VOC. The two flows from rotameters 3 and 4 are then combined into a mixing chamber (6). The setting of rotameter 3 determines the VOC concentration in the gas mixture to be fed into the reactor. This concentration is then measured by gas chromatographic analysis of samples withdrawn at the exit of the reactor prior to the application of the corona discharge: this analysis provides the value of $[VOC]_0$. In the second part of the line it is possible to change the relative humidity of the gas mixture by using the same kind of system described above and a bubbler containing distilled water (9). The resulting relative humidity, RH, can be varied between 0 and 80 % and is measured with a Rotronic A1H humidity probe (10). The total flow-rate can be varied within the interval of 150 to 800 $mL \bullet min^{-1}$.

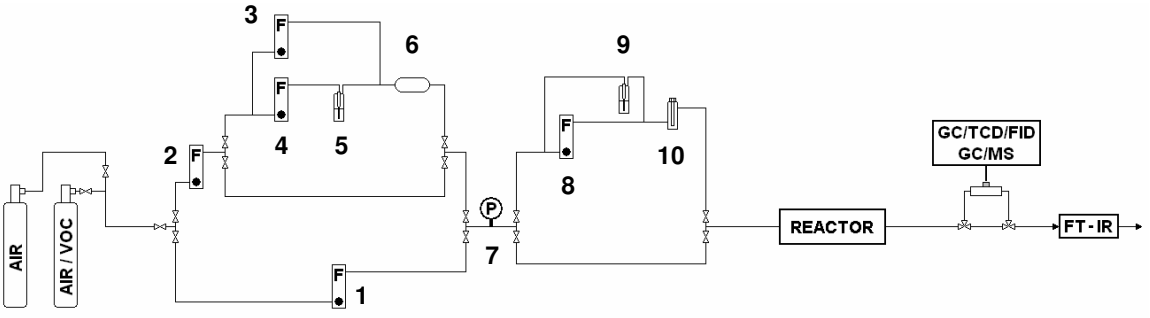

Figure 3.2: Gas feeding line schematic.

3.3.1.3 Power supply and energy determination

The reactor could operate under three different electrical conditions:

- A continuous positive voltage (+DC);
- A continuous negative voltage (–DC);
- A positive pulsed voltage (+Pulsed).

The electrical power supply circuit for DC voltage is sketched in *Figure 3.3*. The AC voltage from the grid is manually regulated with an autotransformer (Variac), elevated by a transformer and rectified through a Graetz bridge and a low pass filter. The maximum voltage (nominal) which can be applied to the

reactor is 30 kV. The series resistance of the low pass filter also serves to limit the current in case of sparks occurring in the reactor. In order to limit current oscillations, a damping resistor (R_{DAMP}) of 7.7 kΩ is connected in series with the reactor. To avoid breakdown current through the power supply a limiting resistor (R_{LIMIT}) of 10 kΩ is connected in series to it. A home made coaxial shunt (R_{SHUNT}) of 52 Ω with a bandwidth up to 200 MHz is included in the circuit for measuring the current across the reactor. To determine the Specific Input Energy (SIE), i.e. the energy per unit volume ($kJ \cdot L^{-1}$), we use the following equation:

$$\mathbf{SIE} = \frac{\mathbf{V} \cdot \mathbf{I}}{\mathbf{F}} \qquad (1)$$

where:

- V is the effective voltage (V);
- I is the discharge current (A);
- F is the gas flow rate through the reactor ($L \cdot s^{-1}$).

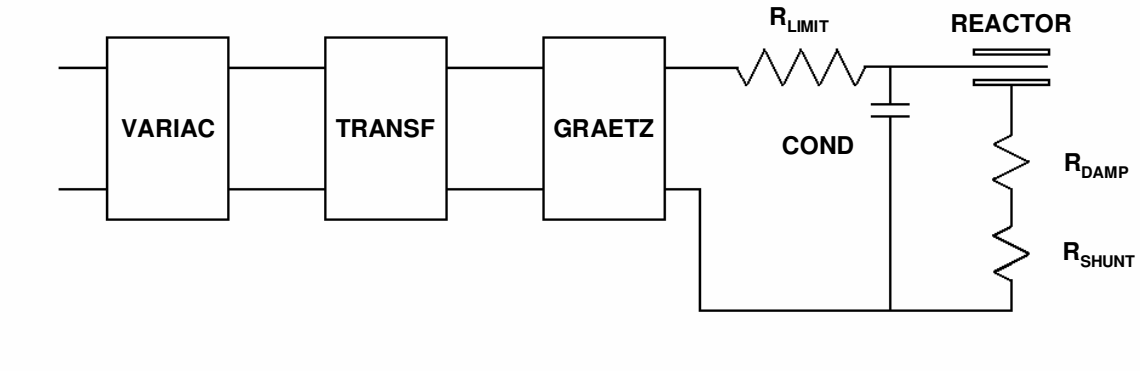

Figure 3.3: Electrical schematic of the DC power supply.

The electrical scheme for Pulsed High Voltage power with DC bias (PHVDC) is sketched in *Figure 3.4*. It is based on a spark gap switch with air blowing, with the following specifications: DC bias 0 – 14 kV (input voltage 0 – 100 V), peak voltage 25 – 40 kV with DC bias (input voltage 120 - 220V) peak current 100A, frequency between 33 – 300 Hz, rise-time of pulses less than 50 ns.

The working principle is described as follows: the power supply is divided into two parts, one is the pulsed power and the other is the DC bias.

For pulsed power; the energy is stored in the capacitor C1 that is charged by V1 (which is the same Graetz bridge high voltage power supply). Then the pulsed capacitor C2 is charged through the circuit of C1, R2 and R3; after that

an ignitor, whose frequency can be changed by an external frequency generator triggers the gap switch. When it closes the charged capacitor C2 discharges through the gap switch and the narrow pulse voltage supplies the reactor through capacitor C3.

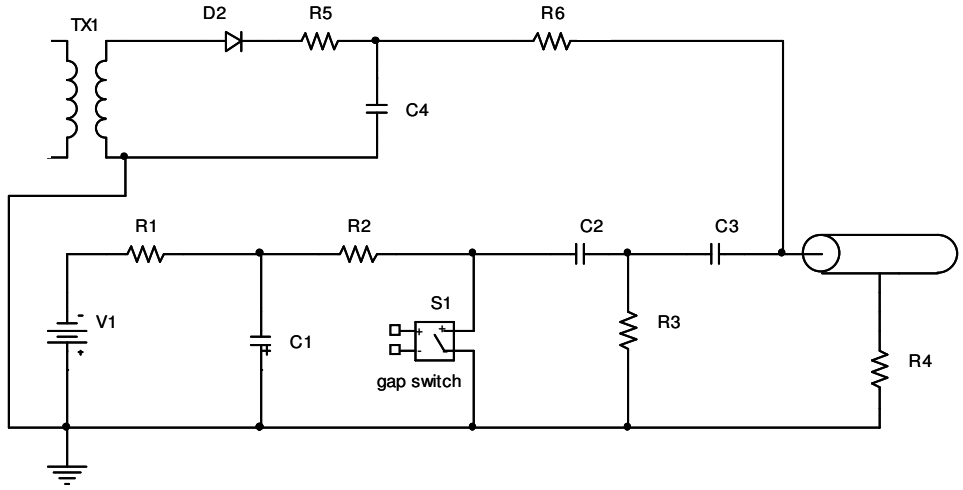

Figure 3.4: Electrical schematic of the high voltage pulses discharges.

For the DC bias; the AC voltage from the grid is manually regulated with an autotransformer (Variac), and elevated by a transformer TX1. To rectify the voltage a diode D2, a resistor R4 and a capacitor C4 are used. The power is applied to the reactor through R6 of 420 kΩ. R4 is the current shunt.

The functions of R3 are two: first it builds a loop for charging the capacitor C2, second it serves to adjust the “tails” of the pulses. If the “tails” of the pulses with high value of R3 are too long, they can cause sparks in the reactor, and if the value of R3 is too low, some energy would be dissipated into it.

The spark gap is shown in *Figure 3.5*. The distance between the electrodes can be adjusted from 4 to 6 mm. The air is supplied to the spark gap switch to enhance the operation frequency.

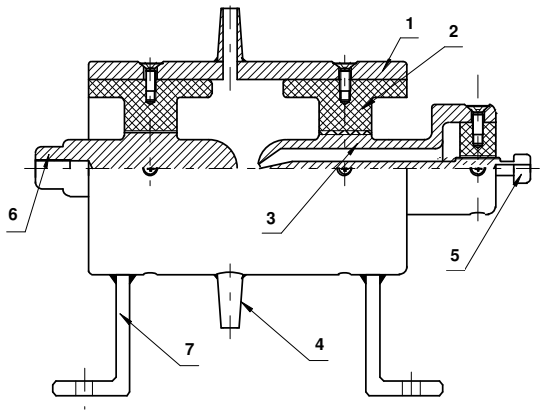

Figure 3.5: Sectional view of the spark gap switch.

Measurements of power input are made using a digital oscilloscope (Tektronix type 410A, bandwidth 200 MHz, two channels), a high voltage probe by Tektronix (ratio 1000:1, bandwidth 75 MHz, peak voltage 40 kV), and two homemade current probes with 10 resistors in parallel housed in an electromagnetic shield (52 Ω for DC only current measurement and 1.1 Ω for PHVDC current measurement). In order to shield the oscilloscope and the other measuring devices from the radio frequency waves generated by the discharge the power supply is enclosed into a Faraday cage.

The total power fed to the reactor (P_{TOT}) is then given by:

$$\mathbf{P_{TOT} = P_{DC} + P_{PULSE}} \qquad (2)$$

where:

- P_{DC} is the power supplied by the DC bias (W);
- P_{PULSE} is the power supplied by the pulses (W).

Because the pulses of current and voltage are added on a DC bias, we can't use the formula of DC power to calculate P_{DC} directly. We used instead equation (3) which employs digital data recorded by the oscilloscope obtained within a time interval comprising two consecutive pulses:

$$\mathbf{P_{DC} = \frac{1}{T}\int_0^T u(t)\cdot i(t)\cdot dt = \frac{1}{T}\sum_{i=1}^{N} U_i \cdot I_i \cdot \Delta T} \qquad (3)$$

where:

- T is the time interval considered for the calculation (s);
- N is the number of acquired data points;
- U_i are the voltage data (V);
- I_i are the current data (A);
- ΔT is the time interval between two consecutive data (s).

Similarly, the pulsed power, P_{PULSE}, can de determined as follows:

$$\mathbf{P_{PULSE} = f \cdot E_{pp} = f \cdot \int_0^T u(t)\cdot i(t)\cdot dt = f \cdot \sum_{i=1}^{N} U_i \cdot I_i \cdot \Delta T} \qquad (4)$$

where:

- f frequency of the pulses (Hz);
- E_{pp} energy of a single pulse;
- T is the time interval considered for the calculation (s);
- N is the number of acquired data points;
- U_i are the voltage data (V);

- I_i are the current data (A);
- ΔT is the time interval between two consecutive data (s).

When the voltage is lower than or very near to the corona onset, the current is very low comparable to the zero floating of the oscilloscope, so we have to subtract this contribution (P_0). P_0 is determined by the same procedure used for P_{DC}, but the current data are taken after the power supply is switched off.

So the total power input is calculated according to this formula:

$$\mathbf{P_{TOT} = (P_{DC} - P_0) + P_{PULSE}} \quad (5)$$

Finally we can determine the specific input energy (SIE, in kJ•L^{-1}), using the following equations:

$$\mathbf{SIE} = \frac{\mathbf{P_{TOT}}}{\mathbf{F}} \quad (6)$$

where F is the gas flow rate through the reactor (L•s^{-1}).

:

3.3.2 Experimental procedures

3.3.2.1 Determination of the process efficiency and product analysis

The following standard procedure was developed to achieve stable and reproducible conditions for the discharge and for the gas flow rate and composition. The reactor is first flushed with air at 4 L•min^{-1} (rotameter 1) for a few minutes. VOC-containing air is then allowed in at a flow rate of 0.8 L•min^{-1} (rotameter 2) for 3 min, at which point the VOC concentration measured at the reactor outlet is the same as that at its entry. The desired flow rate for the specific experiment is then set and the high potential is applied. After a stabilization time of about 5 residence times to obtain a steady concentration of the residual VOC at the reactor outlet, the gas flow is stopped, the valve located after the reservoir is closed, and the high potential is switched off.

Accurately measured samples (0.5 or 1 mL) of the treated gas are withdrawn from the gas reservoir using a gas-tight Hamilton syringe and subjected to GC analysis. The apparatus is finally cleaned by flushing air at 4 L•min^{-1} for 15 min. In experiments with humidified gas, preconditioning of the reactor is achieved by flushing humidified air through it for 30 min. Then, the VOC-containing air, humidified as described above, is introduced into the system. The experimental

procedure is the same if we use pre-constituted gas mixture from gas cylinder or if we prepare it using rotameter 3 and 4 of the gas line (see *Figure 3.2*)

The identification of volatile organic by-products was achieved by means of GC/MS analysis and by the use of standards. Their concentration and that of their precursor (n-hexane, toluene, CH_2Br_2, CF_2Br_2) was determined by means of quantitative GC/FID (hydrocarbons) and GC/FID-TCD (halomethanes) analysis based on individually established calibration curves. Calibration was performed using external standards prepared by injecting an accurately measured volume of liquid VOC (1-10 µL) into large calibrated glass flasks filled with nitrogen at ambient pressure and temperature and equipped with a porthole closed by a gas tight septum.

CO, CO_2 and ozone were quantified by on-line FT-IR analysis. The instrument response for CO_2 and CO was calibrated by means of commercial standards as specified above in *Section 3.1*. The ozone concentration was determined by quantitative FT-IR analysis of its two characteristic bands at 1030 and 1060 cm^{-1}. Calibration of the instrument response was performed by carrying out simultaneous determinations of ozone in the treated gas by FT-IR and by the well established iodometric titration method, based on the following reactions:

$$H_2O + O_3 + 2I^- \longrightarrow I_2 + O_2 + 2\ OH^-$$

$$I_2 + I^- \longrightarrow I_3^-$$

$$I_3^- + 2\ S_2O_3^{2-} \longrightarrow 3\ I^- + S_4O_6^{2-}$$

The gas exiting the reactor was allowed to flow for 15 min through two bubblers placed in series and containing each 150 mL of a 0.12 M KI solution in phosphate buffer at pH 7. 5 mL of H_2SO_4 4.5 M were then added to each solution and I_3^- was titrated with a 0.1 M standardized tiosulphate solution.

Since the numbers of moles of thiosulfate introduced were determined, by the stoichiometry of reactions moles of ozone were calculated by the equation:

$$\text{moles of } O_3 = \text{moles of } I_3^- = \tfrac{1}{2} \text{ moles of } S_2O_3^{=} \qquad (7)$$

Using the following equation is possible to switch the concentration to ppm_v:

$$\mathbf{C\,(ppm_v) = \frac{moles\ of\ ozone\ (mol) \cdot 24450\ (mL \cdot mol^{-1}) \cdot 10^6}{F\ (mL \cdot min^{-1}) \cdot t_g\ (min)}} \qquad (8)$$

where:

- F is the gas flow rate (it is more accurately a volumetric flow rate, but is commonly referred to flow);
- t_g is the bubbling time (min).

The carbon mass balance is calculated as the ratio C_{DET}/C_{TOT} where, C_{DET}, the detected carbon is the sum of contributions due to unreacted VOC, CO, CO_2, and volatile organic by-products, and C_{TOT} is the carbon initially present in the VOC. The percentage of undetected carbon ($\%C_{UNDET}$) is, therefore, expressed by equation 9:

$$\%\,\mathbf{C_{UNDET}} = \frac{(\mathbf{C_{TOT}} - \mathbf{C_{DET}})}{\mathbf{C_{TOT}}} \cdot \mathbf{100} = \\ = \left(\mathbf{1} - \frac{([\mathbf{VOC}] \cdot \mathbf{n_{VOC}} + [\mathbf{CO_2}] + [\mathbf{CO}] + \sum [\mathbf{byproduct}] \cdot \mathbf{n_{byproduct}})}{[\mathbf{VOC}]_0 \cdot \mathbf{n_{VOC}}} \right) \cdot \mathbf{100} \quad (9)$$

where n_{VOC} and $n_{byproduct}$ are the number of carbon atoms present in the VOC molecule (i.e., 6 for n-hexane and 7 for toluene) and in each one of the various by-products, respectively, and the terms into square brackets are concentrations of the indicated species.

The process efficiency is evaluated by interpolating the fraction of residual VOC, $[VOC]/[VOC]_0$, as a function of the specific input energy (SIE in $J \bullet L^{-1}$), using the exponential equation

$$\frac{[\mathbf{VOC}]}{[\mathbf{VOC}]_0} = \cdot \mathbf{e}^{-\mathbf{k_E} \cdot \mathbf{SIE}} \quad (10)$$

where $[VOC]_0$ is the initial VOC concentration, [VOC] is its concentration after applying the specific input energy SIE and k_E ($J^{-1} \bullet L$) is the characteristic energy constant for the given VOC under the specific experimental conditions used. For the calculation of SIE see *Section 3.3.1.3*.

3.3.2.2 Determination of current-voltage (I-V) characteristics of DC corona

Current/voltage characteristics of DC corona were monitored both in the presence and in the absence of the hydrocarbon. For each applied voltage the mean current intensity was measured with a multimeter after a stabilization time of 5 min.

3.3.2.3 In situ spectroscopic measurements

In order to make in situ emission spectroscopy measurements in air treatment experiments the end cup of the entrance of the reactor was adapted to mount an optic lens with an optic fibre placed coaxially to the active electrode (see *Figure 3.1*, *Detail 13*). At the opposite end the fibre was connected to a Czerny Turner spectrometer equipped with holographic grating of 1200 g/mm. A retro-illuminated CCD camera (512 x 512 pixel) was used as detector. We monitored the spectral window between 305 and 780 nm, in particular the region around 305 nm corresponding to $^{\bullet}OH$ emission, 777 nm lines corresponding to $O(^3P)$ emission (generally used also in astrophysics and astronomy), [1] and the region between 335 and 400 nm to observe the emission lines of N_2 and N_2^+ useful for the determination of electronic (T_e), vibrational (T_v), and rotational (T_r) temperature. Details about the determination of T_e, T_v and T_r are described in *Section 4.3*

3.3.2.4 Ion analysis

Atmospheric Pressure Chemical Ionization (APCI) mass spectra were acquired with a TRIO 1000 II instrument (Fisons Instruments, Manchester, U. K.), equipped with a Fisons APCI source. A schematic representation of this source, and of the apparatus used for sample introduction, is shown in *Figure 3.6*.

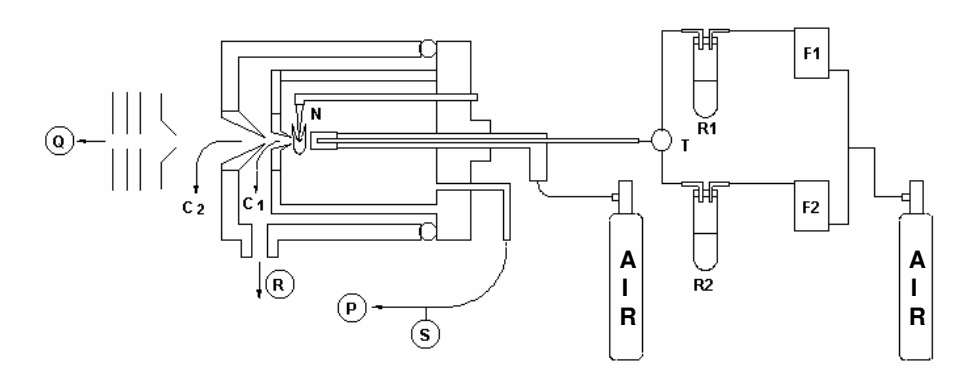

Figure 3.6: Schematics of the APCI-MS mass spectrometer.

The ion source is kept at atmospheric pressure by a flow of synthetic air at 4000–5000 $mL \cdot min^{-1}$ through the nebulizer line, a capillary of ≈ 2mmi.d. Vapours of the hydrocarbon to be analyzed are stripped from a small reservoir

containing a liquid sample of the same, by an auxiliary flow of air (typically 5–50 mL•min^{-1}) and enter the APCI source through a capillary (i.d. = 0.3 mm) running coaxially inside the nebulizer line. A needle electrode is energized by a DC corona discharge of ±3000 V. Ions, produced via ionization and ion-molecule reactions occurring during a time period of 500 ms, leave the source through an orifice, ca 50 mm in diameter, in the counter electrode (the 'sampling cone', held at 0–150 V relative to ground), cross a region pumped down to ca. 10^{-2} Torr and, through the orifice in a second conical electrode (the 'skimmer cone', kept at ground potential), reach the low pressure region hosting the focusing lenses and the quadrupole analyzer. Ion identities were inferred based on their m/z values and characteristic fragmentation pattern as observed in CID (collision induced decomposition) experiments. These were performed by varying the potential difference between the two exit electrodes, the 'sampling cone' and the skimmer cone.

3.4 OXIDATION OF ORGANIC COMPOUNDS IN AQUEOES SOLUTION

3.4.1 The experimental set-up

Two different experimental set-ups were developed and tested for the oxidation of organic compounds in water by the effect of non-thermal plasma produced in the air above the aqueous solution. Each experimental set-up comprises an electrical power supply and a distinct reactor plus a gas line for air circulation and analysis of volatile products. The two experimental set-up are described in the following sections.

3.4.1.1 The two-wires DBD reactor – "Reactor 1"

The first reactor developed (*Figure 3.7*) is made with a glass vessel of size equal to 95x75x60 mm (length x width x height) and is equipped with a Teflon cover. The cover has four electrode holders made of stainless steel. The active electrodes are two 75 mm long parallel wires that are fixed on the tips of

holders. They are placed at a distance of 38 mm one from the other, and are kept above the aqueous solution. The outside surface of the reactor base is covered with silver film and connected to ground. The reactor is mounted on a metal plate which is held in place by screws on the cover. A Viton gasket is placed between glass and Teflon to avoid gas leakage. On the cover there are two connectors for inlet and outlet of an air flow and in the middle there is a sampling port for the withdrawal of solution samples during the decomposition experiments.

The reactor is connected to a gas feeding line (*Figure 3.7*). The dry air flown through a bubbler filled with milliQ water in order to saturate it with humidity and prevent evaporation from the treated solution during the experiment. It is possible to change the flow rate value between 20 to 200 mL•min^{-1}.

The volume of treated solution was 70 mL, the thickness of liquid 9.8 mm, the gap between the surface and the electrodes 15 mm, and the volume of air inside reactor 286 mL.

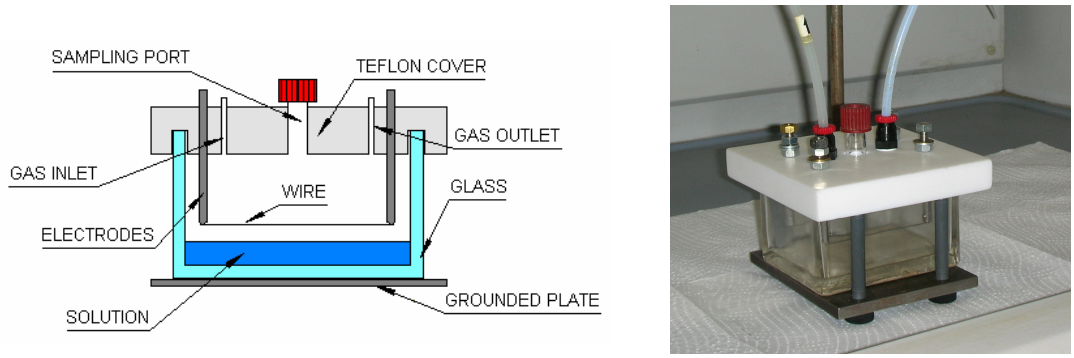

Figure 3.7: Reactor 1 - Sectional view (left) and photo (right).

3.4.1.2 The seven-wires reactor – "Reactor 2"

The second reactor developed and studied is presented in *Figure 3.8*. It is made in two pieces, a base and a cover, both of Plexiglas. The space occupied by gas has the following dimensions: 340x120 mm and 37 mm of height. The base in which the solution is placed is 5.5 mm high and has a capacity of 200 mL. The cover equipped with a entrance and a exit ports for air circulation located at the opposite corners. In the center there is also a sampling port sealed by a silicon septum for withdrawal of samples of the treated solution. Seven parallel wires of 0.15 mm of diameter and 300 mm length, placed at a

distance of 18 mm one from the other, are fixed laterally on stainless steel electrodes screwed on a Teflon structure which can be moved up and down to vary the distance between the wires and the solution. The wires are the active electrodes. The outside surface of the reactor base is covered with a film of colloidal silver paint and connected to a grounded plate. A flow of 100 mL•min^{-1} of air is allowed through the reactor and the discharge occurs in the gas phase above the liquid surface. To minimize evaporation phenomena from the solution to be treated, the gas is humidified by passing it through a water-containing bubbler placed before the reactor.

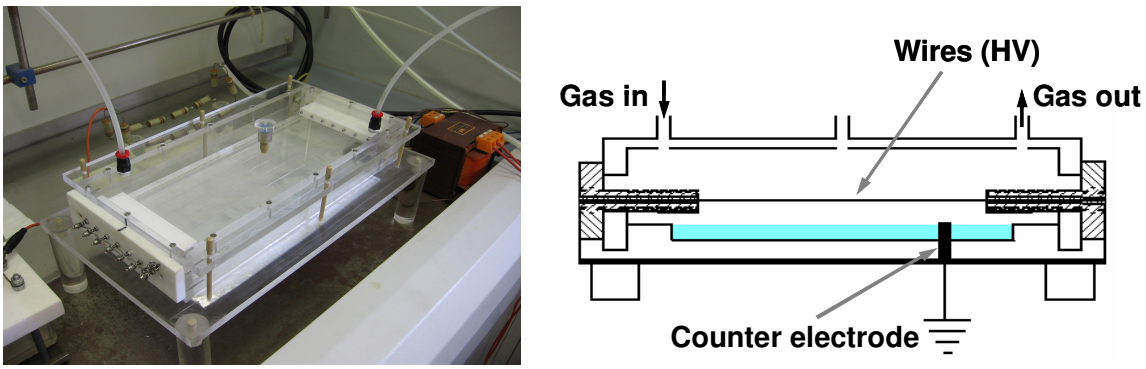

Figure 3.8: Reactor 2 - Photo (left) and sectional view (right).

3.4.1.3 Power supply and energy determinations

The reactor was energized with a high voltage power supply at 50 Hz operating in Dielectric Barrier Discharge (DBD) corona mode. The scheme of power supply is shown in *Figure 3.9*. It includes a voltage regulator autotransformer (Variac – TX1), an isolation transformer (TX2), a voltage rising transformer (TX3) and a resistor (R2) for limiting the current. The function of TX1 is to adjust the voltage from the wall plug with 230 V from 0 to 120 V. Transformer, with a ratio of 1:1, isolates the grounding of wall plugs in case of short-circuit occurring between the oscilloscope (OSC) and the wall plug. TX3 is a voltage transformer that has a ratio of 1:150 and a very low phase shift.

The system of electrical monitoring includes an oscilloscope (Tektronix TDS5032B, Bandwidth 350 MHz, Sample rate 5Gs/s) two 10:1 probes with 500 Hz bandwidth, a current measurement resistor with 50 Ω, and a surging voltage depressor (ZnO).

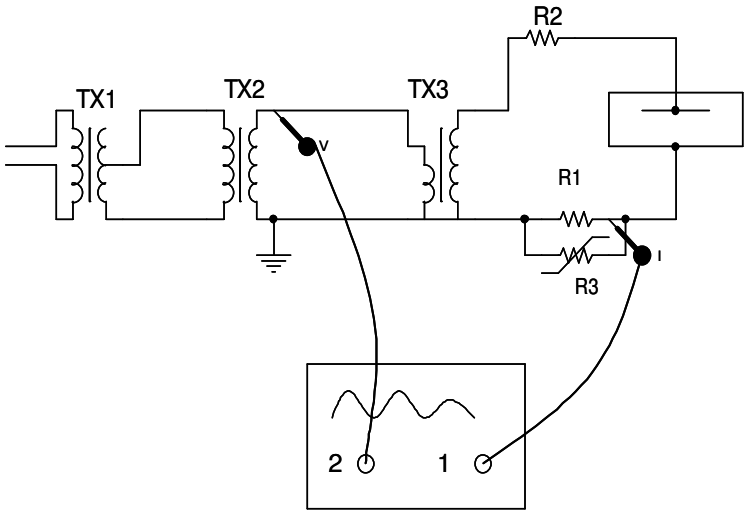

Figure 3.9: Electrical schematic of the AC power supply.

To calculate the power input with this system the following formula is used:

$$\mathbf{P} = \frac{\mathbf{1}}{\mathbf{T}} \int_{0}^{T} \mathbf{u(t)} \cdot \mathbf{i(t)} \cdot \mathbf{dt} \qquad (11)$$

where:

- P is the mean power (W);
- T is the time duration of a voltage period (s);
- u(t) is the voltage applied to the reactor (V);
- i(t) is the current through the reactor (A).

According to Ohm law, the current through the reactor can be obtained from the formula:

$$\mathbf{i(t)} = \frac{\mathbf{u_1(t)}}{\mathbf{R}} \qquad (12)$$

where:

- $u_1(t)$ is the signal recorded on Channel 1 of the oscilloscope (V);
- R is the resistance of R1 (Ω).

The voltage on the reactor, u(t), can be obtained from equation (13):

$$\mathbf{u(t)} = \mathbf{u_2(t)} \cdot \mathbf{K} \qquad (13)$$

where:

- $u_2(t)$ is the signal recorded on Channel 2 of the oscilloscope (V);
- K is the ratio of the voltage rising transformer.

By substituting into (11), one obtains (14) which allows to estimate the power input.

$$P = \frac{K}{R \cdot T} \cdot \int_0^T u_1(t) \cdot u_2(t) \cdot dt = \frac{Kf}{R} \cdot \int_0^T u_1(t) \cdot u_2(t) \cdot dt = 150 \cdot \int_0^T u_1(t) \cdot u_2(t) \cdot dt \quad (14)$$

The power supply frequency f is equal to 50 Hz.

From the mathematical resolution of the formula (14) we can get a digital formula:

$$P = 150 \sum_1^N U_{1n} \cdot U_{2n} \cdot \Delta t = 150 \cdot M \quad (15)$$

where:

- N is the number of data acquired in one period;
- U_1, U_2 are the digital data recorded on Channel 1 and 2 respectively;
- Δt is the interval of time between two consecutive data acquisitions (s);
- M is the value of trace M1 displayed on the screen which is obtained by the mathematical resolution of the numerical sum of voltage and current values within one period (20 ms).

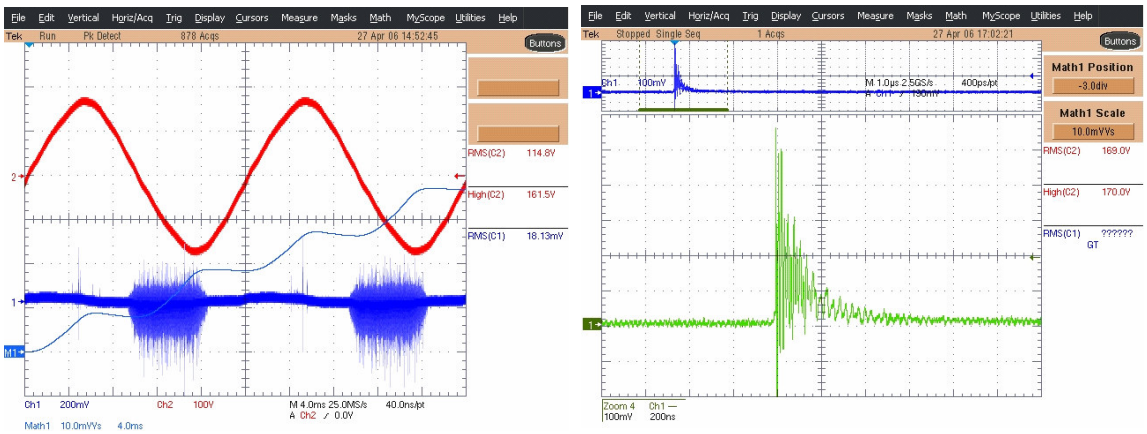

Figure 3.10: Voltage and current measurements (left) and a single pulse (righ).

To make an accurate determination of power input, proper Δt values must be used because the corona discharge pulses are very fast, as shown in *Figure 3.10*. We can find out that the width of most corona discharge is about 200 ns. If Δt is 40 ns, there are 5 data points for every discharge, which are sufficient to get an accurate determination of the power input. The screen of the oscilloscope displays two voltage cycles corresponding to 40 ms, so the memory size should be higher than 1 Mega. The memory size is 2 Mega. With the calculated P values one can get, for any treatment time (t_t), the specific input energy (SIE in $J \cdot L^{-1}$) using the formula:

$$\mathbf{SIE} = \mathbf{P} \cdot \mathbf{t_t} = \mathbf{150} \cdot \mathbf{M} \cdot \mathbf{t_t} \qquad (16)$$

3.4.2 Experimental procedures

The experimental procedures described in following sections were the same for experiments run with both reactors.

3.4.2.1 Determination of process efficiency and products

A volume (70 mL in the case of Reactor 1, 200 mL in the case of Reactor 2) of an aqueous phenol solution $5 \cdot 10^{-4}$ M, prepared in milliQ water, was subjected to plasma treatment under the chosen energization conditions. The efficiency of the decomposition process was determined by measuring phenol conversion as a function of treatment time. To accomplish this, the discharge was interrupted and sample (0.5 mL) of the treated solution were withdrawn at desired treatment times (15, 30, 45, 60, 90, 120, 180, 240 min). The samples were then subjected to HPLC-UV analysis at 210 and 270 nm. The fraction of residual phenol, $[Phenol]/[Phenol]_0$ was plotted against the treatment time and the data were fitted by the equation:

$$\frac{[\mathbf{Phenol}]}{[\mathbf{Phenol}]_0} = \mathbf{e}^{-\mathbf{k} \cdot \mathbf{t}} \qquad (17)$$

to obtain k, the rate constant of the process. [2]

For the identification of intermediate products of the oxidation of phenol selected samples were analyzed also with an HPLC instrument connected to a diode array and a mass spectrometer detector. The ionization was performed by electro spray (ESI). The assignment of the intermediate products was confirmed by comparison with standards.

The sampled solution was also analyzed by ion chromatography to investigate the anions formed during the plasma treatment. pH and conductivity of the initial and final solutions were monitored during the experiments. The gas exiting the reactor was subjected to on line FT-IR analysis using a 10 cm long flow cell equipped with CaF_2 windows.

An alternative procedure was used when larger volumes of the treated solution were necessary for the analysis, like in the case of determinations of pH and conductivity at intermediate treatment times. This procedure consisted in analyzing the whole volume of treated solution and in replacing it with a fresh batch for the next treatment time. Control experiments showed that both procedures gave the same experimental results as far as kinetics and products are concerned.

3.4.2.2 Determination of reactive species

The following methods were made only for the first reactor otherwise were specified.

Ozone

Determination of ozone concentration in the aqueous solution was done using the indigo method. [3] The lower detection limit was determined with pure water treated for 1, 1.5 and 2 h. After the desired treatment time, the discharge was interrupted and the flow rate of air was increased to 200 $mL \cdot min^{-1}$ for 2 minutes. This procedure was followed to eliminate any ozone present in the gas phase to avoid interferences with the measurement of dissolved ozone. Then, 10 mL of $4 \cdot 10^{-4}$ M of indigosulfonate in phosphate buffer 50 mM were added into the reactor through the sampling port by a pipette the tip of which was maintained well into the solution during delivery. The resulting solution was thus analyzed by UV/Vis spectroscopy and its absorbance was compared to a reference solution obtained by adding 10 mL of $4 \cdot 10^{-4}$ M of indigosulfonate in phosphate buffer 50 mM in 70 mL of non-treated pure water. UV/Vis spectra were recorded with a spectrophotometer (Perkin-Elmer Lamdba 16).

The ozone concentration in the gas phase was measured by the iodometric titration method. For all the duration of the experiment the downstream gas was allowed to flow through two bubblers (connected in series) containing each 150 mL of a 0.12 M KI solution in phosphate buffer at pH 7. Sulfuric acid 4.5 M (5 mL) was then added to each solution which was then separately titrated with a standardized thiosulfate solution 0.1 M. The procedure was executed in experiments of treatment of pure water and phenol-containing water for times of 15, 30, 45, 60, 90, 120, 180 and 240 minutes.

OH radical

The production of OH radical in pure water due to the application of the discharge was determined by following the conversion of coumarin 3-carboxylic acid (3-CCA) in coumarin 7-hydroxy-3-carboxylic acid (7OH-CCA), as reported by Newton and Milligan [4] and applied by Hoeben et al. [5] for a similar system. A 10^{-3} M 3-CCA aqueous solution (70 mL) was treated in different experiments for 15, 30, 45, 60, 90 and 120 minutes. The final solution was analyzed by a spectrofluorometer (Perkin-Elmer LS-55).

3.5 CATALYST-ASSISTED NTP OXIDATION OF VOCs IN AIR

This research was carried out at the Advanced Industrial Science and Technology institute of Tsukuba (Japan) using the materials and instruments present in the laboratory of dr. Hyun-Ha Kim situated inside the Environmental Management Technology building.

3.5.1 Chemicals

Pure gases (He, N_2, O_2) and isotopically enriched $^{18}O_2$ in helium (ratio 1:1, isotopic enrichment ≥97 %) were the products of Takachiho Inc. and Cambridge Isotope Labs (purity ≥99 %). The pure grade benzene and silver nitrate were purchased from Takachiho Inc. The solid pellets of TiO_2, molecular sieve MS-13X and γ-Al_2O_3 were used as received from Furukawa Co. Ltd. and Maruzen Chemicals Co. Ltd.

3.5.2 The experimental set-up

The four different types of plasma reactor used for the experiments are shown in *Figure 3.11*.

Reactor (a) is made of a quartz tube of 110 mm length and 28 mm of inner diameter. The active electrode is a stainless steel tip, while the counter electrode is a stainless steel grid. This device is characterized by having both

electrodes in conductive material, and is a classic corona discharge reactor with point-to-plate geometry.

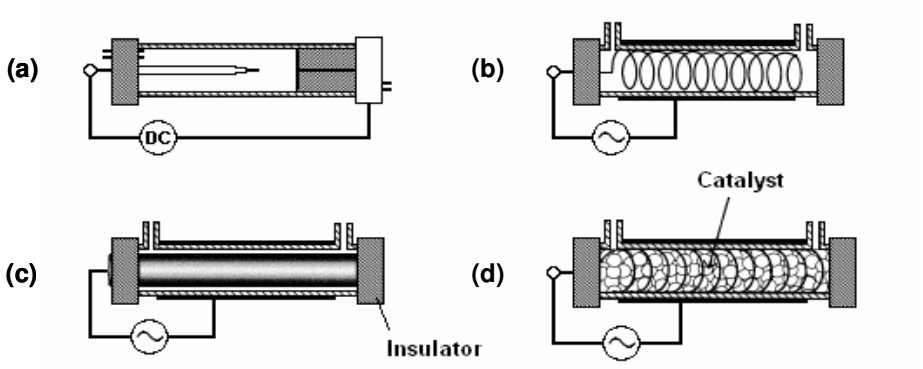

Figure 3.11: Different corona reactor used: (a) pin-to-plate reactor; (b) space discharge reactor; (c) DBD reactor; (d) PDC reactor.

Reactor (b) is made of a quartz tube of 190 mm length and 8 mm of inner diameter. Along the axis of the tube there is a stainless steel wire with a diameter of 0.45 mm coiled, which is the active electrode. The tube is coated with a colloidal silver paste which constitutes the counter electrode. This reactor, characterized by a metal electrode and a counter electrode in insulating material, is called space discharge type.

Reactor (c) is made of a quartz tube of 240 mm length and 10 mm of inner diameter. The active electrode is made by a metal bar covered with ceramic material of 8 mm in diameter. Also in this case the counter electrode is a colloidal silver paste spread on the tube. This reactor, which has both the electrodes made of insulating material, is a DBD type.

Reactor (d) is similar to type (b), but inside it contains an heterogeneous catalyst. This reactor is defined PDC type (Plasma Driven Catalysis).

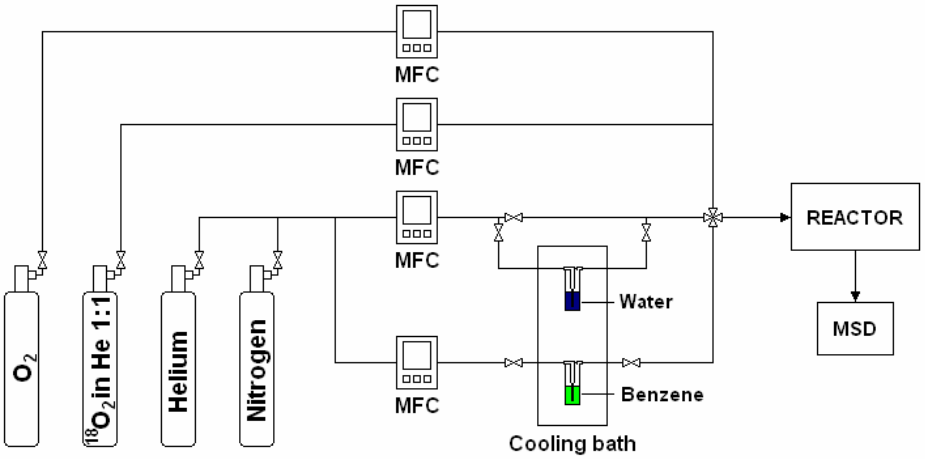

Figure 3.12: Gas feeding line schematic.

A gas feeding line (*Figure 3.12*) was built to be used either with $^{16}O_2$ or $^{18}O_2$ or both the oxygen isotopes. As dilution gas either nitrogen or helium were used. On the carrier gas line there were two bubblers: one containing distilled water, the other liquid benzene. Thus it was possible to add or not humidity or VOC to the plasma reactor in order to investigate different experimental conditions. The flow rates were regulated by calibrated mass flow controllers (MFC) and the total flow rate was set to 200 mL•min^{-1} for all the experiments.

Reactor (a) was powered with DC high voltage of either positive or negative polarity. The electric circuit consists of a high voltage AC power supply which increases the input voltage from 0 – 100 V to 0 – 20 kV. Then 3 rectifying diodes connected in parallel allow switching from positive to negative polarity. A capacitive battery of 0.2 μF is connected before the reactor to get a stable input voltage.

Reactors (b-d) were instead energized with an AC power supply. It consists of a signal amplifier (Trek 20/20B) and a wave function generator (Tektronix AFG 310). To measure the discharge power with reactors (b-d) the Lissajous method was used. The charge Q was determined measuring the voltage between the plates of a 100 nF capacitor connected in series to the ground line of reactors. The applied voltage V was measured with a high voltage probe with ratio 1000:1 (Tektronix P6015A). A digital oscilloscope (Tektronix TDS3034B, bandwidth 500 MHz, sample rate 5 GS/s) recorded V and Q values mediating 16 scans. The discharge power was calculated using the area from V-Q diagram multiplied by the frequency. The Specific Input Energy (SIE) was evaluated by the equation:

$$\mathbf{SIE\ (J \cdot L)} = \frac{\mathbf{P_{DIS}\ (W)}}{\mathbf{gas\ flowrate\ (L \cdot min^{-1})}} \cdot \mathbf{60} \qquad (18)$$

where P_{DIS} is the discharge power and 60 a conversion factor. SIE was modulated varying both the applied voltage and the frequency (10 – 1000 Hz).

The downstream gas was analyzed with a Residual Gas Analyzer instrument (MKS Vision 1000-P) equipped with a high conductance closed ion source (Electron Impact) and a dual detector system (Faraday cup and Secondary Electron Multiplier). It has a mass range between 1 and 200 amu.

3.6 References

[1] Kiselamn, D. *Astrom. Astrophys.* **1993**, 275, 269-282;

[2] Kim, H.-H. *Plasma Processes Polym.* **2004**, 1, 91-110;

[3] Bader, H.; Hoigné, J. *Water Res.* **1981**, 15, 449-456;

[4] Newton, G.L.; Milligan, J.R. *Radiation Phys. Chem.* **2006**, 75, 473-478;

[5] Hoeben, W.F.L.M.; Van Veldhuizen, E.M.; Rutgers, W.R.; Kroesen, G.M.W. *J. Phys. D* **1999**, 32, L133.

4. RESULTS AND DISCUSSION

The results obtained have been elaborated and discussed in a form apt for publication in scientific journals. Ten papers have thus been prepared, each constituting a section of this thesis chapter. The papers presented in *Sections 4.1–4.4* have already been published, whereas those in *Sections 4.5–4.10* are being submitted for publication as specified.

4.1 PRODUCTS AND MECHANISMS OF THE OXIDATION OF ORGANIC COMPOUNDS IN ATMOSPHERIC AIR PLASMAS

IOP PUBLISHING JOURNAL OF PHYSICS D: APPLIED PHYSICS
J. Phys. D: Appl. Phys. **42** (2009) 000000 (10pp) UNCORRECTED PROOF

Products and mechanisms of the oxidation of organic compounds in atmospheric air plasmas

Ester Marotta[1], Milko Schiorlin[1], Massimo Rea[2] and Cristina Paradisi[1,3]

[1] Department of Chemical Sciences, Università di Padova, Via Marzolo 1, 35131 Padova, Italy
[2] Department of Electrical Engineering, Università di Padova, 35131 Padova, Italy

E-mail: cristina.paradisi@unipd.it

Received 2 September 2009, in final form 19 October 2009
Published
Online at stacks.iop.org/JPhysD/42

Abstract
Atmospheric plasma-based technologies are developing as a powerful means for air purification, specifically for the oxidation of organic pollutants. To achieve a better control on the emissions produced by such treatments mechanistic insight is needed in the complex reactions of volatile organic compounds (VOCs) within the plasma. An account is given here of our comparative studies of the behaviour of model VOCs in response to different corona regimes (+dc, −dc and +pulsed) implemented within the same flow reactor. Model VOCs considered include two alkanes (*n*-hexane and *i*-octane), one aromatic hydrocarbon (toluene) and two halogenated methanes, dibromomethane (CH_2Br_2) and dibromodifluoromethane (CF_2Br_2, *halon* 1202). Efficiency and product data are reported and discussed as well as various possible initiation reactions. A powerful diagnostic tool is ion analysis, performed by atmospheric pressure chemical ionization-mass spectrometry: it provides a map of major ions and ion–molecule reactions and a rationale for interpreting current/voltage characteristics of dc coronas. It is shown that, depending on the specific VOC and corona regime adopted, different initiation steps prevail in the VOC-oxidation process and that the presence of a VOC, albeit in trace amounts (500 ppm), can greatly affect some important plasma properties (ion population, current/voltage profile, post-discharge products).

AQ1 (Some figures in this article are in colour only in the electronic version)

1. Introduction

A huge variety of volatile organic compounds (VOCs) are being released in the atmosphere by natural and anthropogenic sources. These compounds differ in respect of their chemical composition, structure, reactivity, environmental impact, toxicity, relative amount, etc. The ever stricter regulations on gaseous emissions and air quality are stimulating continuing efforts to improve existing technologies and to develop novel ones for the removal of organic pollutants. Among these, atmospheric plasmas are most attractive for a number of reasons, which include wide range of applicability, high energy efficiency and low maintenance costs [1–7]. Such plasmas are conveniently produced by means of various types of electric discharges, notably corona and dielectric barrier discharges, in air at atmospheric pressure and ambient temperature. Atmospheric air plasmas are very complex and reactive oxidizing environments which can be applied for the removal of all kinds of VOCs. Despite this high reactivity, however, some selectivity is manifested so that different VOCs are oxidized with different efficiencies [1–7].

Major research efforts in this field initially focussed on improving the process energy efficiency but more recently special attention is being paid to gaining a better control on the emissions produced. Ideally, atmospheric air plasma processing of VOCs should lead to their exhaustive oxidation to CO_2, a goal seldom reached. Only a partial characterization is usually available of the other VOC treatment products, which often include CO, volatile organic oxidation intermediates but

[3] Author to whom any correspondence should be addressed.

JNL: JPD PIPS: 330249 TYPE: SPE TS: NEWGEN DATE: 30/10/2009 EDITOR: MJ

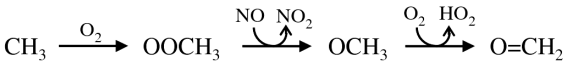

Scheme 1.

also non-volatile organics and aerosols. In addition, electric discharges in air produce undesired side products such as NO_x and ozone. Recent developments in VOC plasma processing concern various combinations of atmospheric plasma with heterogeneous catalysts to achieve better energy efficiency and product selectivity [3, 8, 9].

Product control and process optimization require a good understanding of the chemical reactions involved in the VOC degradation process. Primary plasma events are interactions of high energy electrons with molecules of the bulk gas, N_2 and O_2, producing ionization, excitation and dissociation. The resulting reactive species, ionic and neutral, as well as electrons, react with VOC molecules to initiate a chain of reactions leading eventually to VOC-oxidation all the way to CO_2. This is a complex stepwise process, which proceeds via VOC-derived carbon radical intermediates according to a sequence well known from studies of the natural mechanisms of VOCs degradation in the troposphere [10, 11]. Thus, for example, the simplest VOC of all, methane, is oxidized via the methyl radical as outlined in scheme 1.

Formaldehyde, $CH_2 = O$, is an oxidation intermediate which is in turn oxidized to CO and CO_2 via attack by OH and photolysis. Notably the atmospheric lifetime of formaldehyde is significantly shorter than that of methane [10]: this is also the case for many intermediates detected in the atmospheric plasma processing of various hydrocarbons [12].

How are organic radicals formed from the precursor VOCs within air plasmas? Different reactions are possible [1–7, 13] including reactions with electrons (electron induced bond dissociation, electron ionization and dissociation, dissociative electron attachment), with atoms and radicals (O, OH) and with ions (electron transfer and other ion–molecule reactions). Any one of such processes can activate the oxidation of VOC molecules by converting them into some VOC-derived organic radicals which enter the cycle sketched above. Which initiation step will prevail depends on the specific plasma regime and on the specific VOC and will affect the efficiency of the overall process.

It is well known that different corona regimes are characterized by different distributions in density, energy and space of electrons and other reactive species [1–3]. It is, therefore, to be expected that for a given input energy different power supplies should produce different chemical outcomes.

To gain useful mechanistic insight into these complex reacting systems we have developed a reactor capable of sustaining different corona regimes and are using it to compare their performance in the oxidation processing of selected model VOCs [12, 14–17]. Essential for this analysis is the wealth of kinetic data available in the literature for the reactions of many VOCs with species which are present in atmospheric air plasmas, notably electrons, O atoms, OH radicals and many important atmospheric ions, the cations O_2^+, N_2^+, O^+, N^+, NO^+, the anions O^-, O_2^-, O_3^- and their hydrates. A powerful diagnostic tool in our work is the integrated analysis of dc corona current/voltage characteristics coupled with that of the ionized components of the plasma and of their reactions [15]. To this end we are using atmospheric pressure chemical ionization-mass spectrometry (APCI-MS) which interfaces a corona chamber at atmospheric pressure to a quadrupole mass analyzer. With our APCI-MS apparatus, which has a time window of about 500 μs, we can thus detect and monitor the ion population within the plasma formed from any gas mixture of desired composition (air, VOC, humidity) [15,17–22].

2. Experimental

2.1. Chemicals

Pure air used in the experiments was a synthetic mixture (80% nitrogen–20% oxygen) from Air Liquid with specified impurities of H_2O (<3 ppm) and of C_nH_m (<0.5 ppm). Air mixtures of *n*-hexane (500 ppm ± 3%), *i*-octane (500 ppm ± 2%), CF_2Br_2 (500 ppm, ±3%), CO_2 (520 ppm, ±2%) and CO (499 ppm, ±1%) were purchased from Air Liquid in cylinders loaded to a pressure lower than their respective condensation limits. Liquid samples of *n*-hexane, *i*-octane, benzene, toluene and CH_2Br_2 were the products of Aldrich (purity ⩾99%).

2.2. Experiments with the corona reactor

Corona reactor, power supplies, gas line and the apparatus used for electric and chemical diagnostics were described in detail in previous publications [12, 14, 15]. Briefly, the corona reactor is a stainless steel cylinder (38.5 mm i.d. × 600 mm) which is electrically grounded and has a stainless steel emitting wire electrode (1 mm i.d.) fixed along its axis (figure 1(*a*)). The reactor can be energized by dc or pulsed high-voltage power. The dc power supply has the following features: input voltage 0–220 V, output voltage −25 kV–+25 kV, output current 0–5 mA. The pulse power supply uses a pulsed high voltage with dc (PHVDC) bias, based on a spark gap switch with air blowing, with the following specifications: dc bias 0–14 kV (input voltage 0–100 V), peak voltage 25–35 kV with dc bias (input voltage 120–220 V), peak current 100 A, maximum frequency 300 Hz, rise-time of pulses less than 50 ns. The equipment to measure the power input includes a digital oscilloscope (Tektronix type 410A, bandwidth 200 Hz, two channels), a high voltage probe by Tektronix (ratio 1000 : 1, bandwidth 75 MHz, peak voltage 40 kV) and two homemade current probes with 10 resistors in parallel housed in an electromagnetic shield (1.1 Ω for pulsed current and 52 Ω for dc current).

As shown in the schematic drawing of figure 1(*a*), the reactor is connected to a gas flow line made of teflon tubing (4 mm i.d.). The air/VOC mixtures were purchased in cylinders or prepared by bubbling 'synthetic air' through a sample of liquid VOC and by diluting the outcoming flow with a second flow of synthetic air to achieve the desired gas composition and flow. The gas flow line is equipped with a loop for humidification and with a probe to measure the humidity. The treated gas exiting the reactor goes through a small glass reservoir equipped with a sampling port from which

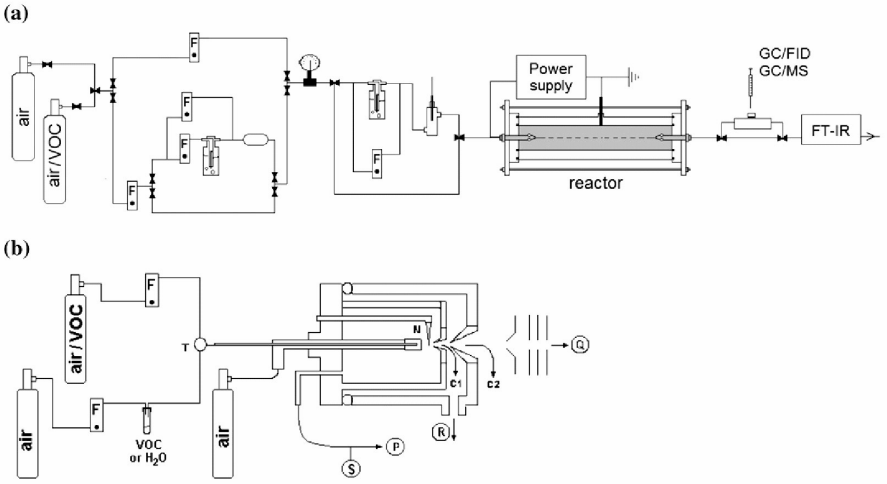

Figure 1. Schematics of the experimental apparatus: (*a*) corona reactor, gas line and diagnostics system; (*b*) APCI-mass spectrometer. Legend for symbols: F = mass flow controller; T = T-junction; P = diaphragm pump; S = septum capped sampling port; N = needle electrode at high voltage; C1 = sampling cone; C2 = skimmer cone; R = rotary pump; Q = quadrupolar mass analyzer. (Published in [32]. Permission to reproduced will be requested).

aliquots are withdrawn with a gas tight syringe for off-line chemical analysis by GC/MS (HP 5973) and GC/FID (Varian 3600). On-line IR analysis is performed with an FTIR Nicolet 5700 spectrophotometer using a 10 cm long gas cell with NaCl windows. Quantitation of ozone, CO and CO_2 was performed as described previously [12].

The reactor is used in a flow-through mode of operation. All experiments reported in this work were conducted by changing the applied voltage at a constant gas flow rate of 450 mL min^{-1} except in the case of CF_2Br_2 processing with +dc, for which a gas flow rate of 150 mL min^{-1} was used to increase the treatment time of this rather inert VOC. The determination of energy input was done as previously described for dc [12] and pulsed [14] corona, respectively. The experimental procedure and analytical protocols were the same as previously described in detail [12]. Current/voltage characteristics of dc corona were monitored in pure air and in air containing the selected VOC in 500 ppm concentration. For each applied voltage the mean current intensity was measured with a multimeter after a stabilization time of 5 min.

2.3. Analysis of ions

APCI spectra in air plasma were aquired with a TRIO 1000 II instrument (Fisons Instruments, Manchester, UK), equipped with a Fisons APCI source as described in earlier publications [18–22]. The ion source, schematically drawn in figure 1(*b*), is kept at atmospheric pressure by a flow of synthetic air (4000–5000 mL min^{-1}) introduced through the nebulizer line, a capillary of ca 2 mm i.d.. The mixture of the desired VOC in air is obtained either directly from a gas cylinder or by stripping vapours from its liquid with an auxiliary flow of synthetic air (typically 5–50 mL min^{-1}). It is then introduced into the APCI source through a capillary (i.d. = 0.3 mm) running coaxially inside the nebulizer line. A second line allows for the introduction of water vapours as desired. The needle electrode for corona discharge was kept at 3000 V. Ions leave the source through an orifice, ca 50 μm in diameter, in the counter electrode (the 'sampling cone', held at 0–150 V relative to ground), cross a region pumped down to ca 10^{-2} Torr and, through the orifice in a second conical electrode (the 'skimmer cone', kept at ground potential), reach the low pressure region hosting the focusing lenses and the quadrupole analyzer. Prior to the introduction of the organic compound, a preliminary analysis is routinely conducted to monitor the 'background' spectra with only air (or humid air) introduced into the APCI source.

3. Results and discussion

The response of CH_2Br_2 to treatment with different types of coronas is similar to that previously observed with saturated and aromatic hydrocarbons. Figure 2 shows the decay profiles of CH_2Br_2 as a function of specific input energy (SIE), i.e. the energy per unit volume (kJ L^{-1}), for processing in our reactor with +dc, −dc and +pulsed corona. Three distinct profiles are clearly evident, showing that the mode by which energy is provided to the system greatly affects the extent of chemical reaction. Thus, any given input of specific energy produces an extent of CH_2Br_2conversion ([CH_2Br_2]/[$CH_2Br_2]_0$), which depends on the corona regime and decreases in the order +pulsed > −dc > +dc. Quantitatively, the process efficiency is conveniently expressed by k_E, the energy constant derived by interpolation of the experimental data with equation (1).

$$[CH_2Br_2] = [CH_2Br_2]_0 e^{-k_E SIE}. \quad (1)$$

The following k_E values are thus obtained for CH_2Br_2 (in L kJ^{-1} units): 0.98, 0.21 and 0.064 for +pulsed, −dc and +dc,

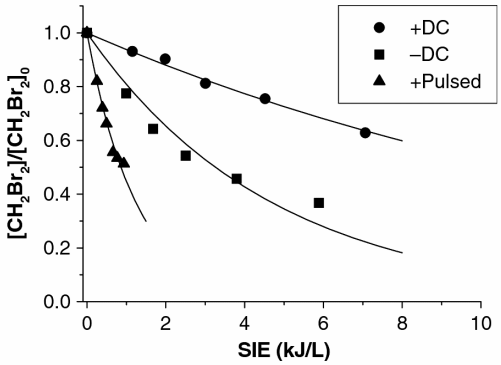

Figure 2. Removal efficiency of CH_2Br_2 (500 ppm in dry air) by different types of corona at room temperature and pressure.

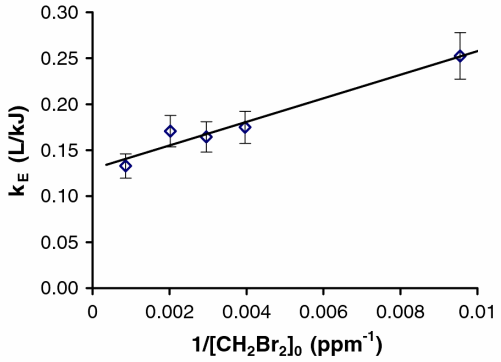

Figure 3. Removal efficiency (k_E) for CH_2Br_2 processing with −dc in dry air as a function of CH_2Br_2 initial concentration, $[CH_2Br_2]_0$.

respectively. It should be noted that k_E depends not only on the specific corona regime, which in turn depends on structural reactor parameters such as configuration, material composition and size of the electrodes, interelectrode distance and more, but also on the VOC type and on its initial concentration $[VOC]_0$ [1–4]. Therefore, a meaningful comparison of different corona regimes, such as dc versus pulsed and positive versus negative polarity, can only be made using the same reactor, as done in this work, and the same $[VOC]_0$. The effect of VOC initial concentration on process efficiency is clearly evident in the plot of figure 3 which reports k_E data as a function of $1/[VOC]_0$ for CH_2Br_2 processing with −dc corona. A linear dependence as shown in figure 3 was previously observed by other researchers in different experiments [23, 24] and explained by a mechanism of inhibition by products which compete with the VOC for the plasma reactive species involved in the initiation step [23]. Such mechanism can be crudely approximated to the three reactions shown in scheme 2 [20]. The first step represents the production of the reactive species, A, from the buffer gas G. The reactive species A attacks the VOC molecule to form an intermediate product I (ii), which in turn can react with A, thus competing with step (ii). For example, in the methane oxidation cited in the introduction, A could be the OH radical and I the $CH_2 = O$ oxidation intermediate.

$$G \rightarrow A, \qquad \text{(i)}$$

$$A + VOC \rightarrow I + \text{other products}, \qquad k_1, \qquad \text{(ii)}$$

$$I + A \rightarrow Z + \text{other products}, \qquad k_2. \qquad \text{(iii)}$$

Scheme 2.

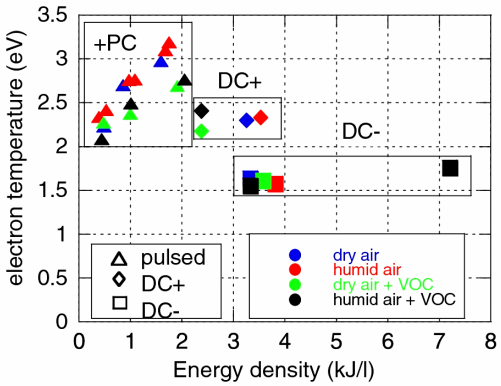

Figure 4. Electron temperature T_e as a function of energy density for different coronas and gas compositions. VOC was hexane (500 ppm). +PC stands for positive pulsed corona. (Published in [16]. Permission to reproduce is enclosed).

The kinetic expressions derived for such reaction scheme [23] are (2) and (3):

$$\frac{d[A]}{dt} = S - k_1[A][VOC] - k_2[A][I], \qquad (2)$$

$$\frac{d[VOC]}{dt} = -k_1[A][VOC], \qquad (3)$$

where S is the rate of formation of A. By assuming that A is in the stationary state, i.e. $d[A]/dt = 0$, that k_1 is similar to k_2, and that $[Z] \ll [I]$, as in the process initial stages, so that $[VOC]_0 = [VOC] + [I]$, then the differential equations are integrated to provide the kinetic expression (4)

$$[VOC] = [VOC]_0 e^{(-S/[VOC]_0 t)} = [VOC]_0 e^{(-k_E SIE)}. \qquad (4)$$

which predicts that k_E depends inversely on $[VOC]_0$ and directly on S, the rate of formation of the reactive species A [23].

The reasonably good fit of the experimental points to a linear trend shown in figure 3 suggesting that the approximations made are reasonable within the scope of the experimental conditions tested for CH_2Br_2 processing in this study. Much of the following discussion will focus on the identity of the process initiation step and of the reactive species A in the case of different VOCs and of different corona regimes.

The observed greater efficiency of +pulsed corona with respect to dc corona of either polarity is consistent with the results of a previous emission spectroscopy investigation on the same reactor which provided a map of the average electron temperature (figure 4) and of the relative densities of excited O atom (figure 5) as a function of SIE and corona

type [16]. Figure 4 shows that at any SIE a significantly greater average electron energy is obtained with +pulsed corona than with dc coronas. Correspondingly, a greater density of excited O atoms is also observed with +pulsed corona than with dc coronas (figure 5). It is well known that, due to the filamentary nature of the streamers of +pulsed corona, not only the energy but also the spatial distribution of electrons (and of other short-lived reactive species) is very different from that in glow dc coronas: the plasma occupies a relatively larger volume thus accounting for a more efficient process.

The response of CH_2Br_2 to the presence of humidity in the feed gas is also similar to that previously observed with hydrocarbons [12, 17]. The data in table 1 show that for CH_2Br_2 as well as for *i*-octane and toluene previously studied, humidity has opposite effects on the process efficiency depending on the discharge polarity: it produces an increase in efficiency with –dc corona and a decrease in efficiency with +dc corona.

The effect of humidity is usually attributed to OH radicals which are formed from water via electron dissociation (5) and via reaction with excited O atoms (6) [25]

$$H_2O + e^- \rightarrow OH + H + e^-, \quad (5)$$

$$O(^1D) + H_2O \rightarrow 2OH \quad (6)$$

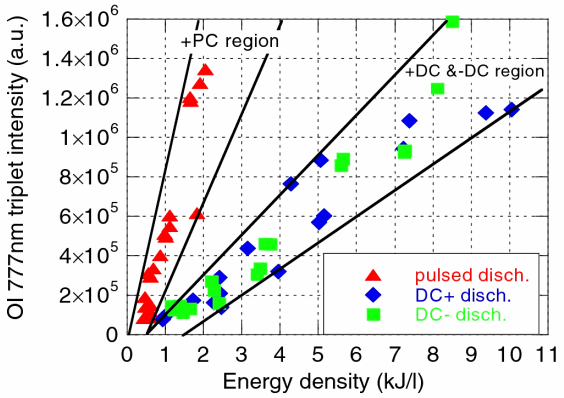

Figure 5. O I 777 nm triplet intensity in all the explored conditions of corona discharge. The distinction between +pulsed (+PC) and ±dc discharges is evident. (Published in [16]. Permission to reproduce is enclosed).

as well as, in the case of corona of positive polarity, via highly efficient ionic paths (7)–(11) [26]

$$N_2^+ + H_2O \rightarrow N_2H^+ + OH, \quad (7)$$

$$\rightarrow H_2O^+ + N_2, \quad (8)$$

$$H_2O^+ + H_2O \rightarrow H_3O^+ + OH, \quad (9)$$

$$O_2^+ + H_2O + M \rightarrow O_2^+(H_2O) + M, \quad (10)$$

$$O_2^+(H_2O) + H_2O \rightarrow H_3O^+ + OH + O_2. \quad (11)$$

Thus, the increase in efficiency of CH_2Br_2 and of hydrocarbon processing observed with −dc in humid air is attributed to the presence of OH radicals which are known to react very efficiently with hydrocarbons, such as with *i*-octane (12) [11c],

$$i - C_8H_{18} + OH \rightarrow \text{products}$$

$$k = 3.34 \times 10^{-12}\,\text{cm}^3\,\text{molecule}^{-1}\,\text{s}^{-1} \quad (T = 298\,\text{K}) \quad (12)$$

and with CH_2Br_2 (13) [27]

$$CH_2Br_2 + OH \rightarrow \text{products}$$

$$k = 1.1 \times 10^{-13}\,\text{cm}^3\,\text{molecule}^{-1}\,\text{s}^{-1} \quad (T = 298\,\text{K}) \quad (13)$$

via H-abstraction to form H_2O and an organic carbon radical.

In dry air similar reactions can be performed by ground state atomic oxygen, although much less efficiently. Thus, for *i*-octane a rate constant of $9.13 \times 10^{-14}\,\text{cm}^3\,\text{molecule}^{-1}\,\text{s}^{-1}$ ($T = 307\,\text{K}$) is reported for reaction with $O(^3P)$ [28], which is 37 times smaller than that with OH. Similar k_{OH}/k_O ratios also apply for other hydrocarbons, such as hexane and toluene, for which we found that processing with –dc is promoted by the presence of humidity in the air [10, 14]. No data are available for the reaction of $O(^3P)$ with CH_2Br_2, but it is reasonably expected to be similarly slower than reaction with OH.

Support for the conclusion that reaction with OH is important in −dc corona oxidation of CH_2Br_2 and of hydrocarbons comes from the results obtained with CF_2Br_2, halon 1202. Like any other perhalogenated saturated hydrocarbon, including the chlorofluorocarbons (CFCs) and the perfluoroalkanes, halons are notoriously inert towards OH and other atmospheric radicals. The persistence of such compounds has caused environmental problems due to their photolysis in the stratosphere and consequent catalytic destruction of ozone [10]. Specifically, the reaction of CF_2Br_2

Table 1. Efficiency data (k_E, in L kJ^{-1} units) of VOC processing by −dc and +dc corona in dry and humid air (40% RH)[a,b].

		CH_2Br_2	*i*-octane [12]	Toluene [17]	CF_2Br_2
−Dc	Dry	2.1×10^{-1}	4.2×10^{-1}	4.1×10^{-1}	1.4×10^{-1}
	Humid	2.6×10^{-1}	7.5×10^{-1}	8.1×10^{-1}	1.1×10^{-1}
	k_{humid}/k_{dry}	1.2	1.8	2.0	0.79
+Dc	Dry	6.4×10^{-2}	1.3×10^{-1}	1.4×10^{-1}	4.5×10^{-2}
	Humid	5.1×10^{-2}	1.2×10^{-1}	1.3×10^{-1}	3.9×10^{-2}
	k_{humid}/k_{dry}	0.80	0.92	0.93	0.87

[a] This work, unless otherwise specified.
[b] VOC intial concentration was 500 ppm.

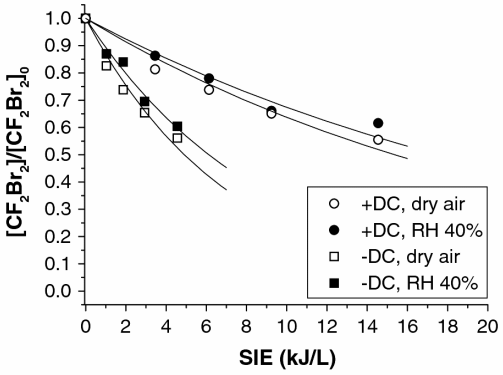

Figure 6. Removal efficiency of CF_2Br_2 (500 ppm) by +dc and −dc corona in dry and in humid (40% RH) air at room temperature and pressure.

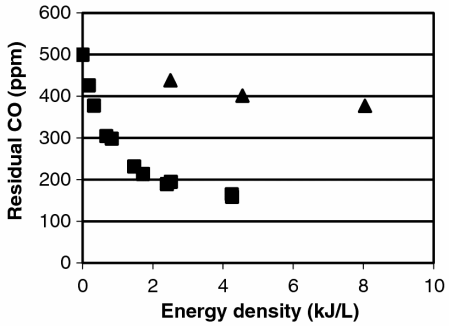

Figure 7. Conversion of CO (500 ppm in humid air, $RH = 40\%$) as a function of energy density in experiments with −dc (■) and +dc (▲) corona. (Published in [15]. Permission to reproduce is enclosed).

with OH (14) is more than 220 times slower [27] than that of CH_2Br_2.

$$CF_2Br_2 + OH \rightarrow \text{products}$$

$$k = 5 \times 10^{-16}\,\text{cm}^3\,\text{molecule}^{-1}\,\text{s}^{-1} \quad (T = 298\,\text{K}). \tag{14}$$

Expectedly, there is no efficiency enhancement for −dc processing of CF_2Br_2 in the presence of humidity (figure 6 and table 1). Quite the opposite, a slight decrease in the efficiency is instead observed with respect to dry air, which is attributed to reaction (5). Notably reaction (5) contributes to reduce the average electron energy while producing a species, OH, which is unable to attack this specific VOC.

Less straightforward to explain is the decrease in efficiency observed with +dc for the hydrocarbons and for CH_2Br_2 (table 1), since these compounds do react with OH radicals. To make sure that OH radicals are present in the +dc induced plasma and to compare their density in +dc and −dc plasmas we applied a chemical probe [29] based on the well-known reaction of OH with CO to form CO_2 (15) [30].

$$CO + OH \rightarrow CO_2 + H$$

$$k = 2.28 \times 10^{-13}\,\text{cm}^3\,\text{molecule}^{-1}\,\text{s}^{-1} \quad (T = 296\,\text{K}). \tag{15}$$

In a control experiment we found that, as expected, in dry air CO does not react under the effect of either +dc or −dc corona. In contrast, in humid air (40% RH) reaction (15) occurs under the effect of both –dc and of +dc (figure 7), thus proving the presence of OH radicals in such plasmas. Since with +dc reaction of hydrocarbons and of CH_2Br_2 is less efficient in the presence of OH radicals than it is in dry air, it is concluded that reaction with OH radicals is not the dominant initiation channel for their oxidation in +dc corona. Moreover one can conclude that reaction with O atoms is also not a major initiation route with +dc corona, since their transformation into the more reactive OH radicals should increase the efficiency of CH_2Br_2 decomposition and not decrease it as found in our experiments. Electron interaction is a viable channel for CH_2Br_2 (16), requiring 2.75 eV. This route is also available for −dc processing.

$$CH_2Br_2 + e^- \rightarrow CH_2Br + Br + e^-. \tag{16}$$

Water is expected to inhibit this reaction by competing for the electrons in a process, (5), which, however, produces OH radicals and thus promotes reaction (13). The net balance between such opposing effects is difficult to predict, but it is unlikely that it should operate in such a way so as to slow down the decomposition of CH_2Br_2 with +dc and to enhance it with −dc. As proposed earlier for hydrocarbons [15, 17], a more reasonable possibility is initiation via ion–molecule reactions, of which direct evidence is found in the analysis of ions within the plasma conducted via APCI-mass spectrometry. Figure 8 shows the positive ion mass spectra recorded with pure air (figure 8(*a*)) and with air containing CH_2Br_2 in 500 ppm concentration (figure 8(*b*)). The spectra are very different and reflect the different ion populations in pure air and in CH_2Br_2-containing air plasmas. As described earlier [15,18–22] the major ions in pure air are $H_3O^+(H_2O)_n$ (n = 2–3: m/z 55,73) and $NO^+(H_2O)_n$ (n = 0–2; m/z 30, 48 and 66) (figure 8(*a*)). In contrast major ions observed in air containing CH_2Br_2 (500 ppm) are $CH_2Br_2^+$ and CH_2Br^+, seen here as ion–molecule complexes with a neutral CH_2Br_2 molecule (figure 8(*b*)). Such ions are most likely formed via charge transfer (17) and dissociative charge transfer (18) reactions with O_2^+, which are both exothermic processes and are expected to be highly efficient [31].

$$O_2^+ + CH_2Br_2 \rightarrow O_2 + CH_2Br_2^+$$

$$\Delta H = -152.3\,\text{kJ mol}^{-1}, \tag{17}$$

$$O_2^+ + CH_2Br_2 \rightarrow O_2 + CH_2Br^+ + Br$$

$$\Delta H = -116.4\,\text{kJ mol}^{-1}. \tag{18}$$

Corona current is due to ion transport across the drift region of the interelectrode gap and depends on the mobility of the ions. Since the ions detected in CH_2Br_2-containing air have different compositions, sizes and shapes from those detected in pure air, it is reasonably expected that they should also have different mobilities and thus produce different

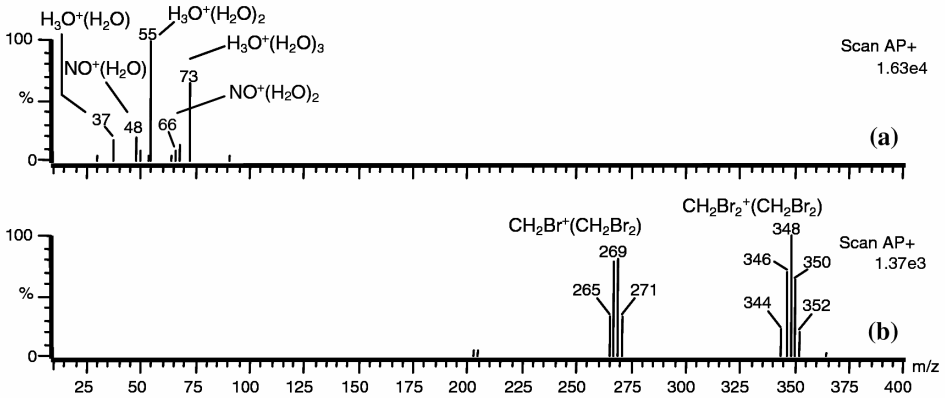

Figure 8. Positive ion APCI-mass spectra obtained at ambient temperature and pressure with: (*a*) pure air, (*b*) CH_2Br_2 500 ppm in air.

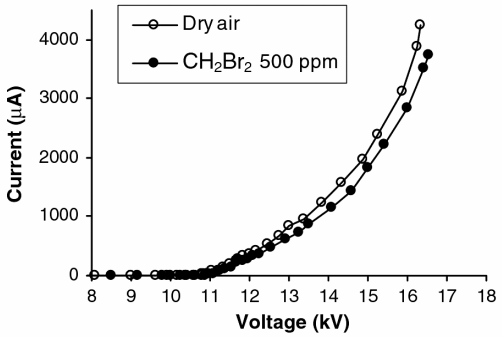

Figure 9. Current/voltage characteristics for +dc corona in pure air and in air containing CH_2Br_2 500 ppm.

current/voltage characteristics. This is indeed the case, as shown in figure 9 which compares corona current/voltage characteristic measured for +dc corona in pure air and in air containing 500 ppm of CH_2Br_2. It is seen that the current detected in CH_2Br_2-containing air is significantly lower than in pure air indicating that the average ion mobility is lower in CH_2Br_2-containing air than in pure air.

Thus, trace amounts (500 ppm) of CH_2Br_2 produce major effects on the ion population formed by +dc in air and, consequently, on the corona current/voltage characteristic. This behaviour is very similar to that previously observed with hydrocarbons, notably hexane [15], *i*-octane [15], toluene [17] and benzene [32]. Such observations, combined with the evidence presented above that OH radicals do not take part in the rate limiting initiation of hydrocarbon oxidation by +dc corona, suggest that ion–molecule reactions play an important role in these processes.

In contrast to hydrocarbons, CH_2Br_2 also produces many negative ions in −dc corona. As shown in figure 10, the spectra of pure air (*a*) and of CH_2Br_2-containing air (*b*) are quite different due to major signals in the latter due to Br^- and to various ion–neutral complexes thereof. The favourable effect of humidity on the efficiency of −dc corona processing of CH_2Br_2, however, is not consistent with a decomposition mechanism proceeding via negative ion chemistry. This conclusion is based on the observation that in the presence of humidity ions form hydrate complexes ('solvated' ions) [15,19–21], which are less reactive than the 'naked' ions, and should therefore reduce and not increase the process efficiency. The greater efficiency in humid air supports instead the proposal of a radical mechanism initiated by reaction with OH radicals.

Other major differences between CH_2Br_2 and hydrocarbons concern the products detected in the plasma processed gas. Figure 11 reports FTIR spectra of pure air (figure 11(*a*)), air plus 500 ppm of toluene (figure 11(*b*)) and air plus 500 ppm of CH_2Br_2 (figure 11(*c*)) processed under the same experimental conditions. Thus, while for CH_2Br_2 the only C-containing products detected are CO and CO_2, for toluene formic acid, an oxidation intermediate, is also observed. Moreover, it is seen that ozone, a major product in the experiment with pure air, is less abundant in the toluene experiment [17], and is not detected at all in the CH_2Br_2 experiment. Conversely, the amounts of HNO_3 and N_2O formed in this experiment appear to be greater than in the toluene experiment. These results can be explained considering the known reactions involving Br atoms, ozone and NO_x which are summarized in scheme 3 [10].

Cycles I and II are responsible for the efficient conversion of 'odd' oxygen species (O and O_3) into 'even' oxygen (O_2) mediated by reaction of the highly reactive species Br and BrO which act as chain propagators. In nature such cycles occur in the stratosphere and are involved in the depletion of the ozone layer. They are very efficient, a single Br atom catalyzing the destruction of up to 10^6 molecules of ozone in the stratosphere prior to being quenched by a termination reaction [10].

Within our corona reactor Br atoms can form directly from CH_2Br_2 by way of reaction with electrons (16) and, in positive corona, with positive ions (18). In addition, Br atoms are formed in a number of secondary reactions initiated by the bromomethyl radical, CH_2Br, and by the dibromethyl radical, $CHBr_2$, as shown in scheme 4.

The reaction sequence of scheme 4 reproduces the well-known oxidation route of organic radicals in air shown in the introduction (scheme 1), but also contains additional features due to the presence of bromine in the organic radicals.

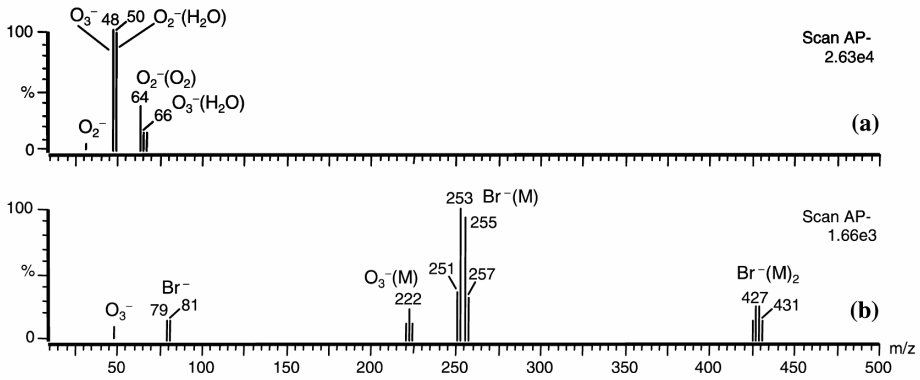

Figure 10. Negative ion APCI-mass spectra obtained at ambient temperature and pressure with: (*a*) pure air, (*b*) CH_2Br_2 500 ppm in air.

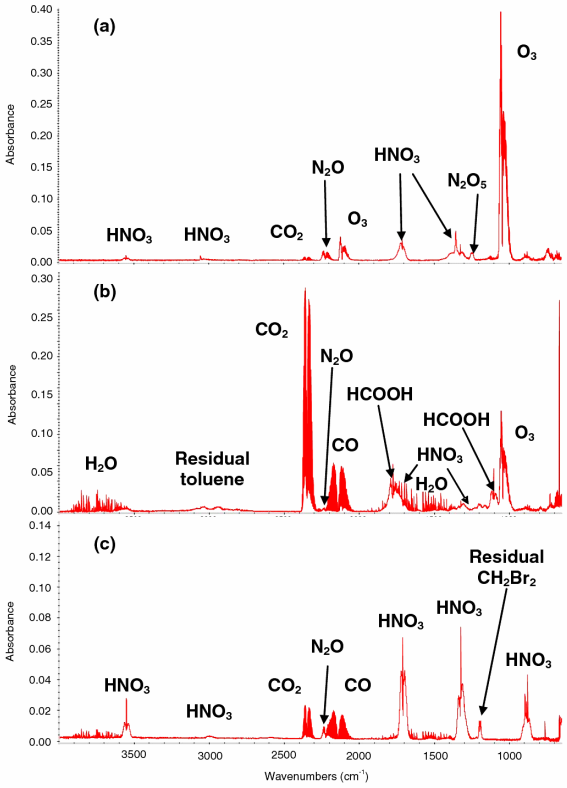

Figure 11. FTIR spectra of the gas flowing out of the reactor after processing with −dc corona at −19 kV. The feed gas was (*a*) pure air; (*b*) air containing toluene (500 ppm) and (*c*) air containing CH_2Br_2 (500 ppm).

Specifically, the decay of radicals $CHBr_2O$ and CH_2BrO via C-Br bond dissociation shown in scheme 4 is supported by the results of experimental and theoretical investigations showing that there is no appreciable barrier to dissociation [33–36].

As for the NO_x species, the formation of NO in corona induced air atmospheric plasmas is well documented and supported by detection of NO^+ in our APCI-MS experiments with +dc corona. In the presence of Br atoms the NO to NO_2 oxidation is strongly promoted via cycle II of scheme 2.

In turn NO_2 can react to form HNO_3 according to reaction (19)

$$NO_2 + OH + M \rightarrow HNO_3 + M \qquad (19)$$

and, in the presence of Br atoms, also via reactions (20)–(21)

$$NO_2 + BrO + M \rightarrow BrONO_2 + M, \qquad (20)$$

$$BrONO_2 + H_2O \rightarrow HNO_3 + HBrO. \qquad (21)$$

NO_2 is also a precursor, by way of reaction (22), of N_2O, the stable nitrogen oxide which is detected among the products of air plasma treatments (figure 11).

$$NO_2 + N \rightarrow N_2O + O. \qquad (22)$$

4. Conclusions

Trace amounts of organic compounds (VOCs) produce quite dramatic effects on the composition of plasmas produced by corona discharges in air at atmospheric pressure. Such effects are largely VOC-specific and can be rationalized on the basis of known properties of the organic compound which can then be used as molecular probes. One feature of the plasma which is drastically affected is its ion population: different ions are observed depending on the specific VOC used, albeit in very low relative concentrations. Thus, while in pure air +dc plasma the major ions are $H_3O^+(H_2O)_n$ and $NO^+(H_2O)_n$, in air containing hexane or *i*-octane various $C_nH^+_{2n+1}$ carbon ions are the prevailing ionized species [15, 18]; in air containing toluene (T), mostly ionized (T^+) and protonated (TH^+) toluene are detected [17] and in air containing CH_2Br_2, the ions are mostly $CH_2Br_2^+$ and CH_2Br^+. Such different ion populations reflect in VOC-specific current–voltage characteristics. Ion analysis therefore provides a rationale to interpret current–voltage profiles of coronas at the molecular level.

Neutral products and intermediates of air plasmas are likewise greatly affected by the presence of very small amounts of a specific VOC. Thus, no ozone was detected in the treated gas when air containing 500 ppm CH_2Br_2 was processed in

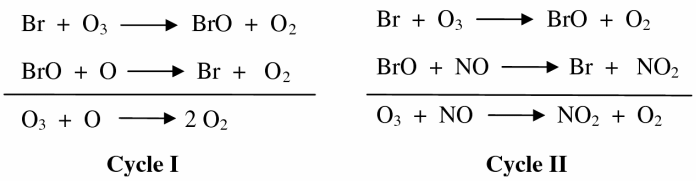

Scheme 3.

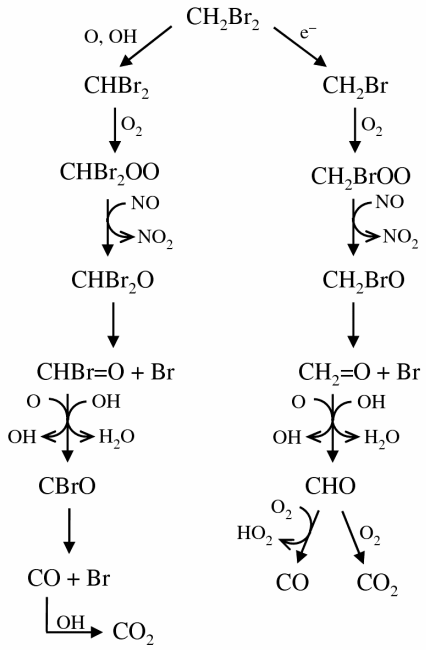

Scheme 4.

the corona reactor, as a consequence of the very efficient catalytic cycles leading to ozone destruction, in which Br atoms are propagating species. NO also enters one such cycle to be oxidized to NO_2, thus accounting for the production of significant amounts of HNO_3 in these experiments.

It is becoming increasingly evident that besides energy efficiency, product selectivity is a most important process feature which needs to be optimized in corona induced removal of organic pollutants from air. The study of the reactions and mechanisms of VOC-oxidation induced by corona in air at atmospheric pressure reveals a great variety of chemical behaviours depending on VOC type, corona regime and other experimental conditions, notably the presence and extent of humidity in the air. Such findings will hopefully be useful for the advancement of plasma-based depuration technologies.

Acknowledgments

The authors thank Marta Dal Molin for performing some of the experiments during her undergraduate thesis. Financial support by the University of Padova (PRAT 2005) is gratefully acknowledged.

References

[1] Van Veldhuizen E M 2000 *Electrical Discharges for Environmental Purposes: Fundamentals and Applications* (New York: Nova Science Publishers)
[2] Fridman A 2008 *Plasma Chemistry* (Cambridge: Cambridge University Press)
[3] Kim H-H 2004 *Plasma Process. Polym.* **1** 91
[4] Penetrante B M 1993 *Nonthermal Plasma Techniques for Pollution Control* (New York: Springer)
[5] Mizuno A 2007 *Plasma Phys. Control. Fusion* **49** A1
[6] Odic E, Paradisi C, Rea M, Parissi L, Goldman A and Goldman M 1999 *The Modern Problems of Electrostatics with Applications in Environment Protection* (Bucharest: Springer) pp 143–60
[7] Urashima K and Chang J-S 2000 *IEEE Trans. Dielectr. Electr. Insul.* **7** 602
[8] Hakoda T, Matsumoto K, Mizuno A, Kojima T and Hirota K 2008 *Plasma Chem. Plasma Process.* **28** 25
[9] Van Durme J, Dewulf J, Leys C and Van Langenhove H 2008 *Appl. Catal. B: Environ.* **78** 324
[10] Seinfeld J H and Pandis S N 1998 *Atmospheric Chemistry and Physics* (New York: Wiley-Interscience)
[11] (a) Atkinson R 1998 *Pure Appl. Chem.* **70** 1327
(b) Atkinson R 2000 *Atmos. Environ.* **34** 2063
(c) Atkinson R 2003 *Atmos. Chem. Phys.* **3** 2233
[12] Marotta E, Callea A, Rea M and Paradisi C 2007 *Environ. Sci. Technol.* **41** 5862
[13] Tosi P, Ascenzi D, Franceschi P and Guella G 2009 *Plasma Sources Sci. Technol.* **18** 034005
[14] Marotta E, Callea A, Ren X, Rea M and Paradisi C 2007 *Int. J. Plasma Environ. Sci. Technol.* **1** 39
[15] Marotta E, Callea A, Ren X, Rea M and Paradisi C 2008 *Plasma Process. Polym.* **5** 146
[16] Zaniol B, Schiorlin M, Gazza E, Marotta E, Ren X, Puiatti M E, Rea M, Sonato P and Paradisi C 2008 *Int. J. Plasma Environ. Sci. Technol.* **2** 65
[17] Schiorlin M, Marotta E, Rea M and Paradisi C submitted AQ2
[18] Marotta E and Paradisi C 2009 *J. Am. Soc. Mass Spectrom.* **20** 697
[19] Marotta E, Scorrano G and Paradisi C 2005 *Plasma Process. Polym.* **2** 209
[20] Donò A, Paradisi C and Scorrano G 1997 *Rapid Commun. Mass Spectrom.* **11** 1687
[21] Nicoletti A, Paradisi C and Scorrano G 2001 *Rapid Commun. Mass Spetrom.* **15** 1904
[22] Marotta E, Bosa E, Scorrano G and Paradisi C 2005 *Rapid Commun. Mass. Spectrom.* **19** 391
[23] Slater C and Douglas-Hamilton D H 1981 *J. Appl. Phys.* **52** 5820
[24] Rudolph R, Francke K P and Miessner H 2002 *Plasma Chem. Plasma Process.* **22** 401
[25] Herron J T and Green D S 2001 *Plasma Chem. Plasma Process.* **21** 459
[26] Sieck L W, Herron J T and Green D S 2000 *Plasma Chem. Plasma Process.* **20** 235

[27] Lias S G 2006 Ionization energy evaluation *NIST ChemistryWebBook, NIST Standard Reference Database No 69* ed W G Maillard and P J Linstrom (Gaithersburg MD: National Institute of Standards and Technology) http://webbook.nist.gov/chemistry/
[28] Herron J T 1988 *J. Phys. Chem. Ref. Data* **17** 967
[29] Su Z-Z, Ito K, Takashima K, Katsura S, Onda K and Mizuno A 2002 *J. Phys. D: Appl. Phys.* **35** 3192
[30] Atkinson R, Cox R A, Crowley J N Jr, Hampson R F, Hynes R G, Jenkin M E, Kerr J A, Rossi M J and Troe J 2006 *Summary of Evaluated Kinetic and Photochemical Data for Atmospheric Chemistry. Section II—Organic Reactions. Data sheet HOx_VOC10* http://www.iupac-kinetic.ch.cam.ac.uk/
[31] (a) Spanel P and Smith D 1999 *Int. J. Mass Spectrom.* **189** 213
(b) Spanel P and Smith D 1999 *Int. J. Mass Spectrom.* **184** 175
[32] Marotta E, Schiorlin M, Rea M and Paradisi C *Industrial Plasma Technology* (Weinheim: Wiley) at press
[33] Orlando J J, Tyndall G S, Wallington T J and Dill M 1996 *Int. J. Chem. Kinet.* **28** 433
[34] (a) Chen J, Young V, Catoire V and Niki H 1996 *J. Phys. Chem.* **100** 6580
(b) Chen J, Young V, Catoire V and Niki H 1995 *Chem. Phys. Lett.* **245** 519
[35] McGivern W S, Kim H, Francisco J S and North S W 2004 *J. Phys. Chem.* A **108** 7247
[36] Bayes K D, Friedl R R and Sander S P 2005 *J. Phys. Chem.* A **109** 3045

4.2 COMPARISON OF TOLUENE REMOVAL IN AIR AT ATMOSPHERIC CONDITIONS BY DIFFERENT CORONA DISCHARGES

Environ. Sci. Technol. 2009 43, 9386–9392

Comparison of Toluene Removal in Air at Atmospheric Conditions by Different Corona Discharges

MILKO SCHIORLIN,[†] ESTER MAROTTA,[†] MASSIMO REA,[‡] AND CRISTINA PARADISI*,[†]

Department of Chemical Sciences, and Department of Electrical Engineering, Università di Padova, 35131 Padova, Italy

Received August 1, 2009. Revised manuscript received October 9, 2009. Accepted October 20, 2009.

Different types of corona discharges, produced by DC of either polarity (±DC) and positive pulsed (+pulsed) high voltages, were applied to the removal of toluene via oxidation in air at room temperature and atmospheric pressure. Mechanistic insight was obtained through comparison of the three different corona regimes with regard to process efficiency, products, response to the presence of humidity and, for DC coronas, current/voltage characteristics coupled with ion analysis. Process efficiency increases in the order +DC < −DC < +pulsed, with pulsed processing being remarkably efficient compared to recently reported data for related systems. With −DC, high toluene conversion and product selectivity were achieved, CO_2 and CO accounting for about 90% of all reacted carbon. Ion analysis, performed by APCI−MS (Atmospheric Pressure Chemical Ionization−Mass Spectrometry), provides a powerful rationale for interpreting current/voltage characteristics of DC coronas. All experimental findings are consistent with the proposal that in the case of +DC corona toluene oxidation is initiated by reactions with ions ($O_2^{+\bullet}$, H_3O^+ and their hydrates, NO^+) both in dry as well as in humid air. In contrast, with −DC no evidence is found for any significant reaction of toluene with negative ions. It is also concluded that in humid air OH radicals are involved in the initial stage of toluene oxidation induced both by −DC and +pulsed corona.

1. Introduction

Nonthermal plasma is currently viewed as an important entry in the field of environmental control for air purification, especially for the removal of diluted volatile organic compounds (VOCs) (*1*−*5*). In nonthermal plasmas (NTPs), which are conveniently produced by electric corona discharges in air at atmospheric pressure, high energy electrons induce ionization, excitation, and dissociation of the bulk gas molecules (N_2 and O_2), producing excited molecules, atoms, ions, and radicals, as well as thermalized electrons. VOC molecules which are present, albeit highly diluted, in the air are then efficiently intercepted by one or more of such reactive species and enter a sequence of reactions leading eventually to their oxidation. Depending on the reacting species, different initiation steps will occur: excitation, bond dissociation, atom abstraction, radical addition, electron attachment, charge transfer, and ion−molecule reactions. From the vast scientific literature on this subject the general consensus emerges that the prevailing initiation steps involve electron induced bond dissociation or attack by O atoms in dry air and of OH radicals in ambient humid air. However, a few reports have pointed out that under some conditions ionic reactions might indeed prevail (*6*−*12*).

Different initiation steps have in common the production of VOC-derived radicals. Such organic radicals (R•) are then trapped by molecular oxygen to form a peroxy radical (ROO•) which is in turn reduced to the corresponding oxy radical (RO•), as is well-known from atmospheric chemistry studies (*13*). Subsequent reactions of such oxy radicals either via hydrogen abstraction by molecular oxygen and/or (isomerization and) fragmentation lead to carbonyl derivatives, notably aldehydes and ketones. In turn these carbonyl intermediates suffer the same fate and eventually form the ultimate oxidation product, CO_2 (*13*). Recent developments in VOC plasma processing concern various combinations of NTP with heterogeneous catalysts to achieve better energy efficiency and product selectivity (*14, 15*).

Despite the numerous well-established applications of NTP and the important recent technological advancements in the field of plasma assisted catalysis, fundamental knowledge of the underlying chemical processes is still unsatisfactory: product analysis and mass balance data are not often available and the reactions and mechanisms involved in VOCs decay are far from being well understood and characterized. With the intent to gain insight into the chemistry of corona induced VOC abatement, especially with regard to the crucial initiation steps, we have recently undertaken studies of the processing of model hydrocarbons with different types of corona but otherwise under identical experimental conditions. To this end a corona reactor of wire/cylinder configuration was built, which can be energized with DC or with pulsed voltage of either polarity, and standard protocols were developed for chemical and electrical diagnostics for VOC processing in this system (*7, 16, 17*). With this experimental apparatus we are exploring the chemistry of some model VOCs under different energization conditions and interpreting the results on the basis of known chemical and physical features pertaining to the ensuing specific corona regimes. Detection and monitoring of reactive species, both neutral (*18*) and ionized (*7*−*9, 19*), has been most informative to this end.

The investigation is now being extended to different families of VOCs to evaluate and interpret the effect of chemical structure on the oxidation process within NTP generated under different corona regimes. In this paper we report and discuss the oxidation of toluene, one of the environmentally most important aromatic hydrocarbons, in dry and humid air using −DC, +DC, and +pulsed corona discharges. Specifically, we used APCI−MS (Atmospheric Pressure Chemical Ionization−Mass Spectrometry) (*7*−*9, 19*) to investigate ions and ionic reactions within the corona induced NTP. The interpretation of the results is greatly aided by the wealth of kinetic and product data available in the literature on the gas phase reactions of toluene with electrons and many of the reactive species, neutral as well as ionized ones, formed in air NTPs. Moreover toluene has been a favorite model in testing and comparing the performance of different experimental set-ups for NTP and plasmochemical VOC processing (*15, 20*−*25*). In particular, detailed accounts have appeared on the products, both gaseous and particles, formed from toluene NTP processing under various experi-

* Corresponding author e-mail: cristina.paradisi@unipd.it; tel.: +39 049 827 5661; fax: +39 049 827 5239.
† Department of Chemical Sciences.
‡ Department of Electrical Engineering.

10.1021/es9021816 CCC: $40.75
Published on Web 11/09/2009

mental conditions (*23, 26*). Although there are a great number of reports dealing with toluene nonthermal plasma processing and more generally with a comparison of different types of experimental reactors and conditions (*27–29*), this is, to the best of our knowledge, the first study in which the response of toluene to treatment with three different types of corona was investigated within a common reactor and under otherwise identical experimental conditions.

2. Experimental Section

The experimental apparatus was described in detail previously (*16*). Briefly, the corona reactor is a stainless steel cylinder (38.5 mm i.d. × 600 mm) that is electrically grounded and has a stainless steel emitting wire electrode (1 mm i.d.) fixed along its axis. The reactor can be energized by DC or pulsed high-voltage power. The DC power supply has the following features: input voltage 0–220 V, output voltage −25 kV to +25 kV, output current 0–5 mA. The pulse power supply uses a pulsed high voltage with DC bias (PHVDC), based on a spark gap switch with air blowing, with the following specifications: DC bias 0–14 kV (input voltage 0–100 V), peak voltage 25–35 kV with DC bias (input voltage 120–220 V), peak current 100 A, maximum frequency 300 Hz, rise-time of pulses less than 50 ns. The equipment to measure the power input includes a digital oscilloscope (Tektronix type 410A, bandwidth 200 Hz, two channels), a high voltage probe by Tektronix (ratio 1000:1, bandwidth 75 MHz, peak voltage 40 kV), and two homemade current probes with 10 resistors in parallel housed in an electromagnetic shield (1.1 Ω for pulsed current and 52 Ω for DC current).

The reactor is connected to a gas flow line made of Teflon tubing (4 mm i.d.). The air/toluene mixture is prepared by bubbling "synthetic air" (80% nitrogen:20% oxygen from Airliquide) through a sample of liquid toluene and by diluting the outcoming flow with a second flow of synthetic air to achieve the desired gas composition and flow (500 ppm of toluene, 450 mL·min^{-1}). The gas flow line is equipped with a loop for humidification and a probe to measure the humidity. The treated gas exiting the reactor goes through a small glass reservoir equipped with a sampling port from which aliquots are withdrawn with a gastight syringe for off-line chemical analysis by GC/MS (HP 5973) and GC/FID (Varian 3600). Online IR analysis is performed with an FTIR Nicolet 5700 spectrophotometer using a 10 cm long gas cell with NaCl windows. Quantitation of ozone, CO, and CO_2 was performed as described previously (*16*).

All experiments were run at a constant gas flow rate by changing the specific input energy, SIE, the energy per unit volume. For any given experimental condition with regard to gas composition and type of corona, the efficiency of the process was measured by monitoring the amount of residual toluene as a function of SIE. The SIE was determined as described previously for DC (*16*) and pulsed (*17*) corona, respectively. The experimental procedure and analytical protocols were the same as described previously in detail (*16*).

Current/voltage characteristics of DC corona were monitored both in the presence and in the absence of the hydrocarbon. For each applied voltage the mean current intensity was measured with a multimeter after a stabilization time of 5 min.

APCI mass spectra in an air plasma were acquired with a TRIO 1000 II instrument (Fisons Instruments, Manchester, U.K.), equipped with a Fisons APCI source as described in earlier publications (*8, 9*). The ion source is kept at atmospheric pressure by a flow of synthetic air (4000–5000 mL·min^{-1}) introduced through the nebulizer line, a capillary of ca. 2 mm i.d. Vapors of the desired VOC, stripped from a liquid sample by an auxiliary flow of synthetic air (typically 5–50 mL·min^{-1}), enter the APCI source through a capillary (i.d. = 0.3 mm) running coaxially inside the nebulizer line. A second line allows for the introduction of water vapors as desired. The needle electrode for corona discharge was kept at 3000 V. Ions leave the source through an orifice, ca. 50 μm in diameter, in the counter electrode (the "sampling cone", held at 0–150 V relative to ground), cross a region pumped down to ca. 10^{-2} Torr and, through the orifice in a second conical electrode (the "skimmer cone", kept at ground potential), reach the low pressure region hosting the focusing lenses and the quadrupole analyzer. Prior to the introduction of the organic compound, a preliminary analysis is routinely conducted to monitor the "background" spectra with only air (or humid air) introduced into the APCI source.

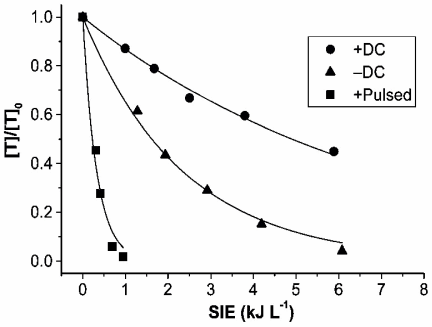

FIGURE 1. Removal efficiency of toluene (500 ppm in dry air) by different types of corona at room temperature and pressure.

3. Results and Discussion

The efficiency of a plasma process for VOC removal is measured by monitoring the VOC residual fraction ([VOC]/[VOC]$_0$) as a function of Specific Input Energy (SIE), i.e., the energy per unit volume (kJ·L^{-1}). Representative data for toluene (T) decomposition in our reactor are shown in Figure 1 for three experiments run in dry air under different corona regimes: +DC, −DC and +pulsed corona. As is typically found, the data of each experiment fit to a good approximation an exponential function (eq 1), from which the energy constant k_E is derived:

$$[T] = [T]_0 e^{-k_E^{SIE}} \quad (1)$$

It should be noted that an alternative way to describe the same function uses the fitting parameter β (*1, 2, 10*), otherwise called the characteristic energy density ϵ_0 (*23*), which is equal to $1/k_E$. For analogy with chemical kinetics we prefer to express the efficiency in terms of k_E: thus, the larger k_E, the more efficient the process, much as fast chemical reactions are characterized by large kinetic constants. Regardless of whether one uses β or k_E, however, it should be kept in mind that both depend on $[VOC]_0$, the VOC initial concentration, the process efficiency usually decreasing with increasing $[VOC]_0$ (*1, 2, 10*). Therefore the efficiency of different processes can be compared only when the same $[VOC]_0$ is used. This is the case for the experiments shown in Figure 1 for which the initial toluene concentration ($[T]_0$) was 500 ppm. It is seen that the efficiency decreases markedly in the order +pulsed > −DC > +DC. Thus, 1 kJ·L^{-1} specific input energy determines an almost quantitative conversion of toluene in pulsed corona, but only about 35% and 10% conversion in −DC and +DC corona, respectively. Relevant k_E values are summarized in Table 1 which also includes efficiency data for experiments run in humid air.

The effect of humidity is indeed of great interest since practical applications deal with ambient air which usually contains large amounts of water. Efficiency data for toluene

TABLE 1. k_E Values for Decomposition of Toluene in Air at Room Temperature and Atmospheric Pressure under Different Conditions of Power Supply and Humidity (% RH)

	k_E (L·kJ^{-1})				
		humid air[a]			
power supply	dry air	20%	40%	60%	80%
+DC	0.14	0.13	0.13	0.13	0.13
−DC	0.43	0.63	1.1	1.2	0.94
+pulsed	3.0	-	3.5	-	-

[a] Relative humidity data.

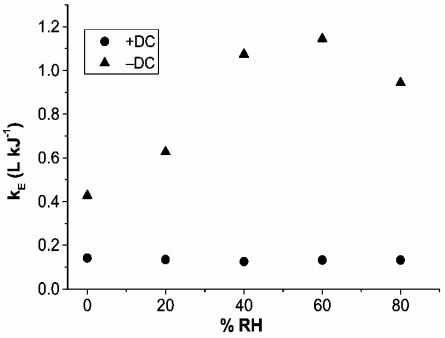

FIGURE 2. Effect of humidity on the removal efficiency of toluene (500 ppm in air) by DC corona.

processing in humid air are reported in Table 1 and Figure 2. It is seen that, while there is no effect on the removal efficiency with +DC, with −DC the efficiency increases significantly with increasing water content up to 60% relative humidity (RH). At higher levels of humidity a trend inversion occurs, with the efficiency at 80% RH becoming slightly lower than at 60% RH. In the case of +pulsed corona the process in air with 40% relative humidity is about 25% more efficient than in dry air. As discussed later, the effect of humidity is to be interpreted considering that corona discharges in humid air produce OH radicals which are among the strongest known oxidants of VOCs (*13*).

The efficiency of our process with +pulsed corona is remarkable when compared with recent data for atmospheric plasma processing of toluene. For example, our k_E value of 3.0 L·kJ^{-1} for toluene at 500 ppm initial concentration in dry air compares very favorably with values of 0.5 L·kJ^{-1}, reported for processes in a 3-stage packed bed reactor (*21*) and in a single stage DBD reactor (*30*), and of 20 L·kJ^{-1} for a corona process (*23*), considering that these experiments were all conducted with much lower toluene initial concentrations (110, 50, and 0.5 ppm, respectively). It is well-known that k_E decreases significantly with increasing toluene initial concentration (*10, 22, 31*).

Important mechanistic insight was gained from studies of the DC corona current/voltage characteristics (Figure 3a and b) and of the ions formed within the plasma conducted by means of APCI−mass spectrometry (Figure 3c−f). The data of Figure 3a and b show that, while for −DC the *I*/*V* curves determined in pure air and in air containing toluene (500 ppm) are nearly superimposed (Figure 3a), for +DC a significantly lower current intensity is detected, at any applied voltage, in the presence of toluene than in pure air (Figure 3b). Since corona current is due to ion transport across the drift region of the interelectrode gap, our results suggest that with +DC corona different ions are present in pure air and in toluene (500 ppm) containing air. Accordingly, different average ion mobilities are derived from the current/voltage characteristics of Figure 3b using the Townsend formula (*32*−*34*): 2.35 cm^2·V^{-1}·s^{-1} for pure air and 1.79 cm^2·V^{-1}·s^{-1} for toluene-containing air, respectively.

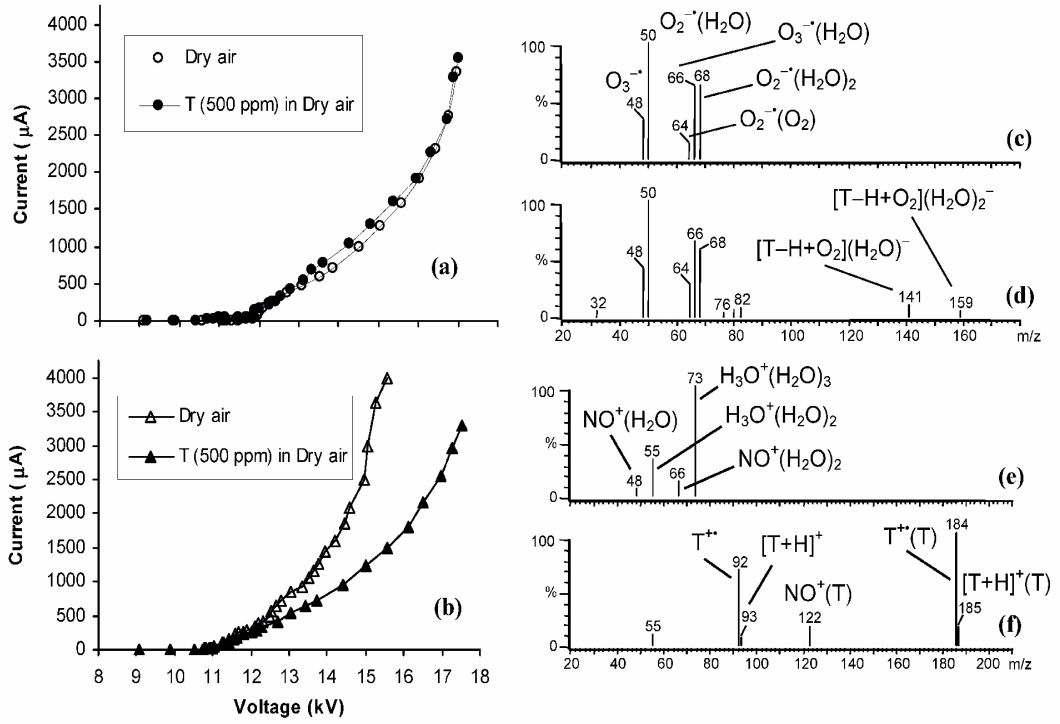

FIGURE 3. Current/voltage characteristics measured in air and in air containing toluene (500 ppm) for (a) −DC and (b) +DC corona; negative APCI mass spectra of (c) synthetic air and (d) toluene in synthetic air recorded at 30 °C; positive APCI−mass spectra of (e) synthetic air and (f) toluene in synthetic air recorded at 30 °C.

APCI−mass spectrometry is a powerful tool for monitoring and characterizing the ions formed by corona discharges and their reactions. Thus, the APCI−mass spectra reported in Figure 3c and d show that with −DC the major negative ions in the plasma when toluene is present (Figure 3d) are the same as in pure air (Figure 3c). The major signals in both spectra are due to $O_2^{-\bullet}(H_2O)_n$ (n = 0−2: m/z 32, 50, 68), $O_3^{-\bullet}(H_2O)_n$ (n = 0−1: m/z 48, 66), and $O_2^{-\bullet}(O_2)$ (m/z 64), originating from air and water molecules. These observations are fully consistent with and provide a rationale for the *I*/*V* curves of Figure 3a. On closer inspection of the APCI−mass spectrum of toluene-containing air (Figure 3d), two minor signals are found at m/z 141 and 159, which must be formed via some ion−molecule reaction of toluene and are attributed to $[T - H + O_2](H_2O)_n^-$, with n = 1 (m/z 141) and n = 2 (m/z 159), respectively. The core anion of these hydrates could likely be the benzylperoxyanion $C_6H_5CH_2OO^-$ or any isomer thereof. Notably, the bezylperoxyradical is a known intermediate in the oxidation of toluene in air (*35*). Since there are no data in the literature, to the best of our knowledge, about gas phase reactions of toluene with $O_2^{-\bullet}$, $O_3^{-\bullet}$, and their hydrates, we have no leads for proposing any specific ion−molecule reaction as the source for these $[T - H + O_2](H_2O)_n^-$ minor product ions. Their contribution to the overall −DC corona current (Figure 3a) is, however, evidently negligible.

In contrast, in the case of +DC the spectrum of pure air (Figure 3e) is completely different from that of air plus toluene (Figure 3f). Thus, while major ions in air are $H_3O^+(H_2O)_n$ (n = 2 − 3: m/z 55, 73) and $NO^+(H_2O)_n$ (n = 1 − 2; m/z 48, 66), in air contaminated with a few hundred ppm of toluene the prevailing charged species are instead $T^{+\bullet}$ (m/z 92) and $[T + H]^+$ (m/z 93), along with their ion−molecule complexes $T^{+\bullet}(T)$ (m/z 184) and $[T + H]^+(T)$ (m/z 185). These ions form (*12, 36, 37*) via exothermic charge− and proton transfer ion−molecule reactions (eq 2 and 3), characterized by rate constants of 1.8×10^{-9} and 2.2×10^{-9} cm^3 molecule^{-1} s^{-1}, respectively (*12*), followed by ion−molecule complex formation (eqs 2a and 3a).

$$T + O_2^{+\bullet} \rightarrow T^{+\bullet} + O_2 \quad (2)$$

$$T^{+\bullet} + T + M \rightarrow T^{+\bullet}(T) + M \quad (2a)$$

$$T + H_3O^+ \rightarrow [T + H]^+ + H_2O \quad (3)$$

$$[T + H]^+ + T + M \rightarrow [T + H]^+(T) + M \quad (3a)$$

Finally, the $NO^+(T)$ (m/z 122) ion−molecule complex is also observed. These APCI−MS results provide detailed experimental evidence that in the presence of toluene, +DC corona produces a very different ion population with respect to pure air. Thus, mass spectroscopic ion analysis provides a rationale for interpreting the *I*/*V* curves of Figure 3b at the molecular level. In addition, these results suggest that ionic reactions might be responsible for the initial stages of toluene decomposition induced by +DC corona. This hypothesis is consistent with the observed insensitivity of the +DC process efficiency to the presence of humidity, which rules out a significant role of the OH radical.

In contrast, the APCI−MS data suggest that with −DC corona the role of ionic species is negligible in the removal of toluene. In this case electron induced dissociation (*22, 24*) and exothermic reactions with radical and neutral chemical species, as shown in eqs 4 and 5 (*38*), must be considered.

$$C_7H_8 + {}^{\bullet}OH \rightarrow \text{products} \qquad k_{298} = 5.7 \times 10^{-12}\ \text{cm}^3\ \text{molecule}^{-1}\ \text{s}^{-1} \quad (4)$$

$$C_7H_8 + O \rightarrow \text{products} \qquad k_{298} = 2.32 \times 10^{-13}\ \text{cm}^3\ \text{molecule}^{-1}\ \text{s}^{-1} \quad (5)$$

Reaction 4 prevails in humid air and accounts for the increase of efficiency observed with increasing humidity up to 60% RH (Figure 2). The trend inversion observed for humidity levels greater than 60% can be attributed to saturation and inhibition of the $^{\bullet}$OH-forming reactions, i.e., dissociation of H_2O molecules induced by interaction with electrons or by reaction with $O(^1D)$. Ono and Oda observed a similar trend inversion in a positive pulsed corona discharge system for water concentrations >1% by volume (corresponding to a relative humidity of 32% at room temperature) and ascribed this effect to a decrease in the electron mean energy due to H_2O molecules (*39*). In the case of +pulsed power supply, the increase in efficiency observed in humid air (RH 40%) with respect to dry air suggests that, similarly to −DC, the OH radical must be involved in the initiation step.

Since corona discharges in air produce ozone (eqs 6a and 6b), another possible route to be considered for toluene oxidation is reaction 7, with a rate constant of 3.85×10^{-22} cm^3 molecule^{-1} s^{-1} at 298 K (*38*).

$$O_2 + e \rightarrow O(^3P) + O + e \quad (6a)$$

$$O(^3P) + O_2 + M \rightarrow O_3 + M \quad (6b)$$

$$C_7H_8 + O_3 \rightarrow \text{products} \qquad k_{298} = 3.85 \times 10^{-22}\ \text{cm}^3\ \text{molecule}^{-1}\ \text{s}^{-1} \quad (7)$$

We measured the ozone formed in our experiments by means of quantitative FT−IR analysis. Figure 4a reports ozone concentration data as a function of specific input energy for experiments run under different corona regimes in pure air and in air containing toluene. It is seen that in the case of −DC and of +pulsed corona the presence of toluene causes

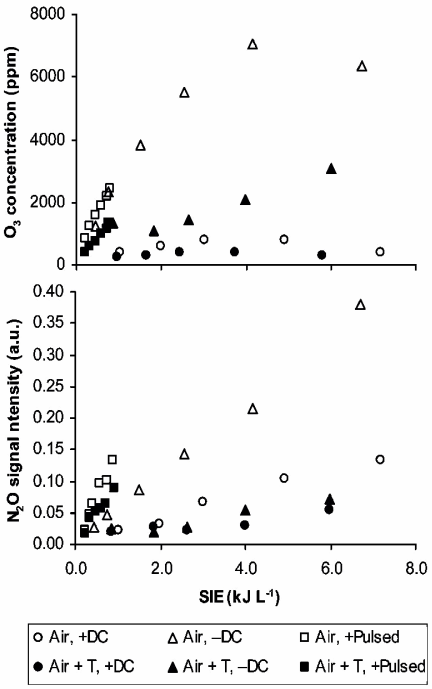

FIGURE 4. (a) Ozone concentration and (b) FT−IR signal intensity of N_2O as a function of specific input energy by different types of corona in pure air (open symbols) and toluene (500 ppm)-containing air (closed symbols).

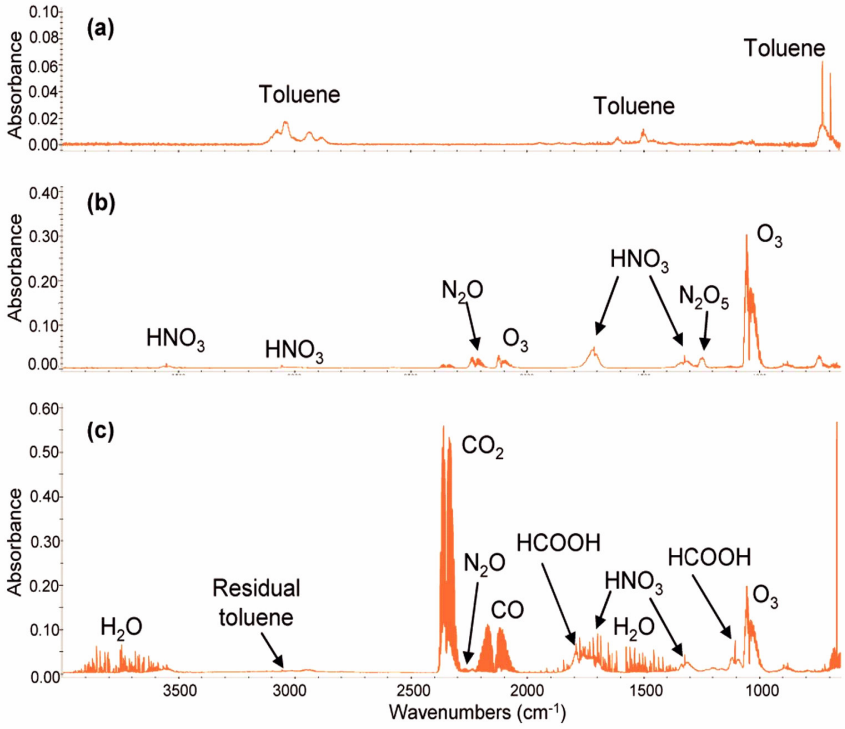

FIGURE 5. FT−IR spectra of the gas flowing out of the reactor: (a) air containing toluene (500 ppm) before corona processing, (b) pure air, and (c) air containing toluene (500 ppm) after processing with −DC corona at −21.5 kV.

a significant decrease in ozone concentration with respect to pure air. This effect might indeed be due either to ozone consumption by reaction 7 or to inhibition of ozone formation (reaction 6b) due to competing reaction of $O(^3P)$ atoms with toluene. The possible involvement of reaction 7 in our process was assessed as follows. Under the hypothesis that toluene were to decay exclusively via reaction with ozone, eq 8 should hold, where k is the time constant for reaction 7 reported above and t is the reaction time, given by the reactor volume divided by the gas flow rate.

$$\ln \frac{[T]}{[T]_0} = k_E \cdot SIE = k \cdot [O_3] \cdot t \qquad (8)$$

One can then use eq 8 to calculate, for any specific corona regime (k_E) and specific input energy, the concentration of ozone which would be necessary to produce the observed toluene conversion ($[T]/[T]_0$). By doing this calculation one obtains an ozone concentration much higher than that experimentally found: for example, for the −DC process the ozone concentration that would be necessary to decompose toluene to the observed extent is 10^3 times greater than that experimentally found. Moreover, since the concentration of ozone is very similar in −DC and +pulsed plasma, the proposal that toluene decays via reaction with ozone is not consistent with the observed different efficiencies of −DC and +pulsed in toluene processing. It is therefore concluded that the reaction with ozone is not a significant path for the oxidation of toluene in the investigated plasma processes. Thus, the decrease in ozone concentration observed in the presence of toluene must be ascribed to less efficient ozone production due to competing reaction of O atoms with toluene.

As for the products of toluene processing with the different corona regimes considered in this study, FT−IR and gas chromatography coupled to FID and MS detectors allowed for the analysis of all gaseous components present in the treated air flowing out of the reactor. These included C-containing products from toluene oxidation as well as other volatile products which do not contain carbon, notably ozone, already discussed, and N oxides (Figure 4b). FT−IR analysis has shown that the major volatile product of toluene oxidation is CO_2, with considerable amounts of CO being also formed (see for example Figure 5). Also evident are the characteristic absorption bands of formic acid, a product of toluene oxidation detected in previous studies (*23, 40*), and of water. Since water was not detected in the gas prior to the plasma treatment (Figure 5a), that observed in the spectrum of Figure 5c was evidently formed from toluene oxidation.

Quantitative analysis data for CO_2 and CO produced under different corona regimes are shown in Figure 6a as a function of toluene conversion. It is seen that for all types of corona, the selectivity for (CO_2 + CO) increases with toluene conversion, that is with specific input energy (Figure 6b). This observation suggests that some organic material (intermediates and nonvolatile products) formed at low specific input energy can in turn be oxidized under somewhat harsher conditions, as reported earlier (*17*). Consistent with this picture is the order of (CO_2 + CO) selectivity observed for the three corona regimes at any given toluene conversion: a significantly greater value is found with +DC than with either −DC or +pulsed. This is a consequence of the fact that to achieve a given toluene conversion, higher and higher specific input energy values are required in the order +pulsed < −DC < +DC (see Figure 1). The data of Figure 6b show that −DC processing is quite satisfactory in that high conversion can be achieved accompanied by high product selectivity.

The substantial production of CO observed in our experiments is reasonably attributed to reaction of glyoxal, one of the most important products of toluene oxidation (*23, 41*), via the HC(O)CO radical. This radical is known to form CO via unimolecular dissociation and via reaction with O_2 (*42*). There are numerous papers reporting that CO can be oxidized by a catalytic post-treatment which uses the ozone produced in the plasma reactor (*43, 44*). The catalyst

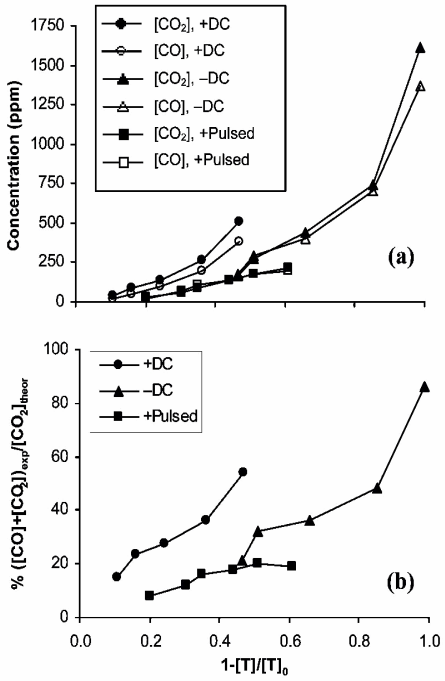

FIGURE 6. CO_2 and CO production from toluene (500 ppm initial concentration) processing with different corona regimes: (a) concentration in ppm and (b) selectivity. The data are shown as a function of toluene conversion.

could be possibly spared for nonthermal plasma processing of ambient air which generally contains large amounts of water since CO is oxidized to CO_2 by the OH radical (*45*). Indeed we found that CO (500 ppm initial concentration) in air with 40% RH is converted to CO_2 by +pulsed corona with a k_E of 1.07 kJ^{-1} L (*17*).

The missing carbon fraction is likely to be found in various toluene oxidation intermediates, nonvolatile products (*23, 41*), and aerosols (*26*). Indeed gas chromatographic analysis revealed the presence of trace amounts of several volatile organic compounds which are in turn decomposed at higher specific input energy values. It should be noted that the complex oxidation pathways of toluene, which are of environmental relevance both for tropospheric oxidation and remediation technologies, have not yet been fully characterized and are the object of current interest and research efforts (*23, 41*).

As for NO_x products, the major species detected by FT−IR is HNO_3 (Figure 5b and c), which can form either via reaction of NO_2 with the OH radical or via hydrolysis of N_2O_5 (*1*). The latter is in turn formed via reaction of NO_2 with NO_3, which are the products of sequential oxidation of NO (*1*). None of these oxides, NO, NO_2, and NO_3, were ever detected in air with or without toluene by FT−IR after-plasma analysis under any experimental conditions we used. As for N_2O_5, its characteristic absorption is seen in air (Figure 5b) but not in toluene-containing air (Figure 5c). This observation is explained considering that water produced by the oxidation of toluene is available to hydrolyze N_2O_5 to HNO_3. Thus, a greater amount of HNO_3 should be formed in toluene-containing air: unfortunately this expectation could not be verified due to significant overlap of the absorption bands due to HNO_3 with those due to water and HCOOH. Finally, N_2O was also detected in the treated gas, its abundance being greatly reduced in the presence of toluene under all corona conditions tested (Figure 4b). Considering that N_2O forms via reaction of NO with N (*1*), its lower yield in the presence of toluene is reasonably attributed to competing reactions of NO with organic peroxy radicals (*13*).

A few concluding remarks can be made on the performance of different corona regimes (+DC, −DC, and +pulsed) in the treatment of toluene-contaminated air. Toluene processing is most efficiently carried out with +pulsed corona, a result consistent with measurements made previously in the same reactor on processing of saturated hydrocarbons (*17*) and on electron energy and relative O atom density (*18*). Thus, both electron energy and O atom density are significantly higher with +pulsed than with DC corona of either polarity (*18*). Notably, the efficiency of pulsed corona treatment in our reactor is remarkable in comparison with values reported recently for toluene processing (*21, 23, 30*). Humidity, an important and variable component of ambient air, affects the efficiency of toluene oxidation by −DC and +pulsed corona, but not with +DC, no effect being observed at all over a wide range of relative humidity. A rationale for the different response of +DC and −DC to changes in the humidity content comes from the analysis of the ions formed within the plasma coupled with the results of current/voltage characteristics. It is proposed that the initial steps of toluene decomposition differ depending on the plasma regime applied: ionic reactions are favored with +DC in dry as well as in humid air, whereas reactions with O atoms and OH radicals prevail in the case of −DC and +pulsed corona discharges. These conclusions are of immediate practical relevance. As for products, the selectivity for (CO_2 + CO) increases with specific input energy. Notably, high toluene conversion and product selectivity were achieved in −DC processing. Moreover, the presence of toluene has a beneficial effect on the amount and type of undesired side products, notably ozone and NO_x. Thus, toluene reduces the formation of ozone and promotes the conversion of NO_x to HNO_3. The formation of nitric acid, a side product which is more readily disposed of than the NO_x, is favored by production of water and of NO_2 due to toluene oxidation. NO_2 is formed from oxidation of NO coupled to the conversion of organic peroxyradicals (ROO·) to the corresponding oxy radicals (RO·) along the well-known route of VOC oxidation to CO_2 (*13*).

Acknowledgments

Financial support by the University of Padova (Progetto Interarea 2005) is gratefully acknowledged.

Literature Cited

(1) Van Veldhuizen, E. M. *Electrical Discharges for Environmental Purposes: Fundamentals and Applications*; Nova Science Publishers: New York, 2000.
(2) Kim, H.-H. Nonthermal plasma processing for air-pollution control: A historical review, current issues, and future prospects. *Plasma Process. Polym.* **2004**, *1*, 91–110.
(3) Fridman, A. *Plasma Chemistry*; Cambridge University Press: Cambridge, UK, 2008.
(4) Penetrante, B. M. *Nonthermal Plasma Techniques for Pollution Control*; Springer Verlag: New York, 1993.
(5) Odic, E.; Paradisi, C.; Rea, M.; Parissiv, L.; Goldman, A.; Goldman, M. Treatment of organic pollutants by corona discharge plasma. In *The Modern Problems of Electrostatics with Applications in Environment Protection*; Inculet, I. I., Tanasescu, F. T., Cramariuc, R., Eds; Springer: Bucarest, 1999; Vol. 63, pp 143−160.
(6) Penetrante, B. M.; Hsiao, M. C.; Bardsley, J. N.; Merritt, B. T.; Vogtlin, G. E.; Wallmann, P. H. Electron beam and pulsed corona processing of volatile organic compounds in gas streams. *Pure Appl. Chem.* **1996**, *68*, 1083–1087.
(7) Marotta, E.; Callea, A.; Ren, X.; Rea, M.; Paradisi, C. DC corona electric discharges for air pollution control. Part 2. Ionic intermediates and mechanisms of hydrocarbon processing. *Plasma Process. Polym.* **2008**, *5*, 146–154.
(8) Marotta, E.; Scorrano, G.; Paradisi, C. Ionic reactions of chlorinated volatile organic compounds in air plasma at

4.3 AN EMISSION SPECTROSCOPY STUDY OF ATMOSPHERIC PLASMAS FORMED BY DC AND PULSED CORONA DISCHARGES IN HYDROCARBON CONTAMINATED AIR

An emission spectroscopy study of atmospheric plasmas formed by DC and pulsed corona discharges in hydrocarbon contaminated air

B. Zaniol[1], M. Schiorlin[2], E. Gazza[1], E. Marotta[2], X. Ren[2], M. Puiatti[1], M. Rea[3], P. Sonato[1,3], and C. Paradisi[2]

[1]Consorzio RFX, 35127 Padova, Italy
[2]Department of Chemical Sciences, Università di Padova, 35131 Padova, Italy
[3]Department of Electrical Engineering, Università di Padova, 35131 Padova, Italy

Abstract—Optical emission spectroscopy was used to characterize the plasma produced by DC and pulsed corona discharges in air at ambient pressure in a wire-cylinder reactor. The experiments have been performed both in dry and humid air and also in the presence of *n*-hexane, used in 500 ppm concentration as a model pollutant. The results provide a thorough characterization of different plasma regimes in terms of electron, vibrational and rotational temperature and are discussed with reference to chemical reactivity data.

Keywords—Atmospheric air plasma, corona discharge, emission spectroscopy, electron temperature, vibrational temperature, rotational temperature, OH radical, atomic oxygen

I. INTRODUCTION

Among the novel approaches for air pollution control, non-thermal plasma processing is especially suited for the removal of volatile organic compounds (VOCs) in low concentrations [1-4]. Corona discharges are one of the convenient means to produce such plasmas. Current applications range from the large devices for treatment of industrial emissions to the minute air purifiers with USB-connection used to improve the air quality around the PC. However, despite the rather advanced technological developments, the chemical reactions resulting in the decomposition of organic pollutants in the plasma are far from being well characterized. To contribute some insight into these processes a corona reactor of wire/cylinder configuration has been developed to study the mechanisms of VOC decomposition induced by different types of corona discharges [5-7]. Using as a model VOC the hydrocarbon *n*-hexane the process efficiency, the products and the reactive intermediates both in dry and humid air under different energization conditions, negative DC (–DC), positive DC (+DC) and positive pulsed corona (+PC), have been compared. One interesting conclusion drawn from this comparison is that different mechanisms occur depending on the specific corona regime adopted [5-7]. Specifically, the proposal was advanced that, in contrast to +DC corona for which ionic reactions prevail, in the case of –DC and of +PC, hydrocarbon decomposition is initiated by reactions with atoms and/or radicals, notably $O(^3P)$ in dry air and OH in humid air [6,7]. Support for this proposal came from the results of chemical probes (ozone formation and CO oxidation) applied to compare the average concentrations of the reactive species $O(^3P)$ and OH obtained in the plasma formed by +DC, –DC and +PC in dry and humid air [6,7]. These results suggest that, for any given energy input, the concentrations of $O(^3P)$ and OH (in humid air), decrease in the order +PC > –DC > +DC corona.

Direct measurements of the OH radical density in non-thermal plasmas produced by electrical discharges are usually made by means of laser-induced fluorescence [8] or resonant absorption spectroscopy [9]. In a few instances, however, diagnosis of OH was also done by optical emission spectroscopy [10]. In order to better characterize the different plasma regimes produced in our reactor by DC (±DC) and +PC, we thus resorted to optical emission spectroscopy diagnostics which provides data on excited neutral and ionized molecular and atomic species. From these data the characteristic plasma temperatures T_e (electron temperature), T_v (vibrational temperature) and T_r (rotational temperature) can also be obtained.

This paper reports, compares and discusses the emission spectra obtained under different corona regimes (–DC, +DC and +PC) in pure dry and humid air and also in air doped with the pollutant *n*-hexane in 500 ppm concentration. From the spectral data the plasma temperatures T_e, T_v and T_r were determined for all the different experimental conditions tested.

II. EXPERIMENTAL SETUP

A. Discharge chamber

The discharge chamber, described in detail in [5], was used after minor adaptations to incorporate an optical lens at the centre of one of the end caps. An out of scale sketch of the reactor with the layout of the main components is shown in Fig. 1.

The corona reactor has a wire/cylinder configuration with a length of 60 cm and a diameter of 3.85 cm. The wire is made of Stainless Steel and has a diameter of 1 mm.

Corresponding author: Cristina Paradisi
e-mail address: cristina.paradisi@unipd.it

Received; March 4, 2008, Accepted; March 27, 2008

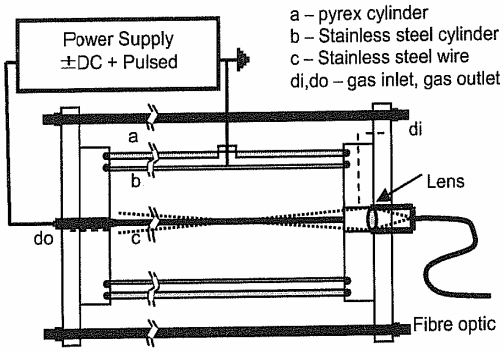

Fig. 1. Sketch of the wire-cylinder reactor adapted for measurements of emission spectroscopy.

Both DC (+DC, –DC) and positive pulsed corona (+PC) discharges were investigated.

The voltage range explored for DC corona is between 14 and 18 kV, the current is in the order of a few mA with a DC power ranging from 9 to 85 W.

For pulsed corona discharge a positive DC bias of 12 kV was used with superimposed a pulsed waveform having a peak of about 15 kV and a frequency range between 30 Hz and 300 Hz. The typical waveform of the pulsed discharge is shown in Fig. 2 for a single pulse at 75 Hz of repetition rate. As shown in Fig. 2 the pulse duration is in the order of 60 ns. The peak power reaches a value of 100 kW, while the mean input power is within the range of 3.5 to 15 W. The bias voltage, approximately 12 kV in Fig. 2, is recovered after 5-10 μs depending on operational conditions.

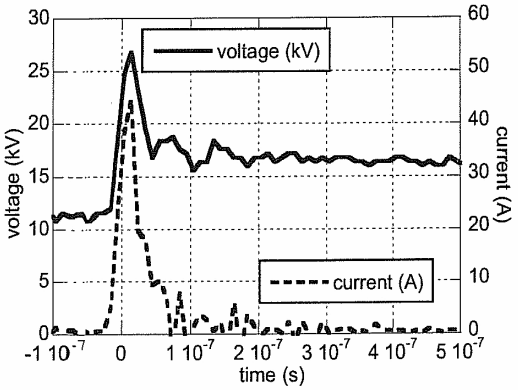

Fig. 2. Typical waveform of a single pulse at 75 Hz of repetition rate.

B. Optical emission spectroscopy and analysis methods

The plasma radiation has been detected by a Czerny Turner spectrometer, 75 cm of focal length, equipped with a 1200 g/mm holographic grating. A back-illuminated CCD camera (512x512 pixels) has been used as a detector. Different spectral windows have been acquired over the range between 305 nm (corresponding to OH emission) and 780 nm (where a triplet from O I is observed). In particular the region between 380 and 400 nm has been considered for the evaluation of the electron and gas temperatures from the N_2 and N_2^+ molecular emission spectra.

In non-thermal plasmas heavy particles (neutrals and ions) and electrons do not have the same temperature. While the electrons have a relatively high energy (several eV), sufficient to produce ionization, excitation and dissociation of the gas, the heavy particle temperature is close to room temperature.

In a N_2 discharge the electron temperature (T_e) can be easily determined from the band head intensities of the first negative system of $N_2^+(B\ ^2\Sigma_u^+ - X\ ^2\Sigma_g^+)$ at 391.4 nm and of the second positive system of $N_2(C\ ^3\Pi_u^+ - B\ ^3\Pi_g^+)$ at 394.3 nm [11]. The ratio of the two bands is very sensitive to variations of T_e, and it is well suited for measuring it. Fig. 3 shows an example of the experimental N_2 spectrum used for the determination of T_e. The peaks of N_2^+ and N_2 emission are shown with their curve fits.

The overall uncertainty in the determination of the T_e is in the range of 10% of its value.

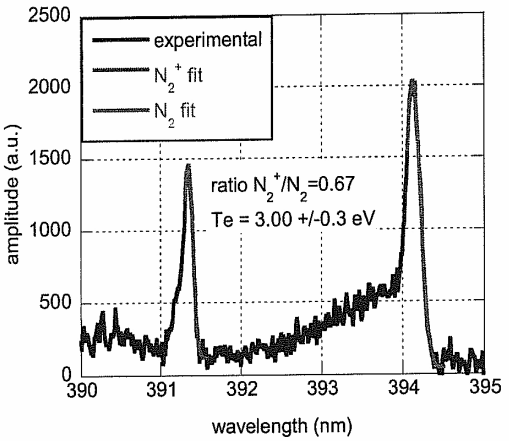

Fig. 3. Example of the N_2 spectrum used for the determination of the electron temperature T_e.

The vibrational temperature (T_v), related to the temperature of the neutral monoatomic species, is measured from the nitrogen second positive system when considering more than one band emission. The series corresponding to $\Delta v=2$ and vibrational numbers (v'-v"): (3-5), (2-4), (1-3), (0-2) (Fig. 4), leads to the determination of the T_v [11].

Regarding the rotational temperature (T_r), a different approach has been used. Since the dependence on T_r affects the spectral profile of each nitrogen band emission, following a published protocol [12,13], the spectrum was simulated at different T_r to find the best match with the experimental data. This method provided T_r with an error of about +/- 50 K. Fig. 5 shows an example of experimental data overlapped with the simulations at different T_r.

It has to be mentioned that the temperature evaluations do not need absolute intensity calibrated signals.

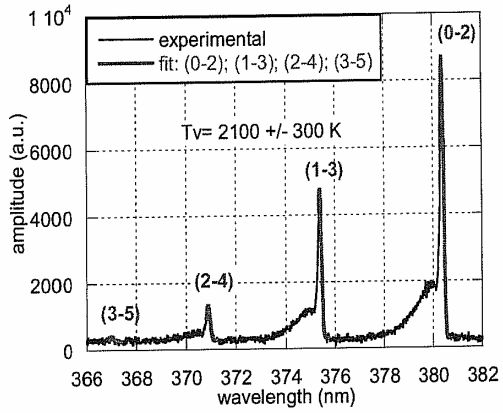

Fig. 4. N_2 spectrum used for the determination of the vibrational temperature T_v.

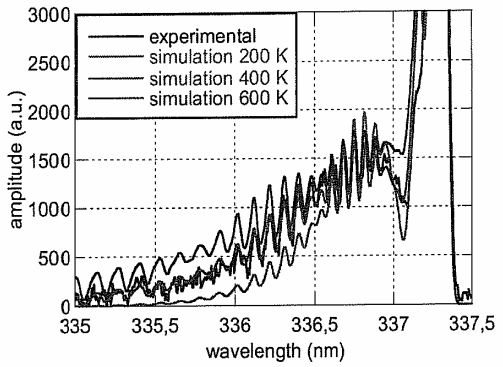

Fig. 5. N_2 spectrum used for the determination of the rotational temperature T_r.

The T_r can also be obtained from the UV OH band at 306.357 nm ($A\ ^2\Sigma, v=0 - X\ ^2\Pi, v'=0$).

Unfortunately the OH emission turned out to be too low also in very humid air to be detected by our instrument. Only under very particular conditions, discussed in section IV, the OH rotation pattern could be detected and identified.

C. *Chemical measurements*

The experimental setup for the gas flow line, the humidification loop and the chemical diagnostics are shown in the simplified scheme of Fig. 6 and are described in detail in a previous publication [5].

In experiments with *n*-hexane contaminated air, for each energy condition investigated by emission spectroscopy, the extent of VOC decomposition was also determined. This was done by quantitative GC analysis of an aliquot of the treated gaseous mixture using the experimental protocol described in previous publications [5-7].

It was thus verified that the minor changes introduced in the reactor in order to accommodate the quartz lens, involving specifically one of the wire (active electrode) connections (see Fig. 1), did not produce significant changes in the process efficiency with respect to those reported earlier [5-7].

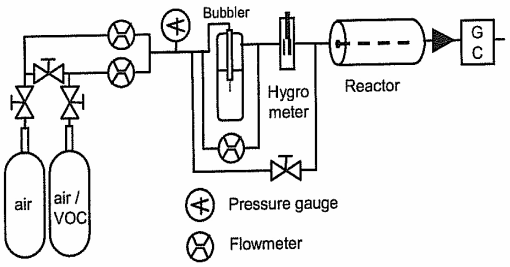

Fig. 6. Simplified scheme of the gas flow line experimental setup.

The process efficiency is measured by k_E ($J^{-1}\cdot L$), the energy constant evaluated by interpolating the fraction of residual VOC as a function of the energy density deposited in the gas (E, $J\cdot L^{-1}$), according to the exponential Eq. 1:

$$[VOC] = [VOC]_0 \cdot e^{-k_E \cdot E} \qquad (1)$$

where $[VOC]_0$ is the initial VOC concentration and [VOC] is its residual concentration after applying the energy density E.

III. EXPERIMENTS

Various experimental campaigns have been performed to investigate the presence and the behaviour of excited species within the plasma, together with the various temperature parameters, as a function of the different experimental conditions tested, i.e. different corona regimes and gas composition.

In addition, the efficiency of *n*-hexane processing was also measured to compare the different corona regimes with regard to their capabilities in promoting the oxidative degradation of this model VOC. Table 1 reports all the experimental conditions used in the present work. Three different scenarios in a wide energy range have been explored, pertaining to +DC, –DC corona and +PC discharge.

For each experimental condition, the voltage between the electrodes and the current were measured and used to calculate the mean power and the energy density as previously described [5-7]. In particular, the DC discharges can achieve a larger mean power with respect to the pulsed ones because the energy is supplied

continuously. Mean power and energy density data are also reported in Table 1.

Emission spectra were acquired in dry and humid air with two different levels of humidity (R_H = 40 and 80%). The same experiments were also conducted in the presence of *n*-hexane, used in 502 ppm concentration as a model VOC pollutant.

For each experimental condition tested, characterised by a given imposed voltage and gas composition, many spectroscopic lines have been measured to perform the analysis of the plasma temperatures and to explore and characterize which type of corona leads to the most efficient chemical process.

TABLE 1
SUMMARY OF THE EXPERIMENTAL CONDITIONS. FOR + PC THE FREQUENCY WAS IN THE RANGE OF 33 TO 300HZ. THE DC BIAS VOLTAGE IS ABBREVIATED AS D AND THE PULSED ONE AS P.

	Types of Corona Discharge	Voltage (kV)	Mean Power (W)	Energy Density (kJ/l)
Dry air	+ DC	14-17.3	13-86	1.8-11.5
	– DC	14-18	12-71	1.6-9.5
	Pulsed	12D+ 15P	4.4-12.3	0.6-1.6
Humid air (R_H=40 %)	+ DC	14-17,45	10-81	1.3-10.8
	– DC	14-18	9.2-70	1.2-9.4
	Pulsed	12D+ 15P	4.5-12.5	0.6-1.7
Humid air (R_H=80%)	+ DC	14-16	8.9-31	1.2-4.1
	– DC	14-15	10-18	1.3-2.4
	Pulsed	12D+ 15P	3.5-13.7	0.5-1.8
Dry air + Hexane (502ppm)	+ DC	14-18	7.6-42	1.0-5.6
	– DC	14-18	11-62	1.5-8.2
	Pulsed	12D+ 15P	3.6-14.3	0.5-1.9
Humid air (R_H=40%) + Hexane (502ppm)	+ DC	14-18	7.6-42	1.0-5.6
	– DC	14-18	10.3-63	1.4-8.4
	Pulsed	12D+ 15P	3.3-15.4	0.5-2.0

Specifically, we monitored the O I oxygen triplet, corresponding to the emission lines around 777 nm, and the OH radical (309 nm). In addition, the N_2^+ (391.4 nm) and N_2 (394.1 nm) molecular lines were acquired and used to calculate T_r, and the N_2 molecular group in the spectral range between 365 and 385 nm was acquired to perform the calculation of T_e and T_v, respectively.

Each spectral range was collected using different acquisition times spanning from a few seconds for N_2 molecular emission lines to ten minutes for the OH radical.

IV. RESULSTS AND DISCUSSION

Using the analysis and elaboration protocols described in section II B, T_e, T_v and T_r data have been calculated for all types of experimental corona discharge (+DC, –DC and +PC), exploring most of the imposed voltages. The results are reported, as a function of energy density, in Fig. 7, 8, and 9 for T_e, T_v and T_r, respectively.

As expected, three different well separated groups of temperatures have been found, with T_e (see Fig. 7) being much greater than T_v (see Fig. 8), which in turn is higher than T_r (see Fig. 9).

It is seen that the type of corona has a major effect on T_e (Fig. 7). Thus, T_e exhibits a positive dependence on energy density only for +PC discharges, while it remains fairly constant in the case of +DC and –DC discharges. Interestingly, T_e is significantly higher for +DC than for

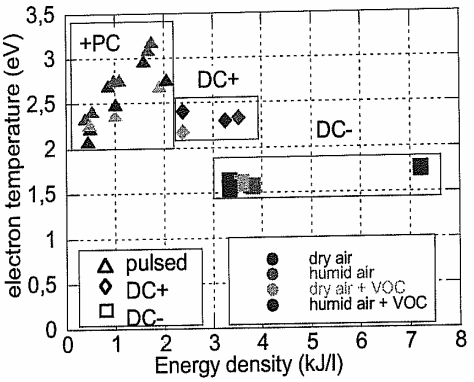

Fig. 7. Electron temperature T_e as a function of energy density for different coronas and gas compositions.

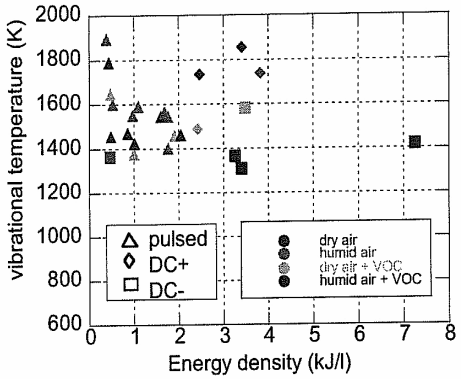

Fig. 8. Vibrational temperature T_v as a function of energy density for different coronas and gas compositions.

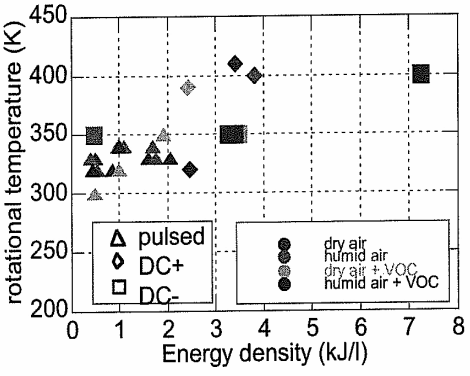

Fig. 9. Rotational temperature T_r as a function of energy density for different coronas and gas compositions.

–DC discharges, which appear to be less efficient in the electron heating, as in this case the negatively charged particles move towards the cathode, i.e. the reactor wall. In any case the electrons, thermalized during the discharge, reach an equilibrium regime independently on the energy supplied to the reactor. The uncertainty attributable to the T_e for each experimental point has been calculated to be in the order of 10 %.

In contrast T_v, which is related, as aforementioned, to the temperature of the neutral monoatomic particles, does not exhibit any clear dependence on the type of discharge applied or on the specific energy supplied (Fig. 8). Also the composition of the gas used does not influence significantly the final T_v which remains fairly constant around a value of 1600 K also in the presence of water and/or *n*-hexane. In conclusion, T_v does not show any clear dependence on the experimental conditions used and the observed spread in its experimentally determined value may be attributed to normal statistical errors.

This is also true for T_r, which indicates the equilibrium temperature of the molecular bulk gas (Fig. 9). T_r is not significantly affected by the energy density of the plasma, remaining rather stable around an average value of 340-350 K. The uncertainty in T_r data, which depends on the quality of the simulation fit to the experimental data, can be estimated around 30-50 K.

A systematic study on the presence of neutral atomic oxygen has been performed, to verify in which kind of corona regime it is more abundant.

The use of the emission lines of O I triplet in the visible region at 777 nm, well known in astrophysics and astronomy [14], gives an indication of the quantity of excited $O(^3P)$. This information is particularly important since, as mentioned in section I, O atoms are very reactive towards hydrocarbon molecules and are likely involved in the initiation steps of the degradation process in dry air.

It has to be noted that the spectroscopic methods used in this work, do not give the absolute value of the O density inside the corona plasma, but only an indication of the relative concentration and efficiency in the production of the excited $O(^3P)$; this with the assumption that the only O atom transition to a lower level considered is $O(3p\ ^5P \rightarrow 3s\ ^5S^0)$, corresponding to the 777 nm emission line. In Fig. 10, the intensity (counts normalized to the acquisition time) of O I triplet are reported as a function of the energy, for all the different experimental conditions explored. It is seen that in all cases the production of excited $O(^3P)$ is proportional to the energy injected, but also that the excitation by means of +PC discharges is more efficient than in the case of +DC and –DC discharges.

The spectrum reported in Fig. 11 (red trace, dotted line), shows evidence for the presence of some roto-vibrational structures observed at lower wavelengths relative to the O I triplet lines, due to the excitation of N_2 molecules, visible at 778-779 nm. Since these structures are superimposed to the emission lines of interest (blue trace, solid line), it has been necessary to deconvolve their contributions. For this purpose, emission spectra

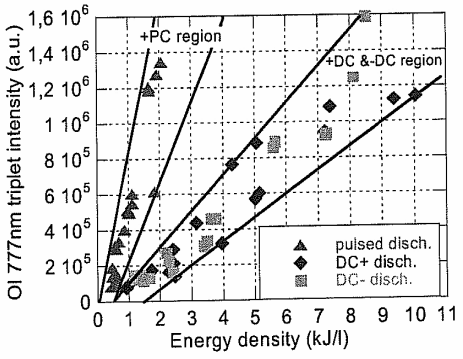

Fig. 10. O I 777 nm triplet intensity in all the explored conditions of corona discharge. The distinction between +PC and ±DC discharges is evident.

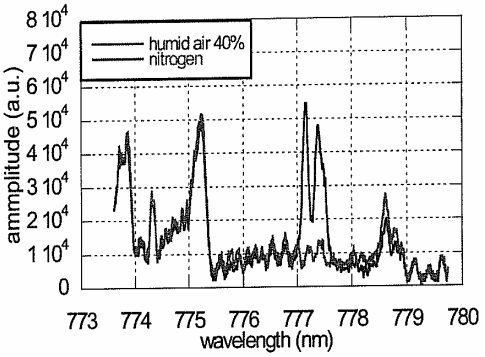

Fig. 11. Emission spectra recorded in pure nitrogen and in air (the bands due to O I are evident around 777 nm).

were recorded with pure N_2 atmosphere inside the reactor (Fig. 12).

As expected, the N_2 spectrum does not show any signal within the range of the O I triplet lines (Fig. 12); thus this spectrum was used to subtract the roto-vibtrational contribution of the N_2 molecular structure from the O I spectrum lines, after a normalisation procedure.

The O I triplet was then interpolated using a three gaussian fit with only three free parameters (intensity, width and position of only one of the three peaks), since

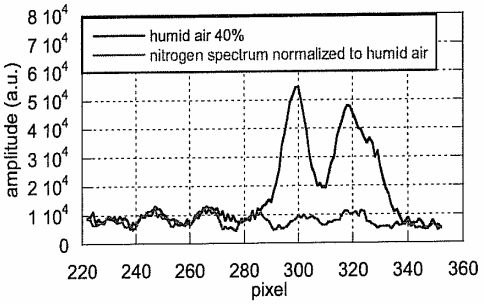

Fig. 12. Normalization of the nitrogen spectrum peaks to allow for background subtraction.

the relative positions and intensities of the three Gaussian curves are fixed by atomic data, and their width must be the same. Fig. 13 shows the experimental spectrum together with the interpolating curve. As it can be noted in Fig. 13, the superimposition is considerably better than in the case without the N_2 spectrum subtraction. It has to be investigated whether there are other unknown emission lines under the O I triplet, some quenching phenomenon, or some aspects related to the efficiency of the spectrometer in that region.

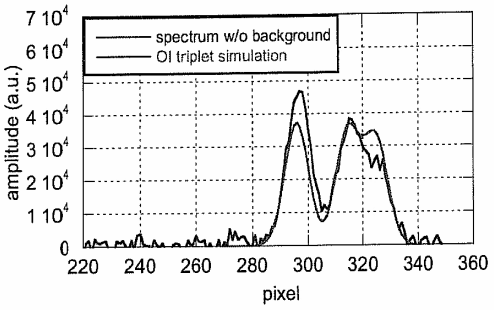

Fig. 13. Spectrum with subtracted background compared with the simulation of the O I triplet around 777 nm.

The spectroscopic analysis was then extended to the study of the OH radical production in +PC, +DC and –DC discharges; the OH radical is one of the strongest oxidizing agents in humid air non-thermal plasmas. Since the transition of excited OH mainly appears at 309 nm, our measurements were concentrated in the spectral region around this wavelength. In an attempt to detect such species we acquired several spectra with integration time up to 10 minutes, as it is known that the lifetime of excited OH radicals does not exceed one millisecond under the best conditions (humid air). For example in atmospheric dry air, the life time of OH ($A^2\Sigma$) generated by collision and radiation is nearly 10^{-9} s and 700 ns, respectively and all the excited radicals return to the ground state by collision and radiation in a very short time [10].

Despite our efforts, we could not detect the OH transition in air under any of the different energization conditions explored, ±DC and +PC, not even in air with up to 80% relative humidity.

The OH transition was instead observed when the corona reactor was filled with N_2 containing a high level of relative humidity (80% relative humidity). An example of the spectral emission line of OH excited radicals at 309 nm observed in humidified nitrogen gas with +PC corona is reported in Fig. 14.

Following [15], the intensity ratios of three groups of unresolved rotational lines have been used for inferring T_r (see Fig. 14). In this particular case a T_r value of about 800 K was obtained, with an uncertainty of +/- 200 K due to the poor signal to noise ratio of the data. The difference between the T_r calculated in humid N_2 discharge using the OH emission (Fig. 14) rather than the

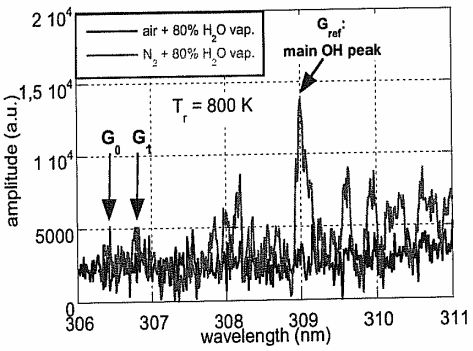

Fig. 14. OH spectrum used for the determination of the rotational temperature.

N_2 emission can be the effect of two different excitation regions.

Finally, Table 2 reports our experimental data on the efficiency (k_E) of *n*-hexane decomposition obtained under the different corona regimes applied in dry and humid air. It is seen that, in agreement with earlier reports [5,6], pulsed corona processing is much more efficient than –DC which in turn is somewhat better than +DC corona. The better performance of pulsed corona discharges in dry air is perfectly coherent with the higher density of O I reached under these discharge conditions (Fig. 10).

TABLE 2
EFFICIENCY OF *N*-HEXANE DECOMPOSITION BY PLASMA PROCESSING UNDER THE SPECIFIED CONDITIONS.

Types of Corona Discharge	Gas condition	k_E ($L \cdot kJ^{-1}$)
+ DC	Dry air	0.196
+ DC	Humid air (R_H=40%)	0.176
– DC	Dry air	0.77
– DC	Humid air (R_H=40%)	1.06
+ PC	Dry air	2.11
+ PC	Humid air (R_H=40%)	2.23

V. CONCLUSION

An extensive and comprehensive set of emission spectra was acquired under different discharge conditions (–DC, +DC, +PC) in air but under otherwise identical experimental conditions (same reactor, same gas composition, same experimental and diagnostic protocols). The data, therefore, provide a unique opportunity for the direct comparison of the non-equilibrium atmospheric plasmas produced by the different energization modes, i.e. –DC, +DC and +PC.

The results are quite useful in differentiating the various corona regimes tested. Specifically the relatively higher concentrations of O I and of OH (in humid air) observed in +PC discharges with respect to DC

discharges parallel the higher efficiency in *n*-hexane processing. The results are therefore consistent with current views that the initial step of hydrocarbon oxidation in pulsed corona plasma in air is due to attack by O and/or, in humid air, by OH [1].

REFERENCES

[1] H.-H. Kim, "Nonthermal plasma processing for air-pollution control: a historical review, current issues, and future prospects", *Plasma Process. Polym.*, vol. 1, no. 2, pp. 91-110, September 2004.

[2] E. M. van Veldhuizen, *Electrical Discharges for Environmental Purposes, Fundamentals and Applications*. Huntington, Nova Science Publishers, Inc., New York, 2000.

[3] S. Pasquiers, "Removal of pollutants by plasma catalytic processes", *Eur. Phys. J. Appl. Phys.*, vol. 28, no. 3, pp. 319-324, December 2004.

[4] B. M. Penetrante and S. E. Schultheis, *Nonthermal plasma techniques for pollution control*. Springer Verlag: New York, 1993.

[5] E. Marotta, A. Callea, M. Rea and C. Paradisi, "DC corona electric discharges for air pollution control. Part 1. Efficiency and products of hydrocarbon processing", *Environ. Sci. Technol.*, vol. 41, no. 16, pp. 5862-5868, August 2007.

[6] E. Marotta, A. Callea, X. Ren, M. Rea and C. Paradisi, "A mechanism study of pulsed corona processing of hydrocarbons in air at ambient temperature and pressure", *Int. J. Plasma Environ. Sci. Technol.*, vol. 1, no. 1, pp. 39-45, March 2007.

[7] E. Marotta, A. Callea, X. Ren, M. Rea and C. Paradisi, "DC Corona Electric Discharges for Air Pollution Control. Part 2. Ionic Intermediates and Mechanisms of Hydrocarbon Processing", *Plasma Process. Polym.*, vol. 5, no. 2, pp. 146-154, February 2008.

[8] R. Ono and T. Oda, "Dynamics of ozone and OH radicals generated by pulsed corona discharge in humid-air flow reactor measured by laser spectroscopy", *J. Appl. Phys.*, vol. 93, no. 10, pp. 5876-5882, May 2003.

[9] C. Hibert, I. Gaurand, O. Motret, J. M. Pouvesle, "[OH(X)] measurements by resonant spectroscopy in a pulsed dielectric barrier discharge", *J. Appl. Phys.*, vol. 85, no. 10, pp. 7070-7075, May 1999.

[10] M. Sun, Y. Wu, J. Li, N. H. Wang, J. Wu, K. F. Shang and J. L. Zang, "Diagnosis of OH by optical emission spectroscopy in atmospheric pressure unsaturated humid air corona discharge and its implication to desulphurization of flue gas.", *Plasma Chem. Plasma Process.*, vol. 25, no. 1, pp. 31-40, February 2005.

[11] N. Britun, M. Gaillard, A. Ricard, Y. M. Kim, K. S. Kim and J. G. Hanet, "Determination of the vibrational, rotational and electron temperatures in N_2 and Ar-N_2 rf discharge" *J. Phys. D: Appl. Phys.*, vol. 40, no. 4, pp. 1022-102, February 2007.

[12] G. Herzberg, *Molecular Spectra and Molecular Structure I: Spectra of Diatomic Molecules*. New York: Van Nostrand, 1950.

[13] G. Hartmann and P.C. Johnson, "Measurements of relative transition probabilities and the variation of the electronic transition moment for N_2 C $^3\Pi_u$ - B $^3\Pi_g$ ", *J. Phys. B: Atom. Molec. Phys.*, vol. 11, no. 9, pp. 1597-1612, May 1978.

[14] D. Kiselman, "The 777 nm oxygen triplet in the Sun and solar-type stars, and its use for abundance analysis", *Astron. Astrophys.*, vol. 275, no. 1, pp. 269-282, August 1993.

[15] C. de Izarra, "UV OH spectrum used as a molecular pyrometer" *J. Phys. D: Appl. Phys.*, vol 33, no. 14, pp. 1697-1704, July 2000.

4.4 CHEMISTRY OF ORGANIC POLLUTANTS IN ATMOSPHERIC PLASMAS

7
Chemistry of Organic Pollutants in Atmospheric Plasmas

Ester Marotta, Milko Schiorlin, Massimo Rea, and Cristina Paradisi

7.1
Introduction

Atmospheric air plasmas are very complex oxidizing environments which are easily and conveniently produced by means of various types of electric discharges. Such plasmas can be exploited for many environmental applications [1, 2], including air pollution control especially for the removal of volatile organic compounds (VOCs) in low concentration [1–6]. Major research efforts in this field focused initially on improving the process energy efficiency and, more recently, on gaining a better control on the emissions produced. Ideally, atmospheric air plasma-processing of VOCs should lead to their exhaustive oxidation to CO_2, a goal seldom reached. Only a partial characterization is usually available of the other products of VOC plasma treatment, which often include CO, volatile organic oxidation intermediates but also nonvolatile organics and particles. In addition, electric discharges in air produce undesired side products such as NO_x and ozone. Recent developments in VOC plasma processing concern various combinations of atmospheric plasma with heterogeneous catalysts to achieve better energy efficiency and product selectivity [1, 2, 7, 8].

Product control and process optimization require a good understanding of the chemical reactions involved in the VOC degradation process. The strong oxidizing power of atmospheric air plasmas makes them applicable to the processing of all kinds of VOCs, which come in huge numbers and in a large variety of chemical composition, structure, and reactivity. Despite their abovementioned strong oxidizing power, such plasmas display some selectivity so that it has been found that different VOCs are oxidized with different efficiencies [9]. As organic chemists we intend to exploit such differences to arrive at a better characterization and understanding of the chemistry of atmospheric plasmas. Essential for this analysis is the wealth of kinetic data available in the literature for the reactions of many VOCs with species which are also present in atmospheric air plasmas, notably electrons, O atoms, OH radicals, and many important atmospheric ions: the cations $O_2^{+\bullet}$, $N_2^{+\bullet}$, O^+, N^+, NO^+, the anions $O^{-\bullet}$, $O_2^{-\bullet}$, $O_3^{-\bullet}$, and their hydrates.

Depending on the attacking species, different initiation steps will occur in the oxidation of any specific VOC: excitation, bond dissociation, atom abstraction,

Industrial Plasma Technology. Edited by Yoshinobu Kawai, Hideo Ikegami, Noriyoshi Sato, Akihisa Matsuda, Kiichiro Uchino, Masayuki Kuzuya, and Akira Mizuno

ISBN: 978-3-527-32544-3

radical addition, electron attachment, charge transfer, and ion–molecule reactions [2]. Anyone of such processes activates the oxidation of VOC molecules by converting them into some VOC-derived organic radicals, $R^{\bullet}$. The subsequent oxidation of such radicals initiates with their trapping by molecular oxygen and is known from studies of the natural oxidative degradation pathways of VOCs in the troposphere [10].

It is well known that different corona regimes are characterized by different distributions in density, energy, and space of electrons, and other reactive species [2]. It is, therefore, to be expected that for a given input energy different power supplies should produce different chemical outcomes. However, despite the wealth of literature data on VOC processing, the results produced by different corona regimes with a single VOC could not usually be compared, because the experiments were performed with different reactors and under different experimental conditions with regard to the composition of the gas being treated (relative amounts of oxygen and humidity, VOC concentration). Thus, it is well known that the corona phenomenon depends strongly on the configuration and size of the electrodes and on the interelectrode distance. On the other hand, it is also well known that the efficiency of VOC processing within a given corona reactor, under well-defined experimental conditions, changes greatly with the initial concentration of VOC (VOC_0), usually decreasing significantly with increasing VOC_0. [1, 2, 11, 12]. It was therefore of interest to develop a single reactor capable of sustaining different corona regimes and to compare their performance in the oxidation processing of selected VOCs. A brief account is offered here of our comparative studies made with the developed apparatus, a large wire/cylinder bench-top corona reactor which can be powered by DC and pulsed voltages of either polarity. It will be shown that through these comparisons important mechanistic insight can be gained and that the oxidation of VOCs is initiated by reaction with different species depending on the specific corona regime used. A powerful diagnostic tool in our work is the integrated analysis of DC corona current/voltage characteristics coupled with that of the ionized components of the plasma and of their reactions. To this end we are using APCI-MS (atmospheric pressure chemical ionization–Mass Spectrometry) which interfaces a corona chamber at atmospheric pressure with a quadrupole mass analyzer. With our APCI-MS apparatus, which has a time window of about 500 μs, we can thus detect and monitor the ion population within the plasma formed from any gas mixture of desired composition (air, VOC, humidity).

7.2 Experimental

7.2.1 Chemicals

Pure air used in the experiments was a synthetic mixture (80% nitrogen–20% oxygen) from Air Liquid with specified impurities of H_2O (<3 ppm) and of C_nH_m

(<0.5 ppm). Air mixtures of *n*-hexane (500 ppm ± 3%), *i*-octane (500 ppm, ±2%), CO_2 (520 ppm, ±2%), and CO (499 ppm, ±1%) were purchased from Air Liquid in cylinders loaded to a pressure lower than their respective condensation limits. Liquid samples of *n*-hexane, *i*-octane, benzene, and toluene were the products of Aldrich (purity ≥ 99%).

7.2.2
Experiments with the Corona Reactor

Corona reactor (wire/cylinder configuration; cylinder size: 38.5 mm i.d. × 600 mm; wire size 1 mm × 620 mm), power supplies, gas line, and the apparatus used for electric and chemical diagnostics were described in detail in previous publications [13–15]. As shown in the schematic drawing of Figure 7.1a, the reactor is used in a flow-through mode of operation, which allows changing of the input energy by either of the two ways: the applied voltage is changed while maintaining a constant gas flow rate; alternatively, the gas flow rate is changed while maintaining a constant applied voltage. All experiments reported in this work were conducted by changing the applied voltage at a constant gas flow rate of 450 mL min^{-1}. The experimental procedure and the analytical protocols used were as described previously [13–15]. Briefly, for each applied voltage, a 1-mL aliquot of the treated gas mixture was withdrawn with a gastight volumetric syringe from the sampling port just downstream of the reactor. GC-FID quantitative analysis of the aliquots yielded VOC conversion data, $[VOC]/[VOC]_0$. Plots of $[VOC]/[VOC]_0$ against E,

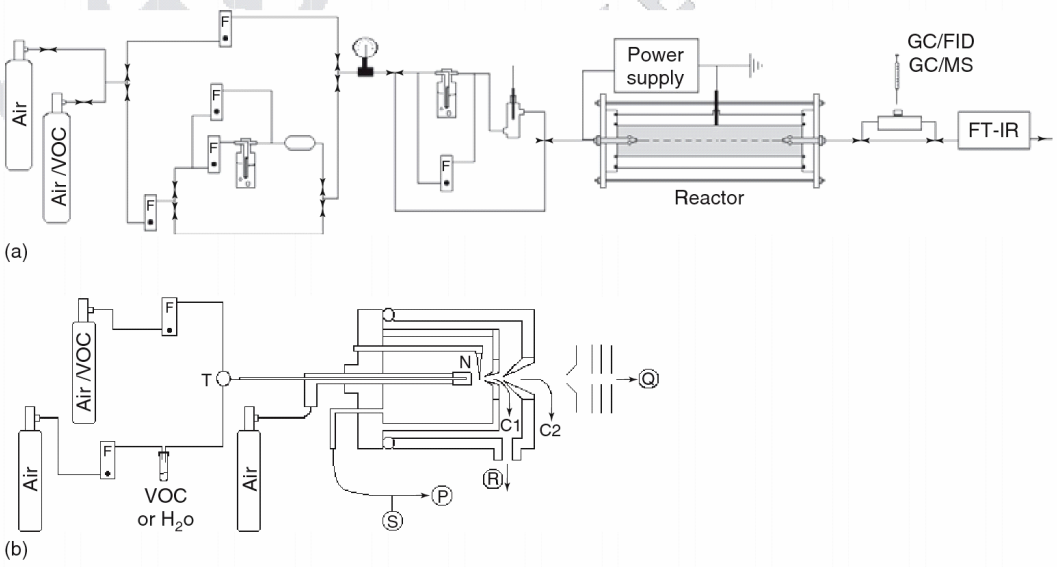

Figure 7.1 Schematics of the experimental apparatus: (a) corona reactor, gas line, and diagnostics system; (b) APCI-mass spectrometer. Legend for symbols: F = mass flow controller; T = T-junction; P = diaphragm pump; S = septum-capped sampling port; N = needle electrode at high voltage; C1 = sampling cone; C2 = skimmer cone; R = rotary pump; Q = quadrupolar mass analyzer.

the corresponding energy per unit volume or *specific input energy* ($kJ \cdot L^{-1}$), were interpolated with the exponential function of Eq. (7.1) to determine the energy constant k_E, which is a measure of the process energy efficiency.

$$[VOC] / [VOC]_0 = e^{-k_E E} \tag{7.1}$$

The specific input energy for DC [14] and pulsed [15] corona was determined as described previously. Since k_E depends on $[VOC]_0$ [1, 2, 11, 12], in order to compare the efficiency of the different corona regimes, all experiments were conducted at the same initial concentration of VOC (500 ppm).

Current/voltage characteristics of DC corona were monitored both in the presence and in the absence of the selected VOC, always in 500 ppm concentration. For each applied voltage the mean current intensity was measured with a multimeter after a stabilization time of 5 min.

7.2.3 Analysis of Ions

APCI spectra in air plasma were acquired with a TRIO 1000 II instrument (Fisons Instruments, Manchester, U.K.), equipped with a Fisons APCI source as described in earlier publications [16, 17]. The ion source, schematically drawn in Figure 7.1b, is kept at atmospheric pressure by a flow of synthetic air (4000 – 5000 $mL \cdot min^{-1}$) introduced through the nebulizer line, a capillary of about 2 mm i.d.. Vapors of the desired VOC, stripped from a liquid sample by an auxiliary flow of synthetic air (typically 5–50 $mL \cdot min^{-1}$), enter the APCI source through a capillary (i.d. = 0.3 mm) running coaxially inside the nebulizer line. A second line allows for the introduction of water vapors as desired. The needle electrode for corona discharge was kept at 3000 V. Ions leave the source through an orifice, about 50 μm in diameter, in the counter electrode (the "sampling cone," held at 0–150 V relative to ground), cross a region pumped down to about 10–2 torr, and, through the orifice in a second conical electrode (the "skimmer cone," kept at ground potential), reach the low-pressure region hosting the focusing lenses and the quadrupole analyzer. Prior to the introduction of the organic compound, a preliminary analysis is routinely conducted to monitor the "background" spectra with only air (or humid air) introduced into the APCI source.

7.3 Results and Discussion

In Figure 7.2, we report the decay of *n*-hexane in dry air as a function of specific input energy in our corona reactor under identical experimental conditions (dry air, initial concentration of VOC: 500 ppm) except for the power supply: +DC (•), −DC(▲), and +pulsed (♦) [13, 15, 18]. Not only is a much greater efficiency observed when energy is provided by pulsed corona than by DC corona, but also significant differences are found between +DC and −DC corona. Similar trends were also

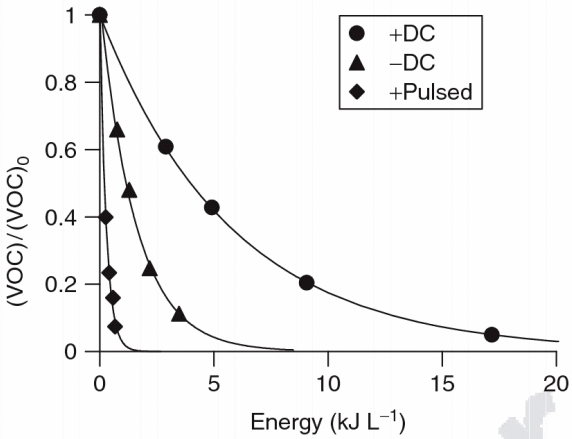

Figure 7.2 Efficiency of removal of *n*-hexane (500 ppm initial concentration in dry air) by different types of corona at room temperature and pressure.

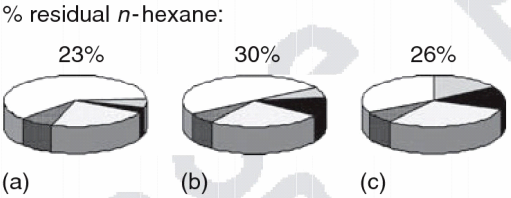

Figure 7.3 Comparison of product distributions in *n*-hexane processing with (a) +pulsed, (b) −DC, and (c) +DC corona at similar conversion extents. Color code: dots = residual *n*-hexane, spheres = volatile organic byproducts, white = unaccounted carbon, gray = CO_2, black = CO.

observed with *i*-octane [15] and toluene [19] thus indicating that the efficiency of hydrocarbon processing decreases in the order +pulsed > −DC > +DC. Interestingly, the observed product distributions are also significantly different for the three energization modes tested. An example is shown in Figure 7.3, which compares product data for three experiments in which *n*-hexane was decomposed by treatment with +pulsed, +DC, and −DC corona to achieve similar conversions (the residual hexane was 23, 30, and 26%, respectively). It is evident that different product distributions are obtained under the different energization modes. Notably, the extent of unaccounted carbon, due to nonvolatile and/or particulate byproducts, is the largest with +pulsed corona (60%) and decreases in the order −DC (50%) > +DC (32%). In contrast, the selectivity for CO_2 production follows an opposite trend, namely +DC (16%) is better than −DC and + pulsed (6% for both).

The process response to the presence of humidity in the air is also very characteristic of the mode of corona energization. Figure 7.4 shows decomposition data for *i*-octane induced by +DC (circle symbols) and −DC (triangle symbols) in dry (open symbols) and humid air (40%RH•) (closed symbols). It is seen that the

Q1

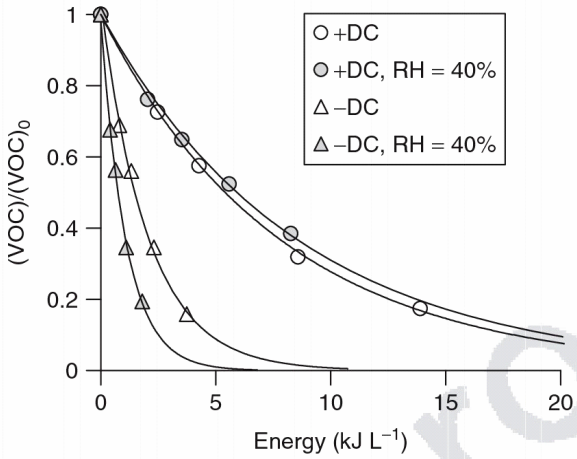

Figure 7.4 Effect of humidity on the efficiency of removal of *i*-octane (initial concentration 500 ppm in air) by DC corona.

efficiency of the process induced by −DC corona increases in humid air whereas a slight decrease is found with +DC corona. Similar observations were also made with *n*-hexane [14] and toluene [19], as shown by the energy constants summarized in Table 7.1. As for +pulsed corona, the presence of humidity in the air improves the efficiency of hydrocarbon processing, but the effect is much less pronounced than for −DC corona. This can be appreciated by the data reported in Table 7.1 under the heading "%Δ" which represents the percent efficiency change in going from dry to humid (40% RH) air. In the case of toluene, for example, with −DC corona the efficiency of hydrocarbon processing in humid air doubles with respect to dry air, whereas with +pulsed corona a modest increment of 15% is experienced under the same conditions.

Note that for *n*-hexane two sets of data are reported in Table 7.1 for +DC and −DC experiments. The data in parentheses were recorded with the reactor in an earlier configuration [14], which was later slightly modified to allow for the acquisition of optical emission spectra [18]. The modification to house the optical lens required increasing slightly the length of the emitting wire while maintaining its original diameter (1 mm) and composition (stainless steel). Moreover, the wire morphology also changed from the original entwined threads, not anymore available, to a smooth cylindrical shape. This new electrode was used in the present work as well as in that reported in [13, 18, 19].

The data in Table 7.1 also serve to establish relative reactivity scales for the investigated hydrocarbons and thus to address the question of structure/reactivity relationship. Relative reactivity data are shown in Table 7.2, taking *n*-hexane as the reference compound and using consistent sets of data. Thus, the relative reactivity of *i*-octane versus *n*-hexane was calculated using, for the latter, the data in parentheses which were obtained at the same time and with the same reactor configuration as the data for *i*-octane [14]. Table 7.2 shows that *n*-hexane is more

Table 7.1 Efficiency of VOC processing by +DC, −DC, and +pulsed corona in dry and humid (40% RH) air.

	k_E(kJ · L^{-1})								
	+DC			−DC			+pulsed		
VOC[a]	Dry	Humid	% − Δ[b]	Dry	Humid	% − Δ[b]	Dry	Humid	% − Δ[b]
n-Hexane[c]	0.20 (0.17[d])	0.18 (0.15[d])	−10%	0.77 (0.58[d])	1.1 (1.1[d])	+43% (+90%)	2.1	2.2	+30%
i-Octane[d]	0.13	0.12	−8%	0.42	0.75	+79%	–	–	–
Toluene[e]	0.14	0.13	−7%	0.41	0.81	+98%	3.1	3.5	+15%

[a] Initial concentration of VOC was 500 ppm.
[b] Percentage increment/decrement of k_E in humid air relative to dry air.
[c] Ref. [19].
[d] Ref. [14].
[e] Ref. [18].

Table 7.2 VOCs relative reactivity data in processing by +DC, −DC, and +pulsed corona in dry and humid (40% RH) air.

	+DC		−DC		+pulsed	
VOC[a]	Dry	Humid	Dry	Humid	Dry	Humid
n-Hexane	(1.00)	(1.00)	(1.00)	(1.00)	(1.00)	(1.00)
i-Octane	0.76	0.80	0.72	0.68	–	–
Toluene	0.70	0.72	0.53	0.74	1.45	1.59

[a] Initial concentration of VOC was 500 ppm.

reactive than both *i*-octane and toluene under DC corona conditions, whereas an inversion in the relative order of reactivity is found under +pulsed corona conditions, with toluene being about 1.5 times more reactive than *n*-hexane.

The effect of humidity is most interesting not only for obvious practical implication but also because it provides important clues on the mechanisms of VOC oxidation. One major outcome due to the presence of water within the air plasma is the formation of OH radicals which are among the strongest known oxidants of VOCs. There are many ways by which OH radicals can be formed by corona discharges in humid air. These include H_2O reactions with electrons, neutrals and ions as shown in Eqs. (7.2)–(7.6b).

$$H_2O + e \rightarrow {}^{\bullet}OH + {}^{\bullet}H + e \tag{7.2}$$

$$O(^1D) + H_2O \rightarrow 2^{\bullet}OH \tag{7.3}$$

$$N_2^{+\bullet} + H_2O \rightarrow N_2H^+ + {}^{\bullet}OH \tag{7.4a}$$

$$\rightarrow H_2O^{+\bullet} + N_2 \tag{7.4b}$$

$$H_2O^{+\bullet} + H_2O \rightarrow H_3O^+ + {}^{\bullet}OH \tag{7.5}$$

$$O_2^{+\bullet} + H_2O + M \rightarrow O_2^{+\bullet}(H_2O) + M \tag{7.6a}$$

$$O_2{}^{+\bullet}(H_2O) + H_2O \rightarrow H_3O^+ + {}^{\bullet}OH + O_2 \tag{7.6b}$$

In "dry" air, the origin of OH radicals is to be attributed to any residual water present and to the reaction of VOC molecules with atomic oxygen, as shown for toluene, as an example, in Eq. (7.5c)

$$O(^1D) + C_6H_5CH_3 \rightarrow {}^{\bullet}OH + C_6H_5CH_2^{\bullet} \tag{7.7}$$

How important are these reactions for each of the different corona regimes compared in this work? How many OH radicals are present in each case? To compare the relative $^{\bullet}OH$ density produced by +DC, −DC, and +pulsed corona in our reactor, we have used a chemical reactivity probe which was developed for atmospheric chemistry determinations [20] and later used also for determinations in atmospheric plasmas [13, 15, 21, 22]. The probe is based on the known reaction of OH radicals with CO for which a rate constant of 2.28×10^{-13} cm^{-3} · molecule^{-1} · s^{-1} was reported at 296 K [23].

$$CO + {}^{\bullet}OH \rightarrow CO_2 + {}^{\bullet}H$$
$$k = 2.28 \cdot 10^{-13}\text{cm}^3 \cdot \text{molecule}^{-1} \cdot \text{s}^{-1}\ (T = 296\ \text{K}) \tag{7.8}$$

The experiments were conducted by subjecting CO (500 ppm in air) to +DC, −DC, and +pulsed treatment in our reactor, both in dry and in humid (40% RH) air. The results are summarized in Figure 7.5. It is seen that the concentration of CO does not change in dry air even under conditions of high input energies, indicating that the reactive species present in dry air plasmas are not capable of oxidizing carbon monoxide. In contrast, a decay of CO concentration is observed in all experiments conducted in humid air, with the efficiency of reaction (7.8) being, however, greatly different depending on the mode of energization: +pulsed > −DC > +DC.

In the light of these results one can now interpret the reactivity data of Table 7.1 and conclude that the oxidation of hydrocarbons in humid air is greatly favored by attack of OH radicals in −DC, while in +DC this reaction route is not important since in the presence of OH radicals a slight decrease in efficiency is observed. Considering that OH radicals are much more reactive than O atoms toward hydrocarbons (see, for example, Eqs. (7.9) and (7.10) concerning *i*-octane [24, 25]), the fact that OH radicals are not involved in hydrocarbon oxidation in +DC processing reasonably suggests that reaction with O atom is also not very likely in this systems and that alternative routes should be considered.

$$i\text{–}C_8H_{18} + O(^3P) \rightarrow {}^{\bullet}OH + \text{products}$$
$$k = 9.13 \times 10^{-14}\text{cm}^3 \cdot \text{molecule}^{-1} \cdot \text{s}^{-1}\ (T = 307\ \text{K}) \tag{7.9}$$

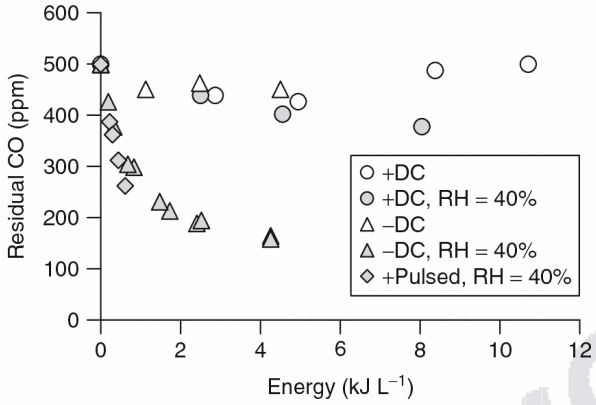

Figure 7.5 Efficiency of CO (500 ppm initial concentration) oxidation under different corona types in dry and humid air.

$$i\text{–}C_8H_{18} + {}^{\bullet}OH \rightarrow H_2O + \text{products}$$
$$k = 3.34 \times 10^{-12}\text{cm}^3 \cdot \text{molecule}^{-1} \cdot \text{s}^{-1}\ (T = 298\ \text{K}) \qquad (7.10)$$

We believe that ion–molecule reactions are important in these systems. Such conclusion is not simply based on the exclusion of a significant role by reactions with neutrals ($^{\bullet}$OHand O) and on the consideration that ion–molecule reactions are intrinsically much faster than reactions with neutrals (compare the rate constants of Eqs. (7.9) and (7.10) with those of Eqs. (7.11–7.14) [26, 27]) but is also supported by direct experimental observations made in the study of current/voltage characteristics of DC coronas and of the corresponding ionized species.

$$i\text{–}C_8H_{18} + O_2^{+\bullet} \rightarrow \text{products} \qquad k = 1.8 \times 10^{-9}\text{cm}^3 \cdot \text{s}^{-1}\ (T = 300\ \text{K}) \qquad (7.11)$$

$$i\text{–}C_8H_{18} + N_2^{+\bullet} \rightarrow \text{products} \qquad k = 2.0 \times 10^{-9}\text{cm}^3 \cdot \text{s}^{-1}\ (T = 300\ \text{K}) \qquad (7.12)$$

$$i\text{–}C_8H_{18} + NO^{+} \rightarrow \text{products} \qquad k = 1.8 \times 10^{-9}\text{cm}^3 \cdot \text{s}^{-1}\ (T = 300\ \text{K}) \qquad (7.13)$$

$$i\text{–}C_8H_{18} + H_3O^{+} \rightarrow \text{products} \qquad k = 4.9 \times 10^{-10}\text{cm}^3 \cdot \text{s}^{-1}\ (T = 300\ \text{K}) \qquad (7.14)$$

Figure 7.6 reports current/voltage characteristics measured for −DC and +DC corona in pure air and in air containing 500 ppm of benzene. The data show that while −DC corona current/voltage profiles show no response to the presence of benzene in the air (Figure 7.6b), with +DC corona the current detected in benzene-containing air is significantly lower than in pure air (Figure 7.6a). Since corona current is due to ion transport across the drift region of the interelectrode gap and depends on the ion mobility, our data indicate that different ions are

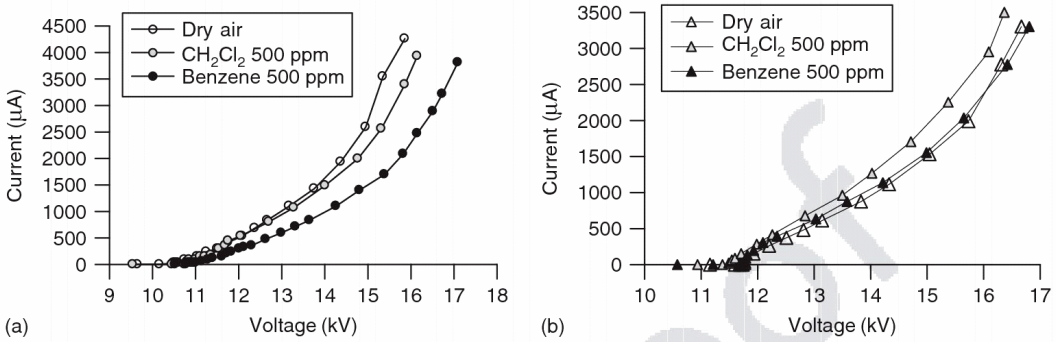

Figure 7.6 Current/voltage characteristics for (a) +DC and (b) −DC corona in pure air and in air containing dichloromethane and benzene.

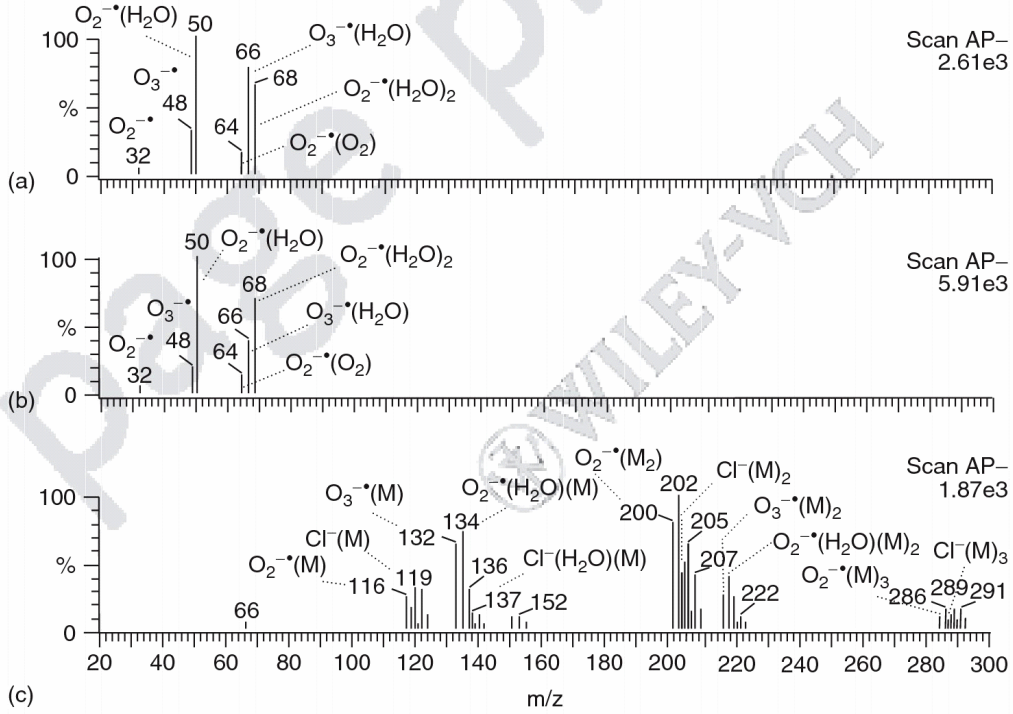

Figure 7.7 Negative-ion APCI mass spectra obtained at ambient temperature and pressure with (a) pure air, (b) benzene in air, and (c) CH_2Cl_2 in air.

involved in pure air and in hydrocarbon-containing air. Specifically, the average ion mobility is lower in hydrocarbon-containing air than in pure air. These observations are supported and rationalized by the results of our ion studies. The APCI-MS mass spectra reported in Figure 7.7 show that with −DC corona the negatively charged ions are observed in pure air (Figure 7.7a) and in benzene-containing

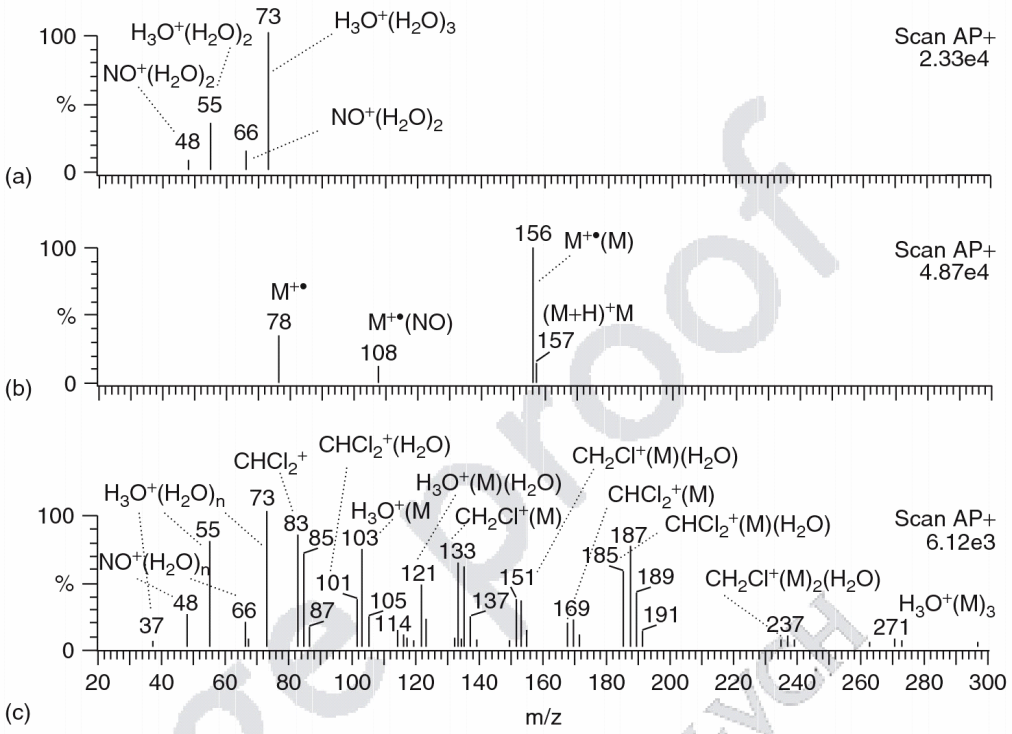

Figure 7.8 Positive-ion APCI mass spectra obtained at ambient temperature and pressure with (a) pure air, (b) benzene in air, and (c) CH_2Cl_2 in air.

air (Figure 7.7b). These are $O_2^{-\bullet}(H_2O)_n$ ($n = 0{-}2$: m/z 32, 50, 68), $O_3^{-\bullet}(H_2O)_n$($n = 0{-}1$: m/z 48, 66), $O_2^{-\bullet}(O_2)$(m/z 64).

In contrast, with +DC corona the spectrum of pure air (Figure 7.8a) differs markedly from that of air containing benzene (Figure 7.8b). Thus, while in pure air major ions are $H_3O^+(H_2O)_n$ ($n = 2{-}3$: m/z 55, 73) and $NO^+(H_2O)_n$ ($n = 0{-}1$; m/z 30, 48), in the presence of benzene the most abundant ions are evidently the benzene radical cation, $C_6H_6^{+\bullet}$ (m/z 78), its cluster with a neutral benzene $(C_6H_6{}^{+\bullet})(C_6H_6)$ (m/z 156) and the complex $(C_6H_6)NO^+$ (m/z 108). Such ions have different compositions, sizes, and shapes from those detected in pure air and are therefore reasonably expected to have different mobilities. Thus, despite its low concentration (500 ppm), benzene produces major effects on the ion population formed by +DC in air and, consequently, on the corona current/voltage characteristic. In contrast, no effects are seen for −DC corona. The behavior of benzene is very similar to that of other hydrocarbons studied previously, notably *n*-hexane [13], *i*-octane [13], and toluene [19].

Such observations, combined with the evidence presented above that OH radicals do not take part in the rate-limiting initiation of hydrocarbon oxidation by +DC corona, suggest that ion–molecule reactions play an important role in these processes.

While these conclusions appear to be of general validity for hydrocarbons (the same behavior was observed with benzene (this work), *n*-hexane [13, 28], *i*-octane [13, 28], and toluene [19]), the picture changes drastically with other VOCs, notably halogen-containing organic compounds. Negative-ion APCI mass spectra of chloro- and bromo-containing VOCs [16, 17, 29, 30] are generally rich in signals due to VOC-derived ions including Cl^-, Br^-, and clusters thereof. This behavior is consistent with the known high electron affinity of alkyl halides, which are readily ionized via electron transfer and charge transfer reactions. Dichloromethane is no exception and produces a wealth of negatively charged ions within the air plasma produced by −DC corona (Figure 7.7c), consisting mainly of ion–molecule complexes of Cl^-, $O_2^{-\bullet}$, and $O_3^{-\bullet}$ with H_2O and dichloromethane molecules. Consistently, significant differences are seen in the current/voltage profiles measured for −DC corona in pure air and in air containing dichloromethane in 500-ppm concentration (Figure 7.6b). As for the effect of dichloromethane on +DC corona, this is similar to that of the hydrocarbons. Thus, the +DC corona current is modified with respect to pure air, being somewhat lower at any applied voltage (Figure 7.6a). The APCI positive mass spectrum of dichloromethane (Figure 7.8c) is very complex and comprises many ions derived from VOC ionization/fragmentation or from ion–molecule complex formation in which VOC molecules are neutral ligands. Tentative attributions are shown on the spectrum (Figure 7.8c), always with reference, in the case of Cl-containing species, to the isotopic peak of the lowest mass, that is, the signal which is due, within each cluster, to ions containing only the isotope ^{35}Cl.

7.4 Conclusions

The results presented and discussed in this paper support the view that different corona regimes (DC or pulsed, positive or negative polarity) applied within the same reactor under the same experimental conditions can support different mechanisms of VOC oxidation. We propose that, in spite of the overall rather similar general features of hydrocarbon processing with +DC, −DC, and +pulsed corona, the crucial initiation steps are different. Specifically, with +DC corona ionic reactions, which are intrinsically much faster than radical reactions, prevail not only in dry air but also in humid air. In contrast, with −DC and +pulsed corona radical initiation steps occur, involving mainly $O(^3P)$ in dry air and $^{\bullet}OH$ in humid air. Electron-induced bond dissociation is also probably an important decay channel, especially for toluene [12]. This might be the reason for the inversion in the relative reactivity order observed for toluene in +pulsed corona with respect to DC processing. The elemental composition and chemical structure of the decomposing VOC have expectedly a major effect on its reactivity under the specific corona regime considered. We have shown here that, in contrast to the behavior of hydrocarbons, the currents measured for −DC corona in air are significantly increased by the addition of trace amounts of dichloromethane (500 ppm). Consistently, the

negative-ion APCI mass spectra are also greatly affected due to the prevalence of VOC-derived Cl-containing anions.

Acknowledgments

Financial support by the University of Padova (Progetto Interarea 2005) is gratefully acknowledged.

References

1. Van Veldhuizen, E.M. (2000) *Electrical Discharges for Environmental Purposes: Fundamentals and Applications*, Nova Science Publishers, New York.
2. Fridman, A. (2008) *Plasma Chemistry*, Cambridge University Press, Cambridge.
3. Kim, H.-H. (2004) *Plasma Processes Polym.*, **1**, 91–110.
4. Penetrante, B.M. (1993) *Nonthermal Plasma Techniques for Pollution Control*, Springer-Verlag, New York.
5. Odic, E., Paradisi, C., Rea, M., Parissi, L., Goldman, A., and Goldman, M. (1999) Treatment of organic pollutants by corona discharge plasma, in *The Modern Problems of Electrostatics with Applications in Environment Protection*, Vol. 63 (eds I.I. Inculet, F.T. Tanasescu, and R. Cramariuc), Springer, Bucharest pp 143–160.
6. Urashima, K. and Chang, J.-S. (2000) *IEEE Trans. Dielectr. Electr. Insul.*, **7**, 602–614.
7. Van Durme, J., Dewulf, J., Leys, C., and Van Langenhove, H. (2008) *Appl. Catal. B: Environ.*, **78**, 324–333.
8. Harling, A.M., Demidyuk, V., Fischer, S.J., and Whitehead, J.C. (2008) *Appl. Catal. B: Environ.*, **82**, 180–189.
9. Harling, A.M., Glover, D.J., Whitehead, J.C., and Zhang, K. (2008) *Environ. Sci. Technol.*, **42**, 4546–4550.
10. Atkinson, R. (2000) *Atmos. Environ.*, **34**, 2063–2101.
11. Rudolph, R., Francke, K.-P., and Miessner, H. (2002) *Plasma Chem. Plasma Process.*, **22**, 401–412.
12. Blin-Simiand, N., Jorand, F., Magne, L., Pasquiers, S., Postel, C., and Vacher, J.-R. (2008) *Plasma Chem. Plasma Process.*, **28**, 429–466.
13. Marotta, E., Callea, A., Ren, X., Rea, M., and Paradisi, C. (2008) *Plasma Process. Polym.*, **5**, 146–154.
14. Marotta, E., Callea, A., Rea, M., and Paradisi, C. (2007) *Environ. Sci. Technol.*, **41**, 5862–5868.
15. Marotta, E., Callea, A., Ren, X., Rea, M., and Paradisi, C. (2007) *Int. J. Plasma Environ. Sci. Technol.*, **1**, 39–45.
16. Marotta, E., Scorrano, G., and Paradisi, C. (2005) *Plasma Processes Polym.*, **2**, 209–217.
17. Donò, A., Paradisi, C., and Scorrano, G. (1997) *Rapid Commun. Mass Spectrom.*, **11**, 1687–1694.
18. Zaniol, B., Schiorlin, M., Gazza, E., Marotta, E., Ren, X., Puiatti, M.E., Rea, M., Sonato, P., and Paradisi, C. (2008) *Int. J. Plasma Environ. Sci. Technol.*, **2**, 65–71.
19. Schiorlin, M., Marotta, E., Rea, M., and Paradisi, C. (2009) *Environ. Sci. Technol.*, manuscript submitted for● publication. Q2
20. Campbell, M.J., Farmer, J.C., Fitzner, C.A., Henry, M.N., Sheppard, J.C., Hardy, R.J., Hopper, J.F., and Muralidhar, V. (1986) *J. Atmos. Chem.*, **4**, 413–427.
21. Su, Z.-Z., Ito, K., Takashima, K., Katsura, S., Onda, K., and Mizuno, A. (2002) *J. Phys. D: Appl. Phys.*, **35**, 3192–3198.
22. Rudolph, R., Francke, K.-P., and Miessner, H. (2003) *Plasmas Polym.*, **8**, 153–161.
23. Lias, S.G. (2006) Ionization energy evaluation, in *NIST Standard Reference Database*, Vol. 69 (eds W.G. Maillard

and P.J. Linstrom), National Institute of Standard and Technology, Gaithersburg.
24. Herron, J.T. (1988) *J. Phys. Chem. Ref. Data*, **17**, 967–1026.
25. Atkinson, R. (1998) *Pure Appl. Chem.*, **70**, 1327–1334.
26. Arnold, S.T., Viggiano, A.A., and Morris, R.A. (1997) *J. Phys. Chem. A*, **101**, 9351–9358.
27. Arnold, S.T., Viggiano, A.A., and Morris, R.A. (1998) *J. Phys. Chem. A*, **102**, 8881–8887.
28. Marotta, E. and Paradisi, C. (2009) *J. Am. Soc. Mass Spectrom.*, **20**, 697–707.
29. Marotta, E., Bosa, E., Scorrano, G., and Paradisi, C. (2005) *Rapid Commun. Mass Spectrom.*, **19**, 391–396.
30. Nicoletti, A., Paradisi, C., and Scorrano, G. (2001) *Rapid Commun. Mass Spectrom.*, **15**, 1904–1911.

4.5 A COMPARISON OF CF_2Br_2 AND CH_2Br_2 OXIDATION IN AIR AT ROOM TEMPERATURE INDUCED BY ELECTRIC CORONA DISCHARGES

A comparison of CF_2Br_2 and CH_2Br_2 oxidation in air at room temperature induced by electric corona discharges

Ester Marotta, Milko Schiorlin, Marta Dal Molin and Cristina Paradisi*

Department of Chemical Sciences, Università di Padova, 35131 Padova, Italy

The oxidation of two halomethanes, CH_2Br_2 and CF_2Br_2, in air at room temperature and atmospheric pressure was studied in a corona reactor which can be energized with +DC, -DC and +pulsed high voltage. The resulting corona discharges produce non-thermal plasmas (NTP) which are strongly oxidizing environments. For both CH_2Br_2 and CF_2Br_2 the oxidation efficiency depends on the corona regime, +pulsed providing the best among the three types of corona tested. Despite their high reactivity, NTPs display some substrate selectivity, the reaction of CH_2Br_2 being significantly more efficient than that of CF_2Br_2 under all conditions tested. The two halomethanes also form different products: FT-IR analysis of post-discharge gas has shown that CH_2Br_2 produces both CO_2 and CO, whereas CF_2Br_2 forms CO_2 and $F_2C=O$. The latter product is a long-lived oxidation intermediate due to its low reactivity with atmospheric radicals. It is however very rapidly hydrolized to CO_2 and HF as shown by combined ion chromatography and FT-IR analysis of the solution and exhaust gas obtained after a water scrubbing step. Other non-carbon containing products of the discharge were analyzed by FT-IR analysis, including ozone, HNO_3 and N_2O. For both halomethanes evidence was found for bromine-sustained catalytic ozone destruction cycles, responsible also for increased conversion of NOx into HNO_3. Finally, it was found that the two halomethanes respond differently to the presence of humidity in the air. It is concluded that, while for CH_2Br_2 the mechanisms of initial VOC attack are different in +DC and –DC, for CF_2Br_2 a common mechanism operates under all corona regimes tested.

Introduction

Air quality control is a major issue of our days which stimulates the search of ever more efficient and cleaner remediation procedures. Many hundreds of different organic compounds are being released into the atmosphere from natural or anthropogenic sources and many more are being produced from their reactions in the atmosphere. Depending on their structure and reactivity the impact of these organic compounds ranges from toxic effects for living organisms including humans, to greenhouse gas effects, to depletion of the stratospheric ozone layer. What on small scale (in terms of time and space) is highly desirable (lack of reactivity) often brings serious hazards on the wide environmental scale. A prototype example [1] is given by the chemically and biochemically inert chlorofluorocarbons (CFCs) which were successfully developed and used as safe substitutes for refrigerating fluids like ammonia but turned out to be dangerous pollutants in the stratosphere which they reach just in virtue of their persistency, to contribute to the depletion of the ozone layer by releasing chlorine atoms. This problem was overcome with a new generation of substitutes, the hydrofluorocarbons (HFCs), likewise inert and non toxic, but dangerous in their green house gas performance [1].

Electric discharges in air at room temperature and atmospheric pressure have long been used in various technologies including environmental applications for air and water purification [2-8]. Non-thermal plasma (NTP) are thus produced which are characterized by very high electron temperatures in a gas which remains near ambient temperature. These air plasmas are very reactive, strongly oxidizing media which are ideal for the oxidative degradation of multiple pollutants. NTP processing is very advantageous for a number of reasons, which include among others, wide range of applicability, high energy efficiency and low maintenance costs [2-8]. Despite their high reactivity, NTPs display some selectivity which makes it possible to use molecular probes to study and characterize both the plasma and the mechanisms of the reactions it can promote.

We report in this paper a study of corona induced oxidation of two important environmental models, CF_2Br_2 and CH_2Br_2. The first is a fascinating man-made molecule which, like CFCs is inert towards the OH radical and other strong oxidizing species of the troposphere, notably the NO_3 radical and ozone. We have used a reactor capable of sustaining different corona regimes and allows to compare their performance in the oxidation processing of selected model VOCs [9-13]. Essential for this analysis is the wealth of kinetic data available in the literature for the reactions of many VOCs with species which are present in atmospheric air plasmas, notably electrons, O atoms, OH radicals and many important atmospheric ions.

Experimental

Chemicals. Pure air used in the experiments was a synthetic mixture (80% nitrogen - 20% oxygen) from Air Liquid with specified impurities of H_2O (< 3 ppm) and of C_nH_m (< 0.5 ppm). Air mixtures of CF_2Br_2 (500 ppm, ± 3%), CO_2 (520 ppm, ± 2%) and CO (499 ppm, ± 1%) were purchased from Air Liquid in cylinders loaded to a pressure lower than their respective

condensation limits. Liquid CH_2Br_2 was purchase from Aldrich (purity ≥99%).

Experiments with the corona reactor. Corona reactor, power supplies, gas line and the apparatus used for electric and chemical diagnostics were described in detail in previous publications [9-11]. Briefly, the corona reactor is a stainless steel cylinder (38.5 mm i.d. x 600 mm) which is electrically grounded and has a stainless steel emitting wire electrode (1 mm i.d.) fixed along its axis. The reactor can be energized by DC or pulsed high-voltage power. The DC power supply has the following features: input voltage 0 - 220V, output voltage –25 kV - +25 kV, output current 0 - 5 mA. The pulse power supply uses a pulsed high voltage with DC bias (PHVDC), based on a spark gap switch with air blowing, with the following specifications: DC bias 0 - 14 kV (input voltage 0 - 100 V), peak voltage 25 - 35 kV with DC bias (input voltage 120 - 220 V), peak current 100 A, maximum frequency 300 Hz, rise-time of pulses less than 50 ns. The equipment to measure the power input includes a digital oscilloscope (Tektronix type 410A, bandwidth 200 Hz, two channels), a high voltage probe by Tektronix (ratio 1000:1, bandwidth 75 MHz, peak voltage 40 kV), and two homemade current probes with 10 resistors in parallel housed in an electromagnetic shield (1.1 Ω for pulsed current and 52 Ω for DC current).

The reactor is connected to a gas flow line made of teflon tubing (4 mm i.d.). For experiments with CF_2Br_2 a commercial mixture of the VOC in air was used whereas for CH_2Br_2 the desired mixture was prepared by bubbling 'synthetic air' through a sample of the liquid VOC and by diluting the outcoming flow with a second flow of synthetic air to achieve the desired gas composition and flow. The gas flow line is equipped with a loop for humidification and with a probe to measure the humidity. The treated gas exiting the reactor goes through a small glass reservoir equipped with a sampling port from which aliquots are withdrawn with a gas tight syringe for off-line chemical analysis by GC/MS (HP 5973), GC/FID (Varian 3600) and GC/TCD/FID (Agilent Technologies 7890). On-line IR analysis is performed with an FTIR Nicolet 5700 spectrophotometer using a 10 cm long gas cell with NaCl or CsF windows. Quantitation of ozone, CO and CO_2 was performed as described previously [9].

The reactor is used in a flow-through mode of operation. All experiments reported in this work were conducted by changing the applied voltage at a constant gas flow rate of 450 mL·min^{-1} except in the case of CF_2Br_2 processing with +DC, for which a gas flow rate of 150 mL·min^{-1} was used to increase the treatment time for this rather inert VOC. The determination of energy input was done as described previously for DC [9] and pulsed [10] corona, respectively. The experimental procedure and analytical protocols were the same as described previously in detail [9]. Current/voltage characteristics of DC corona were monitored in pure air and in air containing the selected VOC in 500 ppm concentration. For each applied voltage the mean current intensity was measured with a multimeter after a stabilization time of 5 minutes.

Analysis of ions. APCI spectra in air plasma were aquired with a TRIO 1000 II instrument (Fisons Instruments, Manchester, U.K.), equipped with a Fisons APCI source as described in earlier publications [14-18]. The ion source, schematically drawn in Fig. 1b, is kept at atmospheric pressure by a flow of synthetic air (4000-5000 mL·min^{-1}) introduced through the nebulizer line, a capillary of ca. 2 mm i.d.. The mixture of the desired VOC in air is obtained either directly from a gas cylinder or by stripping vapors from its liquid with an auxiliary flow of synthetic air (typically 5-50 mL·min^{-1}). It is then introduced into the APCI source through a capillary (i.d. = 0.3 mm) running coaxially inside the nebulizer line. A second line allows for the introduction of water vapors as desired. The needle electrode for corona discharge was kept at 3000 V. Ions leave the source through an orifice, ca 50 μm in diameter, in the counter electrode (the 'sampling cone', held at 0 - 150 V relative to ground), cross a region pumped down to ca. 10^{-2} Torr and, through the orifice in a second conical electrode (the 'skimmer cone', kept at ground potential), reach the low pressure region hosting the focusing lenses and the quadrupole analyzer. Prior to the introduction of the organic compound, a preliminary analysis is routinely conducted to monitor the 'background' spectra with only air (or humid air) introduced into the APCI source.

Results and Discussion

The oxidation efficiency was measured by monitoring VOC residual concentration as a function of energy input per unit volume (*SIE, Specific Input Energy* in kJ·L^{-1}). In a flow reactor *SIE* can be changed either by changing the applied voltage at a constant flow rate (constant residence time) or by changing the gas flow rate at a constant applied voltage. We have shown previously that either procedure provide the same experimental results. The decay of VOC concentration as a function of *SIE* fits reasonably well the exponential curve of equation (1)

$$\frac{[VOC]}{[VOC]_0} = e^{-k_E \cdot SIE} \qquad (1)$$

where k_E, the energy constant, is a measure of the process efficiency. Typical decay curves for CH_2Br_2 processing with +DC are shown in Figure 1 for experiments carried out with two different initial concentrations, 100 and 1000 ppm, respectively. It is seen that the process efficiency depends on the VOC initial concentration, an effect that is better appreciated in Figure 2 which shows that, within the concentration range explored, k_E increases linearly with $1/[CH_2Br_2]_0$. This behaviour is typical of non-thermal plasma oxidation of VOCs and is consistent with a simple inhibitor kinetic model proposed by Slater and Douglas-Hamilton [19] almost thirty years ago and

found to fit many experimental data thereafter [20-21]. This behaviour makes NTP processing particularly convenient for remediation of large gas masses contaminated by pollutants in low concentration, conditions which make alternative methods, like combustion, very expensive.

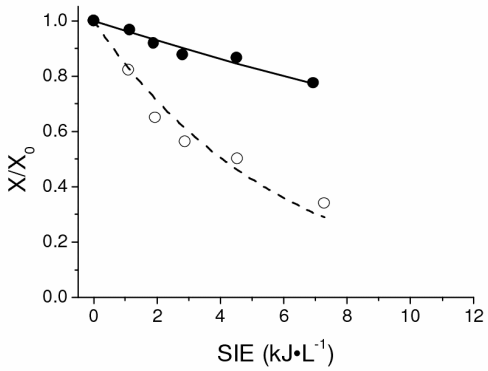

Figure 1. Comparison of the decomposition efficiency between 100 and 1000 ppm of CH_2Br_2 with +DC corona discharge.

Process efficiency also depends on the way by which energy is being provided, -DC corona being more efficient than +DC corona for all VOC examined so far in our reactor. CH_2Br_2 and CF_2Br_2 are no exception, k_E being 3.3 times and 3.1 times greater with –DC than with + DC, respectively [21]. Despite the high oxidizing power of such air plasma, substrate selectivity is observed. Thus, CH_2Br_2 is more reactive than CF_2Br_2 both in –DC and in +DC processing, specifically 1.5 and 1.4 times more reactive, respectively [21].

Products are also different as can be appreciated from the FT-IR spectra recorded in the post-plasma window (Figure 3). Thus, while both CO_2 and CO are found in the case of CH_2Br_2, only CO_2 is present in the case of CF_2Br_2 alongside with the carbonyl intermediate $F_2C=O$. Besides these C-containing products, also HNO_3 and N_2O are detected in both cases, but no ozone which is instead present in the control experiment performed with only air being fed into the reactor (Fig. 3 a).

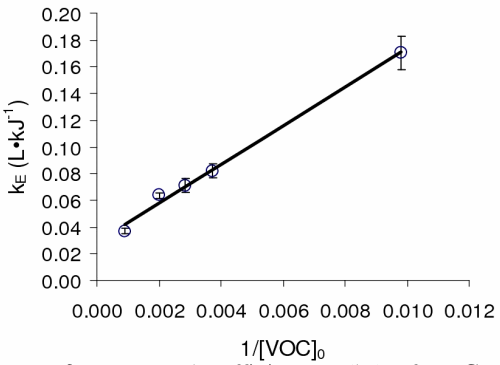

Figure 2. Removal efficiency (k_E) for CH_2Br_2 processing with +DC in dry air as a function of CH_2Br_2 initial concentration, $[CH_2Br_2]_0$.

Common to experiments with either CF_2Br_2 or CH_2Br_2 is the lack ozone in the treated gas. Ozone is an important product of corona discharges in air, as can be appreciated from the FT-IR spectrum of Fig. 3a. As already reported in the literature, we found that the ozone yield for any given input energy depends on the corona regime applied, being much higher for –DC and +pulsed than for +DC corona (Fig. 4). Fig. 4, based on FT-IR analyses, also shows that ozone was not detected at all under any of the corona conditions and specific input energy values applied when the air contained CF_2Br_2 (500 ppm initial concentration). This outcome can be explained considering the well known catalytic cycles for ozone destruction in which Br atoms act as chain propagators (Scheme 1).

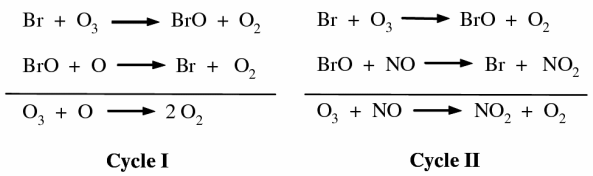

Scheme 1

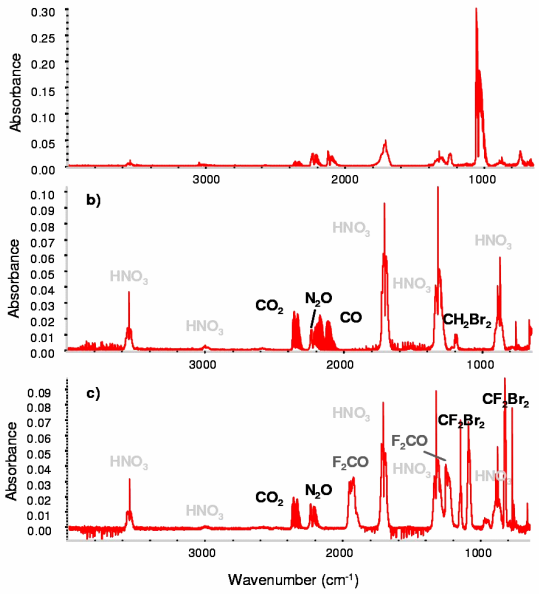

Figure 3. FT-IR spectra of the gas flowing out of the reactor after processing with +DC corona. The feed gas was: (a) pure air; (b) air containing CH_2Br_2 (500 ppm) and (c) air containing CF_2Br_2 (500 ppm).

Both CF_2Br_2 and CH_2Br_2 can form bromine atoms in primary events such as electron induced bond dissociation (eq. 2), the C-Br bond being the weakest bond in both molecules, as well as in dissociative ionization reactions due to interaction with high energy electrons, or, more likely to charge exchange with plasma ions, as shown in eq. (3).

$$CF_2Br_2 + e^- \rightarrow CF_2Br + Br + e^- \qquad E_a = 2.86\ eV \qquad (2)$$

$$O_2^+ + CH_2Br_2 \rightarrow O_2 + CH_2Br^+ + Br \qquad \Delta H = -116.4\ kJ\ mol^{-1} \qquad (3)$$

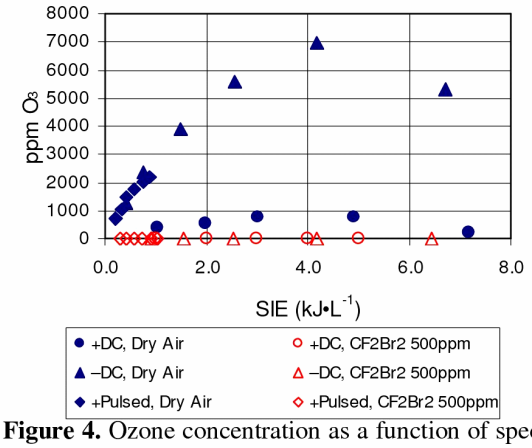

Figure 4. Ozone concentration as a function of specfic input energy in the gas flowing out of the reactor after processing pure air and CF_2Br_2 –containing air (500 ppm initial concentration) with +DC, -DC and +pulsed corona.

As discussed later, Br atoms also form in secondary processes involving the VOC-derived alkoxy radicals.

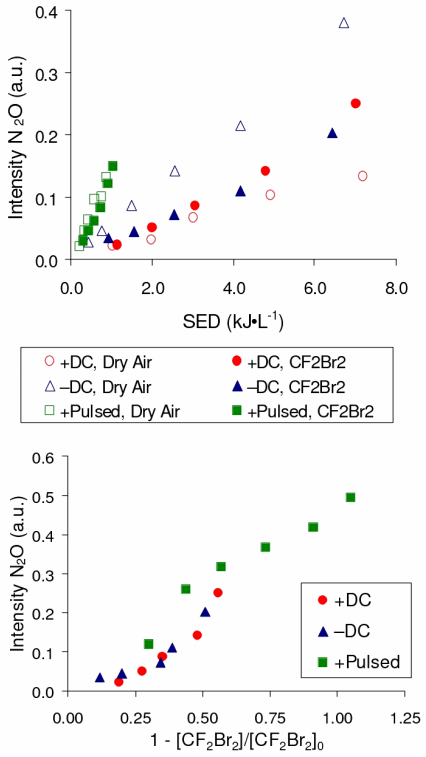

Figure 5. N_2O concentration, expressed as the area of its FT-IR absorption bands, as a function of (a) specific input energy and (b) CF_2Br_2 conversion in experiments performed with +DC, -DC and +pulsed corona discharges.

It also appears that, compared to experiments with pure air, larger amounts of HNO_3 form in the presence of either CF_2Br_2 or CH_2Br_2 (Fig. 3). Considering that HNO_3 derives from the reaction of NO_2 with OH radicals, this result can be viewed as the consequence of NO_2 production via Cycle II of Scheme 1 as well as of reactions (4) and (5) also involving active bromine species.

$$NO_2 + BrO + M \rightarrow BrONO_2 + M \quad (4)$$

$$BrONO_2 + H_2O \rightarrow HNO_3 + HBrO \quad (5)$$

It should be noted that NO_2 is also the precursor of N_2O, the stable nitrogen oxide which is detected among the products of air plasma treatments (Fig. 3), formed according to eq. (6).

$$NO_2 + N \rightarrow N_2O + O \quad (6)$$

Figure 5 shows the profile of N_2O concentration, expressed as the area of its FT-IR absorption bands, as a function of specific input energy (Fig. 5a) and of CF_2Br_2 conversion (Fig. 5b) in experiments performed with +DC, -DC and +pulsed corona discharges. It can be seen that, regardless of the specific corona regime used, all experimental points describe a reasonably homogeneous profile displaying a roughly linear increase of N_2O concentration with the reaction progress.

Similar conclusions are also reached for CF_2O and for CO_2, the C-containing products of CF_2Br_2 plasma induced oxidation. The concentration profiles for these two products as a function of reaction progress are shown in Figure 6. As for N_2O production, there is no appreciable difference or discontinuity in these trends to suggest that different plasma regimes support different oxidation mechanisms.

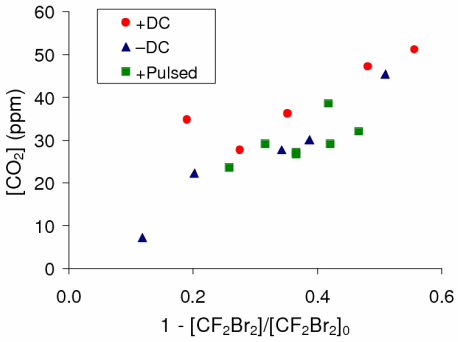

Figure 6. CF_2O (a) and CO_2 (b) concentrations as a function of CF_2Br_2 conversion in experiments performed with +DC, -DC and +pulsed corona discharges.

Highly informative were also the results of ion chromatography (IC) analysis of the aqueous solution obtained by bubbling, for a set time, the gas coming out of the reactor through a water scrubber. These analyses have shown that, besides NO_3^-, also Br^- and, for CF_2Br_2 processing, F^- are found in the aqueous solution. FT-IR analysis of the gas emerging from the water scrubber has shown that the signals due to $F_2C=O$ have disappeared. This observation is consistent with the known properties of $F_2C=O$, an important fluorine-containing reservoir in the atmosphere, having low reactivity towards gas phase radical species. Its removal in the atmosphere is thus attributed to reaction with water. In the condensed phase (aqueous solution or rain droplets) hydrolysis is

very fast ($t_{1/2}$ = 0.16 s). In the gas phase the same reaction (7)

$$F_2C{=}O + H_2O \rightarrow CO_2 + 2HF \quad (7)$$

is exothermic (ΔH = - 25 kcal/mol). Calculations have shown that the reaction proceeds in a stepwise manner and that some of these steps have high activation energy (30-36 kcal/mol). These barriers are however drastically reduced when one additional water molecule is considered in the calculations (it stabilizes and lowers the energy of some of the transition states), making the hydrolysis extremely fast. Accordingly, in our NTP treatments in dry air $F_2C{=}O$ is a long-lived intermediate and we are able to detect it by FT-IR analysis (Fig. 3c). The little water that there is around under these conditions is responsible for the production of CO_2 via reaction (7) and there is no route to CO production for CF_2Br_2, since CO is formed via radical reactions.

Another remarkable difference between CH_2Br_2 and CF_2Br_2 is their response to the presence of humidity within the plasma. Experiments in humid air are most relevant to practical applications since water is a major component of ambient air. Earlier work had shown that with –DC the oxidation of various hydrocarbons [9,13] and of CH_2Br_2 [21] is more facile in humid than in dry air, an effect attributed to the OH radical which is known to react very efficiently with C-H bonds in organic compounds, like for example with CH_2Br_2 via H-abstraction to form H_2O and an organic carbon radical (eq. 8) [22].

$$CH_2Br_2 + OH \rightarrow \text{products}$$
$$k = 1.1\times10^{-13}\ cm^3\ molecule^{-1}\ s^{-1}\ (T = 298\ K) \quad (8)$$

In contrast, the oxidation of CF_2Br_2 in humid air is not favored at all, but rather somewhat hindered relative to dry air (Figure 7). This observation is consistent with the well known poor reactivity of CF_2Br_2 with OH, reaction (9) being over two orders of magnitude slower [22] than that with CH_2Br_2.

$$CF_2Br_2 + OH \rightarrow \text{products}$$
$$k = 5\times10^{-16}\ cm^3\ molecule^{-1}\ s^{-1}\ (T = 298\ K) \quad (9)$$

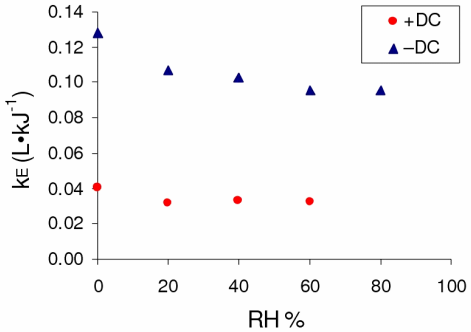

Figure 7. Efficiency of CF_2Br_2 (500 ppm initial concentration) removal with +DC and –DC as a function of relative humidity (RH%) in the air.

The slight decrease in efficiency of CF_2Br_2 in humid with respect to dry air is attributed to reaction (10) which contributes to lower the average electron energy of the plasma to produce OH radicals, which are, however, unable to attack this specific VOC.

$$H_2O + e^- \rightarrow OH + H + e^- \quad (10)$$

Similar observations (Figure 7) and conclusions also apply to +DC processing of CF_2Br_2 in humid air suggesting that the underlying chemistry is also the same. A different response was obtained earlier for CH_2Br_2 [21]. Thus, while –DC processing is favoured by the presence of humidity, +DC processing is not, suggesting that different mechanisms might be involved for this VOC in –DC and in +DC corona plasmas. Similar conclusions were also reached for hydrocarbons [11,13] leading to the proposal that ionic initiation reactions are important in +DC corona induced hydrocarbon oxidation. Support for this proposal came from analyses of the ions formed in the plasma and of current/voltage characteristics for +DC corona [11,13,14,21].

The combination of all results reported here support the proposal that corona induced oxidation of CF_2Br_2 in air proceeds via a common mechanism with any of +DC, -DC and +pulsed corona. Most likely initiation step is the electron induced dissociation shown in eq. (2), which requires about 2.86 eV, reasonably within the range of our NTPs produced by either DC or pulsed corona. The greater efficiency of +pulsed with respect to DC corona processing is consistent with the higher mean electron energy we measured for this regime in an emission spectroscopy investigation performed using the same reactor [12]. Once the CF_2Br radical is formed (eq. 2) it reacts with molecular oxygen (eq. 11), followed by reaction of the peroxy radical with NO to form the oxy radical (eq. 12).

$$CF_2Br + O_2 + M \rightarrow CF_2BrOO + M \quad (11)$$

$$CF_2BrOO + NO \rightarrow CF_2BrO + NO_2 \quad (12)$$

The CF_2BrO radical is known to dissociate to release Br as shown in eq. 13

$$CF_2BrO \rightarrow F_2C{=}O + Br \quad (13)$$

In our experiments in dry air $F_2C{=}O$ is a major C-containing product of CF_2Br_2 oxidation, the other one being CO_2. Note that the fact that we do not observe CO in our product mixture is consistent with the known chemical inertia of $F_2C{=}O$ towards atmospheric radicals. On the other hand this product is most efficiently hydrolized by bubbling the exhaust gas in water as shown by the complementary detection of fluoride ion in ion chromatographic analysis and disappearance of FT-IR absorption bands due to $F_2C{=}O$.

In contrast to $F_2C{=}O$, the corresponding carbonyl derivatives formed from CH_2Br_2, i.e. $CH_2{=}O$ and CHBr=O, react with radicals and produce CO, as found in our FT-IR product studies (Fig. 3b).

Finally, it is worth noting that the key intermediate in the oxidation of CF_2Br_2, the radical CF_2Br, in –DC corona could also form via charge transfer reaction with O_2^- which is slightly exothermic (the estimated electron affinity of CF_2Br_2 is 0.46 eV vs 0.45 eV for

O_2). This charge transfer can be dissociative (14a) or non dissociative (14b):

$$CF_2Br_2 + O_2^- \rightarrow CF_2Br + Br^- + O_2 \quad (14a)$$

$$CF_2Br_2 + O_2^- \rightarrow CF_2Br_2^- + O_2 \quad (14b)$$

Consistently, we found that negative ion APCI-MS spectra of air/CF_2Br_2 mixtures contain signals due to both the molecular anion, $CF_2Br_2^-$, and Br^-.

Acknowledgements

Financial support by the University of Padova (PRAT 2005) is gratefully acknowledged.

References

[1] J. H. Seinfeld, S. N. Pandis 'Atmospheric chemistry and physics' 1998, Wiley-Interscience, New-York

[2] Van Veldhuizen E M 2000 *Electrical Discharges for Environmental Purposes: Fundamentals and Applications* (New York: Nova Science Publishers)

[3] Fridman A 2008 *Plasma Chemistry* (Cambridge: Cambridge University Press)

[4] Kim H-H 2004 *Plasma Process. Polym.* **1** 91

[5] Penetrante B M 1993 *Nonthermal plasma techniques for pollution control* (New York: Springer Verlag)

[6] Mizuno A 2007 *Plasma Phys. Contr. Fusion* **49** A1

[7] Odic E, Paradisi C, Rea M, Parissi L, Goldman A and Goldman M 1999 in *The Modern Problems of Electrostatics with Applications in Environment Protection* (Bucarest: Springer) pp 143-160

[8] Urashima K and Chang J-S 2000 *IEEE Trans. Diel. Electr. Insul.* **7** 602

[9] Marotta E, Callea A, Rea M and Paradisi C 2007 *Environ. Sci. Technol.* **41** 5862.

[10] Marotta E, Callea A, Ren X, Rea M and Paradisi C 2007 *Int. J. Plasma Env Sci. Technol.***1** 39

[11] Marotta E, Callea A, Ren X, Rea M and Paradisi C 2008 *Plasma Process. Polym.* **5** 146

[12] Zaniol B, Schiorlin M, Gazza E, Marotta E, Ren X, Puiatti M E, Rea M, Sonato P and Paradisi C 2008 *Int. J. Plasma Environ. Sci. Technol.* **2** 65

[13] Schiorlin M, Marotta E, Rea M and Paradisi C submitted for publication.

[14] Marotta E and Paradisi C 2009 *J. Am. Soc. Mass Spectrom.* **20** 697

[15] Marotta E, Scorrano G and Paradisi C 2005 *Plasma Process. Polym.* **2** 209

[16] Donò A, Paradisi C and Scorrano G 1997 *Rapid Commun. Mass Spectrom.* **11** 1687

[17] Nicoletti A, Paradisi C and Scorrano G 2001 *Rapid Commun. Mass Spetrom.* **15** 1904

[18] Marotta E, Bosa E, Scorrano G and Paradisi C 2005 *Rapid Commun. Mass. Spectrom.* **19** 391

[19] Slater C and Douglas-Hamilton D H 1981 *J. Appl. Phys.* **52** 5820

[20] Rudolph R, Francke K P and Miessner H 2002 *Plasma Chem. Plasma Process.* **22** 401

[21] Marotta E, Schiorlin M, Rea M and Paradisi C 2010 *J. Phys. D: Appl. Phys.* **42** 0000

[22] Lias S G "Ionization Energy Evaluation" *NIST ChemistryWebBook, NIST Standard Reference Database No. 69*, Maillard W G, Linstrom P J, Eds., National Institute of Standards and Technology, Gaithersburg MD, http://webbook.nist.gov/chemistry/, 2006.

4.6 CATALYST-ASSISTED NTP PROCESSES

This paragraph describe the experimental procedure, results and discussion related to the work activity done at the Advanced Industrial Science and Technology institute (AIST) in Tsukuba (Japan), under the supervision of dr. Hyun-Ha Kim, during my doctoral studies.

4.6.1 Introduction

Plasma technology for VOCs abatement is effective for the treatment of moderate flow gas which contains a low amount of pollutant. Urashima e Chang [1] estimated a plasma applicability between 0,01 and 1000 $N \bullet m3 \bullet h^{-1}$ and between 1 and 10000 ppm_v. To the same conclusions arrived Lu et al.[2] A NTP limitations is formation of byproducts including mainly CO. Magureanu et al. [3] report that in trichloroethylene decomposition the selectivity to CO2 is less than 25%, while the majority reaction product is CO with a selectivity near 70%. Van Durme et al. [4] have found several heavier hydrocarbons in downstream gas after the decomposition treatment of toluene, in addition to formic acid, benzaldehyde, benzylic acid, methyl-nitrophenol, etc.

A more effective use of plasma is possible by exploiting its inherent synergistic potential in combination with heterogeneous catalysts. [5-7] We are talking here about plasma-assisted catalysis. For example Wallis et al. [8] found that dichloromethane conversion to CO_2 is greatly improved when γ-Al_2O_3 catalyst was introduced in the plasma discharge. Furthermore, production of by-products such as aerosol, ozone and other oxidation organic intermediates are reduced when using hybrid plasma catalyst technology reactors. [8] Van Durme et al [4] reported that the energy efficiency for toluene degradation strongly increases using TiO_2 as in-plasma catalyst. For example, in dry air with an energy density of 17 $J \bullet L^{-1}$, adding TiO_2 increased the toluene (C_0 = 0.5 ppm_v) removal rate from 27 ± 4 to 82 ± 2 %.

Similarly, introducing 15 g of MnO_2-CuO/TiO_2 downstream the plasma discharge resulted in 78 % toluene removal efficiency for an energy density of 2.5 $J \bullet L^{-1}$, while this was only 2 % in the absence of catalyst.

Based on recent papers (2004–2007) two theories related to the synergistic effect between plasma and catalyst emerged. The first argues that heterogeneous catalyst affects the plasma itself modifying its characteristics, the second claim that NTP initiate and influence catalyst mediated reactions. Aim of this research is to acquire knowledge about chemical mechanisms involved in plasma/catalyst synergy.

Then, we begin studying the exchange reaction between $^{16}O_2$ and $^{18}O_2$ in presence of a corona discharge. We used many different types of reactor in order to investigate different corona regimes. We investigated different experimental conditions: the carrier gas (He, N_2), total oxygen content in the gas, and the humidity grade. Afterwards we studied the same reaction in presence of several different catalysts so as to assess if the different physical-chemical properties may influence or not the reaction.

Finally, some benzene decomposition experiments were done in order to evaluate how the plasma produced oxygen "fission" on catalyst surface, and how this is so actively involved in the decomposition mechanism.

4.6.2 Oxygen exchange

Many experiments were been carried out by introducing into the reactor $^{16}O_2$ and $^{18}O_2$ in 1:1 ratio diluted in different concentrations in the carrier gas, He or N_2, both in the absence or presence of water vapour. During each experiment the energy was increased at regular intervals and the downstream gas was analyzed by mass spectrometry to obtain the signals of the ionized species $O_2^{+\bullet}$ the relative concentrations of $^{16}O_2$, $^{18}O_2$ and $^{16}O^{18}O$. The formation of any other species was not revealed. Unfortunately, in the experimental conditions employed it was not possible to perform a complete calibration of the instrument. However, given the identical nature of the three species, $^{16}O_2$, $^{18}O_2$ and $^{16}O^{18}O$, it was reasonably assumed that they give an almost identical instrumental response. The intensity of each ion species for each recorded value of energy was weighed to total ion intensity, thus obtaining the fraction of each species with different isotopic composition compared to total oxygen.

The first experiments were performed using the space discharge reactor. *Figure 4.1* shows the results obtained using helium as carrier gas and three different percentage of dilution (O_{2TOT} 5%, 10%, 20%). It is possible to see that

increasing the energy, the fraction of $^{16}O^{16}O$ and $^{18}O^{18}O$ are decreasing while $^{16}O^{18}O$ correspondingly increase up to a mole fraction of 0.5 and then remain constant. This result is in agreement with the statistical distribution expected and consistent with the hypothesis that the exchange takes place through a mechanism of dissociation into atomic oxygen and subsequent reaction with molecular oxygen: [10]

$$O_2 + e^- \longrightarrow 2\,O^\bullet + e^- \qquad\qquad O^\bullet + O_2 \longrightarrow O_2 + O^\bullet$$

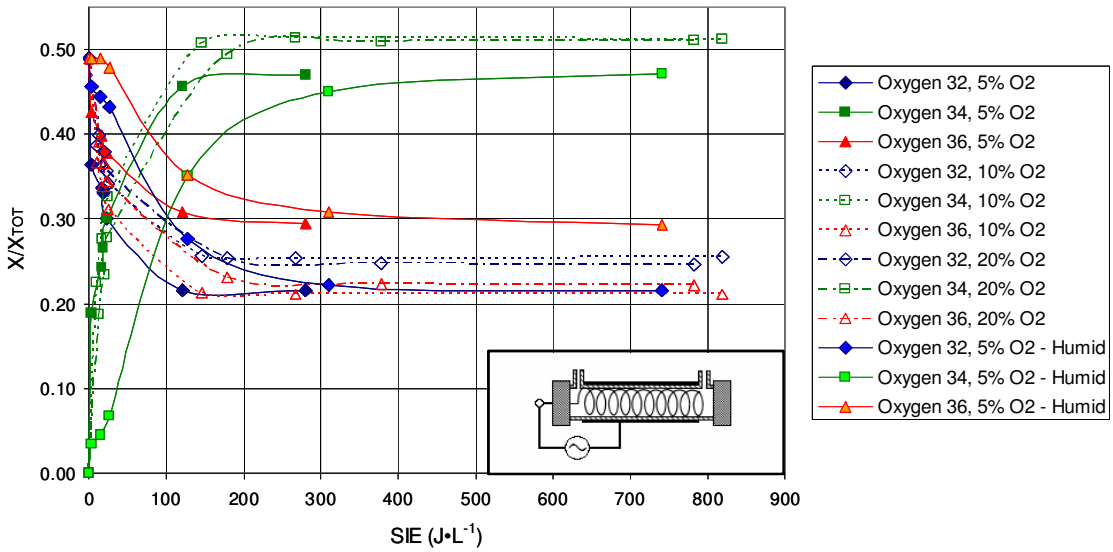

Figure 4.1: Trend of the m/z 32, 34 and 36 species as a function of given energy with different % of O_{2TOT} in dry and humid helium.

As can be seen in *Figure 4.1*, as the total percentage of oxygen increased more energy is required to reach the equilibrium distribution.

This was due to the presence of an increasing number of oxygen molecules that, having a greater cross section compared to helium, require higher energy because the collisions were effective. This trend also happened in wet conditions, in which the water molecules in turn contribute to absorb energy from the plasma by reducing the number of effective collisions for oxygen isotopic exchange.

When nitrogen was used as a carrier gas more energy was needed to reach the steady state in the formation of mixed species, since part of the energy was dissipated in collisions with nitrogen molecules, which have a cross section greater that helium (*Figure 4.2*).

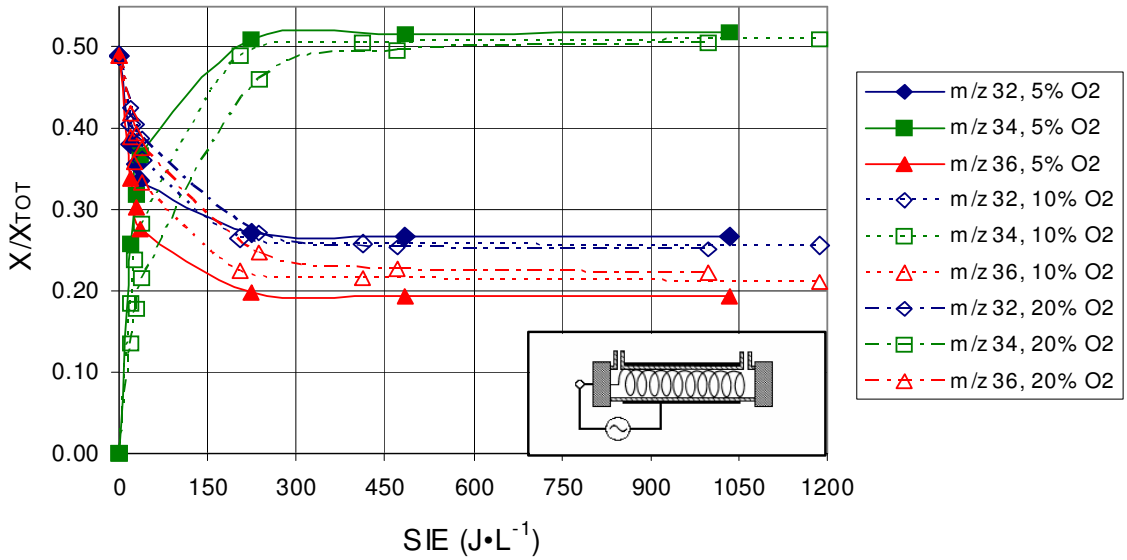

Figure 4.2: Trend of the m/z 32, 34 and 36 species as a function of given energy with different % of O_{2TOT} in dry nitrogen.

To verify that this phenomenon doesn't depend solely on the type of applied corona discharge the same experiments were carried out using the DBD reactor (*Figure 3.11c*). Also in this reactor the isotope exchange reaction occur and the mole fraction of the mixed species with m/z equal to 34 stabilized to the value of 0.5 according to the statistical distribution (*Figure 4.3*).

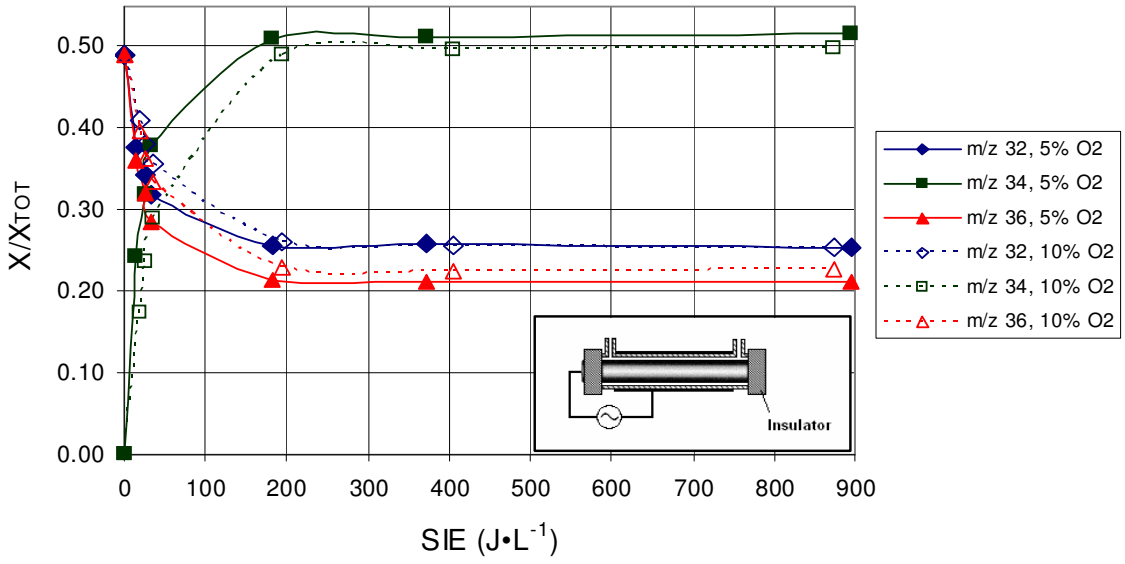

Figure 4.3: Trend of the m/z 32, 34 and 36 species as a function of given energy with different % of O_{2TOT} in dry nitrogen.

In the case of +DC discharge (*Figure 4.4*), obtained using the pin-to-plate reactor (*Figure 3.11a*), the formation of the mixed species is almost negligible. With this reactor was not possible to use the same energy values used with

reactors (b) and (c), because when the voltage was increased there was the formation of the discharge phenomenon known as “breakdown” (in which an electrical discharge is produced in air). With the electrical circuit closing the corona phenomenon disappear entirely, and also continuing to increase the voltage there is the formation of a continuous arc in air. With –DC discharge, however, even if the energy supplied to the reactor is low, you may see a decrease in the proportion of $^{16}O_2$ and $^{18}O_2$ and the subsequent formation of $^{16}O^{18}O$ species, although the steady state was not reached.

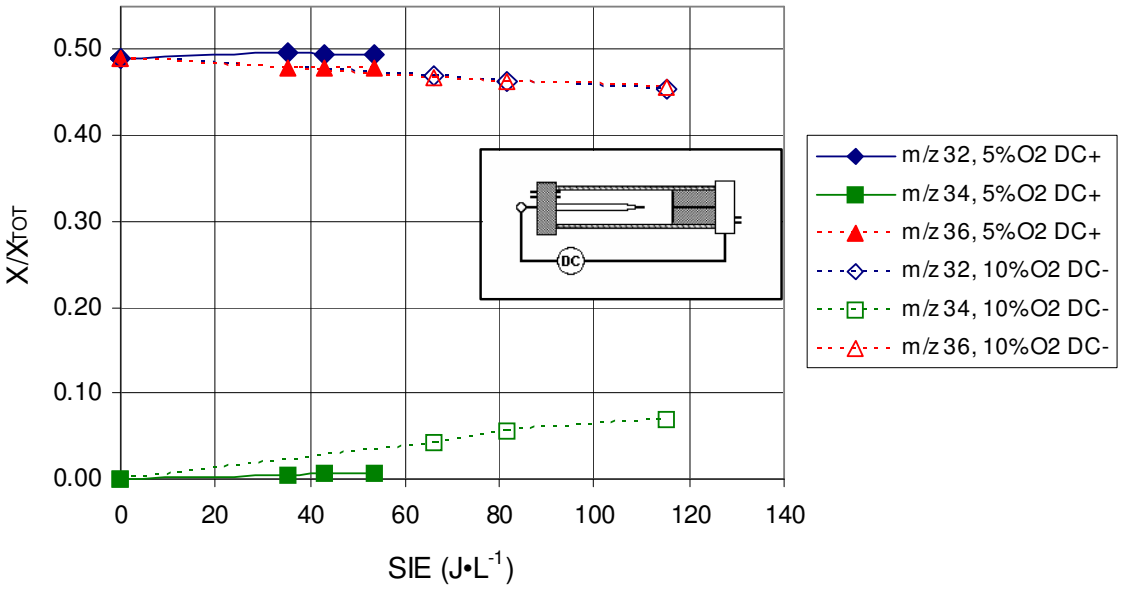

Figure 4.4: Trend of the m/z 32, 34 and 36 species as a function of given energy with different % of O_{2TOT} in dry nitrogen.

Once seen that in any case the reaction was not influenced by the total percentage content of oxygen, the type of carrier gas and particularly the kind of discharge regimes, but was only proportional to the amount of the supplied energy, we made experiments using the PDC reactor (*Figure 3.11d*). We tried different types of catalysts, including: TiO_2, MS-13X and γAl_2O_3. The results are compared in *Figure 4.5*. As showed neither the type of catalyst nor the amount of metal supported on the surface affects the reaction, despite these characteristics influence the efficiency of VOCs decomposition. [11]

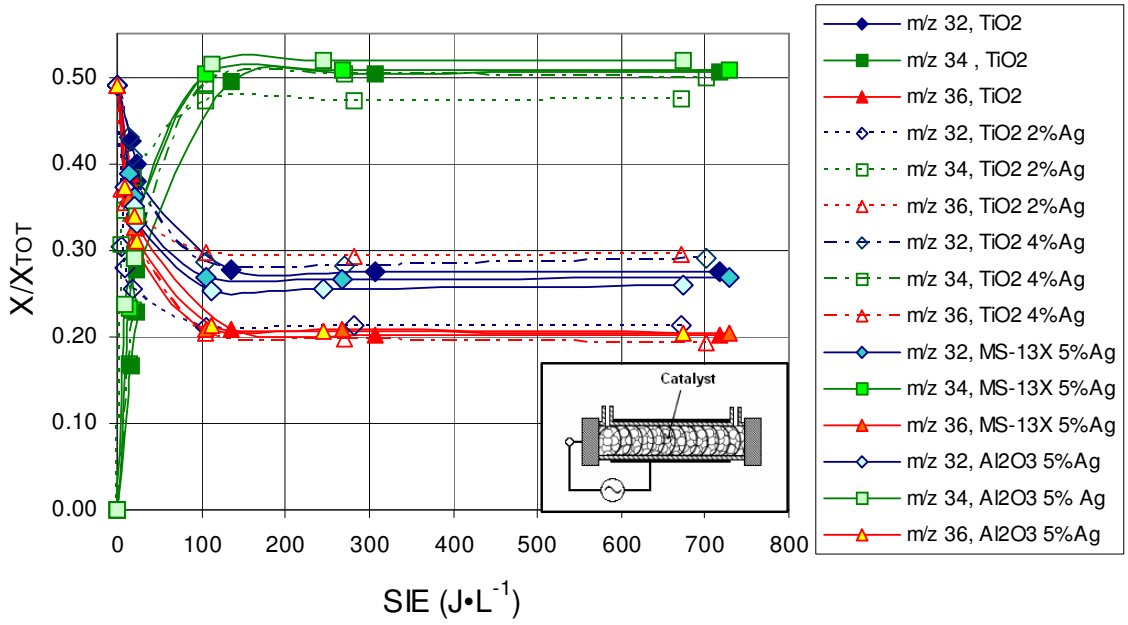

Figure 4.5: Trend of the m/z 32, 34 and 36 species as a function of given energy with different % of O_{2TOT} in dry nitrogen.

4.6.3 Oxygen fission over catalyst surface

Another interesting experiment that was done regard the oxygen exchange on the surface of the catalyst. Using the PDC reactor (*Figure 3.11d*) was seen as the oxygen is "fixed" on the surface of the solid using the corona discharge. The two oxygen isotopes, $^{18}O_2$ and $^{16}O_2$, were transported alternatively into the reactor, and then decomposition experiment, using benzene as model VOC, were carried out to se if among the oxidation products $C^{16}O^{18}O$, $C^{18}O_2$, $C^{16}O_2$, besides $C^{18}O$ and $C^{16}O$ were formed. Again mass spectrometry was used to perform the analysis.

As first experiment, a flow rate of 200 mL•min^{-1} containing 2.5 % of $^{18}O_2$ into helium was passed through the reactor for 10 minutes keeping the discharge off. Then the flow rate of $^{18}O_2$ was interrupted and a flow rate of 2.5 % of $^{16}O_2$ into helium was passed for 30 minutes. Afterwards to the upstream gas benzene was added (around 1000 ppm_v), by bubbling a portion of helium through a bubbler containing the liquid hydrocarbon and the discharge was applied to run the decomposition of the VOC.

The result (*Figure 4.6*) shows only the formation of $C^{16}O_2$ and $C^{16}O$. As there is no chemical species containing ^{18}O this leads us to conclude that in the

absence of discharge, the oxygen doesn't undergo any physisorption phenomenon on the catalyst.

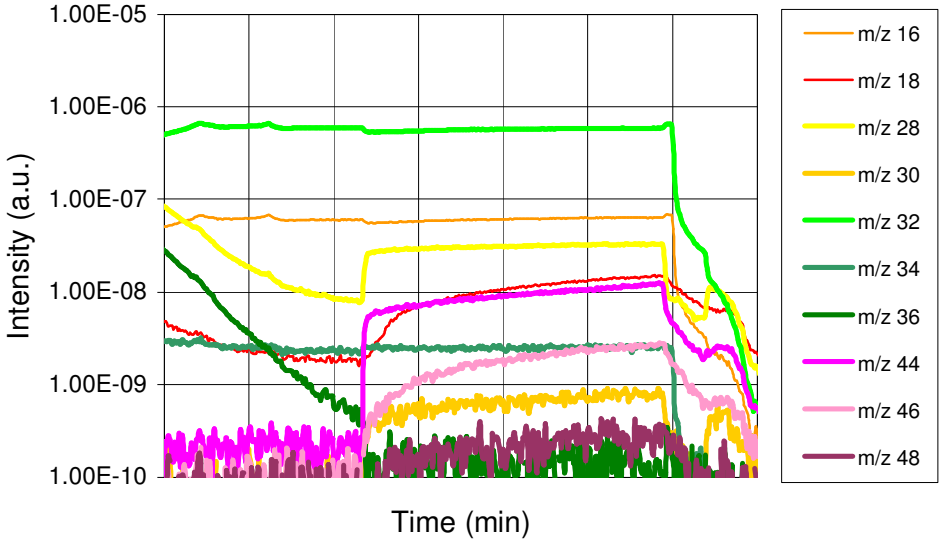

Figure 4.6: Benzene decomposition with TiO_2 after treatment with $^{18}O_2$ without applying corona discharge.

The second experiment consisted on turning on the corona discharge during the 10 minutes in which $^{18}O_2$ (2.5 % in He) was flowing inside the reactor. As in the first experiment a flow rate of $^{16}O_2$ (2.5 % in He) was allowed to pass through the reactor for 30 min, then benzene was added and the decomposition was performed applying the corona discharge. As shown in *Figure 4.7*, in addition to the formation of carbon dioxide with m/z 44, we also note the formation of that of m/z 46 and 48. Similarly was possible to detect an increase of carbon monoxide with m/z 28 and m/z 30.

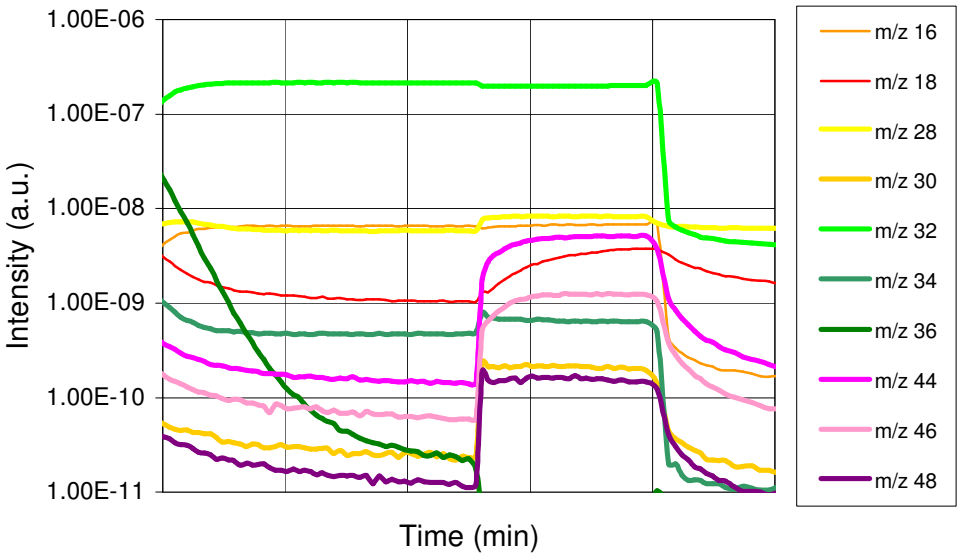

Figure 4.7: Benzene decomposition with TiO_2 after treatment with $^{18}O_2$ applying corona discharge.

The same results were obtained also using TiO2 catalyst with 2 and 4 % of Ag supported on the surface. The same experiments were performed also using various other materials including molecular sieves MS-13X with 5 % of Ag, and gamma-alumina with 5 % of Ag. Even in these cases the results were the same as observed for titanium oxide as received, so the phenomenon of oxygen "fission" on the catalyst does not depend on the chemical and physical properties of the catalyst or the percentage of metal loaded on it. Therefore this result could not be used to explain why changing the type of catalyst, the type and amount of metal supported on it, the efficiency of the VOC decomposition process and the CO_2/CO selectivity increase. The result rather suggested that the catalyst contribution is the increased production of reactive species for the VOC decomposition.

4.6.4 References

[1] Urashima, K.; Chang, J.S. *Trans. Dielectr. Electron. Insul.* **2000**, 7, 602-614;

[2] Lu, B.; Zhang, X.; Yu, X.; Feng, T.; Yao, S. *J. Hazard. Mater.* **2006**, 137, 633-637;

[3] Magureanu, M.; Mandache, N.B.; Parvulescu, V.I.; Subrahmanyam, C.; Renken, A.; Kiwi-Minsker, L. *Appl. Catal. B: Environ.* **2007**, 74, 270-277;

[4] Van Durme, J.; Dewulf, J.; Sysmans, W.; Leys, C.; Van Langenhove, H. *Chemosphere* **2007**, 68, 1821-1829;

[5] Roland, U.; Holzer, F.; Kopinke, F.D. *Appl. Catal. B: Environ.* **2005**, 58, 217–226;

[6] Guo, Y.F.; Ye, D.Q.; Chen, K.F.; He, J.C.; Chen, W.L. *J. Mol. Catal. A: Chem.* **2006**, 245, 93–100;

[7] Grossmannova, H.; Neirynck, D.; Leys, C. *Czech. J. Phys.* **2006**, 56, 1156–1161;

[8] Wallis, A.E.; Whitehead, J.C.; Zang, K. *Appl. Catal. B: Environ.* **2007**, 74, 111–116;

[9] Kim, H.H.; Ogata, A.; Futamura, S. *J. Phys. D: Appl. Phys.* **2005**, 38, 1292–1300;

[10] Anderson, S.M.; Hulsebusch, D.; Mauersberger, K. J. Chem. Phys. 1997, 107, 5385-5392;

[11] RIF: Kim, H.-H.; Ogata, A.; Futamura, S. *IEEE Trans. Plasma Sci.* **2006**, 34, 984-995.

4.7 DETERMINATION OF ATOMIC OXYGEN IN ATMOSPHERIC PLASMA FROM OXYGEN ISOTOPIC EXCHANGE

Determination of atomic oxygen in atmospheric plasma from oxygen isotopic exchange

Milko Schiorlin[1,2], Ester Marotta[2*], Hyun-Ha Kim[1*], Cristina Paradisi,[2] Atsushi Ogata[1]

[1] National Institute of Advanced Industrial Science and Technology (AIST), Tsukuba 305-8569, Japan
[2]Department of Chemical Sciences, Università di Padova, 35131 Padova, Italy

Oxygen scrambling is observed when a 1:1 mixture of $^{16}O_2$ and $^{18}O_2$ 5-20% in nitrogen is treated in a surface discharge plasma reactor. Statistical isotopic distribution ($^{16}O_2$:$^{18}O_2$:$^{16}O^{18}O$ 1:1:2) is achieved with a very low energy input. This process, implemented by kinetic simulations, is proposed as a chemical probe for oxygen atom determination in atmospheric plasma.

Atmospheric plasma are nowadays considered one of the most promising technologies for depuration of air from VOCs in low concentration. The advantages of this technology include the possibility to operate at room temperature and atmospheric pressure, simple working procedures and the highest efficiency in the treatments of diluted gaseous mixtures [1-5] However the knowledge of the mechanisms responsible for VOCs decomposition are not yet completely clarified. In this context the determination of the reactive species concentration is a very important task, from which depends also a rational optimization of the operative conditions.

The main neutral reactive species produced in an air plasma at atmospheric pressure include oxygen atoms in excited and ground state, hydroxyl radicals, particularly important in humid air, and ozone, which is produced in the highest yields by dielectric barrier discharge (DBD) devices. Positive and negative ions have also to be considered, but their lifetime and consequently their role in the reactive system strongly depend on the type of applied discharge.

While reliable analytical procedures have been set up for the determination of stable reactive species as O_3, the measurement of OH radical and O-atom concentration under the same conditions results a difficult task due to the short lifetime of these species and the need of complicated and expensive instruments for performing direct measurements [6,7].

In this paper we propose a chemical method for the determination of O-atom in atmospheric plasma exploiting the molecular oxygen isotopic exchange due to the reaction of $O(^3P)$ with molecular oxygen composed of a different isotope (reaction 1):

$$^{x}O(^3P) + {}^{y}O_2 \rightarrow {}^{x}O^{y}O + {}^{y}O(^3P) \qquad (1)$$

where x,y = 16,18 and x≠y.

This process is known to happen very fast after the application of an electrical discharge [8], but its dependence from the energy applied to the system has never been reported. Herein we report the progress of the reaction as a function of energy and show how, in combination with kinetic simulations, it can be used for determining the averaged $O(^3P)$ concentration produced in the plasma for a given energy input.

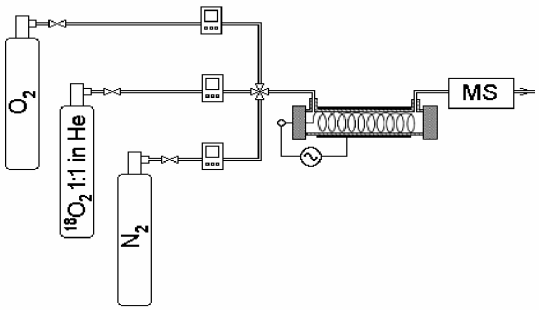

Figure 1. Schematics of the experimental apparatus

In this study we used the experimental apparatus shown in Fig.1. The reactor is a 19 cm long quartz tube with an internal diameter of 0.8 cm externally coated by a silver paste. The high voltage electrode is a stainless steel wire of 0.45 mm of diameter rolled inside the quartz tube. The reactor is energized by an AC high voltage (10 – 1000 Hz).

The energy input per gas flow rate unit (Specific Input Energy, SIE) is calculated by dividing the discharge power P by the flow F (equation 2):

$$SIE\ (J{\cdot}L^{-1}) = P{\cdot}F^{-1} \qquad (2)$$

P is determined using the Lissajous software (Insight Co. Version 1.72) [9]. For the measure of charge (Q) a condenser of 95 nF was connected in series at the ground line. The applied voltage was measured by a high voltage probe (Tektronix, P6015A) and an oscilloscope (Tektronix, TDS3034B).

The gas exiting the reactor was analyzed by a mass spectrometer (MKS Residual Gas Analyzer) equipped with a quadrupole mass analyzer and a Faraday cup and a multiplier as detectors (MKS Microvision IP). In the present experiments the multiplier was used

preferentially as it offered an higher sensitivity. The covered mass range was from m/z 4 to 80.

The gas introduction line is shown in Figure 1. Mixtures of $^{16}O_2$ and $^{18}O_2$ in about 1:1 ratio in nitrogen were prepared by mixing pure O_2 of natural isotope composition (99.9999%, producer) with isotopically enriched $^{18}O_2$ (we received two cylinders 95% and 97%-^{18}O, diluted 50% in helium, from Takachiho Co.). The experiments were performed with overall oxygen concentrations of 5, 10 and 20%. The desired composition was achieved by properly setting the mass flow controllers of the two oxygen cylinders and then adjusting the total gas flow rate to 0.2 L·min^{-1} with pure nitrogen.

During the experiment the energy was progressively increased from 0 to 1.2 kJ·L^{-1}. At fixed energy values the ionic abundance of oxygen-containing species were recorded, notably ^{16}O (m/z 16), ^{18}O (m/z 18), $H_2{}^{16}O$ (m/z 18), $H_2{}^{18}O$ (m/z 20), $^{16}O_2$ (m/z 32), $^{18}O_2$ (m/z 36), $^{16}O^{18}O$ (m/z 34), $N^{16}O$ (m/z 30), $N^{18}O$ (m/z 32), $N_2{}^{16}O$ (m/z 44), $N_2{}^{18}O$ (m/z 46), $N^{16}O_2$ (m/z 46), $N^{16}O^{18}O$ (m/z 48), $N^{18}O_2$ (m/z 50) and O_3 of all possible isotopic composition (m/z 48, 50, 52 and 54). Some mass superimpositions are evident, as for example m/z 32, which could be due both to $^{16}O_2$ and $N^{18}O$. However, as $N^{16}O$ was not revealed, m/z 32 can be reliably attributed to $^{16}O_2$ only. Also the signals at m/z 44 and 46 were absent indicating that at the considered energy values no nitrogen oxides were formed in the plasma. As for ozone formation, it was detected in millionth fraction with respect to molecular oxygen. Of all the listed species the only ones that are of high abundance and change significantly during the process are $^{16}O_2$, $^{16}O^{18}O$ and $^{18}O_2$ (m/z 32, 34 and 36). Their relative abundances were calculated by dividing the intensity of each one by the sum of the intensities of all three. In consideration of the same chemical nature of $^{16}O_2$, $^{16}O^{18}O$ and $^{18}O_2$, it was reasonably assumed that the instrumental response would also be the same and their relative abundances were compared directly.

The obtained results are shown in Figure 2. As SIE is increased the relative abundances of $^{16}O_2$ (m/z 32) and $^{18}O_2$ (m/z 36) decrease and the mixed species $^{16}O^{18}O$ (m/z 34) increases correspondingly. The process of oxygen scrambling proceeds with the increase of the specific energy input until the three isotopic oxygen species reach a stationary state.

The effective initial fractions of $^{16}O_2$,$^{18}O_2$ and $^{16}O^{18}O$ were estimated by mass spectrometry and are reported in Table 1. The initial presence of $^{16}O^{18}O$ is due to the natural isotopic content of ^{18}O in the pure O_2 cylinder and is comprised between 0.1 and 0.2%. The final distribution of the three O_2 isotopic species was compared with that expected for a purely statistical process (reaction 3) of 1:1:2; this was calculated considering the quantities of the different isotopes initially introduced. It was found that the experimental distribution is consistent within a margin of 13% with that expected.

$$^{16}O^{16}O + {}^{18}O^{18}O \rightarrow \frac{1}{2}\,{}^{16}O^{16}O + \frac{1}{2}\,{}^{18}O^{18}O + {}^{16}O^{18}O \quad (3)$$

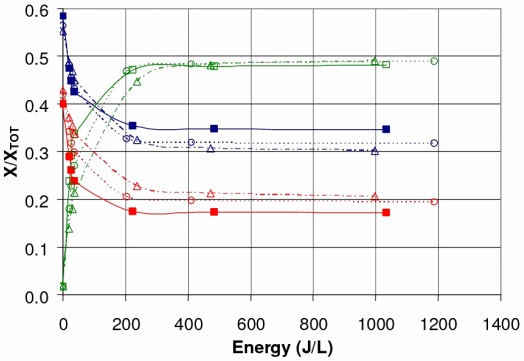

Figure 2. Fraction of $^{16}O_2$ (red trace),$^{18}O_2$ (blue trace) and $^{16}O^{18}O$ (green trace) as a function of energy input in experiments performed with an initial concentration of total oxygen of 5 (square), 10 (circle) and 20% (triangle).

Table 1. Initial fractions of the three O_2 isotopic species and energy constants k_E for isotope oxygen exchange.

% total O_2	$^{16}O_2$ initial fraction	$^{18}O_2$ initial fraction	$^{16}O^{18}O$ initial fraction
5	0.58	0.40	0.02
10	0.56	0.42	0.02
20	0.55	0.43	0.02

Considering that no nitrogen oxides are detected, we neglected the dissociation of nitrogen and considered the reaction system shown below:

$$^{16}O_2 + e^- \rightarrow 2\,{}^{16}O + e^- \quad (4a)$$
$$^{18}O_2 + e^- \rightarrow 2\,{}^{18}O + e^- \quad (4b)$$
$$^{16}O^{18}O + e^- \rightarrow {}^{16}O + {}^{18}O + e^- \quad (4c)$$
$$^{16}O + {}^{18}O_2 \rightarrow {}^{16}O^{18}O + {}^{18}O \quad (5a)$$
$$^{18}O + {}^{16}O_2 \rightarrow {}^{16}O^{18}O + {}^{16}O \quad (5b)$$
$$^{16}O^{18}O + {}^{16}O \rightarrow {}^{18}O + {}^{16}O_2 \quad (5c)$$
$$^{16}O^{18}O + {}^{18}O \rightarrow {}^{16}O + {}^{18}O_2 \quad (5d)$$
$$2\,{}^{16}O + M \rightarrow {}^{16}O_2 + M \quad (6a)$$
$$2\,{}^{18}O + M \rightarrow {}^{18}O_2 + M \quad (6b)$$
$$^{16}O + {}^{18}O + M \rightarrow {}^{16}O^{18}O + M \quad (6c)$$
$$^{16}O + {}^{16}O_2 + M \rightarrow {}^{16}O_3 + M \quad (7a)$$
$$^{16}O + {}^{18}O_2 + M \rightarrow {}^{16}O^{18}O_2 + M \quad (7b)$$
$$^{16}O + {}^{16}O^{18}O + M \rightarrow {}^{16}O_2{}^{18}O + M \quad (7c)$$
$$^{18}O + {}^{16}O_2 + M \rightarrow {}^{16}O_2{}^{18}O + M \quad (7d)$$
$$^{18}O + {}^{18}O_2 + M \rightarrow {}^{18}O_3 + M \quad (7e)$$
$$^{18}O + {}^{16}O^{18}O + M \rightarrow {}^{16}O^{18}O_2 + M \quad (7f)$$
$$^{16}O + {}^{16}O_3 \rightarrow 2\,{}^{16}O_2 \quad (8a)$$
$$^{16}O + {}^{16}O_2{}^{18}O \rightarrow {}^{16}O_2 + {}^{16}O^{18}O \quad (8b)$$
$$^{16}O + {}^{16}O^{18}O_2 \rightarrow {}^{16}O_2 + {}^{18}O_2 \quad (8c)$$
$$^{16}O + {}^{16}O^{18}O_2 \rightarrow 2\,{}^{16}O^{18}O \quad (8d)$$
$$^{16}O + {}^{18}O_3 \rightarrow {}^{18}O_2 + {}^{16}O^{18}O \quad (8e)$$
$$^{18}O + {}^{16}O_3 \rightarrow {}^{16}O_2 + {}^{16}O^{18}O \quad (8f)$$
$$^{18}O + {}^{16}O_2{}^{18}O \rightarrow {}^{16}O_2 + {}^{18}O_2 \quad (8g)$$
$$^{18}O + {}^{16}O_2{}^{18}O \rightarrow 2\,{}^{16}O^{18}O \quad (8h)$$
$$^{18}O + {}^{16}O^{18}O_2 \rightarrow {}^{16}O^{18}O + {}^{18}O_2 \quad (8i)$$

$^{18}O + {}^{18}O_3 \rightarrow 2\ {}^{18}O_2$ (8l)

$^{16}O_3 + M \rightarrow {}^{16}O + {}^{16}O_2 + M$ (9a)

$^{16}O_2{}^{18}O + M \rightarrow {}^{16}O + {}^{16}O^{18}O + M$ (9b)

$^{16}O_2{}^{18}O + M \rightarrow {}^{18}O + {}^{16}O_2 + M$ (9c)

$^{16}O^{18}O_2 + M \rightarrow {}^{16}O + {}^{18}O_2 + M$ (9d)

$^{16}O^{18}O_2 + M \rightarrow {}^{18}O + {}^{16}O^{18}O + M$ (9e)

$^{18}O_3 + M \rightarrow {}^{18}O + {}^{18}O_2 + M$ (9f)

The kinetic constant of reactions (4a)-(4c) depends on the electron mean energy and therefore on the reduced electric field [10]. On the contrary the kinetic constant of reaction (1b) is known from the literature and is equal to $2.9 \cdot 10^{-12}$ $cm^3 \cdot molecole^{-1} \cdot s^{-1}$. [11] The kinetic constant for reaction (1d) is reported as a calculated value in [12] and is equal to about half of k. This is in accordance with the fact that the formation of the products shown in reaction (1d) is in competition with the degenerate reaction $^{16}O^{18}O + {}^{16}O \rightarrow {}^{16}O + {}^{18}O^{16}O$ which does not contribute to changes in the concentration of $^{16}O^{18}O$. In contrast reactions (5a) and (5b) give the products of isotopic exchange whatever is the oxygen atom originating from O_2. Thus, in a first approximation we neglected isotopic effects and consider that reactions (5a) and (5b) progress with the same kinetic constant k_5 and reactions (5c) and (5d) with kinetic constant $k_5/2$. Recombination of O-atom was also considered (reactions 6a-6c); it is reported to take place with a rate constant k_6 equal to $1 \cdot 10^{-32}$ $cm^6 \cdot molec^{-2} \cdot s^{-1}$. [13] Ozone formation (reactions 7a-7f) and destruction by collision with O (reactions 8a-8l) or with the buffer gas M (reactions 9a-9f) were firstly neglected and then taken into account to evaluate if the isotopic species of ozone reach a significant concentration in the system and if the reactions involving ozone affect the trend of O_2 species. The rate constants for reactions (7), (8) and (9) are equal to $k_7 = 5.71 \cdot 10^{-34}$ $cm^6 \cdot molec^{-2} \cdot s^{-1}$, [13] $k_8 = 8.8 \cdot 10^{-15}$ $cm^3 \cdot molec^{-1} \cdot s^{-1}$ [14] and $k_9 = 9.77 \cdot 10^{-24}$ $cm^3 \cdot molec^{-1} \cdot s^{-1}$ [3] and were halved for the reactions which can give different products (8c, 8d, 8g, 8h, 9b-9e).

Therefore the system was submitted to simulation using the application Simbiology of the MatLab R2009b (The MathWorks) program. As k_4 and the electron density are not known and difficult to be estimated, we consider reactions (4a-c) as pseudo-first order reactions including the electron density in the rate constant $k_4' = k_4 \cdot n_e$ in order to have only one unknown variable. Then we performed some simulations attributing to k_4' different values until to fit the concentrations of the isotopic O_2 species obtained in the simulation with the experimental values. This comparison was performed in correspondence of a reaction time equal to the residence time of the gas into the reactor, which is 2.85 s. Moreover, k_4' was recognized as the parameter which varies when the experiments are performed with different energy inputs because energy depends on the electric field, which determines the energy and the density of the electrons.

When one of the value of k_4' was found, we compared two simulations carried out under the same conditions but taking or not into account the reactions involving O_3. In this way it was possible to verify that these reactions (7-10) cannot be neglected because they determine the formation of a significant quantity of ozone and a different shape in the trends of the isotopic O_2 species. Therefore all the simulations were carried out considering the complete reaction system reported above.

A series of simulations with the different total percentage of O_2 (5, 10 and 20%) was thus performed by changing k_4' in order to reproduce the results obtained in the experiment carried out with different SIE. In all cases the trend of the concentration of ^{16}O and ^{18}O increases from zero to the final value in few μs and then remains constant for the total time of the simulation, equal to 10 seconds. In Figure 3 the results relative to the simulation carried out considering a total O_2 percentage equal to 10% and k_4' equal to $3.8 \cdot 10^{-4}$ s^{-1} are reported. This simulation reproduces the results obtained in the experiment carried out with a SIE of 20.4 $J \cdot L^{-1}$ and allows obtaining the concentration of free ^{16}O and ^{18}O present into the system. In Table 2 the concentration of ^{16}O and ^{18}O and finally the total content of O are reported for each energy value lower than that needed to reach the isotopic equilibrium distribution.

Table 2. ^{16}O, ^{18}O and total O concentration determined at different total O_2 percentage in N_2 and energy input.

% total O_2	E (J/L)	^{16}O (10^{10} atoms /cm^3)	^{18}O (10^{10} atoms /cm^3)	total O (10^{10} atoms /cm^3)
5 %	19.8	4.96	3.42	8.38
5 %	27.9	6.20	4.27	10.5
5 %	37.2	7.85	5.40	13.3
10 %	20.4	3.04	2.27	5.31
10 %	27.0	4.80	3.58	8.38
10 %	37.5	5.76	4.29	10.1
20 %	18.6	2.20	1.71	3.91
20 %	29.4	3.14	2.45	5.59
20 %	38.1	4.16	3.24	7.40

Figure 3. Trend of the concentration of ^{16}O and ^{18}O

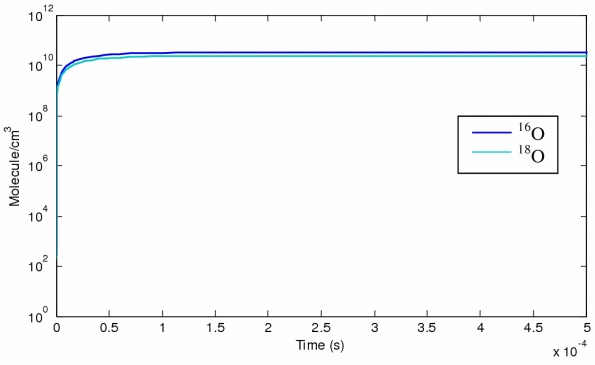

obtained in the simulation with 10% O_2 in N_2 and k_4' equal to $3.8 \cdot 10^{-4}$ s^{-1}.

$^{18}O + {}^{18}O_3 \rightarrow 2\ {}^{18}O_2$ (8l)
$^{16}O_3 + M \rightarrow {}^{16}O + {}^{16}O_2 + M$ (9a)
$^{16}O_2{}^{18}O + M \rightarrow {}^{16}O + {}^{16}O^{18}O + M$ (9b)
$^{16}O_2{}^{18}O + M \rightarrow {}^{18}O + {}^{16}O_2 + M$ (9c)
$^{16}O^{18}O_2 + M \rightarrow {}^{16}O + {}^{18}O_2 + M$ (9d)
$^{16}O^{18}O_2 + M \rightarrow {}^{18}O + {}^{16}O^{18}O + M$ (9e)
$^{18}O_3 + M \rightarrow {}^{18}O + {}^{18}O_2 + M$ (9f)

The kinetic constant of reactions (4a)-(4c) depends on the electron mean energy and therefore on the reduced electric field [10]. On the contrary the kinetic constant of reaction (1b) is known from the literature and is equal to $2.9 \cdot 10^{-12}$ $cm^3 \cdot molecole^{-1} \cdot s^{-1}$. [11] The kinetic constant for reaction (1d) is reported as a calculated value in [12] and is equal to about half of k. This is in accordance with the fact that the formation of the products shown in reaction (1d) is in competition with the degenerate reaction $^{16}O^{18}O + {}^{16}O \rightarrow {}^{16}O + {}^{18}O^{16}O$ which does not contribute to changes in the concentration of $^{16}O^{18}O$. In contrast reactions (5a) and (5b) give the products of isotopic exchange whatever is the oxygen atom originating from O_2. Thus, in a first approximation we neglected isotopic effects and consider that reactions (5a) and (5b) progress with the same kinetic constant k_5 and reactions (5c) and (5d) with kinetic constant $k_5/2$. Recombination of O-atom was also considered (reactions 6a-6c); it is reported to take place with a rate constant k_6 equal to $1 \cdot 10^{-32}$ $cm^6 \cdot molec^{-2} \cdot s^{-1}$. [13] Ozone formation (reactions 7a-7f) and destruction by collision with O (reactions 8a-8l) or with the buffer gas M (reactions 9a-9f) were firstly neglected and then taken into account to evaluate if the isotopic species of ozone reach a significant concentration in the system and if the reactions involving ozone affect the trend of O_2 species. The rate constants for reactions (7), (8) and (9) are equal to $k_7=5.71 \cdot 10^{-34}$ $cm^6 \cdot molec^{-2} \cdot s^{-1}$, [13] $k_8=8.8 \cdot 10^{-15}$ $cm^3 \cdot molec^{-1} \cdot s^{-1}$ [14] and $k_9=9.77 \cdot 10^{-24}$ $cm^3 \cdot molec^{-1} \cdot s^{-1}$ [3] and were halved for the reactions which can give different products (8c, 8d, 8g, 8h, 9b-9e).

Therefore the system was submitted to simulation using the application Simbiology of the MatLab R2009b (The MathWorks) program. As k_4 and the electron density are not known and difficult to be estimated, we consider reactions (4a-c) as pseudo-first order reactions including the electron density in the rate constant $k_4' = k_4 \cdot n_e$ in order to have only one unknown variable. Then we performed some simulations attributing to k_4' different values until to fit the concentrations of the isotopic O_2 species obtained in the simulation with the experimental values. This comparison was performed in correspondence of a reaction time equal to the residence time of the gas into the reactor, which is 2.85 s. Moreover, k_4' was recognized as the parameter which varies when the experiments are performed with different energy inputs because energy depends on the electric field, which determines the energy and the density of the electrons.

When one of the value of k_4' was found, we compared two simulations carried out under the same conditions but taking or not into account the reactions involving O_3. In this way it was possible to verify that these reactions (7-10) cannot be neglected because they determine the formation of a significant quantity of ozone and a different shape in the trends of the isotopic O_2 species. Therefore all the simulations were carried out considering the complete reaction system reported above.

A series of simulations with the different total percentage of O_2 (5, 10 and 20%) was thus performed by changing k_4' in order to reproduce the results obtained in the experiment carried out with different SIE. In all cases the trend of the concentration of ^{16}O and ^{18}O increases from zero to the final value in few µs and then remains constant for the total time of the simulation, equal to 10 seconds. In Figure 3 the results relative to the simulation carried out considering a total O_2 percentage equal to 10% and k_4' equal to $3.8 \cdot 10^{-4}$ s^{-1} are reported. This simulation reproduces the results obtained in the experiment carried out with a SIE of 20.4 $J \cdot L^{-1}$ and allows obtaining the concentration of free ^{16}O and ^{18}O present into the system. In Table 2 the concentration of ^{16}O and ^{18}O and finally the total content of O are reported for each energy value lower than that needed to reach the isotopic equilibrium distribution.

Table 2. ^{16}O, ^{18}O and total O concentration determined at different total O_2 percentage in N_2 and energy input.

% total O_2	E (J/L)	^{16}O (10^{10} atoms /cm^3)	^{18}O (10^{10} atoms /cm^3)	total O (10^{10} atoms /cm^3)
5 %	19.8	4.96	3.42	8.38
5 %	27.9	6.20	4.27	10.5
5 %	37.2	7.85	5.40	13.3
10 %	20.4	3.04	2.27	5.31
10 %	27.0	4.80	3.58	8.38
10 %	37.5	5.76	4.29	10.1
20 %	18.6	2.20	1.71	3.91
20 %	29.4	3.14	2.45	5.59
20 %	38.1	4.16	3.24	7.40

Figure 3. Trend of the concentration of ^{16}O and ^{18}O obtained in the simulation with 10% O_2 in N_2 and k_4' equal to $3.8 \cdot 10^{-4}$ s^{-1}.

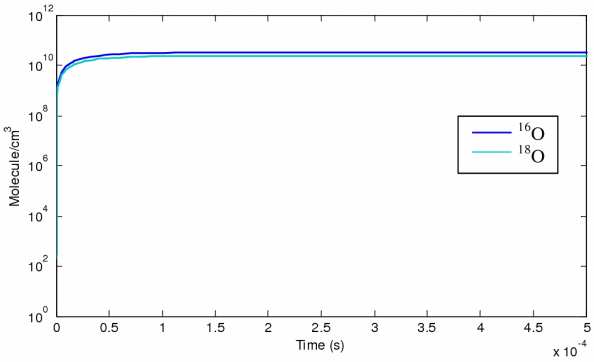

10. O. Eichwald, M. Yousfi, A. hennad, M. D. Benabdessadok. Coupling of chemical kinetics, gas dynamics, and charged particles kinetics models for the analysis of NO reduction from flue gases. *J. Appl. Phys.* **1997**, *82*, 4781-4794.
11. Anderson, S. M.; Klein, F. S.; Kaufman, F. Kinetics of the isotope exchange of ^{18}O with NO and O_2 at 298 K. *J. Chem. Phys.* **1985**, *83*, 1648-1656.
12. Kaye, J. A.; Strobel, D. F. Enhancement of heavy ozone in the earth's atmosphere? *J. Geophys. Res.* **1983**, *88*, 8447-8452.
13. http://kinetics.nist.gov/kinetics/
14. Yanallah, K.; Hadj Ziane, S.; Belasri, A.; Meslem, Y. Numerical modeling of ozone production in direct current corona discharge. *J. Mol. Struct. Teochem.* **2006**, *777*, 125-129.

4.8 OXIDATION OF AQUEOUS PHENOL IN A DIELECTRIC BARRIER DISCHARGE REACTOR

Oxidation of aqueous phenol in a dielectric barrier discharge reactor

Ester Marotta,[1] Milko Schiorlin,[1] Xianwen Ren,[1] Massimo Rea[2] and Cristina Paradisi[1*]

[1]Department of Chemical Sciences, Università di Padova, 35131 Padova, Italy
[2]Retired from the Department of Electrical Engineering, Università di Padova, 35131 Padova, Italy

A novel dielectric barrier discharge reactor was developed for the oxidative degradation of organic pollutants in water. Phenol, chosen as a model compound, is efficiently removed from the aqueous solution according to an exponential decay as a function of treatment time at constant power. The effect of different experimental variables was investigated. The best efficiency was found with active electrodes made of stainless steel wires with a diameter of 0.15 mm and with air flowing above the solution at a rate of 30 mL•min-1. Qualitative analysis of the intermediate and final products of the phenol decomposition was performed and the major reactive species formed upon the application of the discharge in air were identified and determined. It is concluded that the decomposition of phenol is initiated by reactions with ozone, taking place on the surface of the solution, and with hydroxyl radicals, both at the surface and in the bulk of the solution.

Introduction

The application of non-thermalizing discharges in air at atmospheric pressure and room temperature induces the production *in situ* of oxygen-based reactive species which can be conveniently applied for the decomposition of pollutants both in the gas [1-7] and in the aqueous phase [8-19]. The main reactive species are atomic oxygen, hydroxyl radicals, ozone, but also positive and negative ions, including $O2^{+\bullet}$, H_3O^+, $O_2^{-\bullet}$, $O_3^{-\bullet}$ and their clusters with neutral molecules of water and air. When the discharge is applied above the surface of a solution, it is expected that these reactive species reach the water where can dissolve and react directly with the organic pollutants or produce secondary radicals, as shown as an example in reactions (1)-(3) [13].

$$O(gas) + H_2O \longrightarrow 2\ {}^{\bullet}OH(aq) \quad (1)$$

$$O^{-\bullet}(gas) + H_2O \longrightarrow OH^-(aq) + {}^{\bullet}OH(aq) \quad (2)$$

$$O_2^{-\bullet}(gas) + H_2O \longrightarrow OH^-(aq) + {}^{\bullet}O_2H(aq) \quad (3)$$

Ozone also is known to give rise to the production of OH radicals in water, specially when the pH of the solution is basic [20,21].

The application of corona discharges to water purification can be considered a well-established technologies if ozonation processes are considered. In these processes ozone is generally produced ex situ by the application of dielectric barrier discharges in air or pure oxygen and then brought into contact with the liquid to be treated in an absorption column [21,22]. The advantages of applying the discharge directly on the air above the solution consist in the possibility to involve also the other reactive species produced by the discharge in the process of decomposition of the pollutants, because while ozone has a lifetime long enough to be utilized by the conventional ozonation processes, the other reactive species produced in the corona discharge region are characterized by lifetimes extremely short. Moreover an increase in efficiency is reliable and desirable.

However, the efforts to utilize more efficiently the ability of corona discharge to produce short-lived radicals have given rise also to the development of reactors in which the discharge is applied directly into the water [8,19,23-35]. When both the electrodes are submerged the discharge is called electrohydraulic and is characterized by the formation into the water of a plasma channel which can reach temperatures of 14000-50000 K and thus function as a blackbody radiation source. Moreover during the formation and the expansion of the plasma channel, intense shockwaves are generated. These can induce pyrolytic and free radical reactions indirectly via electrohydraulic cavitation. As the plasma channel cools over 1-3 ms, thermal energy is transferred to the surrounding water, resulting in the formation of a steam bubble. Within this bubble the temperature and the pressure are high enough for the formation of transient supercritical water. Thus, the decomposition of organic compounds in such systems is due to direct and indirect photolysis, pyrolytic destruction and free radical reactions in the high-temperature plasma channel. Moreover, while the plasma channel interest a small volume of the solution electrohydraulic discharges induce extreme electromagnetic and mechanical conditions in the bulk allowing there three primary physical processes: ultraviolet (UV) photolysis, electrohydraulic cavitation, and supercritical water oxidation [25].

However it was found that the generation of the corona discharge in water consumes an energy content approximately ten times higher than above the water due to the fact that the production of gas bubbles and plasma channels require heating and vaporization, so leads to energy waste with respect to its employment in the production of reactive species only [11,16,19].

We report here a contribution to this area of

research based on the development and testing of a novel reactor for the oxidative degradation of organic pollutants in water based on the application of dielectric barrier discharges (DBD) above the surface of the solution. DBD discharges are characterized by by the use of an AC high voltage and by the fact that at least one of the electrodes is covered with a thin layer of dielectric material, in our case the glass of the bottom surface of the reactor and also the same water [22]. As model compound for testing our reactor we chose phenol because it is an important pollutant, widely used in industry and also released in the environment via hydrolysis of pesticides and other precursors. Moreover, the oxidative pathways of phenol are the object of many studies in the literature which provide useful information on which products to expect from reaction of phenol with the different species formed by the discharge [36-38].

Experimental Part

Materials. Phenol, coumarin 3-carboxylic acid (97%), 7-hydroxycoumarin carboxylic acid (98%) and potassium indigotrisulfonate were purchased from Aldrich. Ultrapure grade water (milliQ water) was obtained by filtration of deionized water with a Millipore system. Pure air used in the experiments was a synthetic mixture (80% nitrogen and 20% oxygen) from Air Liquide with specified impurities of H2O (< 3 ppm) and of CnHm (< 0.5 ppm).

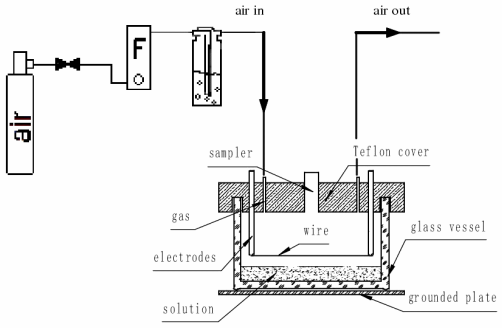

Figure 1. Schematics of the experimental apparatus.

Experimental apparatus. The experimental apparatus developed for water treatment by dielectric barrier discharge is shown in Figure 1. The reactor is a glass vessel (internal dimensions 95x75 mm and 60 mm height) and has a teflon cover with four passing electrodes of stainless steel which support two parallel wires of 75 mm length fixed upon their tips. The wires, made of Ni/Cr or of stainless steel, are placed at a distance of 38 mm between each other and are kept above the aqueous solution. The outside surface of the reactor base is covered with a film of silver and connected to a grounded plate. The reactor is powered with an high voltage transformer with 16.5-18 kV and a frequency of 50 Hz. A flow of air is allowed through the reactor and the discharge occurs in the gas phase above the liquid surface. To minimize evaporation phenomena from the solution to be treated, the air is humidified by passing it through a water bubbler placed before the reactor. During the experiments, electrical power was maintained constant and voltage and current profiles were monitored with a digital oscilloscope (TDS5032B, bandwidth 350 MHz, sample rate 5 Gs/s) to assure the reproducibility of the electrical conditions.

Phenol treatment experiments. A $5 \cdot 10^{-4}$ M aqueous phenol solution (70 mL), prepared in milliQ water, was subjected to plasma treatment. In the reactor, the height of the liquid was 9.8 mm and its distance from the wires was 15 mm. The volume of the air was 286 cm3. The efficiency of the decomposition process was determined by measuring phenol conversion as a function of treatment time. To this end, aliquots of 0.5 mL of the treated solution were withdrawn at desired times (15, 30, 60, 90, 120, 180, 240 min) and analyzed by HPLC (Shimadzu LC-10AT pump with a UV-Vis Shimadzu SPD-10 detector) using an Agilent Technologies column Zorbax SB-Aq 4.6 mm i.d. x 150 mm and phosphate buffer 20 mM at pH=2 containing 1% acetonitrile as eluent. The elution was followed at 210 and 270 nm. The fraction of residual phenol, $[Phenol]/[Phenol]_0$ was plotted against the treatment time and the data were fitted by equation 1

$$\frac{[Phenol]}{[Phenol]_0} = e^{-k \cdot t} \qquad (1)$$

where k is the rate constant of the process.

For the identification of the intermediate products selected samples were analyzed by a different HPLC system (Agilent Technologies 1100 series) connected to a diode array and a mass spectrometer detector (MSD SL Trap). The eluent was a mixture of water/acetonitrile 9:1 containing 0.1% of formic acid. The ionization was performed by electrospray (ESI) source alternating positive and negative polarity with the following parameters: nebulizer 70 psi, dry gas 12 L/min, dry gas temperature 350°C, capillary voltage ±3.5 kV, capillary exit ±101.7 V, skimmer ±40 V. The assignment of the intermediate products was confirmed by comparison with standards.

The sampled solution was also analyzed by ion chromatography (Dionex Series 4000), using a Dionex IonPac AS4A-SC 2x250 mm as column, a mixture of 1.7 mM sodium bicarbonate and 1.8 mM sodium carbonate as eluent and an electrochemical self-regenerating ULTRA II suppressor. The flow rate was 2 $mL \cdot min^{-1}$. pH and conductivity of the initial and final solutions were monitored during the experiments with a pH meter Metrohm 827 and a conductometer Metrohm 660. The gas exiting the reactor was subjected to on line FT-IR analysis (Nicolet 5700) using a 10 cm long flow cell with CaF2 windows.

A second modality to execute the experiments consisted in replacing the solution for every treatment time. In this way a large volume of solution was available and it was possible to measure the pH and the conductivity of the solution after the intermediate treatment times.

Determination of the reactive species. A superior limit for the ozone concentration in pure water treated

for 1, 1.5 and 2 h was determined by the indigo method [39]. Briefly, after the treatment the air flow was increased to 250 mL/min for 2 minutes to eliminate gaseous ozone which could interfere with the measurement. Then, 10 mL of $4 \cdot 10^{-4}$ M of indigotrisulfonate in phosphate buffer 50 mM was added into the reactor through the sampling port by a pipette immersed in the treated water. The resulting solution was thus analyzed by UV/Vis spectrophotometry and its absorbance was compared to a reference solution obtained by adding 10 mL of $4 \cdot 10^{-4}$ M of indigotrisulfonate in phosphate buffer 50 mM to 70 mL of non-treated mQ water. UV/Vis spectra were recorded at 25°C with a Lambda 16 Perkin–Elmer spectrophotometer equipped with water thermostated cell holders. Data were acquired with a slit of 2 nm, a spectral resolution of 0.8 nm and a sampling rate of 480 nm/min. Quartz cells (Hellma) with an optical pathlength of 1 cm were used.

The ozone concentration in the gas phase was determined by the iodometric titration method. For all the experiment duration the gas exiting the reactor was allowed to flow through two bubblers placed in series and containing each 150 mL of a 0.12 M KI solution in phosphate buffer at pH 7. H_2SO_4 4.5 M (5 mL) was then added to each solution and I_3^- was titrated by a standardized tiosulphate solution 0.1 M. The procedure was executed in experiments of treatment of pure water and phenol-containing water for times of 15, 30, 45 and 60 minutes.

The production of OH radical in pure water due to the application of the discharge was determined by following the conversion of coumarin 3-carboxylic acid (CCA) in coumarin 7-hydroxy-3-carboxylic acid, as reported by Newton and Milligan [40] and applied by Hoeben et al. [11] for a similar system. A CCA solution 10^{-3} M (70 mL) was subjected to treatment in different experiments of 15, 30, 45, 60, 90 and 120 min. The final solution was analyzed by Perkin–Elmer LS-55 spectrofluorimeter equipped with a Hamamatsu R928 photomultiplier and thermostated cell holder. Fluorescence spectra were recorded at 25°C by using quartz cells (Hellma) with an optical pathlength of 1 cm. The excitation wavelength was 390 nm. As also CCA exhibits a certain fluorescence using these wavelength, the fluorescence of the solution detected at time zero was subtracted to that measured during the treatment. The sampled solution was analyzed also by HPLC/UV-Vis to follow CCA concentration. The Zorbax SB-Aq 4.6 mm i.d. x 150 mm column with an eluent composed of 90% of phosphate buffer 20 mM at pH=2 and 10% acetonitrile was used and the elution was followed at 390 nm.

Results and discussion

The efficiency of the new apparatus for water decontamination by DBD discharges was evaluated by analyzing the decomposition of an aqueous 0.5 mM phenol solution under different experimental conditions. The air flow rate of the air passing above the solution was changed by setting 30, 50 and 100 $mL \cdot min^{-1}$ and two different types of wires were employed for the active electrodes, one made of Ni/Cr with a diameter of 0.2 mm, the other made of stainless steel with a diameter of 0.15 mm.

The first experiments were performed with the Ni/Cr wires. It was observed that phenol is removed from aqueous solutions according to an exponential curve as a function of the treatment time. The reproducibility of the results was good from the second experiment on, while it was lower than usual in the first experiment performed after new wires are installed. The replacement of the wires was necessary as upon use the Ni/Cr wires undergo oxidative erosion, which, after several experiments of 4 hours each, can lead to their breaking. This anomaly in the efficiency of the system was observed also in the electrical features of the discharge as the waveform of the current in the first experiment performed with new wires is different from that acquired in subsequent experiments (Figure 2). This behavior can be explained considering that the wires are subject to oxidation due to application of the discharge in a strongly humid environment and that the first use implies the biggest change in the features of their surface, which later is only slightly modified. However, the fragility of the wires also depends from their small diameter as wires made of Ni/Cr but with a bigger diameter are commonly used by Locke et al. submerged into the solution [31,32].

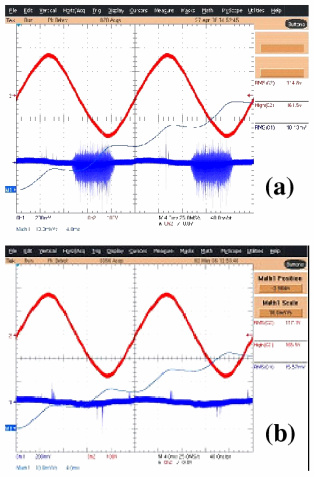

Figure 2. Waveforms of the discharge in experiments with Ni/Cr wires (a) new and (b) after the first experiments.

The effect of the flow rate of the air passing on the surface of the liquid was evaluated by using the Ni/Cr wires. Three air flow rates were considered: 30, 50 and 100 $mL \cdot min^{-1}$. In Figure 3a the decay in time of the residual fraction of phenol under the three different conditions is reported. It is seen that the phenol decomposition rate increases as the air flow rate is decreased. The k values obtained from interpolation of the data with equation 1 and the resulting half-life times of phenol (equation 2) are reported in Table 1.

$$t_{1/2} = \frac{\ln 2}{k} \qquad (2)$$

Table 1. k (s^{-1}) and $t_{1/2}$ (min) values for treatment of a $5 \cdot 10^{-4}$ M phenol aqueous solution in the DBD reactor.

Air flow rate ($mL \cdot min^{-1}$)	Wires	k (s^{-1})	$t_{1/2}$ (min)
100	Ni/Cr 0.2 mm	$6.4 \cdot 10^{-5}$	180
50	Ni/Cr 0.2 mm	$7.8 \cdot 10^{-5}$	148
30	Ni/Cr 0.2 mm	$1.20 \cdot 10^{-4}$	96
30	Stainless steel 0.15 mm	$3.89 \cdot 10^{-4}$	30

Considering that the reactive species responsible for phenol decomposition are produced in the gas phase and then transferred into the solution, the effect of the air flow rate can be understood in terms of their different residence and contact times. Specifically, the residence time of the gas within the reactor is 3, 5.5 and 9 minutes for flow rates of 100, 50 and 30 $mL \cdot min^{-1}$, respectively. Similar results were found by Sano et al., who attributed the dependence of the process efficiency on the gas flow rate mainly to the efficiency by which reactive radicals reach the water surface [13, 14].

Based on the results obtained with the Ni/Cr wires, the flow rate of 30 $mL \cdot min^{-1}$ was chosen for testing the performance of stainless steel wires. The diameter of the new wires was reduced with respect to that of the Ni/Cr ones (0.15 mm instead of 0.2 mm) in order to increase the efficiency of the process.

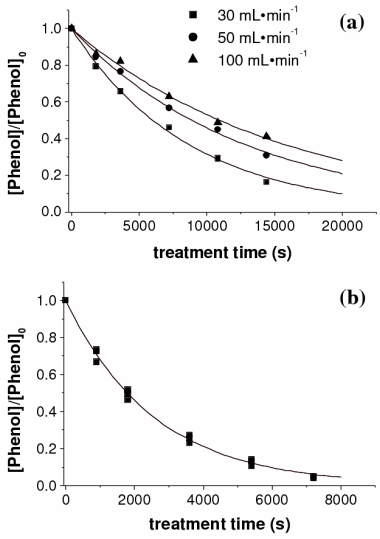

Figure 3. Comparison of phenol conversion as a function of treatment time in experiments performed (a) with Ni/Cr wires and an air flow rate of 30, 50, and 100 $mL \cdot min^{-1}$ and (b) with the stainless steel wires and an air flow rate of 30 $mL \cdot min^{-1}$.

Repeated experiments performed under these conditions have shown that the stainless steel wires are not subject to oxidation and that the reproducibility of the system is good. We performed two experiments by sampling aliquots of a single solution at different times and a third experiment by using a fresh solution batch for each specific treatment time. It is to be noted that no significant differences were observed in the results obtained by the two procedures. This means that the discharge interruption of, which is necessary for withdrawing samples from the treated solution, does not significantly affect the decomposition process. In Figure 3b the experimental data obtained are shown and fitted to a single curve. The k obtained is reported in Table 1.

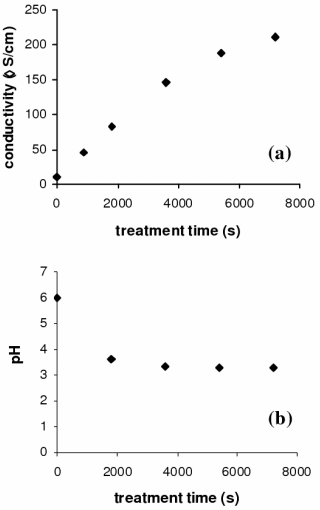

Figure 4. Trend of (a) conductivity and (b) pH in a decomposition experiment of phenol.

As for the efficiency of phenol decomposition, it was found that use of stainless steel wires increases the decomposition rate by a factor of 3.2 (Table 1), resulting in the complete disappearance of phenol after about 2 hours of treatment. On the contrary, with the Ni/Cr wires the extent of phenol removal was about 80% after 4 h of treatment. The increase of the efficiency can be ascribed to the smaller diameter of the stainless steel wires, which makes the electrical field greater. A catalytic effect by the wire material can be excluded due to the high inertia of stainless steel [41]. Figure 4 shows the trend of pH and conductivity detected during the treatment time. The pH decreases drastically from neutrality to 3.3 after 30 minutes and then remains almost stable (Figure 4a). The conductivity increases exponentially to a plateau value (Figure 4b). These data can be rationalized based on the results obtained by means of ion chromatographic (IC) analyses. In Figure 5 the ion chromatograms of a sample analyzed after 1 h of treatment shows two peaks due to the following anions: dissociated organic acids and NO_3^-. The identity of NO_3^- was confirmed by comparison of the peak with that of a $NaNO_3$ standard solution, while the attribution of the first peak to organic acids was deduced based on HPLC results (see later) and known data on phenol decomposition. The column employed for IC analyses was not able to separate different acids. Following the trend of NO_3^-

and organic acids, it appears that the production of NO_3^- increases during the treatment reaching a concentration of about 0.5 mM after 2 hours; on the contrary organic acids initially increase and then are reduced to zero. The trend of pH and conductivity of the solution are in agreement with the concentration of the HNO_3 formed during the treatment. The formation of nitric acid was investigated in the absence of phenol by treating 70 mL of milliQ water for 2h. The same pH decrease was observed as in the presence of phenol and the UV-Vis spectrum of the final solution was superimposable to that of a control HNO_3 solution (Figure not shown). However, HNO_3 is generally detected when the discharge is applied above the solution [9,12,13,15] as NOx produced in the gas phase, also when in low concentration, are effectively absorbed in the aqueous phase, giving rise to the formation of nitric acid. In the case of phenol-containing solutions, no other products were observed besides HNO_3 in the HPLC chromatograms detected at 210 nm or at 270 nm at long treatment time (4h).

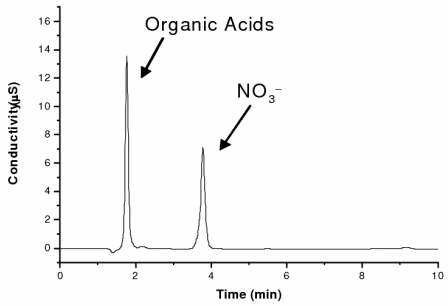

Figure 5. Ion chromatographic analysis of the phenol solution in milliQ water after 1 h of treatment.

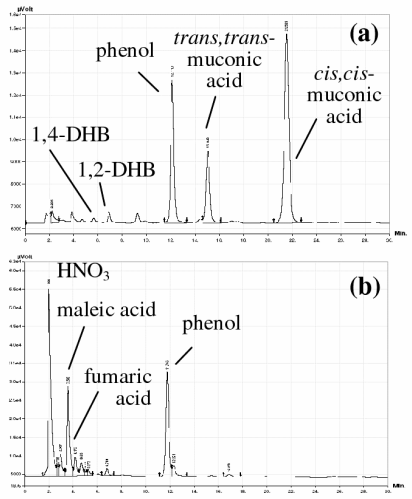

Figure 6. HPLC chromatograms of the phenol solution in milliQ water after 1 h of DBD treatment recorded at (a) 270 nm and (b) 210 nm.

However, at shorter treatment times various intermediate species can be observed. In Figure 6 the chromatograms obtained at 270 nm and 210 nm after 1 h from the discharge application are reported. At 270 nm (Fig 6a), besides of the peak of phenol, two main peaks are observed, due to two isomers of muconic acid. By comparing the retention times of the two peaks with those of standard cis,cis- and trans,trans-muconic acids, we attributed the peak at 21.5 min to the cis,cis isomer, while the peak at 15.0 min to the trans,trans one. The peaks observed at 210 nm (Fig. 6b) are mainly due to organic acids, between which maleic and fumaric were identified as the most abundant. Dihydroxybenzenes are detected both at 210 and 270 nm, but their chromatographic area is very low during all treatment time. Trihydroxybenzenes and benzoquinones were not detected at all under the conditions employed. In Fig. 7 the negative ESI-MS spectra of some of the species indicated above are reported. Due to the change of the elution conditions, made more suitable to electrospray ionization, there was not correspondence between the retention times of the HPLC/UV and LC/MS analysis. Thus, the peak attribution after their recognition performed by mass spectra analysis was confirmed by the use of standard compounds and the method of standard additions.

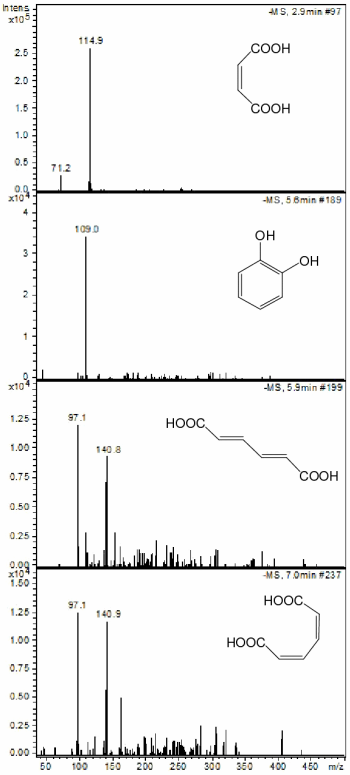

Figure 7. Negative ESI-MS spectra of some of the intermediate products produced from phenol decomposition.

A remarkable feature of the process under investigation is that the species detected constitute intermediate products of phenol oxidation as they are in turn decomposed, as more energy is provided to the system, giving a flat line as a final chromatographic trace. In Fig. 8 the signal intensity due to the isomers of muconic acid is reported as a function of time. It is evident that their concentration initially increases but then drops to zero as the treatment is continued.

As for the final products of the treatment, we have

evidence from FT-IR analysis of the gas exiting the reactor that CO_2 is released from the solution (Figure 9). Quantitative product analysis, including CO_2, is currently underway in our laboratory.

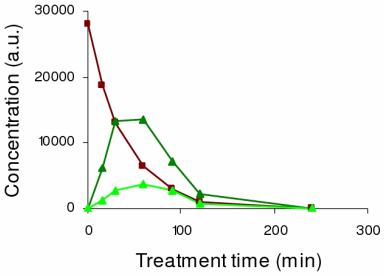

Figure 8. Concentration trend of phenol (■) and muconic acids (▲ and ▲) as a function of time in the treatment of phenol in milliQ water.

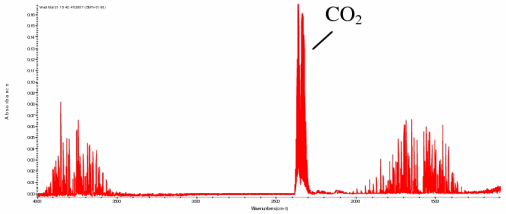

Figure 9. FT-IR spectrum of the gas exiting the reactor during the treatment of phenol in milliQ water.

Some insight about the main reactive species involved in the decomposition process of phenol can be deduced by the analysis of the intermediate products. In particular, the formation of cis,cis-muconic acid is due to the reaction of phenol with ozone and is favoured at low pH [38]. Moreover the low accumulation of dihydroxybenzenes is in accordance with the fact that they are more reactive toward ozone than phenol [42]. Thus, we undertook the quantification of the ozone produced in the gas phase and that dissolved in the solution to covalidate the hypothesis that ozone production is a key factor in the decomposition of phenol. In Figure 10 the concentration of ozone detected in the gas phase in the presence and absence of phenol 0.5 mM was reported as a function of the treatment time. It can be observed that ozone concentration increases linearly with treatment time and its trend can be successfully fitted by a linear interpolation. When phenol is present into the water the ozone detected in the gas phase is lower than that detected when pure water is treated. This difference in concentration increases at longer treatment time and can be attributed to the fact that ozone reacts with the intermediate products formed from phenol. As in the degradation process one molecule of phenol gives rise to the formation of more than one smaller molecule, it follows that an increasing number of ozone moles are consumed with time. The continuous increase of the ozone consumed in the process observed in Figure 9 is in accordance with the fact that after one hour of treatment phenol is not completely destroyed and significant quantities of intermediate products are still present into the solution.

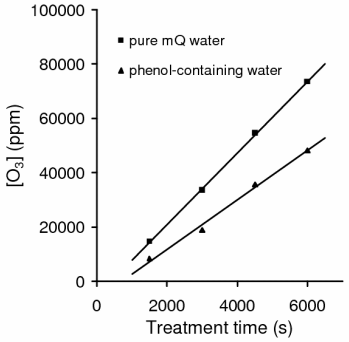

Figure 10. Concentration trend of gaseuous ozone produced during the treatment of pure milliQ water and phenol containing water.

However, the decrease in the gas phase concentration of ozone during the phenol treatment confirms the involvement of ozone in the decomposition process of phenol and allows to estimates the fraction of the produced ozone which can react with the organic compound dissolved into the water. This fraction is comprised between 34 and 44% in the investigated treatment time of 1 hour. A similar disappearance of ozone due to the presence of phenol in the water was observed also by Hoeben [11]. To investigate if the ozone produced in the gas phase can be dissolved in water or reacts with phenol on the surface of the water, we attempted to determine the concentration of ozone in water by the indigo method after different times of treatment of pure water. However, no significant change of the indigo absorption was observed when this dye was added to the treated water with respect to the reference solution, suggesting that if ozone is dissolved into the water during the treatment its concentration will be lower than the detection limit of the applied method, which is equal to $1.4 \cdot 10^{-4}$ mg/mL ($2.9 \cdot 10^{-6}$ M). This result is not surprising considering that ozone decomposes in water [21]. The mechanism of this process was studied by different scientists and is described as a cyclic chain process which globally transforms two molecules of ozone in three molecules of oxygen [21]. During this process OH radicals are produced, which are generally more reactive than ozone with organic compounds as react at rates that are essentially controlled by diffusion [21]. For example, the rate constants for the reactions of O_3 and OH with phenol are $1.3 \cdot 10^3$ $M^{-1} \cdot s^{-1}$ and about $1 \cdot 10^{10}$ $M^{-1} \cdot s^{-1}$, respectively, [36]. The gap is greatly reduced for reaction with the coniugate base, the phenoxide anion, the rate constants for O_3 and $^{\bullet}OH$ being $1.4 \cdot 10^9$ $M^{-1} \cdot s^{-1}$ and about $1 \cdot 10^{10}$ $M^{-1} \cdot s^{-1}$ [43], respectively. On the other hand, as ozone decomposition is initiated mainly by OH^- [21] it is expected that under the pH conditions created during the treatment the direct reaction of ozone with phenol predominates. Previous studies performed on similar reactors [16]. investigated the effect of the pH value on the ozone uptake by measuring the gaseous ozone concentration and found that the ozone concentration above the liquid is higher at low pH than in case of more alkaline solutions.

However, ozone decomposition cannot be completely excluded, therefore, from the above considerations, it follows that hydroxyl radicals can be produced into the system by two sources: electron interaction with water molecules and ozone decomposition in water. To determine the concentration of OH radicals available for reacting with organic compounds we used a well-known chemical probe [40], coumarin 3-carboxylic acid (CCA), which reacts with •OH by addition to the aromatic ring giving coumarin 7-hydroxy-3-carboxylic acid, which is a fluorescent product. Thus, we followed the treatment of CCA 10^{-3} M by fluorescence to quantify the formation of 7-hydroxy-CCA (Figure 11a) and by HPLC/UV-Vis to monitor the concentration of CCA during the treatment. A plot of the concentration of 7-hydroxy-CCA versus time (Fig. 11b), yields the result that $2.94 \cdot 10^{-4}$ µmol/L of 7-hydroxy-CCA are formed per second. Using the literature data that the yield of the reaction of CCA with OH is 4.7% [40], and assuming that the 7-hydroxy-CCA is not decomposed during the experiment duration, the total amount of OH radical formed into the 70 mL of mQ water subjected to the plasma treatment is estimated to be $4.4 \cdot 10^{-4}$ µmol•s^{-1}. The assumption that the formed 7-hydroxy-CCA is not attacked by OH radicals is justified by the fact that during all treatment 7-hydroxy-CCA is 10^4-10^3 times less concentrated than CCA. Thus, the competition for the reactive species present into the system must be largely favoured for CCA with respect to 7-hydroxy-CCA.

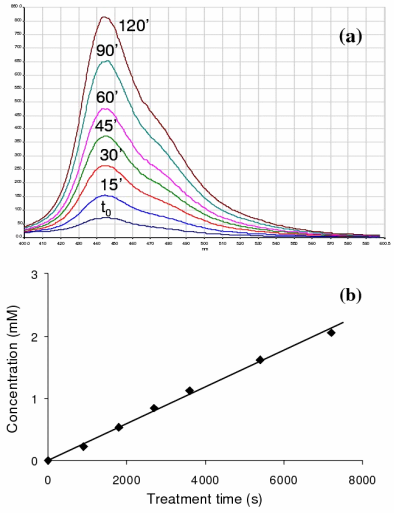

Figure 11. (a) fluorescence spectra of 7-hydroxy-CCA formed in the treatment of CCA and (b) trend of the concentration of 7-hydroxy-CCA as a function of the treatment time.

In conclusion, a new DBD reactor was developed for water purification from organic pollutants and tested using phenol as a model compound. In this system ozone and hydroxyl radical are key species involved in the decomposition process of the organic pollutant. Ozone can react directly with phenol on the surface of the solution, while OH radicals can react both on the surface of the liquid when or into the solution as can be formed in the gas phase from electron interaction with water but also from the ozone decomposition process into the water. The possibility to apply this technology to the treatment of waste water depends on many factors: the process efficiency, the final composition of the treated solution, the general applicability of the system to the organic pollutants. The data obtained until now are very promising mainly because of the absence of any hazardous organic byproduct after a proper treatment time.

Acknoledgements

We thank Roberto Inilli for the construction of the reactor and of the security devices for the power supplies and for the maintenance of the wires), Stefano Mercanzin for technical assistance and Paolo Venturini for the execution of some of the experiments.

References

1. H.-H. Kim. Nonthermal plasma processing for air-pollution control: a historical review, current issues, and future prospects. *Plasma Process. Polym.* **2004**, 1, 91-110.
2. B. M. Penetrante, S. E. Schultheis. *Nonthermal Plasma Techniques for Pollution Control*; Springer-Verlag: New York, 1993.
3. *Electrical Discharges for Environmental Purposes: Fundamentals and Applications.* E. M. van Veldhuizen, Ed., Nova Science Publishers, Inc., Huntington, NY, 2000.
4. K. L. L. Vercammen, A. A. Berezin, F. Lox, J.-S. Chang. Nonthermal plasma techniques for the reduction of VOC in air streams: a critical review. *J. Adv. Oxid. Technol.* **1997**, 2, 312-329.
5. J. Jarrige, P. Vervisch. Decomposition of three volatile organic compounds by nanosceond pulsed corona discharge: study of by-product formation and influence of high voltage pulse parameters. *J. Appl. Phys.* **2006**, 99, art. no. 113303.
6. S. Pasquiers. Removal of pollutants by plasma catalytic processes. *Eur. Phys. J. Appl. Phys.* **2004**, 28, 319-324.
7. E. Odic, C. Paradisi, M. Rea, L. Parissi, A. Goldman, M. Goldman, M. Treatment of organic pollutants by corona discharge plasma. In *The Modern Problems of Electrostatics with Applications in Environment Protection.* NATO Science Series, 2: Environmental Security. I. I. Inculet, F. T. Tanasescu, R. Cramariuc, Eds.. Kluwer Academic Publishers, Dordrecht, The Netherlands, 1999, 63, 143-160.
8. B. R. Locke, M. Sato, P. Sunka, M. R. Hoffmann, J.-S. Chang. Electrohydraulic discharge and nonthermal plasma for water treatment. *Ind. Eng. Chem. Res.* **2006**, 45, 882-905.
9. A. K. Sharma, D. M. Camaioni, G. B. Josephson, S. C. Goheen, G. M. Mong. Formation and measurement of ozone and nitric acid in a high voltage DC negative metallic point-to-aqueous-plane continuous corona reactor. *J. Adv. Oxid. Technol.* **1997**, 2, 239-247.

10. J. L. Brisset. Air corona removal of phenol. *J. Appl. Electrochem.* **1997**, 27, 179-183.
11. W. F. L. M. Hoeben, E. M. van Veldhuizen, W. R. Rutgers, G. M. W. Kroesen. Gas phase corona discharges for oxidation of phenol in an aqueous solution. *J. Phys. D: Appl. Phys.* **1999**, 32, L133–L137.
12. W. F. L. M. Hoeben, E. M. van Veldhuizen, W. R. Rutgers, C. A. M. G. Cramers, G. M. W. Kroesen. The degradation of aqueous phenol solutions by pulsed positive corona discharges. *Plasma Sources Sci. Technol.* **2000**, 9, 361-369.
13. N. Sano, T. Kawashima, J. Fujikawa, T. Fujimoto, T. Kitai, T. Kanki, A. Toyoda. Decomposition of organic compounds in water by direct contact of gas corona discharge: influence of discharge conditions *Ind. Eng. Chem. Res.* **2002**, 41, 5906-5911.
14. N. Sano, T. Fujimoto, T Kawashima, D. Yamamoto, T. Kanki, A. Toyoda. Influence of dissolved inorganic additives on decomposition of phenol and acetic acid in water by direct contact of gas corona discharge. *Sep. Purif. Technol.* **2004**, 37, 169–175.
15. L. R. Grabowski, E. M. van Veldhuizen, W. R. Rutgers. Removal of phenol from water: a comparison of energization methods. *J. Adv. Oxid. Technol.* **2005**, 8, 142-149.
16. L. R. Grabowski, E. M. van Veldhuizen, A. J. M. Pemen, W. R. Rutgers. Corona above water reactor for systematic study of aqueous phenol degradation. *Plasma Chem. Plasma Process.* **2006**, 26, 3-17.
17. M. Sato, T. Tokutake, T. Ohshima, A. T. Sugiarto. Aqueous phenol decomposition by pulsed discharges on the water surface. *IEEE trans. Ind. Appl.* **2008**, 44, 1397-1402.
18. H. Krause, B. Schweiger, J. Schuhmacher, S. Scholl, U. Steinfeld. Degradation of the endocrine disrupting chemicals (EDCs) carbamazepine, clofibric acid, and isopromide by corona discharge over water. *Chemosphere* **2009**, 75, 163-168.
19. T. H. Dang, A. Denat, O. Lesaint, G. Teissedre. Pulsed discharges in water for removal of organic pollutants: a comparative study. Eur. Phys. *J. Appl. Phys.* **2009**, 47, art. n. 22818.
20. L. Forni, D. Bahnemann, E. J. Hart. Mechanism of the hydroxide ion initiated decomposition of ozone in aqueous solution. *J. Phys. Chem.* **1982**, 86, 255-259.
21. W. H. Glaze. Drinking-water treatment with ozone. *Environ. Sci. Technol.* **1987**, 21, 224-230.
22. U. Kogelschatz. Dielectric-barrier discharges: their history, discharge physics, and industrial applications. *Plasma Chem. Plasma process.* **2006**, 23, 1-46.
23. A.K. Sharma, B. R. Locke, P. Arce, W. C. Finney. A preliminary-study of pulsed streamer corona discharge for the degradation of phenol in aqueous-solutions. *Hazard. Waste Hazard. Mater.* **1993**, 10, 209-219.
24. M. Sato, T. Ohgiyama, J. S. Clements. Formation of chemical species and their effects on microorganisms using a pulsed high-voltage discharge in water. *IEEE Trans. Ind. Appl.* **1996**, 32, 106-112.
25. P. S. Lang, W. K. Ching, D. M. Willberg, M. R. Hoffmann. Oxidative degradation of 2,4,6-trinitrotoluene by ozone in an electrohydraulic discharge reactor. *Environ. Sci. Technol.* **1998**, 32, 3142-3148.
26. P. Sunka, V. Babicky, M. Clupek, P. Lukes, M. Simek, J. Schmidt, M. Cernak. Generation of chemically active species by electrical discharges in water. *Plasma Sources Sci. Technol.* **1999**, 8, 258–265.
27. B. Sun, M. Sato, J. S. Clements. Use of a pulsed high-voltage discharge for removal of organic compounds in aqueous solution. *J. Phys. D: Appl. Phys.* **1999**, 32, 1908–1915.
28. B. Sun, M. Sato, J. S. Clements. Oxidative processes occurring when pulsed high voltage discharges degrade phenol in aqueous solution. *Environ. Sci. Technol.* **2000**, 34, 509-513.
29. M. A. Malik, A. Ghaffar, S. A. Malik. Water purification by electrical discharges. *Plasma Sources Sci. Technol.* **2001**, 10, 82–91.
30. P. Sunka, V. Babicky, M. Clupek, M. Fuciman, P. Lukes, M. Simek, J. Benes, B. Locke, Z. Majcherova. Potential applications of pulse electrical discharges in water. *Acta Physica Slovaka* **2004**, 54, 135-145.
31. P. Lukes, A. T. Appleton, B. R. Locke. Hydrogen peroxide and ozone formation in hybrid gas-liquid electrical discharge reactors. *IEEE Trans. Ind. Appl.* **2004**, 40, 60-67.
32. M. J. Kirkpatrick, B. R. Locke. Hydrogen, oxygen, and hydrogen peroxide formation in aqueous phase pulsed corona electrical discharge. *Ind. Eng. Chem. Res.* **2005**, 44, 4243-4248.
33. M. Dors, E. Metel, J. Mizeraczyk. Phenol degradation in water pulsed streamer discharge and Fenton reaction. *Int. J. Plasma Environ. Sci. Technol.* **2007**, 1, 76-81.
34. M. Sahni, B. R. Locke. The Effects of Reaction Conditions on Liquid-Phase Hydroxyl Radical Production in Gas-Liquid Pulsed-Electrical-Discharge Reactors. *Plasma Process. Polym.* **2006**, 3, 668–681.
35. P. Baroch, V. Anita, N. Saito, O. Takai. Bipolar pulsed electrical discharge for decomposition of organic compounds in water. *J. Electrostat.* **2008**, 66, 294-299.
36. H. Bader, J. Hoigné. Rate constants of reactions of ozone with organic and inorganic compounds in water – II Dissociating organic compounds. *Water Res.* **1983**, 17, 185-194.
37. P. C. Singer, M. D. Gurol. Dynamics of the ozonation of phenol – I. *Water Res.* **1983**, 17, 1163-1171.
38. E. Mvula, C. von Sonntag. Ozonolysis of phenols in aqueous solution. *Org. Biomol. Chem.* **2003**, 1, 1749-1756.

39. H. Bader, J. Hoigné. Determination of ozone in water by the indigo method. *Water Res.* **1981**, 15, 449-456.
40. G. L. Newton, J. R.Milligan. Fluorescence detection of hydroxyl radicals. *Radiat. Phys. Chem.* **2006**, 75, 473–478.
41. R. Gasparik, C. Yamabe, S. Ihara, S. Satoh. Comparison of copper and stainless steel used for low voltage electrode in wire-to-plate electrode configuration for NOx treatment. *Jpn. J. Appl. Phys.* **1998**, 37, 5786-5788.
42. Y. Yamamoto, E. Niki, H. Shiokawa, Y. Kamiya. Ozonation of organic compounds. 2. ozonation of phenol in water. *J. Org. Chem.* **1979**, 44, 2137-2142.
43. G. V. Buxton, C. L. Greenstock, W.P. Helman, A. B. Ross. *J. Phys. Chem. Ref. Data* **1988**, 17, 513-886.

4.9 COMPARISON OF THE DECOMPOSITION RATE OF PHENOL IN DEIONIZED AND TAP WATER USING A DIELECTRIC BARRIER DISCHARGE REACTOR

Comparison of the decomposition rate of phenol in deionized and tap water using a dielectric barrier discharge reactor

Ester Marotta,[1] Elisa Ceriani,[1] Milko Schiorlin,[1] Massimo Rea[2] and Cristina Paradisi[1*]

[1]*Department of Chemical Sciences, Università di Padova, 35131 Padova, Italy*

[2]*Retired from the Department of Electrical Engineering, Università di Padova, 35131 Padova, Italy*

The decomposition rate of phenol in a DBD reactor in solutions prepared with milliQ and tap water was compared. Interestingly, a significant increase was found in tap with respect to milliQ water. Conductivity was the first possible reason investigated to explain this observation but it has no effect on the efficiency of the process. The presence of traces of iron, of active chlorine residual after the depuration process operated in the aqueducts of the Italian cities and the presence of bicarbonate anions was thus investigated. The addition of 199 $\mu g \cdot L^{-1}$ of Fe^{2+} was not sufficient to initiate the Fenton's reaction suggesting that a concentration of hydrogen peroxide lower than 1.6 mM is produced into the system. Also the decomposition experiments performed in solutions of $NaClO_4$ containing 202 $\mu g \cdot L^{-1}$ of active chlorine did not show any effect due to the presence of this oxidant. On the contrary, if the removal experiments are carried out in solutions containing the same concentration of bicarbonate anions present in tap water, the same increase in efficiency as observed in tap water is obtained. It is known that bicarbonate anions quench OH radicals but in this case their buffering effect prevails allowing the pH to remain constant at about 7 during the treatment even if a significant concentration of nitric acid is produced. The conclusion, confirmed by experiment with phosphate buffer, is that the increase in the decomposition rate of phenol in tap with respect to milliQ water is due to the higher pH of the solution generated by the presence of bicarbonate salts.

Introduction

The application of electrical discharges for water purification is currently under investigation both into [1-14] and above aqueous solutions [14-22]. Hybrid reactors, which utilize both gas phase non-thermal plasma formed above the water solution and direct liquid phase corona-like discharge in the water, have also been developed [23,24] and proved to be more efficient in the production of OH radicals [11] and in the degradation of organic compounds [24] than single-liquid-phase discharge reactors. Other typologies of reactors include systems in which the solution to be treated is supplied into the discharge zone as a cloud of aerosol [19,25] or as a falling-water film [26,27], in order to optimize the transfer of the reactive species.

Many different parameters affect the process of removal of the organic compounds depending on the system employed [14]. In particular, the initiation of a discharge in water requires a certain initial

conductivity, generally of a few of μS/cm. On the other hand, a high conductivity (> 400 μS/cm) makes streamers shorter and decreases the production of radicals [2,3]. Thus, a high conductivity affects the efficiency on the removal of organic compounds from the solution. For example, Mizeraczyk et al. [10] compared the removal percentage of phenol in distilled water (1 μS/cm), water containing NaCl (200 μS/cm) and tap water (600 μS/cm) and found a significant decrease in the efficiency of the process, with phenol in tap water being not decomposed at all. As tap water was used as a model for the application of the process to drinking water and wastewater purification, we undertook a similar investigation by using our DBD reactor, where the discharge is applied above the solution [28]. In such a system it is expected that the water conductivity does not have influence on the voltage to generate corona discharge and on the production rate of radicals in the gas above the solution [8,11]. However, the use of tap water in our system significantly affects the decomposition rate of phenol, but in the opposite sense with respect to the result found by Mizeraczyk et al., as an increase in the decomposition rate of phenol is observed in tap water with respect to deionized water. We firstly verified that this effect can not be attributed to water conductivity, thus we undertook an investigation on the effects of different variables which could affect the efficiency in tap with respect to milliQ water, as the presence of bicarbonate salts, traces of iron ions or residual chlorine due to the depuration process operated in the aqueducts of the Italian cities.

Experimental Part

Materials. Phenol, NaClO solution with available chlorine ≥4 %, and Titanium(IV) oxysulfate-sulfuric acid solution were purchased from Aldrich, $FeSO_4 \cdot 7H_2O$ from Riedel-de Haen, $NaHCO_3$ from Normapur and KCl, $NaH_2PO_4 \cdot H_2O$ and $NaHPO_4 \cdot 12H_2O$ from Carlo Erba. Ultrapure grade water (milliQ water) was obtained by filtration of deionized water with a Millipore system. Tap water was sampled from the building 170 of the Department of Chemical Sciences of the University of Padova. Pure air used in the experiments was a synthetic mixture (80% nitrogen - 20% oxygen) from Air Liquide with specified impurities of H_2O (< 3 ppm) and of C_nH_m (< 0.5 ppm).

Experimental apparatus. The experimental apparatus employed in the experiments was described in a previous report [28]. Briefly, the reactor is a glass vessel (internal dimensions 95x75 mm and 60 mm height) and has a teflon cover with four passing electrodes of stainless steel which support two parallel wires of 75 mm length and 0.15 mm diameter fixed upon their tips. The wires, made of stainless steel, are placed at a distance of 38 mm between each other and are kept above the aqueous solution. The outside surface of the reactor base is covered with a film of silver and connected to a grounded plate. The reactor is powered with an AC high voltage transformer with 16.5-18 kV and a frequency of 50 Hz. A flow of air of 30 $mL \cdot min^{-1}$ is allowed through the reactor and the discharge occurs in the gas phase above the liquid surface. To minimize evaporation phenomena from the solution to be treated, the air is humidified by passing it through a water bubbler placed before the reactor. During the experiments, the electrical power was maintained constant (1.9 W) and voltage and current profiles were monitored with a digital oscilloscope (TDS5032B, bandwidth 350 MHz, sample rate 5 Gs/s) to assure the reproducibility of the electrical conditions.

Phenol treatment experiments. A $5 \cdot 10^{-4}$ M aqueous phenol solution (70 mL) was prepared in milliQ water, in tap water and in solutions containing KCl 3 mM or $FeSO_4$ 199 $\mu g \cdot L^{-1}$ or NaClO with available chlorine 202 $\mu g \cdot L^{-1}$ or $NaHCO_3$ 4.4 mM or

$NaH_2PO_4/NaHPO_4$ 4.4 mM and was subjected to plasma treatment. In the reactor, the height of the liquid was 9.8 mm and its distance from the wires was 15 mm. The efficiency of the decomposition process was determined by measuring phenol conversion as a function of the treatment time. To this end, aliquots of 0.5 mL of the treated solution were withdrawn at desired times and analyzed by HPLC (Shimadzu LC-10AT pump with a UV-Vis Shimadzu SPD-10 detector) using a Zorbax-SB 150x4.6 i.d. mm column (Agilent Technologies) and phosphate buffer 20 mM at pH=2 containing 1% acetonitrile as eluent. The elution was followed at 210 and 270 nm. The fraction of residual phenol, $[Phenol]/[Phenol]_0$ was plotted against the treatment time and the data were fitted by equation 1

$$\frac{[Phenol]}{[Phenol]_0} = e^{-k \cdot t} \qquad (1)$$

where k is the rate constant of the process. The half-life time of phenol was thus calculated by equation 2

$$t_{1/2} = \frac{\ln 2}{k} \qquad (2)$$

The sampled solutions were also analyzed by ion chromatography (Dionex Series 4000), using a Dionex IonPac AS4A-SC 4×250 mm as column, a mixture of 1.7 mM sodium bicarbonate and 1.8 mM sodium carbonate as eluent and an electrochemical self-regenerating ULTRA II suppressor. The flow rate was 1.5 $mL \cdot min^{-1}$. pH and conductivity of the initial and final solutions were monitored during the experiments with a pH meter Metrohm 827 and a conductometer Metrohm 660.

Determination of H_2O_2. The production of H_2O_2 after the treatment of pure water for one hour was determined colorimetrically using the reaction of H_2O_2 with titanyl ions [29]. After the interruption of the discharge, 1 mL of the Titanium(IV) oxysulfate-sulfuric acid solution was added into the reactor. Then, 3 mL of the obtained solutions were transferred into a quartz cuvette (Hellma) with an optical path length of 1 cm. The absorbance of the solution was measured at 407.2 nm with a Lambda 16 Perkin–Elmer spectrophotometer equipped with water thermostated cell holders maintained at 25°C.

Results and discussion

When a 0.5 mM phenol solution is prepared in tap water originating from the aqueduct of Padova instead than in milliQ water a significant increase in the decomposition rate of phenol is observed (Figure 1 and Table 1). The first hypothesis to explain this behavior considers the higher conductivity of tap water due to the presence of different dissolved salts. While milliQ water has a conductivity of 1 or 2 units of $\mu S \cdot cm^{-1}$, the tap water of Padova has a conductivity 2 order of magnitude higher (about 400 $\mu S \cdot cm^{-1}$). To verify this hypothesis a phenol solution with the same conductivity as tap water was prepared by adding KCl $3 \cdot 10^{-3}$ M into milliQ water. Under these conditions the decomposition rate of phenol was slightly lower (12%) than in milliQ water. Thus, with this experiment it was confirmed that the discharge applied on the surface of a liquid is not significantly affected by its conductivity [8,11] and it was hypothesized that the increase of the decomposition rate of phenol in tap water was due to the effect by some of the chemical species present in the solution. In Table 2 the results of a typical analysis of the water of Padova are reported. This analysis was executed by the Centro Idrico of Novoledo [30] and reports the average concentrations obtained in March 2006 of the species which have to be monitored as required by the Italian Law 31/2001, issued to implement the Council Directive 98/83/CE on the quality of water intended for human consumption [31]. After careful considerations of these analyses, three possible explanation for the increase in efficiency when the process takes place in a solution with the

composition reported in Table 2 were proposed: i) catalytic effect of traces of iron ions which converts the hydrogen peroxide produced after the application of the discharge into OH radical in accordance with the Fenton's reaction; ii) effect of residual active chlorine present after the depuration process usually applied for drinking water in Italy; iii) buffer effect of bicarbonate salts which prevent the decrease of the pH of the solution during the treatment due to HNO_3 formation. A higher pH leads to higher concentration of dissociated phenol which is more prone to oxidation with respect to the undissociated species [32-34]. Moreover, it favors the decomposition of ozone in water, which leads to the formation of the more reactive OH radical [35,36].

This last hypothesis was suggested by the fact that the trend of the pH in tap water during the DBD treatment is significantly different from that observed in milliQ water: while in milliQ water the pH decreases from 6 to about 3 after half hour of treatment [28], in tap water it remains almost stable at 7 for all the duration of the experiment (4h). As reported above, the decrease of pH observed in milliQ water was attributed to the formation of nitric acid [28]. Nitric acid is formed in tap water as well, as verified by ion chromatographic analyses of the treated solution. However, since the pH does not change, there must be a buffer effect. Bicarbonate ions are the only species present in tap water which can exert such an effect. On the other hand, one must also consider that they are known to quench OH radicals (equation 3) [37].

$$HCO_3^- + {}^\bullet OH \rightarrow CO_3^{-\bullet} + H_2O$$

$$k = 8.5 \cdot 10^6 \ M^{-1}s^{-1} \ [38] \qquad (3)$$

As $^\bullet OH$ is one of the main species leading to the decomposition of organic compounds due to non-thermal plasma, its quenching is expected to have an opposite effect on the decomposition rate of phenol. However, the role of the radical anion $CO_3^{-\bullet}$ formed in the reaction between the bicarbonate ion and the OH radical (equation 3) must be taken into account, as this species is known to efficiently react as an oxidant with organic compounds [39] and in particular with phenol [40]. Though the rate constant of the reaction of phenol with $CO_3^{-\bullet}$ ($k = 1.6 \cdot 10^7 \ M^{-1}s^{-1}$ [40]) is two orders of magnitude lower than that with $^\bullet OH$ ($k = 1 \cdot 10^{10} \ M^{-1}s^{-1}$ [32]), it is four orders of magnitude higher than that with O_3 ($k = 1.3 \cdot 10^3 \ M^{-1}s^{-1}$ [32]). Moreover, at the pH obtained in tap water the reactions of O_3 and $^\bullet OH$ with the phenoxide ion ($k = 1.4 \cdot 10^9 \ M^{-1}s^{-1}$ and $1 \cdot 10^{10} \ M^{-1}s^{-1}$, respectively [38]) become important due to the higher concentration of phenoxide ion. Thus, depending on the pH and on the concentrations of O_3, $^\bullet OH$ and $CO_3^{-\bullet}$, the oxidation by $CO_3^{-\bullet}$ could gain an important role in the decomposition of phenol. From these considerations it is evident that the system becomes significantly more complicated in the presence of bicarbonate salts and that their role is difficult to be predicted.

The first possibility which was investigated for explaining the increase in efficiency in tap water is the effect of iron ions traces. Considering the analyses reported in Table 2, the tap water used in the experiments contains a concentration of iron ions of 5 $\mu g \cdot L^{-1}$, while the law limit for this species in drinking water is 200 $\mu g \cdot L^{-1}$. Due to the very low concentration of iron ions in tap water, the decomposition experiments were performed by adding phenol 0.5 mM to a solution of $FeSO_4$ with a concentration higher than the content of Fe^2/Fe^{3+} in tap water and nearly equal to the highest possible concentration, which is the legal limit (200 $\mu g \cdot L^{-1}$ M). This choice is justified by the fact that if no significant effect is observed with a concentration higher than that present in tap water, no effect is expected with a lower concentration. The result obtained is reported in Table 1 and shown in Figure 2. The decomposition rate of phenol was not significantly different from that obtained in milliQ water, demonstrating that the traces of iron ions in tap

water are not responsible for the increase in efficiency with respect to milliQ water. This result is in contrast with what is generally observed in the reactors in which the discharge is applied underwater, as H_2O_2 is one of the main species formed in these systems and also very low concentrations of Fe^{2+} are sufficient to increase the efficiency of organic compounds removal [1,3,9,10]. Moreover, Grabowski et al. [19], using a reactor similar to ours but energized by pulsed corona discharges, found a significant increase in the decomposition rate of phenol by adding $FeSO_4$ 200 $\mu g \cdot L^{-1}$. Their conclusion is that ozone dissolved in the water is partly converted into H_2O_2 but they did not measure the concentrations of O_3 and H_2O_2 in the water. We performed a measurement of the hydrogen peroxide produced in pure water after one hour of treatment using the reaction of H_2O_2 with titanyl ions but we found that H_2O_2, if present, is lower than the limit of detection estimated for this methodology under our conditions ($1.5 \cdot 10^{-4}$ M). On the other hand, the typical range for observing the Fenton's reaction is 1 part of iron per 5-25 parts of H_2O_2 (wt/wt), so we can confirm that the concentration of H_2O_2 after one hour of treatment is lower than 1.6 mM [41]. Thus, considering the result of the experiment with $FeSO_4$ 200 $\mu g \cdot L^{-1}$ and the lower quantity of iron traces present in tap water, we can safely say that the increase of efficiency found in tap water is not due to the presence of iron ions as the concentration of the hydrogen peroxide produced in our system is too low for the Fenton's reaction to take place at least without a more significant addition of iron ions.

The second hypothesis to be verified is the effect of residual active chlorine after the addition of sodium hypochlorite in the process of water sterilization, usually applied in Italy for drinking water. The concentration of active chlorine when the water exits from the tap is about 0.02 $mg \cdot L^{-1}$ (Table 2), while the law limit is ten times higher (Table 2). In this case also it was preferred to perform the experiments of phenol decomposition in a solution containing an higher concentration of active chlorine than that present in tap water considering that if no effect is observed with an higher quantity, surely the traces present in tap water are ineffective. For this reason the 0.5 mM phenol solution which was subjected to the DBD discharge was prepared in a solution of NaClO containing 0.2 $mg \cdot L^{-1}$ of active chlorine. The results obtained are reported in Table 2 and Figure 2 and show that there is no effect due to the hypochlorite addition.

Finally the effect of bicarbonate salts was considered. First of all, the concentration of the bicarbonate anions in tap water was estimated. As the pH of tap water is 7.1, it can be assumed that carbonates are mainly present as bicarbonate ions, while CO_3^{2-}, H_2CO_3 and dissolved CO_2 are negligible. Thus HCO_3^- was quantified by titration with HCl and resulted to be equal to 4.4 mM. A solution 0.5 mM of phenol in $NaHCO_3$ 4.4 mM was thus prepared and subjected to DBD treatment. In this case the same bicarbonate concentration, as found in tap water, was used as that is a significant quantity and not only a trace. The resulting decomposition rate is reported in Table 1. If compared with that obtained in milliQ water it is evident that an increase in efficiency is observed when sodium bicarbonate is added to the solution. This increase is slightly higher than that observed in tap water, but it is consistent with the experimental error, thus it allows concluding that the presence of carbonate salts is the main reason of the increase in efficiency observed in tap water. As anticipated, the effect of bicarbonate can be due to the buffering effect, which moves the dissociation equilibrium of phenol towards the more reactive phenolate, or to the formation of $CO_3^{-\bullet}$, which is an effective oxidant species. To evaluate these possibilities, a couple of experiments with another salt with similar buffering characteristics of bicarbonate were performed. The chosen saline

system was NaH_2PO_4/Na_2HPO_4 and it was used at the same concentration as that of the bicarbonate. In the first experiment an equal concentration of NaH_2PO_4 and Na_2HPO_4 were used to prepare the solution and the initial and final pH were 6.9 and 5.2. The obtained kinetic constant (Table 1 and Figure 2) supports the hypothesis that the buffering effect is the reason for the increase in efficiency in the case of addition of bicarbonate. However, the kinetic constant obtained with phosphate salts is lower than that obtained with the bicarbonate and this can be attributed to the fact that the buffering power of the prepared phosphate system was not enough for buffering the effect on the pH of the total nitric acid produced. Thus, as the buffering powers of bicarbonate and phosphate are similar, in the second experiment with the system NaH_2PO_4/Na_2HPO_4 we only changed the proportion between the two phosphate species in order to obtain a slight higher initial pH (7.6). During the experiment the pH decreases to 6.3 and the kinetic constant obtained was significant higher than that obtained previously (Table 1). This result was attributed to a big sensitivity of the process to the pH of the solution.

Conclusions

While in reactors which use corona-like dischargse directly applied into the water the conductivity of the solution negatively affect the decomposition rate of the organic compounds, when the discharge is applied above the solution this parameter does not affect significantly the removal process. Moreover, in the DBD reactor developed in our laboratories, bicarbonate anions, generally dissolved in drinking and wastewaters, exert a positive effect on the decomposition of phenol due to their buffering properties, which allow the pH to be constant at about 7 even if a significant quantity of nitrate ions is formed during the treatment. After a careful investigation of the characteristics of tap water which can influence the removal of phenol, we found that the buffering effect of bicarbonate is the determining feature for the increase in the rate constant when the decomposition process is carried out in this water. On the contrary the quenching effect of bicarbonate ions is not significant probably because compensated by the higher proportion of the more reactive phenolate with respect to phenol into the system and by the reactivity of the radical anion $CO_3^{-\bullet}$ produced by the reaction of the bicarbonate anion with the OH radical.

References

1. A.K. Sharma, B. R. Locke, P. Arce, W. C. Finney. A preliminary-study of pulsed streamer corona discharge for the degradation of phenol in aqueous-solutions. *Hazard. Waste Hazard. Mater.* **1993**, *10*, 209-219.
2. M. Sato, T. Ohgiyama, J. S. Clements. Formation of chemical species and their effects on microorganisms using a pulsed high-voltage discharge in water. *IEEE Trans. Ind. Appl.* **1996**, *32*, 106-112.
3. P. Sunka, V. Babicky, M. Clupek, P. Lukes, M. Simek, J. Schmidt, M. Cernak. Generation of chemically active species by electrical discharges in water. *Plasma Sources Sci. Technol.* 1**999**, *8*, 258–265.
4. B. Sun, M. Sato, J. S. Clements. Use of a pulsed high-voltage discharge for removal of organic compounds in aqueous solution. *J. Phys. D: Appl. Phys.* **1999**, *32*, 1908–1915.
5. B. Sun, M. Sato, J. S. Clements. Oxidative processes occurring when pulsed high voltage discharges degrade phenol in aqueous solution. *Environ. Sci. Technol.* **2000**, *34*, 509-513.
6. M. A. Malik, A. Ghaffar, S. A. Malik. Water purification by electrical discharges. *Plasma Sources Sci. Technol.* **2001**, *10*, 82–91.

7. N. Sano, T. Kawashima, J. Fujikawa, T. Fujimoto, T. Kitai, T. Kanki, A. Toyoda. Decomposition of organic compounds in water by direct contact of gas corona discharge: influence of discharge conditions *Ind. Eng. Chem. Res.* **2002,** *41,* 5906-5911
8. N. Sano, T. Fujimoto, T Kawashima, D. Yamamoto, T.Kanki, A. Toyoda. Influence of dissolved inorganic additives on decomposition of phenol and acetic acid in water by direct contact of gas corona discharge. *Sep. Purif. Technol* **2004**, *37*, 169–175.
9. P. Sunka, V. Babicky, M. Clupek, M. Fuciman, P. Lukes, M. Simek, J. Benes, B. Locke, Z. Majcherova. Potential applications of pulse electrical discharges in water. *Acta Physica Slovaka* **2004**, *54*, 135-145.
10. M. Dors, E. Metel, J. Mizeraczyk. Phenol degradation in water pulsed streamer discharge and Fenton reaction. *Int. J. Plasma Environ. Sci. Technol.* **2007**, *1*, 76-81.
11. M. Sahni, B. R. Locke. The Effects of Reaction Conditions on Liquid-Phase Hydroxyl Radical Production in Gas-Liquid Pulsed-Electrical-Discharge Reactors. *Plasma Process. Polym.* **2006,** *3*, 668–681.
12. P. Baroch, V. Anita, N. Saito, O. Takai. Bipolar pulsed electrical discharge for decomposition of organic compounds in water. *J. Electrostat.* **2008**, *66*, 294-299.
13. T. H. Dang, A. Denat, O. Lesaint, G. Teissedre. Pulsed discharges in water for removal of organic pollutants: a comparative study. *Eur. Phys. J. Appl. Phys.* **2009**, *47*, art. n. 22818.
14. B. R. Locke, M. Sato, P. Sunka, M. R. Hoffmann, J.-S. Chang. Electrohydraulic discharge and nonthermal plasma for water treatment. *Ind. Eng. Chem. Res.* **2006,** *45,* 882-905.
15. A. K. Sharma, D. M. Camaioni, G. B. Josephson, S. C. Goheen, G. M. Mong. Formation and measurement of ozone and nitric acid in a high voltage DC negative metallic point-to-aqueous-plane continuous corona reactor. *J. Adv. Oxid. Technol.* **1997**, *2*, 239-247.
16. J. L. Brisset. Air corona removal of phenol. *J. Appl. Electrochem.* **1997**, *27*, 179-183.
17. W. F. L. M. Hoeben, E. M. van Veldhuizen, W. R. Rutgers, G. M. W. Kroesen. Gas phase corona discharges for oxidation of phenol in an aqueous solution. *J. Phys. D: Appl. Phys.* **1999**, *32*, L133–L137.
18. W. F. L. M. Hoeben, E. M. van Veldhuizen, W. R. Rutgers, C. A. M. G. Cramers, G. M. W. Kroesen. The degradation of aqueous phenol solutions by pulsed positive corona discharges. *Plasma Sources Sci. Technol.* **2000**, *9*, 361-369.
19. L. R. Grabowski, E. M. van Veldhuizen, W. R. Rutgers. Removal of phenol from water: a comparison of energization methods. *J. Adv. Oxid. Technol.* **2005**, *8*, 142-149.
20. L. R. Grabowski, E. M. van Veldhuizen, A. J. M. Pemen, W. R. Rutgers. Corona above water reactor for systematic study of aqueous phenol degradation. *Plasma Chem. Plasma Process.* **2006**, *26*, 3-17.
21. M. Sato, T. Tokutake, T. Ohshima, A. T. Sugiarto. Aqueous phenol decomposition by pulsed discharges on the water surface. *IEEE trans. Ind. Appl.* **2008**, *44*, 1397-1402.
22. H. Krause, B. Schweiger, J. Schuhmacher, S. Scholl, U. Steinfeld. Degradation of the endocrine disrupting chemicals (EDCs) carbamazepine, clofibric acid, and isopromide by corona discharge over water. *Chemosphere* **2009**, *75*, 163-168.
23. P. Lukes, A. T. Appleton, B. R. Locke. Hydrogen Peroxide and Ozone Formation in Hybrid Gas–Liquid Electrical Discharge Reactors. *IEEE Trans. Ind. Appl.* **2004**, *40*, 60-67.

24. D. R. Grymonpre, W. C. Finney, R. J. Clark, B. R. Locke. Hybrid gas-liquid electrical discharge reactors for organic compound degradation. *Ind. Eng. Chem. Res.* **2004**, *43*, 1975-1989.
25. R. Burlica, B. R. Locke. Pulsed plasma gliding-arc discharges with water spray. *IEEE Trans. Ind. Appl.* **2008**, *44*, 482-489.
26. N. Sano, D. Yamamoto, T. Kanki, A. Toyoda. Decomposition of phenol in water by a cylindrical wetted-wall reactor using direct contact of gas corona discharge. *Ind. Eng. Chem. Res.* **2003,** *42,* 5423-5428.
27. S. Ognier, D. Iya-sou, C. Fourmond, S. Cavadias. Analysis of mechanisms at the plasma in a gas-liquid discharge reactor used of polluted water. *Plasma Chem. Plasma Process.* **2009**, *29*, 261–273.
28. E. Marotta, M. Schiorlin, X. Ren, M. Rea, C. Paradisi. Oxidation of aqueous phenol in a dielectric barrier discharge reactor. In preparation.
29. G. M. Eisenberg. Colorimetric determination of hydrogen peroxide, *Ind. Eng. Chem. Anal. Ed.* **943**, *15*, 327-328.
30. http://www.centroidriconovoledo.it/
31. http://europa.eu/legislation_summaries/environment/water_protection_management/l28079_en.htm
32. H. Bader, J. Hoigné. Rate constants of reactions of ozone with organic and inorganic compounds in water – II Dissociating organic compounds. *Water Res.* **1983**, *17*, 185-194.
33. P. C. Singer, M. D. Gurol. Dynamics of the ozonation of phenol – I. *Water Res.* **1983**, *17*, 1163-1171.
34. E. Mvula, C. von Sonntag. Ozonolysis of phenols in aqueous solution. *Org. Biomol. Chem.* **2003**, *1*, 1749-1756.
35. L. Forni, D. Bahnemann, E. J. Hart. Mechanism of the hydroxide ion initiated decomposition of ozone in aqueous solution. *J. Phys. Chem.* **1982**, *86*, 255-259.
36. W. H. Glaze. Drinking-water treatment with ozone. *Environ. Sci. Technol.* **1987**, *21*, 224-230.
37. H. Bader, J. Hoigné. The role of hydroxyl radical reactions in ozonation processes in aqueous solutions. *Water Res.* **1976**, *10*, 377-386.
38. G. V. Buxton, C. L. Greenstock, W.P. Helman, A. B. Ross. *J. Phys. Chem. Ref. Data* **1988**, *17*, 513-886.
39. S. Canonica, T. Kohn, M. Mac, F. J. Real, J. Wirz, U. Von Gunten. Photosensitizer method to determine rate constants for the reaction of carbonate radical with organic compounds. *Environ. Sci. Technol.* **2005**, *39*, 9182-9188.
40. C. Busset, P. Mazellier, M. Sarakha, J. De Laat. Photochemical generation of carbonate radicals and their reactivity with phenol. *J. Photochem. Photobiol. A: Chem.* **2007**, *185*, 127–132.
41. http://www.h2o2.com/pages.aspx?pid=143&name=General-Chemistry-of-Fenton-s-Reagent

Table 1. k (s^{-1}) and $t_{1/2}$ values obtained in the treatment of a $5 \cdot 10^{-4}$ M phenol solution by the DBD reactor in different reaction media

Reaction medium	k (min^{-1})	$t_{1/2}$ (min)
milliQ water	(0.018 ± 0.001)	38
Tap water	0.055 ± 0.003	12
KCl 3 mM	(0.016 ± 0.001)	43
$FeSO_4$ (199 µg/L)	0.019 ± 0.001	36
NaClO (202 µg/L of chlorine)	0.019 ± 0.001	35
$NaHCO_3$ (4.4 mM)	0.061 ± 0.003	11
NaH_2PO_4/Na_2HPO_4 (4.4m M)	0.053 and 0.070	13

Table 2. Average quality characteristics of Padova water in March 2006 (according to the analyses performed by the Centro Idrico Novoledo [30])

Parameter	m.u.	Measured value	Legal limit
Temperature	°C	**12.8**	--
Torbidity	NTU	**0.3**	*(1)*
Activity of hydrogen ions	pH	**7.6**	*(6.5÷ 9.5)*
Specific electrical conductivity at 20 °C	$\mu S \cdot cm^{-1}$	**465**	*(2500)*
Total permanent hardness in french degrees		**26.3**	*(15 ÷ 50)*
Conductometric residue	$mg \cdot L^{-1}$	**315**	--
Oxidability according to Kübel	$mg \cdot L^{-1}$	**< 0.5**	*(5.0)*
Calcium	$mg \cdot L^{-1}$	**66.3**	-
Magnesium	$mg \cdot L^{-1}$	**23.7**	-
Sodium	$mg \cdot L^{-1}$	**4.0**	*(200)*
Potassium	$mg \cdot L^{-1}$	**1.0**	-
Clorides	$mg \cdot L^{-1}$	**7**	*(250)*
Nitrates	$mg \cdot L^{-1}$	**18**	*50*
Solfates	$mg \cdot L^{-1}$	**16**	*(250)*
Ammonia	$mg \cdot L^{-1}$	**< 0.05**	*(0.50)*
Nitrites	$mg \cdot L^{-1}$	**< 0.02**	*0.50*
Fluorides	$mg \cdot L^{-1}$	**< 0.1**	*(1.50)*
Residual chlorine	$mg \cdot L^{-1}$	**0.02**	*(0.2)*
Total phenols	$\mu g \cdot L^{-1}$	**< 0.05**	--
Total cyanides	$\mu g \cdot L^{-1}$	**< 0.5**	*50*
Total chlorinated solvents	$\mu g \cdot L^{-1}$	**1**	*10*
Trihalometanes	$\mu g \cdot L^{-1}$	**3**	*30*
Insecticide (single compound)	$\mu g \cdot L^{-1}$	**< 0.1**	*0.10*
Total insecticides	$\mu g \cdot L^{-1}$	**< 0.5**	*0.50*
Benzene	$\mu g \cdot L^{-1}$	**< 0.2**	*1.0*
Toluene, xylenes, alkylbenzenes	$\mu g \cdot L^{-1}$	**< 0.2**	-
Arsenic	$\mu g \cdot L^{-1}$	**< 1**	*10*
Cadmium	$\mu g \cdot L^{-1}$	**< 0.1**	*5,0*
Total chromium	$\mu g \cdot L^{-1}$	**1**	*50*
Total iron	$\mu g \cdot L^{-1}$	**5**	*(200)*
Manganese	$\mu g \cdot L^{-1}$	**2**	*(50)*
Nickel	$\mu g \cdot L^{-1}$	**< 1**	*20*
Lead	$\mu g \cdot L^{-1}$	**< 1**	*25*
Copper	$\mu g \cdot L^{-1}$	**<0.1**	*1,0*
Total coliforms	in 100 mL	**0**	*(0)*
Escherichia coli	in 100 mL	**0**	*0*
Enterococci	in 100 mL	**0**	*0*

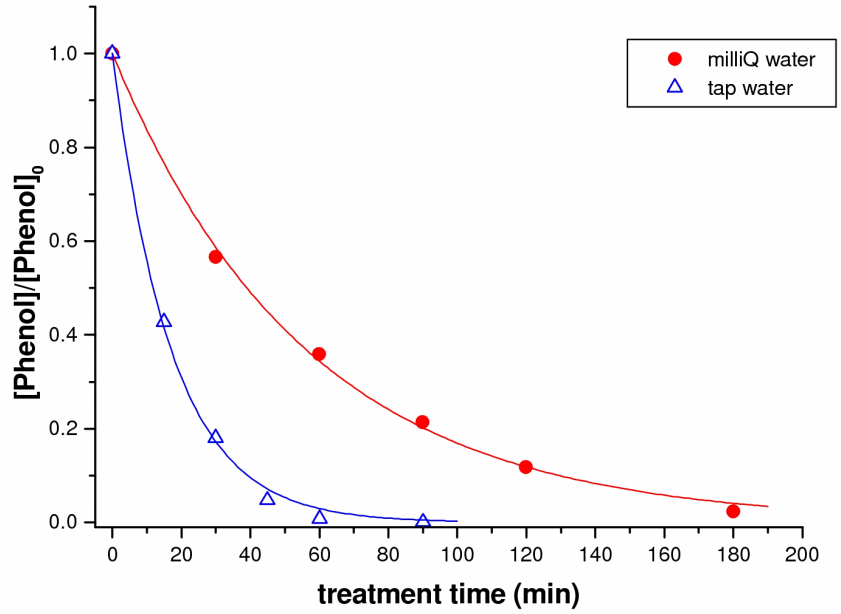

Figure 1. Decomposition of phenol in solutions prepared in milliQ and tap water.

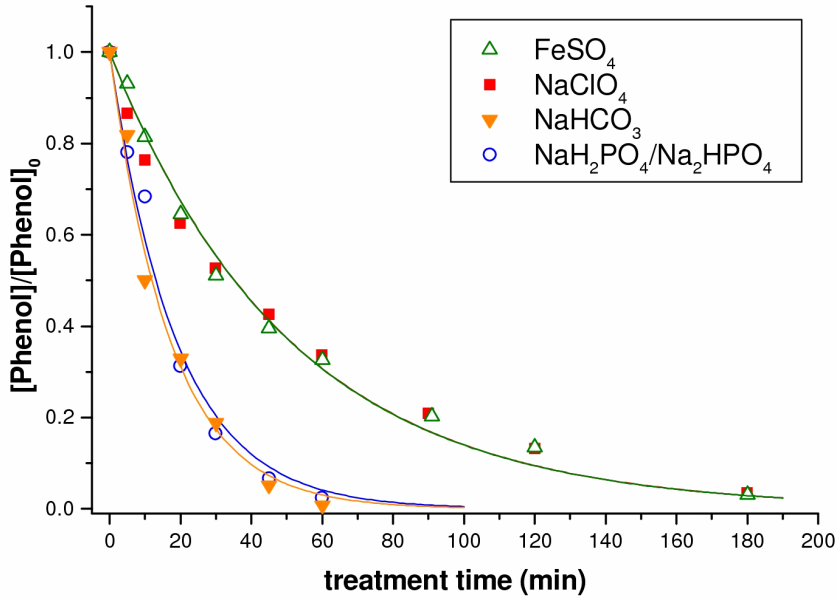

Figure 2. Decomposition of phenol in solutions containing $FeSO_4$ 199 µg·L^{-1}, NaClO 202 µg·L^{-1}, $NaHCO_3$ 4.4 mM and NaH_2PO_4/Na_2HPO_4 4.4 mM (initial pH=6.9).

4.10 COMPARISON OF THE EFFICIENCY OF TWO DIELECTRIC BARRIER DISCHARGE REACTORS IN THE DECOMPOSITION OF PHENOL IN WATER

Comparison of the efficiency of two dielectric barrier discharge reactors in the decomposition of phenol in water

Milko Schiorlin,[1] Ester Marotta,[1] Xianwen Ren,[1] Miroslaw Dors,[2]
Massimo Rea[3] and Cristina Paradisi[1*]

[1]Department of Chemical Sciences, Università di Padova, 35131 Padova, Italy
[2]Centre for Plasma and Laser Engineering, The Szewalski Institute of Fluid Flow Machinery, Gdańsk, Poland
[3]Retired from the Department of Electrical Engineering, Università di Padova, 35131 Padova, Italy

A new reactor for water purification is presented as a development of a first prototype, in which dielectric barrier discharges are applied above the solution to be treated. The objective is to maintain the ability of the first prototype to completely remove the pollutant used as model and its intermediate oxidation products by consuming less energy. The experiments performed with solutions of phenol prepared in deionized and tap water demonstrated the effective increase in efficiency gained by using the new device.

The application of atmospheric plasma to water purification from organic compounds is nowadays object of many studies [1-9]. In these processes non-thermal electrical discharges are applied above the surface of water and the reactive species produced in the gas phase are allowed to interact with the pollutants dissolved in the solution. Different types of discharge have been applied for this scope in reactors characterized by very different geometries and electrode configurations. The objective of these researches is that to obtain the complete degradation of the pollutants with a cost of energy which can make these processes competitive with the technologies actually employed.

In this context, after the development of a first prototype of reactor, in which dielectric barrier discharges (DBD) are applied on the surface of water [10-11], we addressed our efforts to project and test a new reactor which allows a higher efficiency in the removal of organic pollutants. In fact the first prototype appeared very promising in the complete decomposition of the organic compound chosen as model, phenol, since it allowed the complete disappearance both of phenol and of its intermediate products. However, the full decomposition of the organic compounds required a quite long time, specifically two hour for phenol and four hours for the intermediate products. Thus, we developed a new system, bigger and equipped with an higher number of electrodes, to obtain the same results in a shorter time and consuming consequently less energy.

The description of the first reactor developed in our laboratory is reported in [10]. It is made with a glass vessel of size equal to 95x75x60 mm (length x width x height) and is equipped with a Teflon cover. The cover has four electrode holders made of stainless steel. The active electrodes are two 75 mm long parallel wires (diameter of 0.15 mm) made of stainless steel that are fixed on the tips of holders. They are placed at a distance of 38 mm one from the other, and are kept above the aqueous solution. The outside surface of the reactor base is covered with silver film and connected to ground. The reactor is mounted on a metal plate which is held in place by screws on the cover. A Viton gasket is placed between glass and Teflon to avoid gas leakage. On the cover there are two connectors for inlet and outlet of an air flow and in the middle there is a sampling port for the withdrawal of solution samples during the decomposition experiments. The reactor is connected to a gas feeding line. The dry air flows through a bubbler filled with milliQ water in order to saturate it with humidity and prevent evaporation from the treated solution during the experiment. After the optimization of the experimental conditions the air flow rate was set at 30 mL·min^{-1}. The volume of treated solution was 70 mL, the thickness of liquid 9.8 mm, the gap between the surface and the electrodes 15 mm, and the volume of air inside reactor 286 mL.

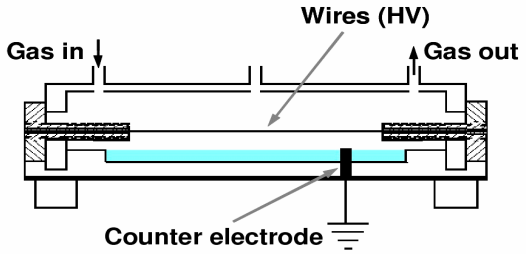

Figure 1 Sectional view of the 'seven-wires' reactor.

The new reactor developed and studied is presented in Figure 1. It is made in two pieces, a base and a cover, both of Plexiglas. The space occupied by gas has the following dimensions: 340x120 mm and 37 mm of height. The base in which the solution is placed is 5.5

mm high and has a capacity of 200 mL. Also in this case, the cover is equipped with a entrance and a exit ports for air circulation located at the opposite corners and in the centre there is a sampling port sealed by a silicon septum for withdrawal of samples of the treated solution. Seven parallel wires of 0.15 mm of diameter and 300 mm length constitute the active electrodes. They are placed at a distance of 18 mm one from the other and are fixed laterally on stainless steel electrodes screwed on a Teflon structure which can be moved up and down to vary the distance between the wires and the solution. The outside surface of the reactor base is covered with a film of colloidal silver paint and connected to a grounded plate. The flow of humidified air allowed through the reactor in this case was of 100 mL•min^{-1}.

The two reactors, which for clarity will be called 'two-wires' and 'seven-wires' reactors, were energized with the same high voltage power supply operating at 50 Hz in DBD corona mode. The scheme of power supply is shown in Figure 2. It includes a voltage regulator autotransformer (Variac – TX1), an isolation transformer (TX2), a voltage rising transformer (TX3) and a resistor (R2) for limiting the current. The function of TX1 is to adjust the voltage from the wall plug with 230 V from 0 to 120 V. Transformer, with a ratio of 1:1, isolates the grounding of wall plugs in case of short-circuit occurring between the oscilloscope (OSC) and the wall plug. TX3 is a voltage transformer that has a ratio of 1:150 and a very low phase shift.

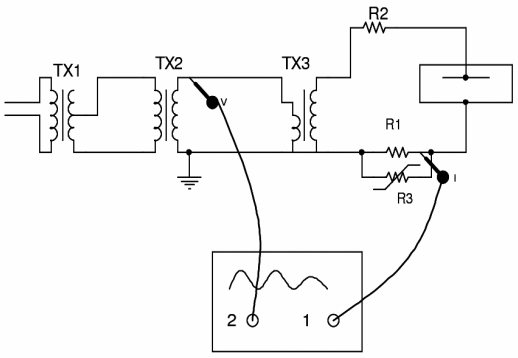

Figure 2 Electrical schematic of the power supply.

The system of electrical monitoring includes an oscilloscope (Tektronix TDS5032B, Bandwidth 350 MHz, Sample rate 5Gs/s) two 10:1 probes with 500 Hz bandwidth, a current measurement resistor with 50 Ω, and a surging voltage depressor (ZnO).

While in the previous papers [10,11] the efficiency of the experimental apparatus was evaluated by the measurement of the degradation rate constant of the pollutant chosen as model, phenol, in this case we calculated the energy per volume unit, Specific Energy Input (SIE), used by the two reactors and we expressed the efficiency in terms of energy constant, as explained below.

Equation (1) was used to calculate the power input:

$$P = \frac{1}{T}\int_0^T u(t)\cdot i(t)\cdot dt \qquad (1)$$

where:

- P is the mean power (W);
- T is the time duration of a voltage period (s);
- u(t) is the voltage applied to the reactor (V);
- i(t) is the current through the reactor (A).

According to Ohm law, the current through the reactor can be obtained from the formula:

$$i(t) = \frac{u_1(t)}{R} \qquad (2)$$

where:

- $u_1(t)$ is the signal recorded on Channel 1 of the oscilloscope (V);
- R is the resistance of R1 (Ω).

The voltage on the reactor, u(t), can be obtained from equation (3):

$$u(t) = u_2(t)\cdot K \qquad (3)$$

where:

- $u_2(t)$ is the signal recorded on Channel 2 of the oscilloscope (V);
- K is the ratio of the voltage rising transformer.

By substituting into (1), one obtains (4) which allows to estimate the power input.

$$P = \frac{K}{R\cdot T}\cdot\int_0^T u_1(t)\cdot u_2(t)\cdot dt = \frac{Kf}{R}\cdot\int_0^T u_1(t)\cdot u_2(t)\cdot dt = 150\cdot\int_0^T u_1(t)\cdot u_2(t)\cdot dt \qquad (4)$$

The power supply frequency f is equal to 50 Hz.

From the mathematical resolution of the formula (4) we can get a digital formula:

$$P = 150\sum_1^N U_{1n}\cdot U_{2n}\cdot \Delta t = 150\cdot M \qquad (5)$$

where:

- N is the number of data acquired in one period;
- U_1, U_2 are the digital data recorded on Channel 1 and 2 respectively;
- Δt is the interval of time between two consecutive data acquisitions (s);
- M is the value of trace M1 displayed on the screen which is obtained by the mathematical resolution of the numerical sum of voltage and current values within one period (20 ms).

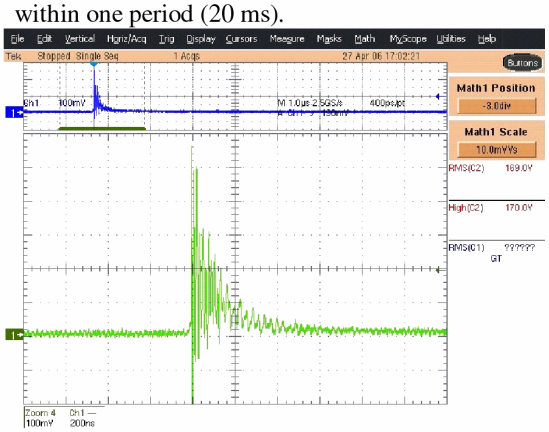

Figure 3 Current trace of a single pulse.

To make an accurate determination of power input, proper Δt values must be used because the corona discharge pulses are very fast, as shown in Figure 3. We can find out that the width of most corona discharge is about 200 ns. If Δt is 40 ns, there are 5 data points for every discharge, which are sufficient to get an accurate determination of the power input. The screen of the oscilloscope displays two voltage cycles corresponding to 40 ms, so the memory size should be higher than 1 Mega. The memory size is 2 Mega. With the calculated P values one can get, for any treatment time (t_t), the SIE ($J \cdot L^{-1}$) using the formula:

$$SIE = P \cdot t_t = 150 \cdot M \cdot t_t \qquad (6)$$

The experiments of removal of pollutants with the two reactors were performed by using solutions of phenol $5 \cdot 10^{-4}$ M. The conversion of phenol at different treatment times was measured by withdrawing aliquots of 0.5 mL of the treated solution and analyzing them by HPLC (Shimadzu LC-10AT pump with a UV-Vis Shimadzu SPD-10 detector). The column used was a Zorbax SB-Aq 150x4.6 mm column (Agilent Technologies) and the eluent was a solution of phosphate buffer 20 mM (pH=2) containing 1% of acetonitrile. The elution was followed at 210 and 270 nm. The fraction of residual phenol, $[Phenol]/[Phenol]_0$ was plotted against SIE and the data were fitted by equation 7

$$\frac{[Phenol]}{[Phenol]_0} = e^{-k_E \cdot SIE} \qquad (7)$$

where k_E is the energy constant expressing the efficiency of the process [12].

The energy constants obtained in the treatment of phenol solutions prepared in milliQ and tap water with the two reactors are reported in Table 1. Those relative to the two-wires reactor are obtained by conversion of the kinetic constants reported in [10-11], possible due to the fact that the experiments were performed maintaining constant the electrical power. New experiments were instead performed with the seven-wires reactor by applying the same experimental conditions both for the experiment execution and for the chemical analyses previously employed with the two-wires reactor. In fact the new reactor was built for allowing the changing of the distance between the wires and the solution and of the power supply and for applying a pump for water recirculation, but it was firstly tested under the same conditions employed with the first reactor in order to verify that only the dimensions, the depth of the solution and the higher number of wires assure an increase in the decomposition efficiency of the organic compounds. Thus, the only differences between the two system were the volume of the treated solution, as the smaller two-wires reactor was filled with 70 mL while the seven-wires reactor with 200 mL, and the depth of the solution, which was 9.8 and 5.5 mm, in the old and the new reactor, respectively.

Table 1. k_E ($L \cdot kJ^{-1}$) obtained in the treatment of a $5 \cdot 10^{-4}$ M phenol solution by the two DBD reactors in milliQ and tap water

Reaction medium	k_E ($L \cdot kJ^{-1}$)	
	Two-wires reactor	Seven-wires reactor
milliQ water	$1.0 \cdot 10^{-2}$	$1.9 \cdot 10^{-2}$
Tap water	$2.9 \cdot 10^{-2}$	$3.2 \cdot 10^{-2}$

The results of the experiments executed with the seven-wires reactor are reported in Figure 4, which shows the phenol conversion as a function of SIE.

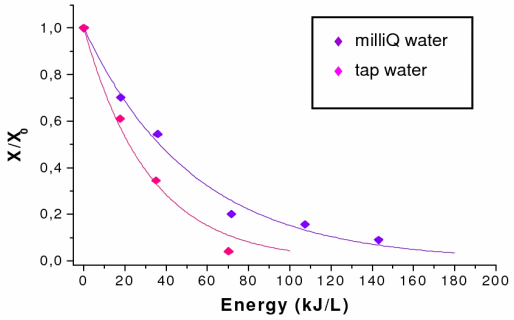

Figure 4. Phenol conversion as a function of SIE in experiments performed with the seven-wires reactor by treating solutions prepared in milliQ and tap water.

If the efficiency of the decomposition process in the two reactors is compared (Table 1), it is evident that the seven-wires reactor allows an increase of about twice when milliQ water is used for the preparation of the solutions. This demonstrates that an higher number of wires allows the development of a more diffuse plasma, which can interest the entire surface of the liquid. The depth of the solution also is considered to have an important role in the decomposition process as it was previously concluded [10] that the most of the reactions responsible for the decomposition of phenol take place on the surface of the liquid. A thin depth of liquid allows also a faster exchange of the surface water as the ionic wind developed by the discharge, clearly visible during the experiments, is sufficient to mix the entire solution.

The experiments performed in phenol solutions prepared with tap water have the scope to consider a model of drinking water, characterized by an higher conductivity and by the presence of dissolved salts with respect to milliQ water. By employing the two-wires reactor it was found that the use of tap water induces an increase in the efficiency of phenol decomposition [11]. After a specific study in which the possible effect of different additives present in tap water was considered, it was concluded that this increase in efficiency is due to the buffer effect of the bicarbonate anions dissolved in the solution, which prevent the decrease of the pH due to the formation of nitric acid during the treatment. To verify if this effect

is obtained also in the seven-wires reactor, this experiment was performed also with the new reactor. Effectively, an increase in efficiency is observed, also if less marked, which confirms that the general mechanism responsible for phenol decomposition is the same in the two reactors.

In conclusion, a new DBD reactor was developed based on a smaller working first prototype based on the application of the discharge to wires placed above the solution to be treated. The calculation of the specific energy input given to the system was performed and this allowed to compare the performance of the two reactors under the same energy input conditions. The new reactor, characterized by bigger dimensions, an higher number of wires and a thinner solution depth demonstrated to be effectively more efficient in the decomposition of phenol, chosen as model, in solutions prepared both in milliQ and tap water.

References

1. B. R. Locke, M. Sato, P. Sunka, M. R. Hoffmann, J.-S. Chang. Electrohydraulic discharge and nonthermal plasma for water treatment. *Ind. Eng. Chem. Res.* **2006,** *45,* 882-905.
2. A. K. Sharma, D. M. Camaioni, G. B. Josephson, S. C. Goheen, G. M. Mong. Formation and measurement of ozone and nitric acid in a high voltage DC negative metallic point-to-aqueous-plane continuous corona reactor. *J. Adv. Oxid. Technol.* **1997**, *2*, 239-247.
3. J. L. Brisset. Air corona removal of phenol. *J. Appl. Electrochem.* **1997**, *27*, 179-183.
4. W. F. L. M. Hoeben, E. M. van Veldhuizen, W. R. Rutgers, G. M. W. Kroesen. Gas phase corona discharges for oxidation of phenol in an aqueous solution. *J. Phys. D: Appl. Phys.* **1999**, *32*, L133–L137.
5. W. F. L. M. Hoeben, E. M. van Veldhuizen, W. R. Rutgers, C. A. M. G. Cramers, G. M. W. Kroesen. The degradation of aqueous phenol solutions by pulsed positive corona discharges. *Plasma Sources Sci. Technol.* **2000**, *9*, 361-369.
6. L. R. Grabowski, E. M. van Veldhuizen, W. R. Rutgers. Removal of phenol from water: a comparison of energization methods. *J. Adv. Oxid. Technol.* **2005**, *8*, 142-149.
7. L. R. Grabowski, E. M. van Veldhuizen, A. J. M. Pemen, W. R. Rutgers. Corona above water reactor for systematic study of aqueous phenol degradation. *Plasma Chem. Plasma Process.* **2006**, *26*, 3-17.
8. M. Sato, T. Tokutake, T. Ohshima, A. T. Sugiarto. Aqueous phenol decomposition by pulsed discharges on the water surface. *IEEE trans. Ind. Appl.* **2008**, *44*, 1397-1402.
9. T. H. Dang, A. Denat, O. Lesaint, G. Teissedre. *Eur. Phys. J. Appl. Phys.* **2009**, *47*, art. n. 22818.
10. E. Marotta, M. Schiorlin, X. Ren, M. Rea, C. Paradisi. Oxidation of aqueous phenol in a dielectric barrier discharge reactor. In preparation.
11. E. Marotta, E. Ceriani, M. Schiorlin, M. Rea, C. Paradisi. Comparison of the decomposition rate of phenol in deionized and tap water using a dielectric barrier discharge reactor. In preparation.
12. H.-H. Kim. Nonthermal plasma processing for air-pollution control: a historical review, current issues, and future prospects. *Plasma Process. Polym.* **2004**, *1*, 91-110.

5. CONCLUSIONS

This thesis reports and discusses the results of studies on non-thermal plasma processes for the oxidation of organic pollutants in air and in water.

The thesis has investigated the great potential of atmospheric plasmas for environmental processes of air and water decontamination from organic pollutants with the specific aim to contribute to the characterization of the major chemical reactions involved. A general conclusion which can be drawn from the results of the experiments conducted in the different systems investigated, is that plasma processing provides a highly efficient means for the advanced oxidation of organic pollutants both in air and in aqueous solution: thus, exhaustive oxidation to CO_2 of various organics, ranging from toluene and CF_2Br_2 in air to phenol in water, was achieved in processes run at ambient temperature and pressure. This extraordinary feature of non-thermal plasma processing makes it highly attractive especially for the decontamination of large volumes of air or water containing pollutants in low concentration.

The energy cost of such treatments is the concern of electrical engineers who are actively pursuing the development and optimization of new reactors and power supplies. A second conclusion of general validity drawn from this thesis is that, within a single reactor and under otherwise identical experimental conditions, the mode by which energy is provided to the system greatly affects the composition and extension of the resulting plasma and consequently the chemical reactions which it can support. Thus, the work described in this thesis shows that the efficiency of VOC oxidation in air plasma (VOC being toluene, CH_2Br_2 or CF_2Br_2) within the same reactor and under the same experimental conditions decreases in the order +Pulsed > –DC > +DC. In other words, any given input of energy produces an extent of VOC conversion ($[VOC]/[VOC]_0$) which depends on the corona regime and decreases in the order +Pulsed > –DC > +DC (see for example *Fig. 1* of *Section 4.2*).

The better performance of +Pulsed corona with respect to +DC and –DC corona regimes found in the oxidation of VOCs in air, which confirms and extends earlier results for processing of saturated hydrocarbons in the same reactor, is perfectly coherent with the results of emission spectroscopy measurements reported in this thesis. These results show that in our reactor

both electron energy and O atom density are, at any value of input energy, significantly higher with +Pulsed than with DC corona of either polarity.

The thesis also shows that trace amounts of organic compounds (VOCs) produce quite dramatic effects on the composition of plasmas produced by corona discharges in air at atmospheric pressure. Such effects are largely VOC-specific and can be rationalized on the basis of known properties of the organic compound which can then be used as molecular probes. One feature of the plasma which is drastically affected is its ion population: different ions are observed depending on the specific VOC used, albeit in very low relative concentrations. Thus, while in pure air +DC plasma the major ions are $H_3O^+(H_2O)_n$ and $NO^+(H_2O)_n$, in air containing toluene (T), mostly ionized (T^+) and protonated (TH^+) toluene are detected and in air containing CH_2Br_2, the ions are mostly $CH_2Br_2^+$ and CH_2Br^+. Such different ion populations reflect in VOC-specific current-voltage characteristics. Similarly, we have shown that the currents measured for –DC corona in air are significantly increased by the addition of trace amounts of dichloromethane (500 ppmv). Consistently, the negative ion APCI mass spectra are also greatly affected due to the prevalence of VOC derived Cl-containing anions.

Perhaps even more than energy efficiency, product selectivity is a most critical process feature which needs to be optimized in corona induced removal of organic pollutants from air. Neutral products and intermediates of air plasmas are likewise greatly affected by the presence of very small amounts of a specific VOC. Thus, no ozone was detected in the treated gas when air containing 500 ppm_v CH_2Br_2 was processed in the corona reactor, as a consequence of the very efficient catalytic cycles leading to ozone destruction, in which Br atoms act as propagating species. NO also enters one such cycle to be oxidized to NO_2, thus accounting for the production of significant amounts of HNO_3 in these experiments. Toluene has similar beneficial effects on the amount and type of undesired side products obtained from corona processing, notably ozone and NOx. Thus, toluene reduces the formation of ozone and promotes the conversion of NOx to HNO_3. The reduced amount of ozone detected in the presence of toluene is attributed to reaction of toluene with O atoms which competes with that forming ozone rather than, as in the case of CH_2Br_2, to some ozone consuming reactions. As for the formation of nitric acid, a side product which is more readily disposed of than the NOx, it is clearly favored by

production of water and of NO_2 due to toluene oxidation. NO_2 is formed from oxidation of NO coupled to the conversion of organic peroxyradicals ($ROO^{\bullet}$) to the corresponding oxy radicals ($RO^{\bullet}$) along the well known route of VOC oxidation to CO_2. The way by which VOC derived organic radicals ($R^{\bullet}$) are formed within the plasma, i.e. the initiation step(s) of the oxidative chain, has been of a central issue of the thesis.

The study of the reactions and mechanisms of VOC-oxidation induced by corona in air at atmospheric pressure has revealed a great variety of chemical behaviours depending on VOC type, corona regime and other experimental conditions, notably the presence and extent of humidity in the air. Thus, humidity, an important and variable component of ambient air, affects the efficiency of toluene oxidation by –DC and +Pulsed corona, but not with +DC, no effect being observed at all over a wide range of relative humidity. A rationale for the different response of +DC and –DC to changes in the humidity content comes from the analysis of the ions formed within the plasma coupled with the results of current/voltage characteristics. It is proposed that the initial steps of toluene decomposition differ depending on the plasma regime applied: ionic reactions are favored with +DC in dry as well as in humid air, whereas reactions with electrons, O atoms and OH radicals prevail in the case of DC and +Pulsed corona discharges. These observations and rationale are of immediate practical relevance. Similar conclusions were reached for CH_2Br_2. In contrast, for the perhalogenated model CF_2Br_2 no evidence or indications were found suggesting that different mechanisms occur within the different plasmas generated by +DC, –DC and +Pulsed corona discharges. A common scheme was thus proposed for the oxidation of this VOC induced by the different coronas tested, initiated by electron induced dissociation into Br atoms and CF_2Br radicals. The scheme is consistent with the results of on-line FT-IR analysis in the post plasma region, which show the absence of CO and the presence of CO_2 and of CF_2O, a compound which is notoriously unreactive with radicals.

Efficiency and, especially, product selectivity can be improved by the combined action of plasma and heterogeneous catalysts which usually result in synergistic effect. The nature and origin of this synergy was the focus of the research I carried out in my second year in graduate school during a stage at the AIST laboratories in Tsukuba, Japan. As molecular probe to compare the

effects of plasma alone and plasma plus catalyst we selected the O-scrambling reaction to form $^{16}O^{18}O$ starting from a mixture of $^{16}O_2$ and $^{18}O_2$. Four different reactors were used and various catalysts, including TiO_2, MS-13X and γAl_2O_3 also containing a few % of Ag. It was possible to conclude that, in the absence of a catalyst the O-exchange reaction occurs in the gas phase and not on the electrodes surface. It was also possible to use the results of these experiments to estimate, for any given energy input the average concentration of O atoms within the plasma. This is a most interesting outcome of these studies since the traditional procedure for obtaining O atom density involves sophisticated laser spectroscopy determinations (LIF experiments). As for the catalyst/plasma interaction, using again a labelled molecular probe, $^{18}O_2$, it was possible to conclude that the plasma induces oxygen fission on the catalyst surface and that this oxygen is then used in the VOC oxidation.

Interesting mechanistic conclusions have been reached also for the plasma-induced oxidation of phenol in aqueous solution. For these studies two prototype reactors were developed and tested, both characterized by application of electric discharges in the air above the solution. The second reactor allowed us to perform some interesting comparisons since it can be powered by different types of high voltage for the generation of plasma. It was shown that ozone and hydroxyl radical are key species involved in the decomposition process of the organic pollutant. Ozone can react directly with phenol on the surface of the solution, while OH radicals can react both on the surface of the liquid when formed in the gas phase from electron interaction with water or into the solution when formed from the ozone decomposition process. The possibility to apply this technology to the treatment of waste water depends on many factors: the process efficiency, the final composition of the treated solution, the general applicability of the system to the organic pollutants. The data obtained until now are very promising mainly because of the absence of any hazardous organic by-product after a proper treatment time.

An interesting and important conclusion is that phenol oxidation in tap water is more efficient in our reactors than in deionized water. This result is attributed to the specific configuration adopted for both reactors, i. e. plasma above the liquid. Thus, while in reactors which use corona-like discharges directly applied into the water the conductivity of the solution affects negatively the decomposition rate of the organic compounds, when the discharge is applied

above the solution this parameter does not affect significantly the removal process. Moreover, in our reactor bicarbonate anions, generally dissolved in drinking and wastewaters, exert a positive effect on the decomposition of phenol due to their buffering properties, which allow the pH to be constant at about 7 even if a significant quantity of nitrate ions is formed during the treatment. After a careful investigation of the characteristics of tap water which can influence the removal of phenol, we found that the buffering effect of bicarbonate is the determining feature for the increase in the rate constant when the decomposition process is carried out in this water. On the contrary the quenching effect of bicarbonate ions is not significant probably because compensated by the higher proportion of the more reactive phenolate with respect to phenol into the system and by the reactivity of the radical anion $CO_3^{-\bullet}$ produced by the reaction of the bicarbonate anion with the OH radical.